Time series analysis and modeling of the statistical properties of heart beat dynamics during atrial fibrillation

Dissertation
zur Erlangung des akademischen Grades
Doktoringenieur (Dr. rer. nat.)

vorgelegt der
Fakultät für Mathematik und Naturwissenschaften
der Technische Universität Ilmenau

von
Dipl.-Ing. Thomas Hennig
geboren am 10.12.1976 in Saalfeld

Gutachter:

1. Univ.-Prof. Dr. rer. nat. habil. Dipl.-Phys. Philipp Maaß,
   Technische Universität Ilmenau
2. Univ.-Prof. Dr. rer. nat. habil. Dipl. Phys. Erich Runge,
   Technische Universität Ilmenau
3. Juniorprof. Priv.-Doz. Jan W. Kantelhardt,
   Martin-Luther-Universität Halle-Wittenberg

eingereicht am: **21.01.2009**
wissenschaftliche Aussprache am: **27.08.2009**
urn: **nbn:de:gbv:ilm1-2009000443**

Contents

1 Introduction

The aim of the present work is to make a contribution to the development of novel and improved methods of the analysis of medical time series. In particular the present study concentrates on the analysis of ECG-signals recorded during atrial fibrillation (AF). This disease is one of the most common arrhythmias of the heart, especially for adults in western industrial countries. AF is a special arrhythmia called supra-ventricular tachyarrhythmia and is characterised by irregular electrical excitations in the atria. This yields an abnormal heart beat and decreases the quality of life. The disease is accompanied with an increased risk of heart attacks and an increased risk of the occurrence of the life-threatening ventricular fibrillation. Due to the increasing life expectancy and due to the fact, that the risk to come down with the disease increases with age, health insurers predict an exponential increase in the costs for the treatment of atrial fibrillation in the coming years.

The precise diagnosis and the successful treatment of the disease is a difficult task, since there exist several kinds of atrial fibrillation for which each of them demands another form of treatment. Often the exact kind of fibrillation that is observed in an individual patient can be determined only by invasive measurements. Medical studies revealed that certain biological parameters, such as the size of the left atrium or the rate of fibrillation, are suitable for indicating the presence of different kinds of the disease. Usually invasive measurements are indispensable for the estimation of such quantities, since they are directly related to the atrium.

This fact is the main point of the present work. It is the aim of this study to investigate the possibility of estimating the rate of fibrillation from the surface ECG by a statistical analysis of the recording itself or of related signals. The importance of such an approach for medical practice is obvious. While atrial ECG-recordings are always connected with invasive measurements and thus are always connected with risks for the patient, the recording of surface ECG signals yields no further physical pressure for the patient and thus can be extended up to any time.

During the last few decades it was already shown that long-time ECG's and long-time tachograms of AF patients do significantly differ from the ones of healthy subjects. Up to now the biological reasons for these differences are not understood. This fact should be improved by the present work. Detailed studies will not only present a new characteristic feature in the time series of ventricular interbeat intervals during AF but will also show that different revealed characteristics are interrelated. Furthermore it will be shown that these features carry important information about a patients health.

Based on this knowledge, the further work concentrates on modeling the conduction of electrical impulses through the AV node. For one particular, well established model the exact analytical description is presented and discussed in detail. This description does not only allow to point out direct relations between the characteristic properties of tachograms

during AF and different biological processes but does also allow to develop novel methods for determining the fibrillation rate directly from the surface ECG.

In the final part of the work both the possibilities and the limits of these methods will be discussed. At the end of the study it will be shown, that in principle the estimation of important atrial parameters without invasive investigations is possible.

Einleitung

Das Ziel der vorliegenden Arbeit ist es, einen Beitrag zur Entwicklung neuer und verbesserter Verfahren für die Analyse medizinischer Signale zu liefern. Die Studie konzentriert sich im Speziellen auf die statistische Analyse von EKG Signalen während Vorhofflimmerns. Vor allem in den westlichen Industrieländern zählt diese Krankheit bei Erwachsenen zu den häufigsten Herzrhythmusstörungen. Vorhofflimmern (AF, abgeleitet vom Englischen *atrial fibrillation*) ist eine supra-ventrikuläre Tachykardie, bei der die Vorhöfe des Herzens unkontrolliert erregt werden. Dies führt zu einem unregelmäßigen Herzschlag und zu einer Beeinträchtigung der Leistungsfähigkeit und der Lebensqualität. Die Krankheit ist mit einem erhöhten Schlaganfallrisiko verbunden und birgt die Möglichkeit in sich, in das lebensbedrohliche Kammerflimmern überzugehen. Da das Risiko an Vorhofflimmern zu erkranken mit dem Alter ansteigt, prognostizieren Krankenkassen im Zuge einer stetig älter werdenden Gesellschaft für die kommenden Jahren einen exponentiell anwachsenden finanziellen Aufwand für die Behandlung dieser Erkrankung.

Die sichere Diagnose und erfolgreiche Behandlung des Vorhofflimmerns wird dadurch erschwert, daß die Krankheit in verschieden Formen aufteten kann, von denen jede eine andere Behandlungsmethode erfordert. In den meisten Fällen läßt sich die Art des Vorhofflimmerns nur durch invasive Eingriffe genau bestimmen. Medizinische Studien haben gezeigt, daß einige ausgesuchte biologische Parameter wie z.B die Größe des linken Vorhofes oder die Flimmerrate als Indikatoren für die speziellen Arten des Vorhofflimmerns verwendet werden können. Da es sich bei diesen Parametern jedoch ausschließlich um solche Größen handelt, die direkt die Vorhöfe des Herzens betreffen, sind invasive medizinische Untersuchungen zu ihrer Bestimmung zumeist unumgänglich.

Dieser Zustand ist der Angriffspunkt der vorliegenden Arbeit. Die vorliegende Studie konzentriert sich auf einen speziellen Parameter - die Rate des Vorhofflimmerns - und hinterfragt inwieweit es möglich ist, diesen Parameter ohne invasive Messungen sondern allein durch die Analyse geeigneter Kenngrößen, direkt aus dem Oberflächen EKG zu gewinnen. Die Bedeutung eines solchen Verfahrens liegt klar auf der Hand. Während invasive Eingriffe stets mit Unanehmlickeiten und Risiken verbunden sind, stellt die Aufzeichnung eines Oberflächen EKG keine weitere Belastung für den Patienten dar und kann infolgedessen über einen nahezu unbegrenzten Zeitraum hinweg ausgedehnt werden.

In den vergangenen Jahren und Jahrzehnten wurde bereits gezeigt, daß sich Langzeit-EKG und Langzeit-Tachogramme von Vorhofflimmerpatienten in charakteristischer Weise von denen gesunder Personen unterscheiden. Die biologischen Ursachen dieser Unterschiede sind bis heute jedoch nicht diskutiert wurden. Dieser Umstand soll mit der vorliegenden Arbeit verbessert werden. Detailierte Studien werden nicht nur ein weitere charakteristische Eigenschaft dieser Zeitreihen zu Tage förden, sondern auch zeigen, daß die verschiedenen Charakteristika miteinander verknüpft sind und wichtige medizinische Informationen über den Gesundheistzustand eines Patienten tragen.

Aufbauend auf diesen Erkentnissen konzentriert sich der weitere Teil der Arbeit auf die Modellierung der biologischen Prozesse die bei der Überleitung elektrischer Impulse über den AV Knoten im Herzinneren ablaufen. Für ein spezielles, etabliertes Modell wird eine exakte analytische Beschreibung vorgestellt und im Detail diskutiert. Mit Hilfe dieser Beschreibung lassen sich nicht nur direkte Zusammenhänge zwischen den charakteristischen Eigenschaften der Tachogramme und verschiedenen biologischen Prozessen aufzeigen sondern auch Verfahren entwickeln mit deren Hilfe die Flimmerrate direkt aus den statistischen Eigenschaften der Herzschlagintervalle bestimmt werden kann.

Die Diskusion über die Möglichkeiten und Grenzen dieser Verfahren bildet den Abschluß der vorliegenden Arbeit. An ihrem Ende wird gezeigt sein, daß eine Bestimmung medizinisch relevanter atrialler Parameter ohne invasive Eingriffe durchaus möglich ist.

2 Theses

1. The generation of shape sensitive morphograms allows to investigate the entire information provided by an ECG-recording without detailed pattern recognition and is suitable for determining different states of health. With view to the level of separation between different groups of subjects, best results are obtained for the analysis of those morphograms in which the information about the ECG morphology during single heart beats and the information about the duration of the heart beats is concatenated.
2. Distributions $w(r)$ of ventricular interbeat intervals r occurring during atrial fibrillation exhibit no common shape but several patterns. On the other hand, the distributions exhibit an exponential decay for large intervals r. This decay is a specific and a characteristic feature of atrial fibrillation.
3. The decay rate γ of the exponential decay is subjected to pronounced diurnal fluctuations which are strongly anticorrelated to the ones of the mean ventricular interval $\bar{r}$.
4. The occurrence of the exponential decay in $w(r)$ is related to the occurrence of the white noise part in the power spectrum of intervals r. The decay rate can be estimated directly from the level of the white noise. Hence, the level of the white noise part in the power spectrum is also subjected to diurnal fluctuations.
5. The time series of ventricular interbeat intervals r occurring during AF can be decomposed into two sub-sequences $\mathcal{S}_1$ and $\mathcal{S}_2$, where $\mathcal{S}_1$ contains those intervals r that are mostly correlated and that barely contribute to the exponential tail in the distribution $w(r)$ and where $\mathcal{S}_2$ contains mostly uncorrelated intervals that encompass accounts for nearly the whole exponential tail in $w(r)$. The shorter the intervals r the weaker are the correlation among them. Intervals r that contribute to the local maxima in the $w(r)$ are stronger correlated than the ones that contribute to other parts in the distributions.
6. The conduction model suggested by Jørgensen *et al* [Jørgensen02] is most suitable for predicting the statistical properties of ventricular interbeat intervals r during AF. The originally model and several of its modifications can be fully analytically described. The stochastic process of blocking atrial impulses at the AV node during its refractory state can be expressed in terms of a first passage time problem of an one-dimensional random walk with moving boundary conditions.
7. The fibrillation rate can be determined from the statistical properties of ventricular intervals r during atrial fibrillation. This can be done (i) by an iterative algorithm which is based on the analysis of the distribution $w(r)$, (ii) by fitting the analytical solutions of modified conduction models to the ventricular response or (iii) by numerical studies in which the parameters of conduction models are fitted to the ventricular response.

3 Overview

The heart is one of the most important organs in the entire human body. It pumps blood throughout the body, beating approximately 72 times per minute. During a single pumping event, the so-called *cardiac cycle*, the four cavities of the heart are filled with blood. The cavities on the top of the heart are named *atria* and the other ones are named *ventricles* (see fig. 3.1). The *septum* separates the heart into a left and a right side. On each side of the heart the atrium and the ventricle are connected by a valve (mitral valve: left side, tricuspid valve: right side).

Several large blood vessels are connected to the top of the human heart. Vessels transporting blood into the heart are named *veins* while vessels transporting blood away from the heart are named *arteries*. The largest veins that carry blood into the heart are the *superior vena cava* and the *inferior vena cava*. The *aorta* on the other hand, carries nutrient-rich blood away from the heart. The *pulmonary artery* connects the human heart with the lungs and thus with the pulmonary circulation system. During every cardiac cycle de-oxygenated blood is pumped from the right atrium into the right ventricle and thus moves via the pulmonary artery into the lungs. At the same time oxygenated blood is collected in the left atrium and pumped into the entire organism.

The contraction and relaxation of the cardiac muscles are governed by electrical impulses provided by the *sinus node*. The node contains a group of modified cardiac cells positioned on the wall of the right atrium near the entrance of the superior vena cava. In principle, all cells in the human heart are capable of generating electrical impulses. The sinus node is the primary pacemaker in the normal working heart since it provides electrical excitations faster than every other cell.

The impulses travel through the heart tissue and cause the mechanical contraction of the muscles. On their way, they pass the *atrioventricular node* (AV node). This node is the only electroconductive connection between the atria and the ventricles [Prystowsky97]. Impulses conducted through the AV node are delayed for about 0.1 s. Thus the node prevents a rapid conduction of excitations to the ventricles in case of rapid atrial rhythms. Furthermore the delay ensures that the ventricles do not contract until the atria have fully ejected their blood.

3.1 Electrocardiogram and tachogram

The interrelation between the electrical activity and the contraction of the heart muscles, allows to observe the state of the heart without complicated invasive investigations. The *electrocardiogram* (ECG) measures electrical potentials between various electrodes, so-called *leads* (see fig. 3.2), which are placed at specific points on the body.

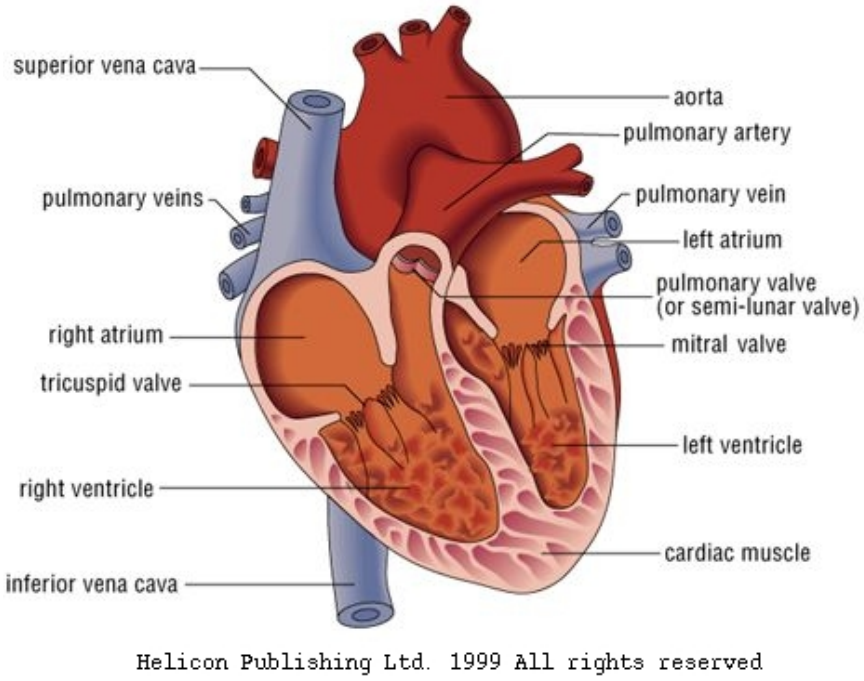

Figure 3.1: Schematic representation of human heart. The picture is taken from `http://www.gonzaga.k12.nf.ca/academics/science/sci_page/biology/biology.html`.

Bipolar leads, such as the standard leads I, II and III detect electrical potentials between two points on the body directly (left panel in fig. 3.2). In contrast to this, *unipolar* leads, such as the *augmented limb leads* aVR, aVL and aVF, measure electrical potentials at one point on the body with respect to a "null point", which is not affected by variations of the electric potentials during the contraction of the heart (right panel in fig. 3.2). For each lead the indifferent point is obtained by adding the potential from the other two leads.

The specific structure of an ECG-signal during a normal cardiac cycle is shown in the left panel of fig. 3.3. According to the notation suggested by Einthoven, the different waves and peaks are assigned to the letters P, Q, R, S and T. The baseline of the signal is named *isoelectric line*.

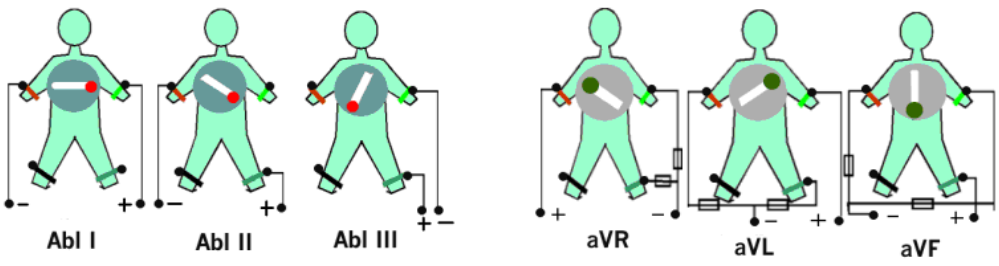

Figure 3.2: Schematic representation of different leads according to Einthoven (left panel) and Goldberger (right panel). The pictures are taken from `http://www.grundkurs-ekg.de/ableitungen/ableitungen.htm`

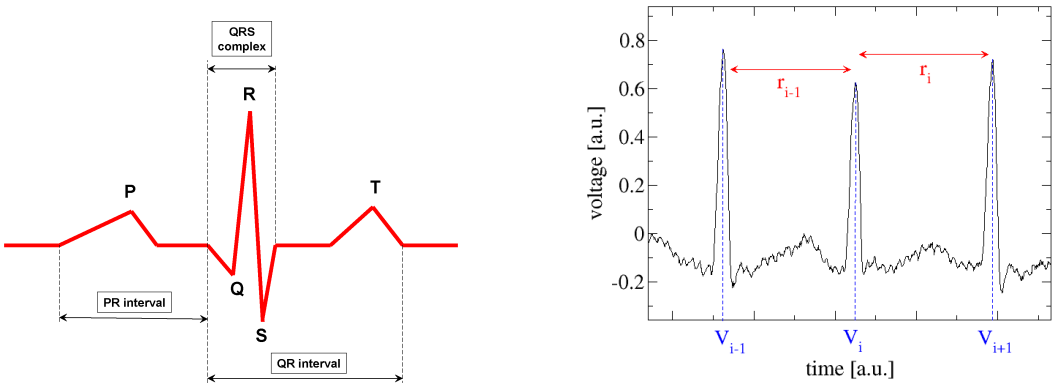

Figure 3.3: Left panel: Schematic representation of an ECG-signal during a single cardiac cycle. The peaks and waves are noted according to the suggestion of Einthoven.
Right panel: Determining the duration of cardiac cycles from the surface ECG.

The *P wave* is observed during the normal depolarisation of the atrium. The depolarisation of the ventricles corresponds to the so-called *QRS complex*. Usually this complex is larger and more pronounced than the P waves, since the ventricles contain more muscle mass than the atria. The repolarisation of the ventricles is assigned to the *T wave* in the ECG. The time interval between the onset of the QRS complex and the apex of this wave corresponds to the *absolute refractory period* of the ventricles. The duration of the second part of the T wave corresponds to the *relative refractory period* of the ventricles. During these periods the ventricles are not or only partly excitable.

The duration of a single cardiac cycle corresponds to the time interval between two consecutive *R peaks* in the surface ECG (see right panel in fig. 3.3). In the following, we denote this time intervals as *ventricular interbeat intervals* r. Time series and sequences of consecutive intervals r are denoted as *tachograms* or as *ventricular responses*. Accordingly, we denote intervals between consecutive atrial excitations as *atrial interbeat intervals* τ and time series or sequences of such excitations as *atrial tachograms*.

In the present work we distinguish two different types of tachograms.

1. **Type I**: Sequence of ventricular intervals r_i

   Type I tachograms are no time series in a strict sense while the intervals r_i are assigned to the number i of the heart beat. Accordingly, they represent equidistant sampled time series on artificial timescales in units of 1 heart beat. The information about the duration of the cardiac cycles is carried only by the amplitudes of the elements r_i. Type I tachograms are normally used in medical practice.

2. **Type II**: Time series of ventricular intervals r_i

   In tachograms of Type II, an interval $r_i = r(t_i = V_i)$ is assigned to the time V_i at which that ventricular excitation is observed, that marks the beginning of the interval. Hence, these tachograms are unevenly sampled time series. The information about the duration of the cardiac cycles is carried by the amplitudes of the elements r_i and by the times V_i that they are assigned to.

Unless otherwise noted, Type I tachograms are used in the present work.

3.2 Atrial fibrillation

All deviations from the normal electrical activity of the heart are summarised as *cardiac arrhythmia*. One distinguishes between (i) *tachycardia*: heart rate faster than 100 beats/minute and (ii) *bradycardia*: heart rate lower than 60 beats/min. Arrhythmias caused by a normal development of the heart rate are denoted as *sinus tachycardia* and *sinus bradycardia*. Tachyarrhythmias that require only atrial and/or atrioventricular (AV) nodal tissues for their initiation and maintenance are called *supraventricular tachycardia*.

A special kind of such tachyarrhythmias is *fibrillation*. In accordance to the part of the heart that is affected by this disease one distinguishes between *atrial fibrillation* (AF) and *ventricular fibrillation*. In contrast to AF the occurrence of ventricular fibrillation is immediately life-threatening.

AF is characterised by uncoordinated atrial excitations with consequent deterioration of the atrial mechanical function. During *sinus rhythm* the atrium is paced by about 72 beats/minute, while during AF rates of about 400-600 beats/minute are observed [Nattel02]. During atrial fibrillation the AV node behaves like a low pass filter. Rapid excitations are not conducted through the ventricles. Thus, the AV node prevents the fibrillation in the atrium to pass over into a ventricular one.

During AF the P waves in the surface ECG are absent ore replaced by rapid oscillations so-called *fibrillatory waves*. When the atrioventricular conduction is intact these waves are associated with an irregular ventricular response [Bellet71]. The ventricular response to AF depends on the electrophysiological properties of the AV node as well as on the levels of the *vagal* and *sympathetic tones*. The pathophysiology is supposed to be determined by *multiple independent re-entrant wavelets* in both atria. The initiation and the maintenance of the disease are supported by the electrophysiological properties of the underlying substrate and repetitive triggers.

AF can occur isolated (so-called *lone AF*) or accompanied with several additional disorders, e.g. *atrial flutter* or *atrial tachycardia*. Atrial flutter may degenerate into AF but it can also be initiated by AF. Some of the most important diseases associated with AF are *hypertensive heart diseases* [Kannel82]. AF is also often found in the presence of other paroxysmal supra-ventricular tachycardias, e.g. *Wolf-Parkinson-White syndrome*: 10% during sinus rhythm to 34% during AF [Bauernfeind81].

According to the classification nowadays used, one distinguishes *paroxysmal*, *persistent* and *chronic* AF ([Saur03], [Levy98]). Paroxysmal AF is characterised by attacks with durations between several minutes and two days. If the AF episode is longer than 48 hours, the disease is denoted as persistent. AF not treatable by medicaments or *electrical cardioversion* is called chronic AF. Other kinds of classification are discussed in sec. 3.2.2.

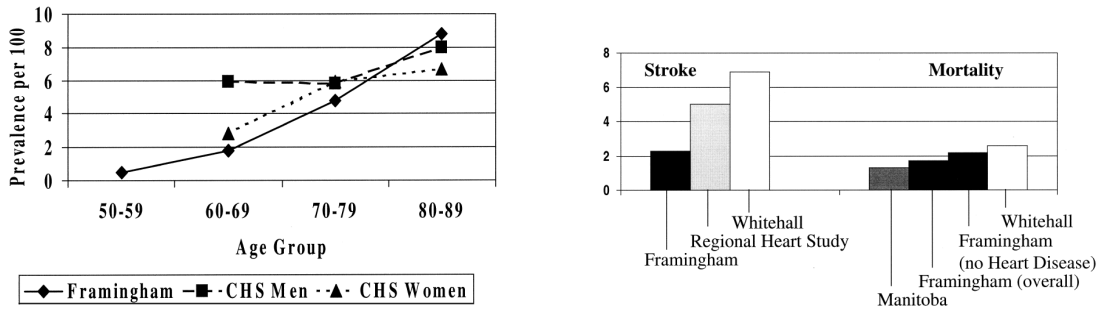

Figure 3.4: Left panel: Prevalence of AF in two american epidemiological studies. Framingham indicates the Framingham Heart Study [Wolf91]; CHS corresponds to Cardiovascular Health Study [Furberg94]. The picture is taken from [Fuster01]. Right panel: Relative risk of strokes and mortality for patients with AF compared to patients without AF. Source data are derived from the Framingham Heart Study [Kannel83], Regional Heart study [Flegel87], Whitehall study [Flegel87], and Manitoba study [Krahn95]. The picture is taken from [Fuster01].

3.2.1 Epidemiology and prognosis

AF is the most relevant arrhythmia in medical practice. Important epidemiological results are provided by the Framingham study where 5184 persons have been observed during 30 years [Kannel82]. AF was detected for 2% of all persons older than 22 years. The incidence of AF increased up to 5% in the age between 50 and 59, and rose up to 9% for all persons in the age between 80 and 89 years. Another study demonstrated a prevalence of AF of 5% for all women and of 6.2% for all men over 65 years [Furberg94]. The prevalence of AF based on the data of the Framingham study (published in 1991) and the Cardiovascular Health Study is shown in the left panel of fig. 3.4.

Furthermore, an increasing risk of strokes in the presence of AF is clearly demonstrated ([Wolf87], [Britton85]). Among patients with AF the rate of ischemic strokes averages about 5% per year, which is two to seven times higher than the rate observed for persons without the disease (see right panel in fig. 3.4) ([Levy99], [Krahn95], [Wolf91]). It was shown by the Framingham study, that the total mortality is approximately doubled for patients with AF compared to those with sinus rhythm. Due to the increasing of the life expectancy the occurrence of AF will rise by 1-2% in the next years. For example, if the population in Europe amounts to 300-500 million, then 6-10 million of AF patients are expected. The associated increase of the medical costs exhibits an exponential trend [Hoffmann02].

3.2.2 Pathophysiological mechanisms

Two main processes are involved in the origin of atrial fibrillation: enhanced automaticity in one or several rapidly depolarising foci and re-entry involving one or more circuits ([Moe59], [Rensma88]). AF can be initiated by rapidly firing atrial foci, located in one or several of the superior pulmonary veins ([Jais97], [Haissaguerre98]).

Moe and coworkers ([Moe62]) proposed the mechanism of AF to be caused by *multiple-wavelets*. Up to now, this hypothesis is the main basis of pathophysiological investigations

and research. It is important to mention, that this model is well accepted but it is still under discussion. Based on numerical simulations, Kneller *et al.* [Kneller02] suggested that AF could also result from relatively sharp primary spiral waves. The number of waves should depend on the refractory period, the mass, the size of the atria and the conduction velocity of impulses. Furthermore, Allessie *et al.* ([Rensma88], [Allessie76]) developed the theory of the *wavelength of re-entry*. This wavelength is given by the product of the refractory period and the conduction velocity and describes the distance an impulse travels during a refractory period. According to Allessie *et al.* this wavelength marks the shortest sustained cycle that can be observed in the atria. Short wavelengths are associated with the presence of a great number of small circuits while long wavelengths indicate only few circuits but large wavefronts in the atria ([Allessie85], [Moe62], [Rensma88]).

A first qualitative classification of AF, that relies on observed patterns of local excitations in the atria, was proposed by Wells *et al.* [Wells78]. According to their classification, discrete electrical signals with intervening isoelectric intervals are defined as Type I AF. The complete absence of periods with complete electrical quiescence in those signals is denoted as Type II AF. Type III AF describes the absence of any clear organisation of the atrial activations. The alternation between Type II and Type III is denoted as Type IV AF. In practice this kind of classification is difficult to use, since the different types of AF are not stable in time as reported by Wells himself. Another limitation is due to the different regional activation patterns that can be observed in the atria. In a medical study of patients undergoing AF, Lie *et al.* [Li96] pointed out the possibility that all three classes of AF are present at the same time but at different locations in the atria.

A well accepted and commonly used pathophysiological classification of AF is based on mapping studies of patients undergoing surgery for the Wolf-Parkinson-White syndrome [Konings94]. These studies distinguish between the observation (i) of single wavefronts, (ii) of single or double wavefronts and (iii) of multiple wavefronts propagating in the right atrium.

3.2.3 General concepts of treatment

In the presence of persistent AF two different ways for the management of the disease are suggested: either restoring and maintaining sinus rhythm or keeping the disease under control of the ventricular rate.

The first way includes the relief of symptoms, avoidance of cardiomyopathy and the prevention of embolism. The *cardioversion* is a commonly used method for the restoration of sinus rhythm despite that it carries a risk of thromboembolism. The risk is highest when the arrhythmia has been persistent for more than 48 hours. A cardioversion can be performed either by electrical shocks or by medication. Restoring and maintaining sinus rhythm is normally chosen as a treatment of paroxysmal AF. It has to be mentioned, that a recurrence to AF does not indicate a failed treatment. Hypertension and an age greater than 55 are indicators for a natural recurrence to AF. Risk factors for a frequent recurrence of fibrillation are female gender and the presence of other heart diseases. For the treatment of patients undergoing lone AF the use of Beta-blockers, Flecainide and Propafenone are suggested.

The second method, the pharmacological cardioversion has become more and more popular

which is due to the further development of new medicaments. This method is less effective than an electrical cardioversion but does not require sedations or anaesthesias. On the other hand, the risk to cause strokes or thromboembolism does not differ for both methods. Pharmacological cardioversion is most effective when initiated during the first seven days after the onset of the disease.

3.2.4 Medical indicators

Up to now, no medical test allows to predict the response of the organism to a chosen treatment. Established AF management guidelines often focus on the duration of the fibrillation episodes as indicator for the choice of the right concept of treatment, but do not take into account the different mechanisms that yield AF ([NHS06], [Fuster01], [NCC06]). Hence, the choice of the therapy often seems to be trial and error. Previous studies pointed out that several medical parameters are useful indicators not only to support the choice but also to predict the outcome of a medical treatment.

The size of the left atrium seems to be one of the most common and well accepted parameters. Beside other parameters, such as the refractory periods of the atrial cells or the conduction velocities of the atrial excitations, the left atrium size mainly predicts the wavelength of the shortest sustained cycle in the atrium. Recent studies showed, that the presence of short cycle lengths correlates with the risk of paroxysmal AF to turn into persistent one ([Asano92], [Boahene90]). Hence, the size of the left atrium has been proposed to be an useful indicator to predict the outcome of a cardioversion. This approach is still under discussion, which is due to the contrary results presented in various medical studies. For example, the finding that patients with left atrial enlargement show higher rates of AF recurrence ([Henry76], [Hoglund85], [Verhorst97]) could not be confirmed in other studies ([Arnar96], [Manabe97], [Omran98]).

A more promising approach to estimate the risk of a recurrence to AF (especially in the presence of paroxysmal AF) relies on the averaging of the P wave signals ([Aytemir99], [Raitt00], [Yamada99]). The sensitivity and specificity of this technique is remarkable (between 70% and 80%). On the other hand, this method can be applied only after the cardioversion and thus during sinus rhythm, since the P wave signal is absent during AF. Consequently, the suggested technique allows not to predict the outcome of cardioversion from the beginning.

During the last years the *averaged fibrillation rate* (inverse mean atrial cycle length) has been studied in detail by several groups. Various studies pointed out the importance of the fibrillatory rate as a classifier of different types of AF as well as an indicator for the prediction of the outcome of several methods of treatment. As an example, slow rates of fibrillation indicate the presence of persistent AF while high rates are observed in patients with AF that terminates spontaneously ([Asano92], [Boahene90]). The conversion to sinus rhythm with Ibutilide is successful only for patients with fibrillation rates lower than 6.25Hz (160ms cycle length) [Stambler97]. Similar results have been reported for medical conversion with Cibenzoline or Procainamide where the conversion is successful when the observed fibrillation rate is lower than 5.95Hz (168ms cycle length) [Fujiki01].

3.2.5 Rate of fibrillation

The *rate of atrial fibrillation* (AFR) is given as the inverse mean atrial cycle length (mean atrial interbeat interval) observed during AF. The majority of ECG-recordings of patients undergoing AF analysed in previous studies, exhibits single narrow banded frequency spectra ([Bollmann98], [Bollmann99], [Pherson98], [Slocum94]). It is suggested that the dominant frequency originates from repetitive activations provided by re-entrant sources [Jais97]. Spectral components of lower frequencies are suggested to be associated with the propagation of waves through the atria ([Jalife98], [Skanes98]). In the literature different values are reported for the dominant fibrillation rates. While some authors noted inter-individual fluctuations of the fibrillation rates in the range between 4 and 9Hz ([Asano92], [Capucci95], [Gaita98], [Hobbs00]), others reported rates between 3 and 12Hz ([Nattel02], [Pherson98]). The AFR is influenced by the refractoriness of cells at any part of the atria that is involved in the travelling of atrial excitations. This influence has been verified in animals [Kim96] as well as in humans ([Misier92], [Capucci95]). A decrease in refractoriness is accompanied with an increase in the AFR. The rate of fibrillation is an indicator not only for the atrial refractoriness but also for the organisation of the activations in the atria [Konings94]. Mean AFR's about 5.7Hz are observed in the presence of Type I AF (according to the classification of Konings, see sec. 3.2.2). Type II AF is associated with rates of about 6.6Hz and Type III with rates of about 7.4Hz.

The electrophysiological properties of the atrial cells are modulated by the autonomous nervous system. The refractory periods are shortened during daytime but prolonged during the night ([Huikuri95], [Cinca86]). Thus, the AFR is affected also by changes of the autonomous tone and therefore subjected to diurnal fluctuations ([Meurling01], [Bollmann00], [Bollmann99]).

3.3 Statistical properties of ECG-signals during atrial fibrillation

The statistical properties of ECG-recordings during AF have been investigated for several decades. First models of the origin of the disease have been presented in the early twenties. Since this time the statistical properties of atrial and surface ECG-recordings have been investigated by many groups all over the world. The earlier works are mostly based on surface ECG-signals. Nowadays multiple synchronous ECG-recordings from the atrium allow to investigate the atrial excitations during AF and their relation to the ventricular response in the surface ECG. In addition to standard techniques of time series analysis new approaches, for example nonlinear analysis, have been used to describe the mechanisms underlying the disease. The present section gives an overview on the different fields of investigations and on the results presented during the last years.

3.3.1 Atrial activations

Atrial activations: General approach

The analysis of intracardiac signals is mainly devoted to methods for recognition and localisation of activation patterns and focus on the following goals:

- Investigation of the mechanisms responsible for the re-entry and self-sustainment of AF
- Investigation of the wavefront propagation with respect to temporal and spatial patterns and organisation
- Identification of atrial regions with self-sustaining re-entrant foci to support ablation
- Estimation of the electrophysiological properties of the atrial tissue and the AV node in order to support the choice of the best medical treatment

First investigations of the morphology of atrial ECG-recordings during AF were made by Wells *et al.* [Wells78]. Their study was based on a visual scoring of the observed activation patterns and was a first attempt in order to classify AF based on electrophysiological measurements. In 1985 Allessie *et al.* [Allessie85] presented the first experimental evidence for the multiple wavelet hypothesis of Moe [Moe62]. Their investigations on dog hearts showed that four to six wavelets are needed for sustaining AF. These findings provided a starting point for further investigations of the multiple wavefronts by several groups ([Allessie96], [Skanes97]).

An alternative hypothesis for the mechanism of atrial fibrillation (the occurrence of rapidly firing re-entrant circuits) was proposed in the early 1920s by Sir Thomas Lewis ([Lewis25b], [Lewis25a]). This hypothesis has been used by several theoretical ([Scherf48], [Scherf53]) and medical studies [Jais97]. Schuessler *et al.* [Schuessler92] showed that activation patterns, observed in an isolated canine right atrial preparation, which are characterised by multiple re-entrant circuits, convert into a single, relatively stable, high-frequency circuit, when increasing the concentrations of Acetylcholine. These findings supported the alternative hypothesis of Lewis. Nowadays it is generally accepted that rapidly firing foci are present in some patients undergoing AF.

Atrial activations: Time domain analysis

The majority of the studies using time domain analysis focus on the development of automated procedures in order to replace the visual scoring of the signals. As a first step, Booteron *et al.* [Botteron95] analysed the spatial organisation of activations during AF by estimating the cross-correlation of closely spaced, bipolar endocardial ECG-recordings. They found that the spatial correlation monotonously decreases with the distance of the electrodes. The more qualitative study of Jais *et al.* [Jais96] pointed out significant differences in the organisation of activations among atrial regions. The synchrony between bipolar ECG-signals has been studied by Sih *et al.* [Sih99]. Their investigations of the linear relationship between different atrial signals pointed out, that the level of organisation decreases under vagal stimulations. The common view that atrial activations during AF are originated from random processes was confuted by Censi *et al.* [Censi00]. Their recurrence

plot analysis of atrial period series demonstrated the presence of deterministic mechanisms. It was furthermore shown, that a certain degree of organisation can be detected between the periods of depolarisation at two atrial sides.

Atrial activations: Frequency domain analysis

In contrast to time domain analysis, high-resolution spectral analysis offers the opportunity to investigate the correlation between spatial distributions of the excitation frequency and the cardiac anatomy. It also allows to monitor the electrophysiological state of the atria during ablation procedures and gives insight into the origin of different types of AF. Sahakian *et al.* [Sahakian92] proposed to characterise the atrial activity during AF by coherence spectra, which are estimated for pairs of short time ECG-recordings. Those spectra allow to investigate the varying relationships between the atrial activities measured at various locations in the atria. Ropella *et al.* [Ropella89] suggested to use coherence spectra for the construction of so-called *coherence maps*, which have been used to monitor the restoration of sinus rhythm during pharmacological conversion. It was shown, that a conversion to sinus rhythm yields an increase of coherence. An innovative approach for the investigation and identification of re-entrant sources of atrial activations during AF was proposed by Jalife *et al.* [Jalife98]. The analysed data are collected *in vitro* by optical recordings. Their work is based on the hypothesis that the fibrillatory frequency is mainly influenced by the most dominant source of activations. Their novel approach allows to identify and to observe rapidly firing foci in the atria in real time.

Atrial activations: Nonlinear analysis

Despite many years of research and investigations the exact mechanisms underlying AF are still poorly understood. Usually, AF is described as a random phenomenon. In contrast to this, medical studies provided evidence that the propagation of atrial excitations during AF is not completely random [Pappone04]. Several experimental and theoretical models have been proposed to describe possible nonlinear mechanisms underlying the propagation mechanisms ([Chialvo90], [Garfinkel97]). Hoekstra *et al.* [Hoekstra95] performed nonlinear analysis based on epicardial atrial ECG-recordings. Their work focused on the estimation of the correlation dimension and the correlation entropy of atrial ECG-signals in a reconstructed phase space. The obtained results are in agreement with the outcomes of high density mappings in medical studies. Their work showed, that there exist significant differences between different types of AF according to Wells definition. While a nonlinear behaviour is observed in ECG-recordings during Type I AF, no feature of low-dimensional chaos is found in ECG-recordings during Type III AF. Furthermore, Pitscher *et al.* [Pitschner98] reported differences in the chaotic behaviour among different locations in the atria.

3.3.2 Ventricular response

Ventricular response: Surface ECG analysis

One characteristic of atrial fibrillation is the absence of P waves and the occurrence of fibrillatory activities (F waves) in the surface ECG. According to the amplitude of the F waves one distinguishes between coarse and fine AF ([Peter66], [Leier80]). Coarse AF is observed if the amplitude of F waves exceeds or equals 0.1mV. Signals with smaller amplitudes are referred to fine AF. The clinical relevance and utility of this classification is limited. Medical studies which focus on the origin of the fibrillatory waves and their medical meaning yield contrary results. Some of them reported a correlation between an enlarged left atrium and the occurrence of high amplitudes in the F waves ([Aysha88], [Bartall78]). Other studies could not confirm this finding ([Blackshear96], [Li95], [Morganroth79]).

Nowadays various studies focus on the extraction of the fibrillation rate from the surface ECG. Rosenbaum *et al.* [Rosenbaum90] and Slocum *et al.* [Slocum92] proposed to identify the AFR by means of Fourier analysis of the surface ECG. While Rosenbaum *et al.* pursued to distinguish atrial flutter from atrial fibrillation, Slocum *et al.* focused on the identification of AF among different rhythms. The latter approach has been only partly successful since atrial and ventricular activities spectrally overlap. Nowadays well accepted methods for the frequency analysis of the surface ECG include various filtering techniques and the elimination of the QRS complexes. These techniques as well as validation has been first presented in two independent publications ([Bollmann98], [Pherson98]). The differences in the algorithms are due to the applied filter techniques and are mainly of technical relevance. The specific algorithm proposed by Bollmann *et al.* resulted in an international patent [Langberg98]. The basic method consists of the following steps: The ECG-signal is bandpass filtered in order to remove all frequencies outside a given range. Afterwards all QRS-complexes are detected and centred around a fiducial point in order to derive the mean signal (the so-called QRS template). This template is aligned to each QRS-complex in the remaining signal and subtracted. The derived signal is Fourier transformed and the AFR is identified as the frequency of the highest peak observed between 3 and 12Hz. A schematic representation of the algorithm is displayed in fig. 3.5. Comparing the estimated fibrillation rates with direct atrial ECG-recordings yield correlation coefficients about 0.98 which demonstrates the potential of the method. The agreement is the better the more pronounced are the F waves in the ECG-recording. The estimation of the AFR from ECG-signals exhibiting only small F waves is difficult or even not possible. Thus, the proposed method yields remarkable results, but is not applicable for all ECG-recordings in medical practice.

Ventricular response: Statistical properties of ventricular interbeat intervals during AF

The statistical properties of ventricular intervals r during AF have been discussed controversially during the last years. The results obtained by different studies are contradictory. On one side it has been reported, that the variation of intervals r mainly results from autonomic modulations of the electrophysiological properties of both the AV node and the atrium [Toivonen90]. The ventricular response is affected by an increase of the sympathetic

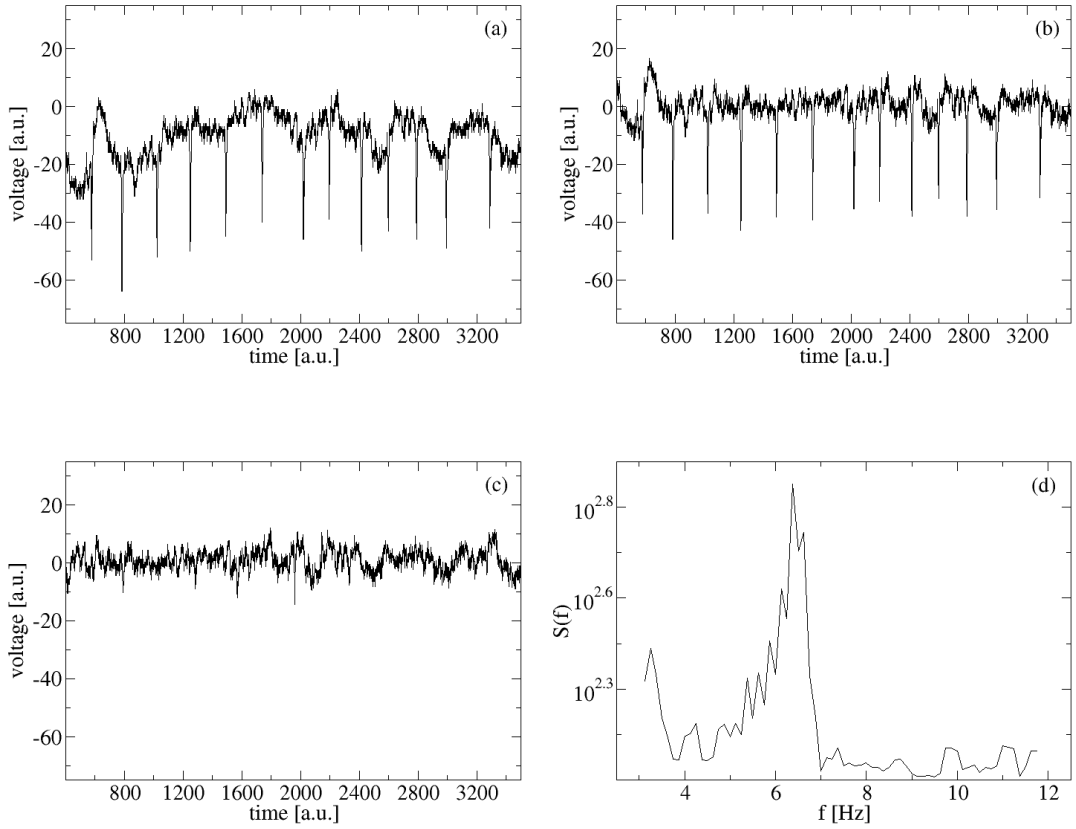

Figure 3.5: Schematic representation of the algorithm proposed by Bollmann *et al.* [Bollmann98] and Pherson *et al.* [Pherson98] for detecting the fibrillation rate from the surface ECG. Original surface ECG-signal (a), remaining signal after Butterworth filtering (b), fibrillatory baseline after QRS averaging and subtracting the QRS template (c), power spectrum of the fibrillatory baseline (d). Both the filtering and the template construction are done according to the algorithm proposed by Bollmann *et al.* [Bollmann98].

tone or a decrease of the parasympathetic tone [Nagayoshi97]. On the other hand, an increase of the sympathetic nerve activity can be caused by the presence of AF [Wasmund03]. This yields a circle, which does not allow to distinguish between cause and effect.

Even the shapes of the distributions $w(r)$ of intervals r are under discussion. While some studies report a unique distribution others directly study the medical meaning of different observed patterns.

Finally the question whether the ventricular response is random or deterministic could not be clarified during the last years.

Ventricular response: Time domain analysis

Several groups investigated the distributions $w(r)$ of intervals r and the distributions $w_\Delta(\Delta_r)$ of their increments $\Delta_r = r_{i+1} - r_i$ ([Konings94], [Goldstein67], [Stackee71], [Cohen83],

[Wittkampf88], [Kirsh88]). These studies mainly focused on the investigation of the specific shape of the distributions and on the occurrence of uni-modal and multimodal structures. For long times the shape of $w(r)$ has been thought to exhibit an uni-modal and characteristic structure. At present, the occurrence of several peaks in $w(r)$ is well accepted, but the previous assumptions are still under investigation [Petrucci05].

The medical meaning of the various shapes is still not well understood and also controversially discussed. On the one hand, the occurrence of multimodal patterns has been suggested to be an indicator for the presence of several conduction pathways in the AV node ([Bootsma70], [Olsson86], [Feld94], [Williamson94], [Morady97], [Pamboucas02]). This approach is mostly supported by the work of Rokas *et al.* [Rokas01]. They showed that the pattern of the distribution $w(r)$ may be an useful indication to predict the outcome of radio frequency modifications of the AV node. On the other hand it was discussed, that multimodal patterns reflect a variable conduction ratio between the atrial and the ventricular activity. In this way, the number of observed peaks indicates the amount of atrial impulses blocked at the AV node. Most of the mathematical models, suggested for the conduction process of atrial impulses through the AV node, follow this approach ([Cammarota05], [Mangin05], [Zeng96], [Cohen83]).

For real medical application, Tateno *et al.* ([Tateno01], [Glass05]) proposed to identify the presence of AF by comparing the distribution $w(r)$, estimated for a single patient, with a so-called *standard distribution*, a template which is obtained by averaging distributions $w(r)$ of intervals r occurred during AF. This approach is based on the assumption, that during AF the distributions $w(r)$ exhibit a unique shape. The remarkable results presented by Tateno *et al.* seem to support this assumption. On the other hand, various studies such as [Murgatroyd95], [Pinciroli86] and [Andresen98] controversially discuss the possibility of detecting AF solely based on $w(r)$. The results of our own investigations (see sec. 6.2) also clearly confute the assumption of an unique shape of distributions $w(r)$ during AF.

Another approach proposed to identify AF, is based on the performance of a so-called *CV test - standard coefficient of variation test* [Tateno01]. The CV is defined as the quotient of the standard deviation σ_r and the mean value $\bar{r}$ of intervals r.[1] The suggested method is directly based on the work of Cammarota *et al.* [Cammarota02] who showed that during AF $\bar{r}$ and σ_r are linearly related. This holds true not only for "global" values, calculated from all observed intervals r, but also for "local values" ($\bar{r}_{\mathrm{loc}}$, $\sigma_{\mathrm{r,loc}}$) obtained by an average over intervals r in limited time windows. Cammarota *et al.* suggested to use *scatter plots* to display the linear relation graphically. This relation is a characteristic feature of AF and can be observed in segments between 300 and 1000 successive intervals r. The origin and the medical meaning of this statistical feature are still under discussion.

Fig. 3.6 shows scatter plots for a representative patient undergoing chronic AF (panels (a), taken from data pool 1), a representative PAF patient (panels (b), taken from the AFDB database in data pool 3) and a healthy subject (panels (c), taken from the NSRDB database in data pool 3). The local values $\bar{r}_{\mathrm{loc}}$ and $\sigma_{r,\mathrm{loc}}$ are calculated for segments of 300 (left panels) and 500 (right panels) successive intervals r. The figures show a pronounced linear relation between $\bar{r}_{\mathrm{loc}}$ and $\sigma_{r,\mathrm{loc}}$ during AF and the absence of this relation during sinus rhythm. The linear relation is less pronounced during paroxysmal AF, since the ECG-

[1] The CV is a constant value in the presence of AF, but it fluctuates during sinus rhythm. The CV value is the inverse of the *signal to noise ratio* (SNR) which is defined as: $SNR = \bar{r}/\sigma_r$.

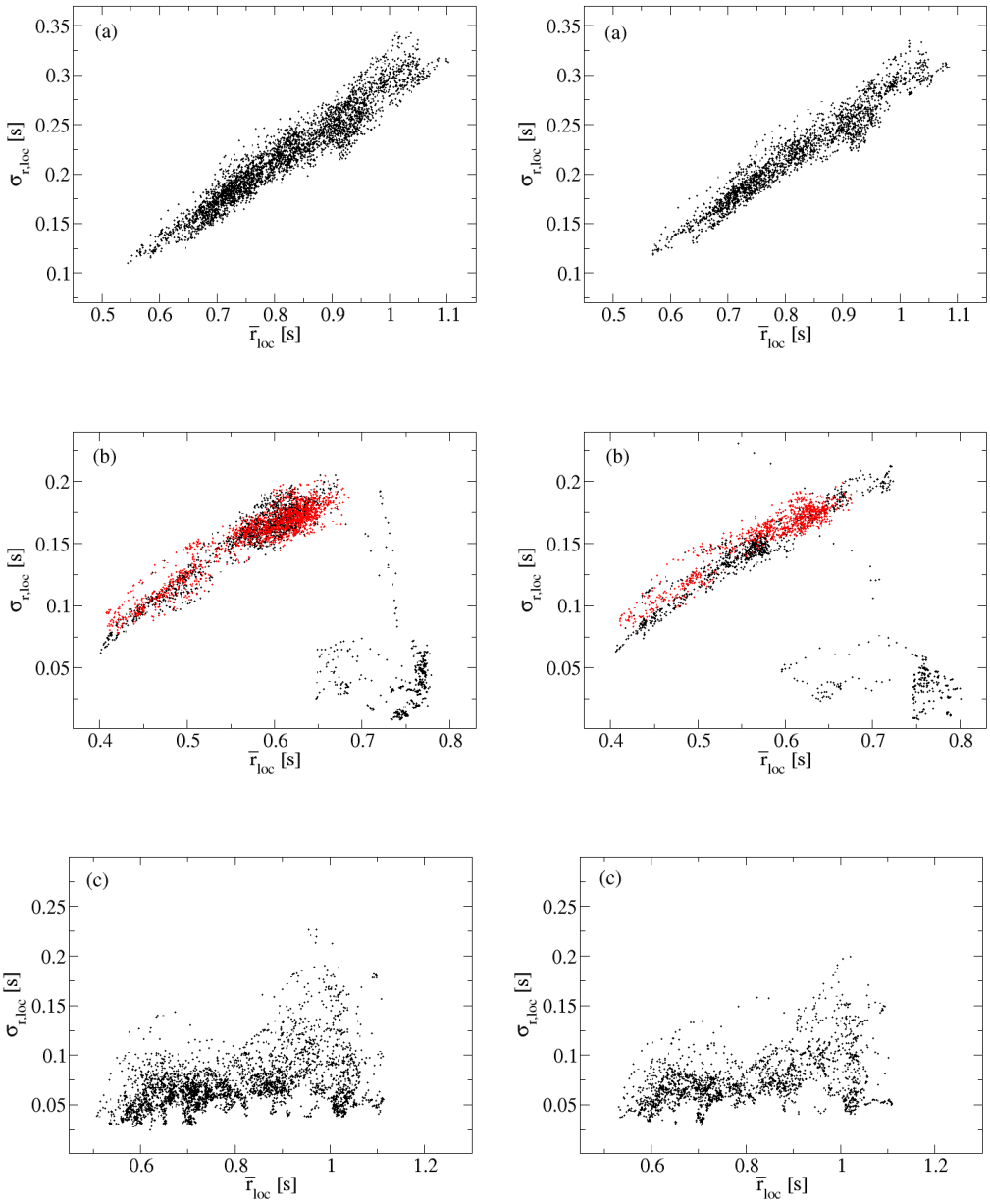

Figure 3.6: Scatter plots of intervals r for representative patients undergoing chronic AF (panels (a)), paroxysmal AF (panels (b)) and a representative healthy person (panels (c)). The data sets are taken from data pool 1 and data pool 3 respectively. The local values $\sigma_{r,\mathrm{loc}}$ and $\bar{r}_{\mathrm{loc}}$ are estimated in segments of 300 (left panels) and 500 (right panels) successive intervals r. For the patient undergoing paroxysmal AF the scatterplots show the local values $\bar{r}_{loc}$ and $\sigma_{r,loc}$ calculated for the whole data set (black points) and for the pure AF episodes only (red points).

recording contains both, episodes of AF and episodes of sinus rhythm [Cammarota05]. The strength of the relationship depends on the length of the fibrillation episodes. The longer the AF episodes are the stronger the linear relation is. For the presented PAF patient the AF episodes encompass about 77% of the whole ECG-recording. The scatter plots exhibit a superposition of the patterns observed during AF and during sinus rhythm. To demonstrate the influence of the episode lengths to the strength of the observed feature the plots show both the local values $\bar{r}_{loc}$ and $\sigma_{r,loc}$ calculated for the whole data set (black points) and for the pure AF episodes (red points) only. Clear to see, the strength of the linear relation improves when intervals during sinus rhythm are rejected.

Although the statistical properties of the ventricular response during AF have been investigated over several decades, the understanding is still rather poor. Nowadays the only commonly accepted finding seems to be the fact, that during AF the distributions $w(r)$ are right skewed; a finding that has already been published in 1967 by Goldstein *et al.* [Goldstein67].

Ventricular response: Correlation and spectral analysis

The characterisation of the ventricular rhythm is also discussed controversially. Short-term randomness [Hayano97] has been reported as well as weak predictability [Stein99] and a short-term deterministic behaviour [Gelzer00].

The power spectral density $S(f)$ of intervals r has been studied in detail by Hayano *et al.* [Hayano97]. Their study included 24 hours tachograms of 45 patients undergoing chronic AF and 30 healthy persons. It has been shown by other groups, that during sinus rhythm $S(f)$ exhibits the typical $1/f$ noise behaviour which indicates the presence of *long-range correlation* ([Saul87], [Shrout79], [Toivonen90], [Van den Berg94], [Yamamoto94]). This can be clearly seen in the left panel of fig. 3.7, where the power spectral density (PSD) of intervals r is displayed in a double-logarithmic representation for a representative healthy person. In contrast, during AF the PSD of intervals r exhibits a striking breakpoint at a critical frequency $f_{\text{crit}} \simeq 0.005\text{Hz}$. For frequencies $f < f_{\text{crit}}$, the PSD follows the same $1/f$ noise as observed for healthy persons, but shows a flat spectrum, so-called *white noise* behaviour, for frequencies higher than f_{crit} (right panel in fig. 3.7). This observation indicates that during AF ventricular intervals have timescale dependent correlation properties. The intervals are uncorrelated on short timescales but they are long-range correlated on large timescales. The presence of the breakpoint and the different regimes in the PSD is a characteristic statistical feature of the ventricular response during AF. The spectral exponents ξ, estimated in the low frequency region by fitting $S(f)$ to $f^{-\xi}$, do not significantly differ between healthy persons ($\xi = 1.36 \pm 0.06$) and AF patients ($\xi = 1.26 \pm 0.40$). Hayano *et al.* concluded that the long-range correlation observed during AF and during sinus rhythm are originated from similar dynamics of the cardiovascular regulatory system [Hayano97].

Contrary to these findings, Stein *et al.* [Stein99] reported *weak predictability* in the ventricular response during AF. This finding resulted from nonlinear investigations of ventricular responses. The main idea of the applied so-called *predictive forecasting algorithms* is to predict the future state of a system by observing sufficiently similar trajectories in a reconstructed phase space.

Given a time series $x_i = x(t_i)$, $t_i = i\Delta_t$, $i = 1, \ldots, N$ of values x_i observed at equidistant times t_i, the state of a dynamical system can be represented in a reconstructed phase space

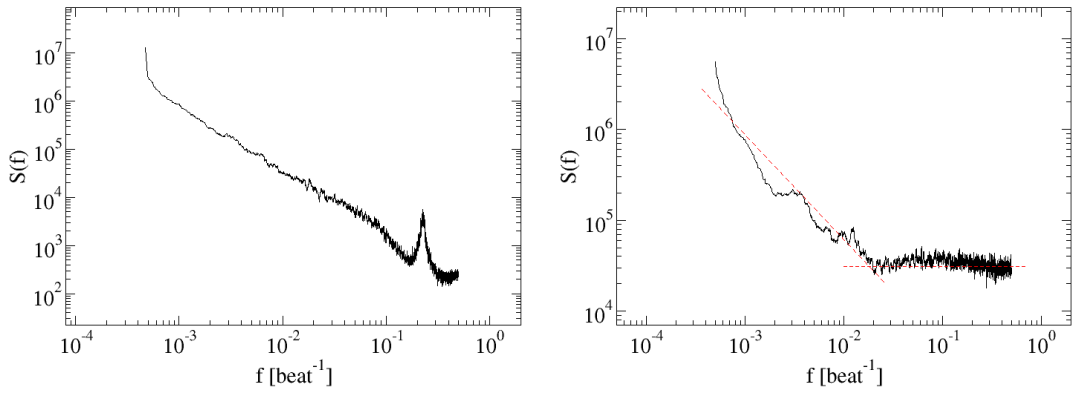

Figure 3.7: Power spectra $S(f)$ of tachograms during sinus rhythm (left panel) and during AF (right panel) in double-logarithmic representations. The data sets are taken from data pool 1 (AF patient) and from the NSRDB database in data pool 3 (healthy person). The red dashed lines mark the scaling behaviours in the different regions. For a better representation both spectra are smoothed with a moving average filter, $N = 50$.

by defining E-dimensional time delay vectors $\vec{Q}_i = (x_i, x_{i+m}, x_{i+2m}, \ldots, x_{i+(E-1)m})$, where m is the time delay and E is the embedded dimension of the reconstructed phase space.

For the special case $E = 2$ the graphical representation of the reconstructed phase space (so-called *recurrence plot*), is commonly used in medical practice for identifying the presence or absence of sinus rhythm and/or other states of health. As an example, fig. 3.8 displays the recurrence plots for (a) a healthy subject, (b) a CHF patient, (c) a PAF patient and (d) a patient undergoing chronic AF.

During sinus rhythm (a) the points in the recurrence plots are arranged close to the main diagonal indicating that successive interbeat intervals do not strongly differ. The so-called *cigar pattern* is a typical feature of sinus rhythm. This pattern is less pronounced but still partly observable in the presence of congestive heart failures (b) . Besides the main diagonal various lines appear resulting from ectopic beats. The cigar pattern is turned into a so-called *butterfly pattern* indicating the partly or complete absence of sinus rhythm. During chronic AF (d) no structure can be recognised since successive interbeat intervals are no longer correlated (see above). The structure observed in the representation for the PAF patient (c) exhibits a superposition of the patterns observed for the AF patient and the ones for the healthy subject. In contrast to the recurrence plot for the CHF patient, besides the main diagonal no clear pattern can be observed. The strength of the diagonal line depends on the length of the fibrillation episodes. The longer the episodes with sinus rhythm are the more pronounced the cigar pattern is.

The weak predictability presented by Stein *et al.* indicates, that the ventricular response during AF is not chaotic in a strict mathematical sense of a deterministic aperiodic system. They reported that the ventricular response was predictable for a significant number of patients (8 of 16 persons). It has to be mentioned that predictability was found only for nearest neighbours in the tachograms. The correlation coefficients between predicted and observed values were always smaller then 0.2. Hence, the presented results can only be

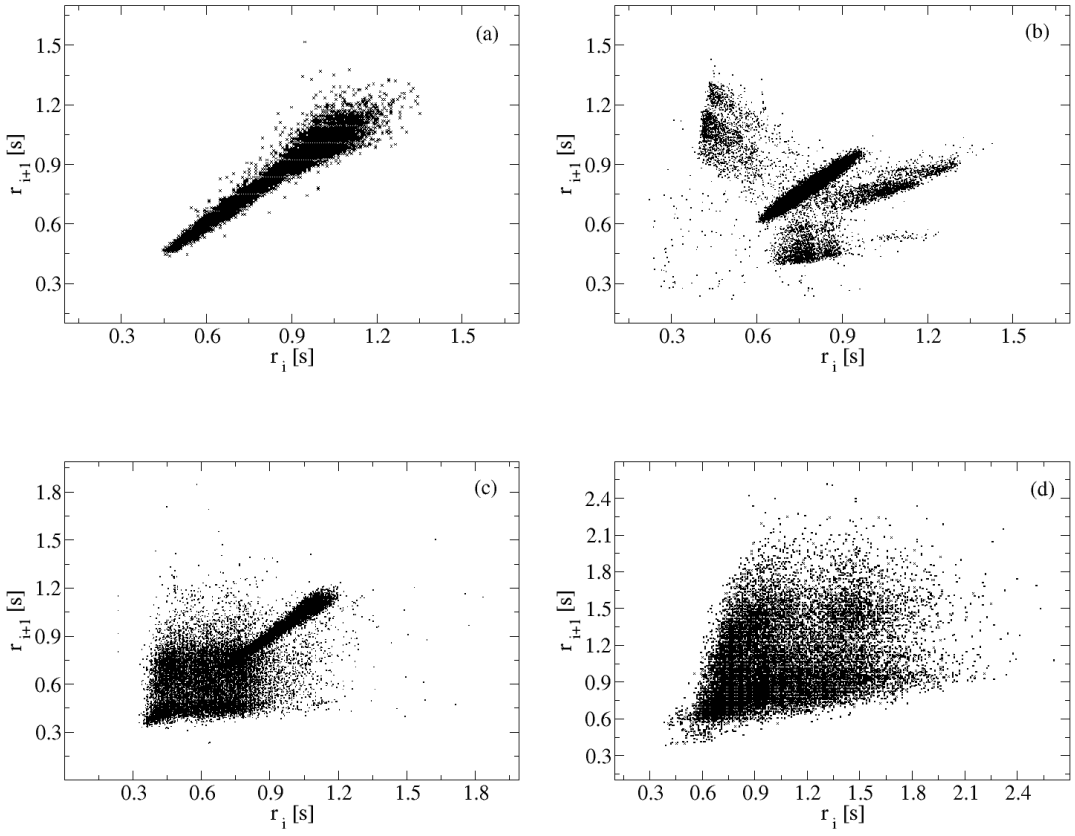

Figure 3.8: Recurrence plots of tachograms for (a) a healthy person (taken from the NSRDB database), (b) a CHF patient (taken from the CHF database), (c) a PAF patient (taken from the AFDB database) and (d) a patient undergoing chronical AF (taken from data pool 1).

.

of theoretical interest and will neither touch the findings of Hayano *et al.* nor yield any practical relevance.

4 Mathematical background

This chapter provides an overview on certain mathematical methods used in present work for time series analysis. The chapter describes the mathematical background and the practical implementations of several methods. In addition to standard measures (moments, probability distributions, etc.) we summarise more advanced techniques, which have particular impact on this thesis.

4.1 Detrended fluctuation analysis

Time series obtained from real physical or medical processes are typically non-stationary. Often they are noisy and/or exhibit several underlying trends. In such cases the estimation of the correlation properties with high accuracy becomes difficult. The *detrended fluctuation analysis* (DFA) allows to estimate the correlation properties in a time series not affected by trends or noise in the data ([Kantelhardt01], [Koscielny-Bunde98], [Peng94]). The basic idea of the analysis is to investigate the mean variance of fluctuations around local trends in the data set, which are estimated in time segments of length s. The *fluctuation function* $F(s)$ obtained by the DFA corresponds to a trend-eliminated root *mean square displacement* $\langle \Delta x^2(s) \rangle$.

The DFA was suggested and developed by Ossadnik *et al.* [Ossadnik94] and by Peng *et al.* [Peng94] for detecting long-range correlation in the base sequence of the DNA. Since that time the method has been modified and successfully applied to time series in different fields of investigations, such as heart rate variability ([Bunde00], [Kantelhardt02]) or climate data ([Eichner03], [Koscielny-Bunde96], [Vjushin04]). The DFA is a further development of other established methods such as the *Fluctuation Analysis* ([Shlesinger87], [Taqqu95], [Ben-Avraham00]) and the *Hurst-Analysis* ([Hurst51], [Mandelbrot68]).

Let be $x_i = x(t_i)$, $i = 1, 2, \ldots, N$ a single realisation of a stochastic process, consisting of N values x_i observed at the equidistant times $t_i = i\Delta_t$, $i = 1, 2, \ldots, N$. The profile $y(k)$ of x_i

$$y(k) = \sum_{i=1}^{k} x_i - \bar{x} \qquad k = 1, 2 \ldots, N$$

is divided into N_s non-overlapping segments of length s. Perhaps some elements in the end of $y(k)$ do not belong to any segment, since in general N is not a multiple of s. To avoid that those parts of the profile yields artifacts in the analysis, the splitting procedure is performed again but starting from the end of the time series. Thus, one obtains $2N_s$ segments in maximum.[1] Elements of $y(k)$ belonging to segment m are denoted as $y_{m,s}(k)$

[1] For simplicity we consider the number of segments to be N_s in the further discussion.

with $k = (m-1)s+1, \ldots, ms$ and $m = 1, 2, \ldots N_s$, respectively.

In every segment m the local trend $\hat{y}_{m,s}(k)$ is estimated by fitting a trend function to the elements $y_{m,s}(k)$. Commonly linear, quadratic, cubic or higher order polynomials are used as trend functions. According to the order of the polynomial the applied method is denoted as DFA1, DFA2, etc. The order of the polynomial determines the kind of trend that is eliminated from the time series. Partly constant trends are removed by subtracting linear polynomials, while local linear trends are removed by subtracting quadratic polynomials.

Next, the *mean squared fluctuation* $F_m^2(s)$ around the local trend is calculated for each segment m by

$$F_m^2(s) = \frac{1}{s} \sum_{k=(m-1)s+1}^{ms} \left[y_{m,s}(k) - \hat{y}_{m,s}(k) \right]^2 .$$

Finally, the *fluctuation function* $F(s)$ is obtained by averaging $F_m^2(s)$ over all segments m and by taking the square root.

$$F(s) = \left[\frac{1}{N_s} \sum_{m=1}^{N_s} F_m^2(s) \right]^{1/2}$$

A graphical representation of the different steps of the DFA is shown in the left panel of fig. 4.1.

The fluctuation function $F(s)$ describes the mean fluctuations in a signal around local trends as a function of the segment length s. The scaling behaviour of $F(s)$ with scale s describes the correlation properties in the analysed time series. For uncorrelated data sets the fluctuation function $F(s)$ scales like $F(s) \sim s^{0.5}$. In the presence of long-range correlation or anticorrelation, the scaling behaviour of $F(s)$ corresponds to the scaling behaviour of the mean squared displacement, $\langle \Delta x^2(s) \rangle \sim s^{2H}$. H is the so-called Hurst exponent. A detailed overview of the different scaling behaviour of $F(s)$ in the presence of different kinds of correlation is given in the next section.

4.2 Correlation properties: Theoretical approach

We consider a continuous stochastic process $X(t)$ which becomes a new process $v(t)$ after subtracting the finite mean of $X(t)$ and a proper trend elimination. Furthermore, we consider the process $v(t)$ to be stationary with correlation function $C(t) = \langle v(t)v(0) \rangle$ and with finite variance $0 < C(0) < \infty$.

First, we introduce the power spectrum $S(\omega) = S(2\pi f)$ as the Laplace transform of the correlation function.

$$S(\omega) = 4 \lim_{\epsilon \to +0} \Re \, \tilde{C}(-\mathrm{i}\omega + \epsilon) , \qquad \tilde{C}(z) = \int_0^\infty dt \, C(t) \, e^{-zt} \tag{4.1}$$

In practice the power spectrum $S_T(\omega)$ is obtained by $S_T(\omega) = 2|\hat{v}_{\mathrm{tr}}(\omega)|^2/T$, where $\hat{v}_{\mathrm{tr}}(\omega) = \int_{-\infty}^{\infty} dt \;\; v(t) e^{\mathrm{i}\omega t}$ is the Fourier Transform of the process $v_{\mathrm{tr}}(t)$ and where T is the time of observation. This is due to the fact that $v(t)$ is truncated beyond the observation time T

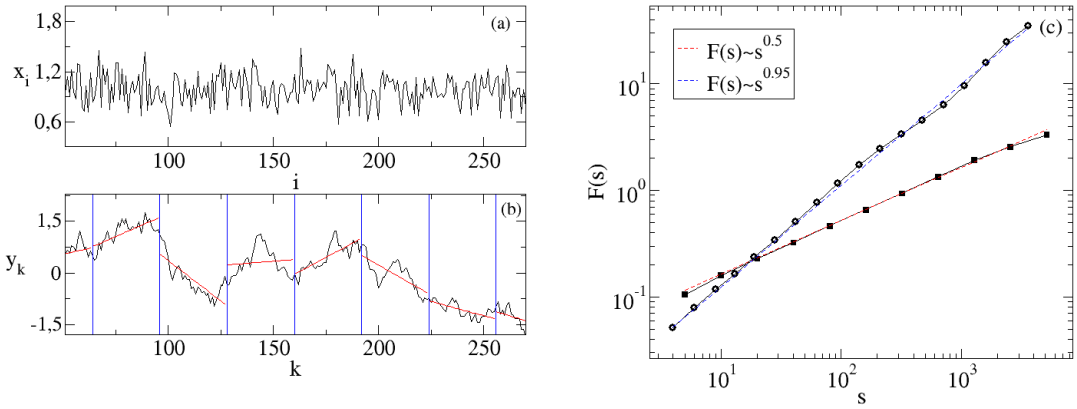

Figure 4.1: Illustration of the detrended fluctuation analysis (DFA). Panel (a) shows a segment of an uncorrelated time series x_i. Panel (b) shows the corresponding profile $y(i)$ and the estimation of local linear trends $\hat{y}_{m,s}(k)$ (red lines) estimated in non-overlapping segments of length $s = 32$. The blue lines mark the borders of the segments. Panel (c) displays two fluctuation functions $F(s)$ (full squares: uncorrelated data set, open circles: long-range correlated data set ($C(s) \sim s^{0.1}$) as functions of the segment length s in a double logarithmic representation. The dashed lines mark the theoretical curves.

($v_{\mathrm{tr}}(t) = v(t)$ for $0 \leq t \leq T$ and zero else). One can show that the process $v(t)$ is ergodic and that $\lim_{T\to\infty} S_T(\omega) = S(\omega)$, when $\int_0^\infty dt\, C(t) < \infty$. We note, that ergodicity is generally broken in the presence of long-range correlations, since $\int_0^\infty dt\, C(t)$ does not exist.

The new process $v(t)$ can be regarded as the velocity in a one-dimensional (correlated) Brownian motion of a particle. Thus the position $x(t)$ of the particle at time s is given by:

$$x(s) = X(0) + \int_0^s dt\, v(t)\,.$$

The mean square displacement $\langle \Delta x^2(s)\rangle = \langle [x(s) - x(0)]^2\rangle$ of the particle at time s, can be expressed as

$$\langle \Delta x^2(s)\rangle = \int_0^s dt_1 \int_0^s dt_2\, C(t_1 - t_2) = 2s \int_0^s dt\, C(t) - 2\int_0^s dt\, t\, C(t) \qquad (4.2)$$

since $v(t)$ is stationary.

For uncorrelated time series, the mean squared displacement increase linearly with s for long times. In that case the integral $\int_0^s dt\, C(t)$ converges to a value different from zero for $s \to \infty$. Thus the behaviour of $\langle \Delta x^2(s)\rangle$ for large times s is dominated by the first term on the right hand side of eq. (4.2) and $\langle \Delta x^2(s)\rangle$ grows linearly with s for $s \to \infty$. Correlation that lead asymptotically to such a normal diffusive behaviour are considered to be "short-ranged".

By contrast, correlation that give rise to an "anomalous" sub- or super-diffusive behaviour, where the mean square displacement grows sub- or super-linearly at large times, are clas-

sified as "long-ranged". There exist different possibilities for $\langle \Delta x^2(s) \rangle$ not to grow linearly in s for $s \to \infty$. One is, that the integral over the correlation function diverges, e.g. $C(t) \sim C_\infty t^{-\gamma_C}$ for $t \to \infty$, $0 < \gamma_C \leq 1$ and $C_\infty > 0$. In this case, both integrals in eq. (4.2) can contribute to the asymptotic behaviour of $\langle \Delta x^2(s) \rangle$. Another possibility is, that the total integral over the correlation function vanishes, $\int_0^\infty dt\, C(t) = 0$. In this case the asymptotic behaviour of $\langle \Delta x^2(s) \rangle$ is determined only by the second integral in eq. (4.2). Here, one has to distinguish two different situations: (i) $|\int_0^\infty dt\, tC(t)| < \infty$, where $\langle \Delta x^2(s) \rangle$ becomes constant for large s and (ii) where $\int_0^s dt\, t\, C(t)$ diverges for $s \to \infty$. In the latter case, one obtains a sub-diffusive behaviour due to long-range anticorrelation, e.g. when $C(t) \sim -C_\infty t^{-\gamma_C}$ for $t \to \infty$, $1 < \gamma_C < 2$ and $C_\infty > 0$.

In the following we study situations in which the autocorrelation functions $C(s)$ decay as power laws and distinguish the following cases:

(i) Long-range correlation

$$C(t) \sim C_\infty\, t^{-\gamma_C}\,,\ t \to \infty\,; \quad 0 < \gamma_C < 1\,,\ C_\infty > 0$$

(ii) Long-range correlation

$$C(t) \sim C_\infty\, t^{-1}\,,\ t \to \infty\,; \quad \gamma_C = 1\,, \quad C_\infty > 0$$

(iii) Long-range anticorrelation

$$C(t) \sim -C_\infty\, t^{-\gamma_C}\,,\ t \to \infty\,; \quad 1 < \gamma_C < 2\,,\ C_\infty > 0\,,\ S(0) = 4 \int_0^\infty dt\, C(t) = 0$$

In these cases, the exponents characterising the scaling of $\langle \Delta x^2(s) \rangle$ with s are readily derived from eq. (4.2). For $s \to \infty$ eq. (4.2) yields:

$$\langle \Delta x^2(s) \rangle \sim \begin{cases} \dfrac{2\,C_\infty}{(1-\gamma_C)(2-\gamma_C)}\, s^{2-\gamma_C} & \text{case } \textit{(i)} \\ 2\,C_\infty\, s\, \ln s & \text{case } \textit{(ii)} \\ \dfrac{2\,C_\infty}{(\gamma_C - 1)(2-\gamma_C)}\, s^{2-\gamma_C} & \text{case } \textit{(iii)} \end{cases} \tag{4.3}$$

Furthermore for $\omega \to 0$ we obtain from eq. (4.1)

$$S(\omega) \sim \begin{cases} 4C_\infty\, \Gamma(1-\gamma_C)\, \sin\left(\dfrac{\pi}{2}\gamma_C\right) \omega^{-(1-\gamma_C)} & \text{case } \textit{(i)} \\ -4C_\infty\, \ln \omega & \text{case } \textit{(ii)} \\ -4C_\infty\, \Gamma(1-\gamma_C)\, \sin\left(\dfrac{\pi}{2}\gamma_C\right) \omega^{\gamma_C - 1} & \text{case } \textit{(iii)} \end{cases} \tag{4.4}$$

by employing Abelian theorems.

Except of case (ii), both the mean squared displacement and the power spectrum exhibit a power law behaviour. The scaling of the power spectrum with the frequency, $S(\omega) \sim \omega^\xi$, is characterised by the spectral exponent ξ and the scaling of the mean squared displacement with the time s, $\langle \Delta x^2(s) \rangle \sim s^{2H}$, is characterised by the Hurst exponent H. In accordance to

eqs. (4.3) and (4.4) these exponents are related to each other by:

$$\gamma_C = 2H - 2 = \xi - 1\,. \tag{4.5}$$

We note, that in the case of anticorrelation the condition $S(0) = 4\int_0^\infty dt\, C(t) = 0$ is crucial to obtain a sub-diffusive scaling behaviour of $\langle \Delta x^2(s) \rangle$ asymptotically. In practice one should check whether this condition is really fulfilled by the analysed data set. Otherwise a finite $S(0) > 0$ appears as an additional contribution in the low-frequency behaviour of the power spectrum. The scaling behaviour of $C(t)$ is then still valid, but the behaviour of $\langle \Delta x^2(s) \rangle$ is altered.

Furthermore, from eq. (4.2) it follows, that the sub-diffusive behaviour of the mean squared displacement according to eq. (4.3) occurs only up to timescales $s \ll s_\times$ with

$$s_\times = \left[\frac{4C_\infty}{(\gamma_C - 1)(2 - \gamma_C) S(0)} \right]^{1/(\gamma_C - 1)}, \tag{4.6}$$

while a normal diffusive behaviour is obtained for timescales $s \gg s_\times$.

4.3 Lomb-periodograms

For unevenly sampled data sets consisting of values $z_i = z(t_i)$, observed at the non-equidistant times t_i, the estimation of the correlation or the spectral properties is a difficult task. Commonly this problem is solved by transferring the unevenly sampled time series into an evenly sampled one, which is done either by interpolating data points or by inserting zeros. Such approaches yield acceptable results only if the number of missing data is small in comparison to the length of the time series and if the episodes of missing values are not too long.

An alternative approach is the autoregressive moving average method (ARMA) estimates the power spectrum (PSD) directly from the unevenly sampled data set. In this approach the signal is considered to be generated by an autoregressive process of a given order. As such the PSD of the time series can be calculated analytically after fitting the parameters of the process to the time series. We note, that this method is not suitable for tachograms since it introduces large dispersion between the real and the estimated PSD [Laguna98].

This problem can be avoided when estimating the PSD by so-called *Lomb-periodograms* $L(\omega)$ [Laguna98]. This technique was originally proposed by N. R. Lomb [Lomb76] who's work based on the previous mathematical studies of Barning [Barning63] and Vanicek [Vanicek71] and was additionally elaborated by Scargle [Scargle82].

The main idea of the approach is to estimate the harmonic components of an unevenly sampled data set $z_i = z(t_i)\,,\ i = 1, 2, ..., N$ by least square fitting the data to

$$z(t_i) = A\cos(\omega t_i) + B\sin(\omega t_i)$$

for a given frequency ω. The Lomb-periodogram $L(\omega)$ of a time series z_i is defined as:

$$L(\omega) = \frac{1}{2\sigma_{z_i}^2} \left[\frac{\left[\sum_{i=0}^{N}(z_i - \bar{z}_i)\cos[\omega(z_i - z^*)]\right]^2}{\sum_{i=0}^{N}\cos[\omega(z_i - z^*)]} + \frac{\left[\sum_{i=0}^{N}(z_i - \bar{z}_i)\sin[\omega(z_i - z^*)]\right]^2}{\sum_{i=0}^{N}\sin[\omega(z_i - z^*)]} \right]$$

where $\omega > 0$ and where $\bar{z}_i$ and $\sigma_{z_i}^2$ are the mean and the variance of z_i respectively. The parameter z^* is given by:

$$z^* = \frac{\sum_{i=0}^{N}\sin(2\omega t_i)}{\sum_{i=0}^{N}\cos(2\omega t_i)}$$

and is a kind of an offset providing that $L(\omega)$ is completely independent from a time shift of all t_i by a constant time. In contrast to the discrete Fourier Transformation, Lomb-periodograms allow to estimate the PSD with an arbitrary spectral resolution. Furthermore the approach allows to detect spectral components for frequencies higher than the Nyquist frequency, which for unevenly sampled data sets is defined as the inverse of the mean time interval between consecutive elements z_i.

A detailed discussion of the application of Lomb-periodograms to time series of interbeat intervals r was given by Castiglioni *et al.* [Castiglioni96] and by Laguna *et al.* [Laguna98]. It was shown that the estimation of the PSD by Lomb-periodograms is more suitable than other suggested methods.

The agreement between the original PSD and the estimated one depends on the distribution of the unevenly sampled intervals in the signal. To demonstrate this dependency the right panel in fig. 4.2 displays Lomb-periodograms of time series z_i with same correlation properties but different sampling properties.

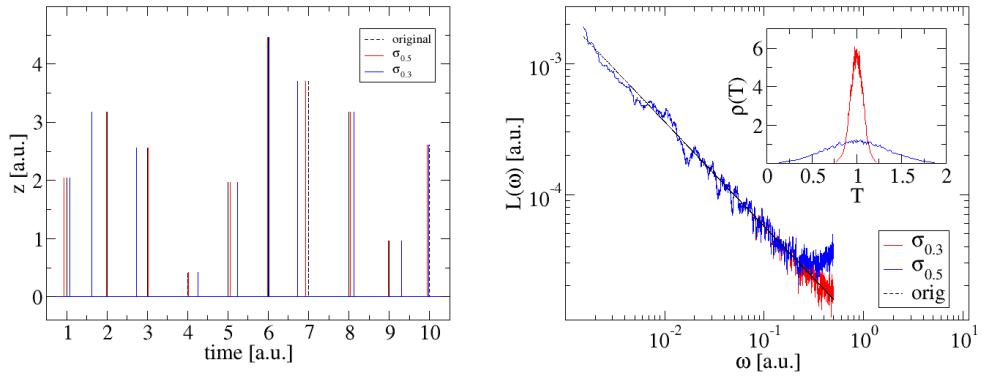

Figure 4.2: Left panel: Segments of a long-range correlated, evenly sampled time series (dashed black line) and two unevenly sampled time series (red and blue curves).Right panel: Double-logarithmic representation of Lomb-periodograms $L(\omega)$. The dashed black line represents the spectrum of the original long-range correlated and evenly sampled time series, while the red and the blue lines represent the Lomb-periodograms of the unevenly sampled time series displayed in the left panel. The inset displays the distributions of the sampling intervals.

The unevenly sampled signals are generated by adding Gaussian distributed white noise

η to the absolute times t_i of an evenly sampled and long-range correlated time series x_i. The different sampling properties of the signal z_i are realised by changing the standard deviation σ_η of the white noise. Segments of the generated signals are shown in the left panel in fig. 4.2. As it is clear to see, the larger σ_η is the stronger the fluctuations in the unevenly sampled time intervals are. The Lomb-periodograms $L(\omega)$ and the distributions of the unevenly sampled time intervals of the signals z_i are shown in the right panel in fig. 4.2. For a better visual impression the Lomb-periodograms are smoothed with a moving average filter, $N = 100$. The PSD of the original and evenly sampled time series is marked by the dashed black line. The agreement between the Lomb-periodograms and the original PSD is getting better if the fluctuations of the sampling intervals are getting smaller. While $L(\omega)$ closely follows the original spectrum for $\sigma_\eta = 0.3$, it differs from the original PSD in the region of high frequencies for $\sigma_\eta = 0.5$.

Castiglioni *et al.* [Castiglioni96] investigated Lomb-periodograms in presence of a $1/f$ noise behaviour in the PSD and showed that the periodograms are in a good agreement with the original spectrum. In addition, a detailed discussion of the application of Lomb-periodograms, ARMA estimates and other techniques for the estimation of the PSD of tachograms is given in [Clifford02].

5 Databases

5.1 Data pool 1: Long time tachograms

A data-pool of long time tachograms of 130 patients undergoing chronic atrial fibrillation was provided by the Core Laboratory at the Nagoya City, University Graduate School of Medical Sciences in a collaboration with our group.

The data pool contains tachograms of 91 men of age 43-89 and 39 women of age 37-84. The tachograms encompass of about 23.64 hours on average (minimal recording time: 14.7 hours, maximal recording time: 25.3 hours). In the present work, data sets that are taken from this data pool are simply labelled as *AF patients*.

Hayano *et al.* [Hayano97] and Heinrichs *et al.* [Heinrichs04] studied in detail the spectral properties of these tachograms. The recording procedure and the preprocessing of the data sets are also discussed therein.

5.2 Data pool 2: Simultaneous surface and atrial ECG-recordings

A data pool of simultaneous surface and intra-atrial ECG-recordings was provided by Prof. Dr. med. J. C. Geller and Dr. med. B. Hügl from Zentralklinik Bad Berka in a collaboration with our group.

The data pool contains 6 patients undergoing different kinds of AF. In contrast to data pool 1, the gender and the age of these patients are unknown. The length of the ECG-recordings differ between 10 and 60 minutes. For each patient 20 ECG-signals have been recorded with a sampling rate of 1kHz. For all patients the main statistical properties of the atrial and the ventricular tachograms are listed in table 5.1. In the present work data sets of this data pool are labelled according to the day on which the signals have been recorded. Thus, we denote signals recorded at 16.01.2006 as *patient_2006_01_16*.

The ventricular excitations in the surface ECG‘s are detected with a *R peak detector*, which is a modified version of the one suggested by Engelse and Zeelenberg [Engelse79]. The algorithm used for the detection of the R peaks follows the one suggested by W. Piechulla ([Piechulla00], [Pan85]).[1] Further information about the detection of peaks and patterns

[1] The implemented modifications do not touch the basic detection algorithm suggested by Engelse and Zelenberg. In fact, the modifications only provide subsequently analysis of the detected peaks. Thus, not all peaks that are detected by the algorithm are accepted as ventricular excitations. Artefacts, such as premature beats are excluded and not labelled as ventricular excitations.

main statistical properties of atrial signals				
patient	$\bar{\tau}$ [s]	σ_τ [s]	SNR_τ	N_τ
2006_01_03	0.15366	0.0229	6.7130	3878
2006_01_16	0.15280	0.0369	4.1340	7720
2006_04_05	0.17294	0.0638	2.7112	6746
2006_11_20	0.23226	0.0078	29.9162	2767
2007_01_31	0.17498	0.0444	3.9403	7135
2007_02_01	0.15177	0.0248	6.1150	7615
main statistical properties of ventricular signals				
patient	$\bar{r}$ [s]	σ_r [s]	SNR_r	N_r
2006_01_03	0.44853	0.0487	9.213	1331
2006_01_16	0.45879	0.0917	5.004	2553
2006_04_05	0.64184	0.1595	4.024	1806
2006_11_20	0.94083	0.2053	4.583	668
2007_01_31	0.75893	0.1398	5.429	1644
2007_02_01	0.54504	0.1200	4.542	2106

Table 5.1: Statistical properties of atrial and ventricular tachograms in data pool 2. The signals (patients) are labelled according to the day of the ECG-recording. The following parameters are listed: mean atrial/ventricular interval ($\bar{\tau}$, $\bar{r}$), standard deviation of atrial/ventricular intervals (σ_τ, σ_r), signal to noise ratio of atrial/ventricular intervals (SNR_τ, SNR_r), number of atrial/ventricular intervals (N_τ, N_r).

in a surface ECG is given in [Clifford02]. The detection algorithm used in the present work yields good results independent of the chosen lead and unaffected by changes in the baseline or in the signal to noise ratio of the ECG-recording (see fig. 5.1).

The detection of atrial excitations is a more difficult task since the corresponding peaks are not clearly observable in the ECG-recordings. In the present work the peaks are detected with respect to their amplitudes. Atrial excitations are defined as those peaks in the signal, which exceed a threshold V_th given by:

$$V_\mathrm{th} = \frac{1}{2}\left(\bar{V} + V_\mathrm{m}\right)$$

where $\bar{V}$ denotes the mean and V_m the median of the absolute amplitudes V of the signal. This approach can be successfully applied since atrial ECG-recordings do not exhibit strong baseline fluctuations. The analysed lead is chosen for every patient separately, since we find pronounced inter-individual differences in the signal quality of the different leads. On the other hand we find that the rates of fibrillation estimated for different leads do not significantly differ. Besides the absolute amplitudes we take into account the intervals between the onset and the offset of the atrial excitations and only accept those whose duration is larger than 20ms. We find that this method yields appropriate results which can not be improved by various preprocessing methods such as a prefiltering of the signal.

As an example, in the left panel of fig. 5.2, a segment of an atrial ECG-recording and the individual threshold V_th (green dashed lines) is shown. First we detect those parts of the

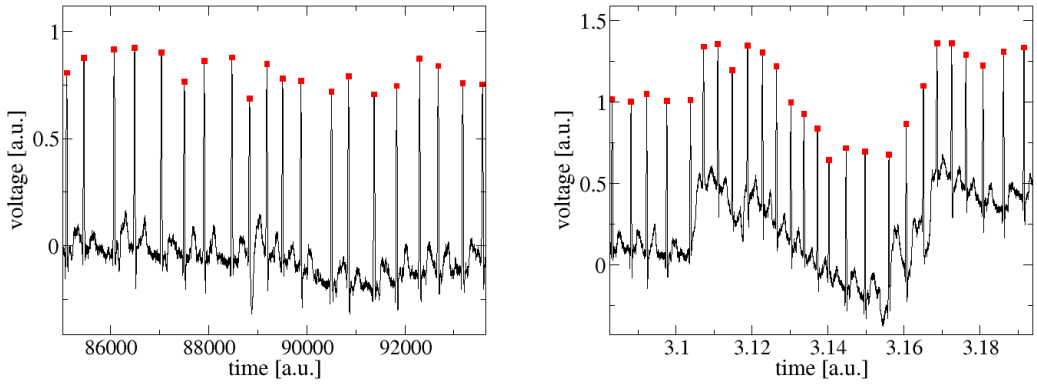

Figure 5.1: Segments of surface ECG-recordings and detected R peaks (red filled squares). The algorithm used for the detection of the R peaks follows the one suggested by W. Piechulla [Piechulla00].

signal that exceed or fall below V_{th}. This allows us to identify the beginning and the end of the atrial excitations (red curve). Afterwards we identify an atrial peak as that point of an excitation that exhibits the highest absolute amplitude (filled blue squares).

Although the detected peaks are controlled manually, the detection can be mistaken sometimes, which is due to the partly high signal to noise ratio in the ECG-signals. To avoid that such mistakes will affect the further analysis, we do not define the AFR by the inverse of the mean atrial interbeat interval but by the inverse of that interval τ that yields the maximum in the distribution $\rho(\tau)$. We find that different definitions of the threshold Vt_{th} yield different sequences of atrial intervals τ, but they do not affect the fibrillation rate estimated according to this definition.

5.3 Data pool 3: PhysioNet

The National Center for Research Resources of the National Institutes of Health provides comprehensive resources for the study of complex physiologic signals in the Internet (`http://www.physionet.org`). A detailed overview about the PhysioNet is given in "PhysioBank, PhysioToolkit, and PhysioNet: Components of a New Research Resource for Complex Physiologic Signals" [Goldberger00]. The resource provides an archive of digital recordings of various physiological signals (ECG-recordings, tachograms, etc) for healthy and diseased persons. The recordings are well characterised and partly pre-analysed. Usually, for each of the recordings three binary files can be downloaded: (i) the original recording, (ii) a *header file* that contains information about the signal, such as sampling rate, age of the patient, etc. and (iii) an *annotation file*, which contains the results of the pre-analysis.

The signals from the following databases are used in the present study:

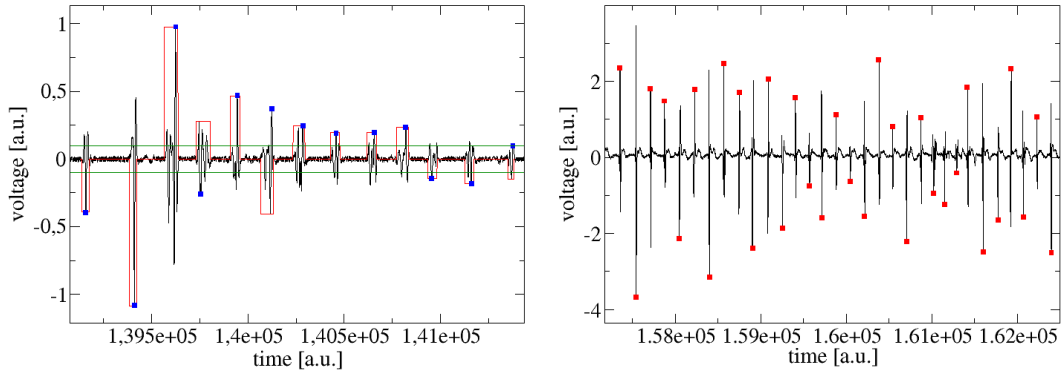

Figure 5.2: Left panel: Detection of atrial excitations. The green dashed lines mark the individual threshold V_{th}. Parts of the ECG-signal that exceed this threshold are identified as atrial excitations (red curve). Excitations with a duration less than 20ms are rejected. Atrial peaks are identified as those points that exhibit the highest absolute amplitude during an atrial excitation (filled blue squares). Right panel: Segment of an atrial ECG-signal and detected atrial peaks.

- **NSR2DB - Normal Sinus Rhythm RR Interval Database**

  The *Normal Sinus Rhythm RR Interval Database* (NSR2DB) provides long time tachograms of 30 men, aged 28.5 to 76 and 24 women, aged 58 to 73. The tachograms encompass of about 23.6 hours on average (minimal recording time: 21.3 hours, maximal recording time: 24.2 hours). The signals result from an automatic analysis of long time ECG-recordings with manual reviews and corrections. The original ECG-recordings (sampling rate: 128 Hz) are not available. Subjects that belong to this database are furthermore denoted as *healthy subjects*.

  The signals in this database have been studied by various groups before ([Stein99], [Bigger95], [Goldsmith92], [Mietus02], [Bartsch05], [Hennig06c]).

- **NSRDB - Normal Sinus Rhythm Database**

  The *Normal Sinus Rhythm Database* (NSRDB) contains long-term ECG-recordings of 18 healthy persons (5 men in age 26 to 45 years and 13 women in age 20 to 50 years). The ECG-signals (sampling rate: 128 Hz) have been recorded at the Boston Beth Israel Hospital (now the Beth Israel Deaconess Medical Center). The recordings encompass of about 21.4 hours on average (minimal recording time: 19.2 hours, maximal recording time 24.2 hours). The annotation files of the ECG-recordings provide detailed information about the detection of several peaks and artefacts. Based on the annotations for every subject we checked the number of heart beat intervals that contain artefacts. In case of four of the patients, more than 2% of the heart beats are affected by artefacts or changes in the signal quality (*16272.dat*, *16773.dat*, *19088.dat* and *19093.dat*). These patients are excluded from all studies in which the correlation properties of the ventricular interbeat intervals are investigated. Patients that belong to this database are also denoted as *healthy subjects*.

- **CHFDB - Congestive Heart Failure Database**

  The *Congestive Heart Failure Database* (CHFDB) includes long time ECG-recordings from 9 patients (7 men, aged between 22 and 71 years and 2 women, aged between 54 and 63 years) undergoing several congestive heart failures.[2] The ECG-recordings encompass of about 19.9 hours on average (minimal recording time: 19.7 hours, maximal recording time: 20 hours). The ECG-recordings are sampled with 250 Hz and have been recorded at the Boston Beth Israel Hospital. The database provides a detailed annotation of all signals, including the detection of artefacts and changes in the signal quality. In the present work we denote patients that belong to this database as *CHF patients*.

  In the past, various studies have been made based on these ECG-recordings ([Poon97], [Ivanov99], [Mietus02], [Bartsch05]).

- **AFDB - Atrial Fibrillation Database**

  The *Atrial Fibrillation Database* (AFDB) contains long time ECG-recordings from 22 subjects undergoing paroxysmal AF.[3] The ECG-recordings encompass of about 9.9 hours on average (minimal recording time: 9.2 hours, maximal recording time: 10 hours). We note, that the duration and the fraction of the AF episodes strongly differ, between 1% and $\sim$ 100% of AF during the recording, for the patients in the database. The ECG-recordings have been made at Boston's Beth Israel Hospital and were sampled with 250 Hz. The database provides a detailed, manually prepared annotation for all signals. In contrast to the other databases, the annotation files of the AFDB database do not provide any further information about artefacts or changes in the signal quality. In the present study, signals and patients in the AFDB database are labelled according to the notation in the PhysioBank. Thus, the signal that is stored in the file *04936.dat* is named as *patient 04936*. Generally the patients in the AFDB database are named as *PAF patients*.

The provided annotation files contain detailed information about the recorded ECG-signals. For example, this information include the positions of R peaks, the beginning and the end of the QRS complexes, but also the detection of artefacts such as extra-systoles. In order to remove those artefacts from our analysis we accept only those interbeat intervals r that are (i) between two consecutive R peaks labelled as *normal* in the annotation files and that (ii) do not contain any abnormal beat. On average we remove 1.6% (NSR2DB), 7.3% (NSRDB), 5% (CHFDB) and less than 0.5% (AFDB) of all interbeat intervals r from the different data sets.

[2] We note, that originally the CHFDB contains 12 and not 9 patients. In the annotation files it is noted, that three patients are undergoing atrial fibrillation (chf02.dat, chf04.dat, chf06.dat). These patients are excluded from the group of CHF patients.

[3] We note, that originally the AFDB contains 25 and not 22 patients. The datasets *00735.dat* and *03665.dat* are rejected, since the original ECG-recordings are not available. Furthermore we reject the set *08455.dat*, since the recorded ECG-signals contains episodes of atrial flutter.

6 Time series analysis of ECG-recordings during atrial fibrillation: New approaches and results

This work discusses the possibility of detecting the fibrillation rate from the statistical properties of the ventricular response during AF. The first and necessary step is to investigate to what extent the presence of the disease can be precisely detected. Hence the present chapter is devoted to a systematic study of the statistical properties of ECG-signals and of ventricular responses during different states of health. We focus on the detection of AF in general and on the investigation of possible relations between different revealed characteristic statistical properties of tachograms during AF in particular. In order to perform a systematical analysis, we distinguish two different kinds of information contained in an ECG-recording. One is the morphology of the signal, which carries information about the electrophysiological states of the heart during a single cardiac cycle. The other one is the duration of single heart beats, which carry information about the rhythm of the heart.

First we concentrate only on the morphology of the ECG and investigate the possibility of an automatic detection of AF by simple measurements of the signal shape. In accordance to investigations of the heart rate variability, we neglect any information about the duration of the heart beats and study the manner the ECG-signal changes between consecutive heart beats.

Secondly, we combine the information about the signal shape during a heart beat and its duration while analysing *non-normalised morphograms*. This approach allows us to analyse the entire information carried in an ECG-recording in one single study.

Thirdly, we neglect any information about the ECG morphology and investigate the statistical properties of ventricular responses. This study will lay open a new characteristic statistical property of intervals r during AF that has not been investigated so far. We will show that the occurrence of this feature is related to the observation of the other previously revealed characteristic statistical properties.

6.1 Analysis of the morphology of ECG-recordings

6.1.1 Time series analysis of normalised morphograms

In the past, the morphology of the ECG-signals has been investigated by various studies in order to provide an automatic detection of the presence or absence of different heart diseases. The common approach pursued by these studies is comparable to the one pursued for the analysis of the heart rate variability. First of all one detects different peaks, waves and segments in the ECG-signal. Afterwards new time series are generated containing specific information of certain patterns, such as the duration of the QRS complex or the length of the ST-segment. These time series are the basis for further investigations.

The application of such analysis in medical practise is rather difficult, since it has two major disadvantages. First, the ECG-signal has to be replaced by a large number of different signals in order to analyse all possible patterns in the signal. The results are not simply single values but various curves and measurements which only in combination describe the patients health. Furthermore, the results depend on the exact labelling of the various waves and peaks in the ECG-signal. This is a difficult task, especially for signals with high noise amplitudes.

We follow another approach and ask if the information contained in the ECG can be analysed without a complicated pattern recognition. We suggest the generation of new, shape-sensitive signals containing information only about the shape of the ECG-signal during cardiac cycles but omitting any information of their duration. These signals are complementary to tachograms, which only contain information about the duration of the heart beats but no information about the ECG-signal itself.

In order to characterise only the morphology of the ECG-signal we perform the following steps:

1. Detection of the ECG-signal of a single heart beat

   First we detect the R peaks in the surface ECG (see panel (a) in fig. 6.1). Then we combine the voltage deflections $\phi_i^{(n)}$ in each heart beat n, into a vector $\vec{\phi}_n = (\phi_1^{(n)}, \phi_2^{(n)}, \ldots, \phi_{i_n}^{(n)})$. The $\phi_i^{(n)}$ are defined as the ECG-signal between the nth R peak and the following one. The number of components i_n is given by $i_n = r_n\, f_{\text{samp}}$, where r_n is the duration of the heart beat n and f_{samp} is the sampling rate of the ECG-recording.

2. Voltage normalisation of the ECG-signal

   The typical values of the components of $\vec{\phi}_n$ will vary from patient to patient and, for a given patient, with the beat number n. This is due to different amplification levels during ECG-recordings and due to baseline changes in the signal. In order to guarantee an analysis of the signal shape, which is independent from those variations, we normalise the signal $\phi_i^{(n)}$ by:

   $$0 \leq \tilde{\phi}_i^{(n)} = \frac{\phi_i^{(n)} - \phi_{\text{min}}^{(n)}}{\phi_{\text{max}}^{(n)} - \phi_{\text{min}}^{(n)}} \leq 1\,. \tag{6.1}$$

   where $\phi_{\text{max}}^{(n)} = \max_i\{\phi_i^{(n)}\}$ is the maximal and $\phi_{\text{min}}^{(n)} = \min_i\{\phi_i^{(n)}\}$ is the minimal compo-

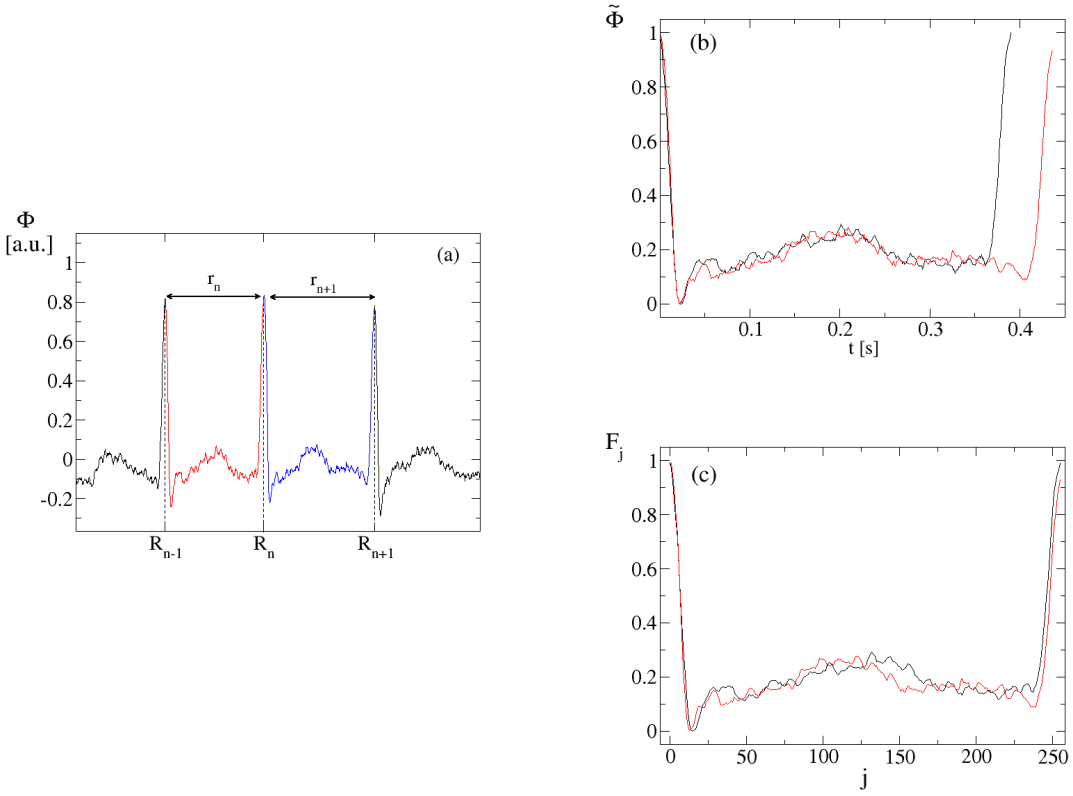

Figure 6.1: Schematic representation of the generation of ECG-morphology sensitive signals. ECG-signals of two interbeat intervals (a) as sampled, (b) after voltage rescaling, and (c) after both voltage and time normalisation, yielding the components F_j of the form vector $\vec{F}_n$.

nent in each heart beat n respectively. As an example, panel (b) in fig. 6.1 displays two rescaled ECG-signals which are obtained after applying eq. (6.1) to the ECG segments shown in panel (a) of fig. 6.1.

3. Time normalisation of the ECG-signal

   To characterise the morphology of the ECG-signals during single heart beats independently from their duration, we normalise the segments in time. Therefore, we decompose each heart beat interval into $N = 256$ equidistant time points. The associated components $F_j^{(n)}$, $j = 1, \ldots N$, of the *form vector* $\vec{F}_n$ are calculated by a linear interpolation of the components $\tilde{\phi}_i^{(n)}$. Rescaled and time normalised signals following from the ECG segments of two successive interbeat intervals are shown in panel (c) of fig. 6.1.

The so-defined form vectors $\vec{F}_n$ carry information on the morphology of each heart beat in the signal within a resolution set by the sampling rate of the recording and by the number N chosen for the time normalisation. The voltage and time normalisation enable us, not only to study changes in the ECG for a single patient, but also to compare the heart beat signals and their changes for different patients undergoing several diseases.

Each heart beat signal is now represented by the form vector $\vec{F}_n$ and thus by a characteristic

point in an N dimensional space. In order to combine the information stored in the form vectors into a simple scalar we generate *normalised morphograms* M_n

$$M_n = \frac{1}{N} \sum_{i=1}^{N} \left(F_i^{(n)} \right)^2 \tag{6.2}$$

which correspond to the total power of the Fourier Transform of the normalised ECG-signal for each heart beat [Bartsch05].

Temporal changes in the morphology of the ECG-signal correspond to a motion of the characteristic point to another position in the N dimensional space. While the actual position of a characteristic point describes the actual heart beat signal, the motion of the point reflects the manner in which the heart beat signal changes in time. To describe the changes in the signal shape between consecutive heart beats we generate *delta morphograms* dM_n.

$$dM_n = \frac{1}{N} \sum_{i=1}^{N} \left(F_i^{(n)} - F_i^{(n-1)} \right)^2 \tag{6.3}$$

Figure 6.2 shows typical sections of normalised morphograms (left panels) and of delta-morphograms (right panels) generated for ECG-recordings during different states of health.[1] In order to remove artefacts and abnormal heart beats from the ECG we take into account only segments between consecutive beats which are classified as "normal" in the corresponding annotation-files. Segments between pairs of normal beats surrounding an ectopic beat are also rejected.

As first step of investigation we analyse standard scaling plots of the probability densities of the M_n and dM_n (or their successive increments $M_{n+1} - M_n, \ldots$ and $dM_{n+1} - dM_n, \ldots$) with respect to the mean and standard deviation but find no characteristic features in the shape of these densities that allow to distinguish between the different states of health. We note that this finding is analogous to the one previously reported for tachograms [Peng94].

Next we perform a DFA in order to study the correlation properties of the normalised morphograms and of the delta morphograms. This yields Hurst exponents very close to one and in a few cases even slightly larger due to statistical fluctuations. Hence we decide to choose the successive increments $M_{n+1} - M_n$ and $dM_{n+1} - dM_n$ to represent the noise in the time series which is analogous to [Peng91]. The fluctuation functions $F(s)$ for the different groups of subjects are shown in fig. 6.3. The left plots refer to the normalised morphograms and the right ones refer to the delta morphograms.

As can be seen from the figure, the normalised morphograms of the healthy subjects exhibit smaller fluctuations on average than the ones for the PAF patients and for the CHF patients. On all timescales the separation of the healthy persons from the diseased ones is very pronounced. For every scale s the level of separation is quantified by the ROC value shown in the upper parts of the plots [Zweig93]. In the present work, the ROC value of a given scale s is the probability that an arbitrary member of one group of subjects has a smaller $F(s)$ value than an arbitrary member of the other group. Thus, the larger the ROC value is the

[1] The ECG-signal for the healthy subject is taken from the NSRDB, the one for the CHF patient from the CHFDB and the one for the PAF patient from the AFDB. The left panels in fig. 6.2 display the segments of morphograms after subtracting the mean $\bar{M}_n$.

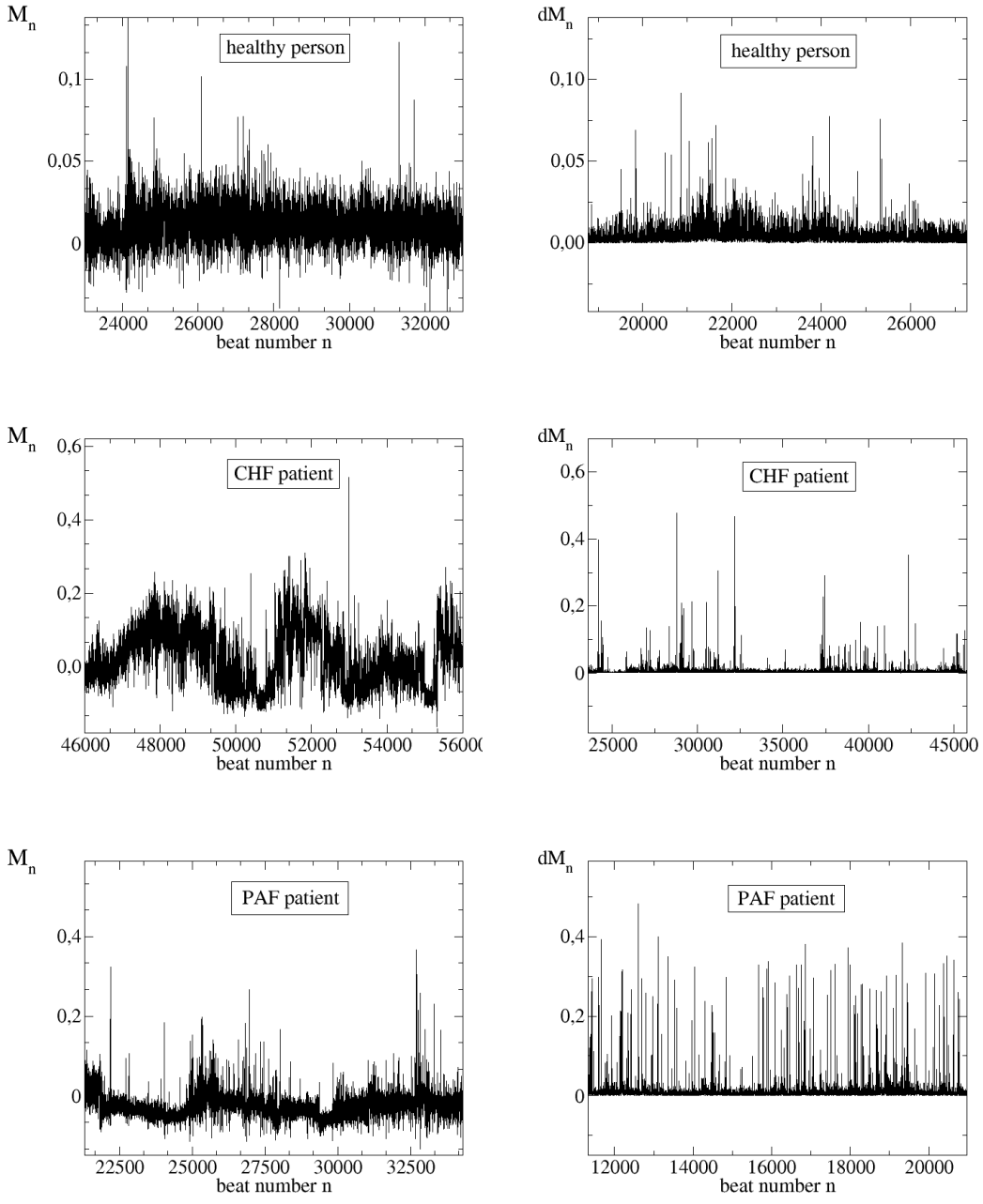

Figure 6.2: Sections of normalised morphograms M_n (left panels) and of delta morphograms dM_n (right panels) for representative healthy and diseased subjects. The left panels show the normalised morphograms after subtracting the global mean $\bar{M}_n$.

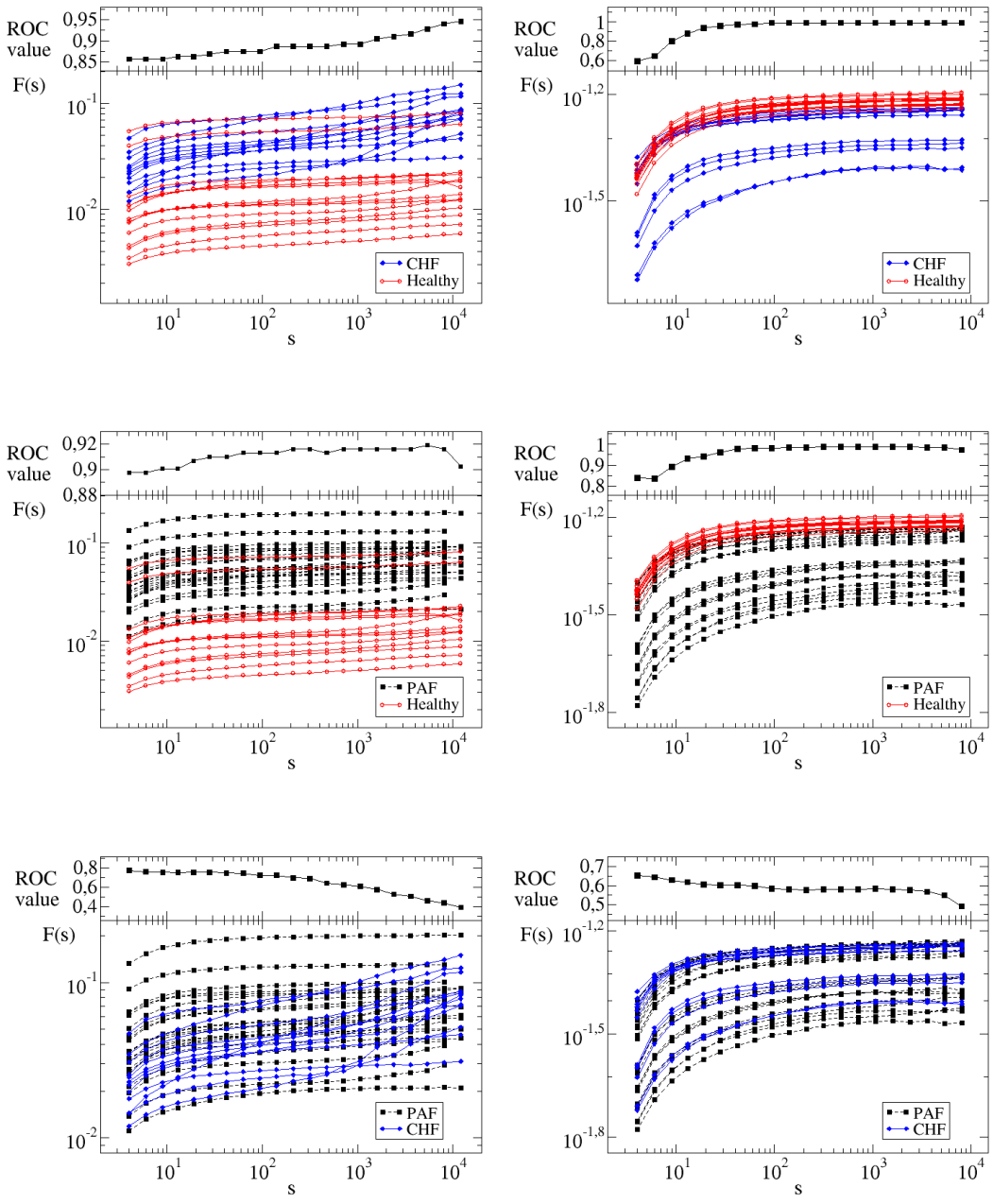

Figure 6.3: Double-logarithmic plots of fluctuation functions $F(s)$ of normalised morphograms M_n (left panels) and of delta morphograms dM_n (right panels) for different groups of patients. The corresponding Hurst exponents H are listed in table 6.1.

	H for normalised morphograms	H for delta morphograms
healthy subjects	0.053 ± 0.045	0.0075 ± 0.0008
CHF patients	0.142 ± 0.076	0.0094 ± 0.0029
PAF patients	0.034 ± 0.034	0.0137 ± 0.0065

Table 6.1: Averaged Hurst exponents H from the analysis of normalised morphograms M_n and delta morphograms dM_n. The errors refer to the standard deviation in each group. The exponents are obtained by fitting the fluctuation function $F(s)$ in the range $s = 10^2 - 10^4$ to a power law.

better the separation between the groups of subjects is. Commonly ROC values between 92% and 97% are classified as "very good" with respect to the discrimination and ROC values larger than 97% are classified as "excellent". An ROC value equal to one points out a complete separation.

The ROC values calculated for the healthy subjects and the PAF patients are nearly constant and are close or even higher than 90% on all observed timescales. In contrast to this the ROC values calculated for the healthy persons and the CHF patients show a strong dependency on the timescale s, with higher ROC values for larger s. Very good ROC values are obtained on all timescales $s \geq 5395$. In contrast, no separation is obtained between the groups of CHF patients and PAF patients.[2]

The fact that healthy persons show smaller fluctuations than the diseased ones is in contrast to the result obtained for the analogous analysis of tachograms [Bartsch05]. This points out, that in comparison with sinus rhythm the other states of health are characterised by more rigid interbeat intervals and a more irregular shape of the ECG-signal.

To quantify the correlation properties we calculate the averaged Hurst exponents H by fitting $F(s)$ in the range $s = 10^2 - 10^4$ to a power law. The Hurst exponents for the normalised morphograms are listed in table 6.1. The averaged exponents are in the range $0.034 \leq H \leq 0.142$. These values indicate the presence of long-range anticorrelation between the increments $M_{n+1} - M_n$. The Hurst exponents obtained for the CHF patients are significantly higher on average than the ones obtained for the other two groups. A complete separation between the groups fails due to the pronounced variations of the averaged Hurst exponents from patient to patient within each group.

In contrast to the normalised morphograms we find, that the delta-morphograms of the healthy persons exhibit stronger fluctuations than the ones for the other subjects. Excellent ROC values are obtained on certain timescales s, when comparing the healthy subjects with the PAF and the CHF patients. We note, that only one healthy subject fails the complete separation. This result clearly points out the strength of this analysis for detecting sinus rhythm. On the other hand, there are no significant differences when comparing the fluctuations in the dM_n for the CHF patients with the ones for the PAF patients. The fluctuation functions overlap on all timescales s and therefore do not allow to distinguish between the

[2] We note, that a complete separation between the CHF patients and the healthy subjects can be obtained when performing a different kind of data preparation [Bartsch05]. In the present work we do not apply this method, since the annotations for the PAF patients differ from the ones for the healthy subjects and for the CHF patients.

different heart diseases. The averaged Hurst exponents listed in table 6.1 are in the range $0.0075 \leq H \leq 0.0139$ and reflect the presence of long-range anticorrelation between the increments of the dM_n. The lowest Hurst exponents and also the smallest fluctuations of the exponents inside of a group are obtained for the healthy subjects. In contrast to the previous analysis, the Hurst exponents for the PAF patients are higher on average then the ones for the other groups. Again a separation between the groups fails due to the variations of the exponents inside the groups.

6.1.2 Time series analysis of non-normalised morphograms

In this section, we combine the information about the shape of the ECG during a cardiac cycle with the information about its duration. As such we generate *non-normalised morphograms* N_n in the same way as the normalised morphograms before, but without the time normalisation.

$$N_n = \sum_{i=1}^{i_n} \left(\tilde{\phi}_i^{(n)}\right)^2 \tag{6.4}$$

where $\tilde{\phi}_i^{(n)}$ are the i_n components of the voltage normalised vector $\vec{\tilde{\phi}}_n$.

According to the definition both variations of the signal shape and variations in the durations of the heart beats yield variations in the N_n values. In case of single heart beats with comparable ECG-signals, the one with the larger duration is designated to a larger N_n value, than the one with the shorter duration. Furthermore the values N_n are affected by the sampling rate of the ECG-recording. To avoid that the information about the sampling of the ECG-recording is contained in the non-normalised morphograms we perform a rescaling to a reference sampling rate, $f_{\text{ref}} = 250Hz$.

We follow the approach of our previous studies and perform a DFA analysis of the increments $N_{n+1} - N_n$ in the non-normalised morphograms. The fluctuation functions $F(s)$ obtained for the different groups of subjects are displayed in the left panels in fig. 6.4. To compare the levels of separations with the ones from the previous study, the right panels in fig. 6.4 display both the ROC values calculated in the present study (red curves) and the ones obtained for the normalised morphograms (black curves).

The plots in fig. 6.4 are in agreement with the ones displayed in the left panels of fig. 6.3. Qualitatively the fluctuation functions $F(s)$ exhibit the same scaling behaviour as the ones obtained for the normalised morphograms. Again, we find the $F(s)$ values for the healthy subjects to be smaller than the ones for the CHF and the PAF patients. Notwithstanding that a complete separation fails, both times there is a significant difference between the healthy persons and the diseased ones. The ROC values calculated for the CHF patients and the healthy subjects do not significantly differ from the ones obtained for the normalised morphograms. Again only two healthy persons fail a complete separation of the groups. The separation between the different groups is much more pronounced than for the normalised morphograms. This becomes clear when comparing the absolute magnitude of the $F(s)$ values. In contrast to this, we find pronounced differences in the ROC values, whenever PAF patients are included in the analysis. The separation between the PAF patients and the other groups is significantly improved when analysing non-normalised morphograms

	H for non-normalised morphograms
healthy subjects	0.0358 ± 0.0247
CHF patients	0.1411 ± 0.0716
PAF patients	0.0336 ± 0.0334

Table 6.2: Averaged Hurst exponents H from the analysis of non-normalised morphograms N_n. The errors refer to the standard deviation in each group. The exponents are estimated by fitting the fluctuation function $F(s)$ in the range $s = 10^2 - 10^4$ to a power law.

instead of normalised ones. This points out, that compared with sinus rhythm or congestive heart failures, paroxysmal AF is characterised not only by a more irregular heart beat (with view to the ECG-signal shape) but also by more irregular heart beat intervals r.

The averaged Hurst exponents for the non-normalised morphograms are listed in table 6.2. They are in the range $0.0336 \leq H \leq 0.1411$, which indicates the presence of long-range anticorrelation between the increments $N_{n+1} - N_n$. The exponents for the CHF and the PAF patients are comparable to the ones listed in table 6.1. For the healthy subjects on the other hand, the variations of the Hurst exponents as well as the averaged exponents are smaller than the ones for the normalised morphograms. Again the complete separation between the groups fails due to the variations of the averaged Hurst exponents within each group.

6.2 Distribution of ventricular interbeat intervals

At last we analyse the statistical properties of ventricular responses during different states of health. First we study the distributions $w(r)$ of interbeat intervals r. As shown in the left panel in fig. 6.5 for three representative AF patients the distributions do not exhibit a characteristic or common shape but various patterns. For 48 patients in data pool 1, $w(r)$ exhibits an uni-modal pattern (a). Bimodal or multimodal patterns are observed for 52 patients (c). *Shoulders* are observed for 30 patients (b). These findings are clearly in contrast to the assumption of a unique shape of $w(r)$ as it is discussed by other groups [Tateno01].

A common feature that can be observed in all distributions is a characteristic decay of $w(r)$ for large intervals r. This decay can be well fitted by a single exponential

$$w(r) \sim p_\infty \exp(-\gamma_{\text{dist}} r)\,, \tag{6.5}$$

with *decay rate* γ_{dist} and *amplitude factor* p_∞. This feature becomes particular clear in the semi-logarithmic plots of the distributions $w(r)$ (right panels in fig. 6.5).

To check the statistical significance of this feature we perform a *Kolmogorov-Smirnov test* for all intervals r that contribute to the *tail region* in $w(r)$, [Honerkamp94]. As a first approximation we specify the tail region with:

$$r \geq \bar{r} + \sigma_r\,, \tag{6.6}$$

where $\bar{r}$ denotes the mean and σ_r the standard deviation of $w(r)$. We find that relation (6.6) provides an appropriate definition of the tail region for AF patients with uni-modal dis-

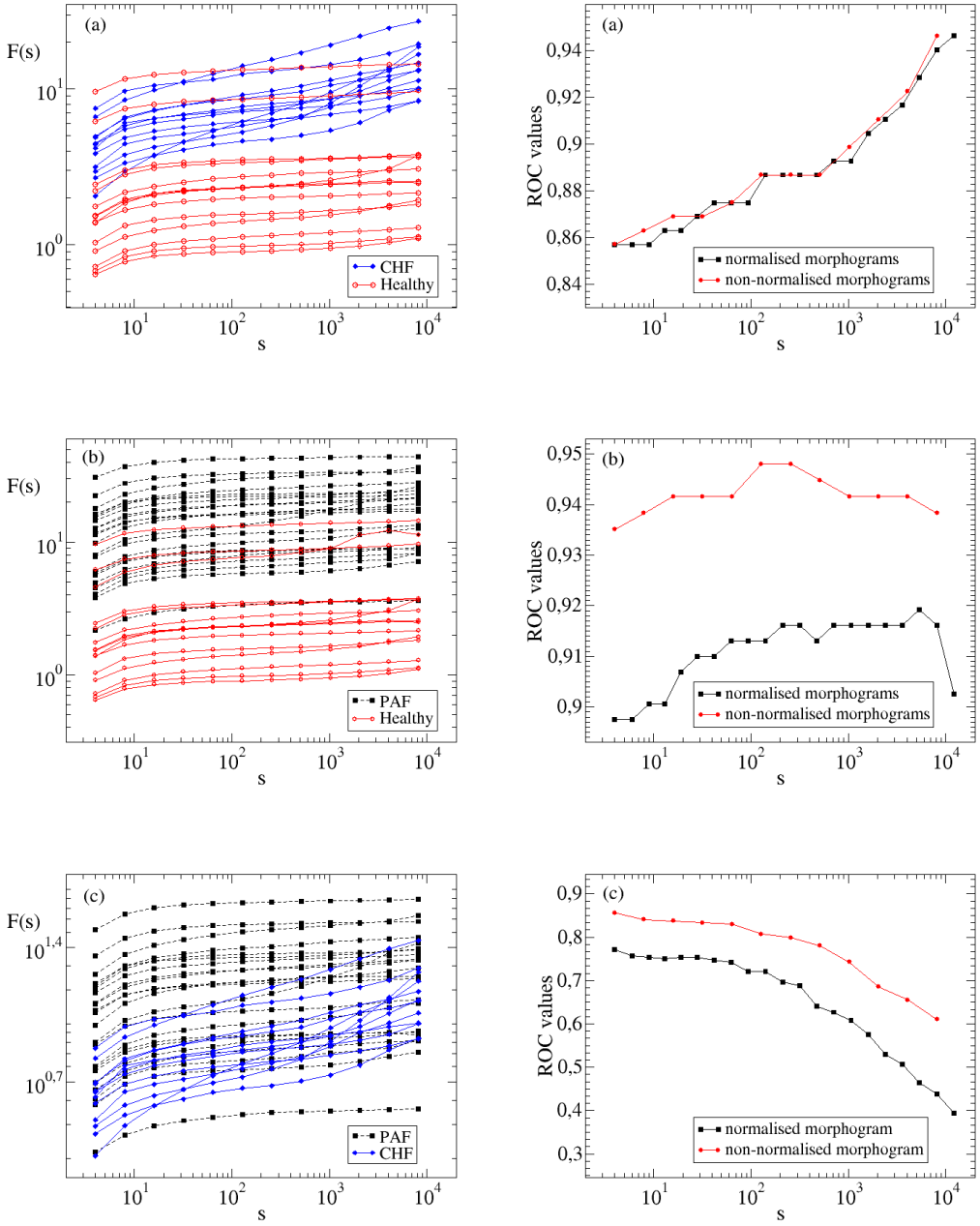

Figure 6.4: Left panels: Double-logarithmic plots of fluctuation functions $F(s)$ of non-normalised morphograms N_n for different groups of patients. The corresponding Hurst exponents H are listed in table 6.2. Right panels: Comparison of the corresponding ROC values calculated for the analysis of non-normalised morphograms (red curves) and normalised morphograms (black curves).

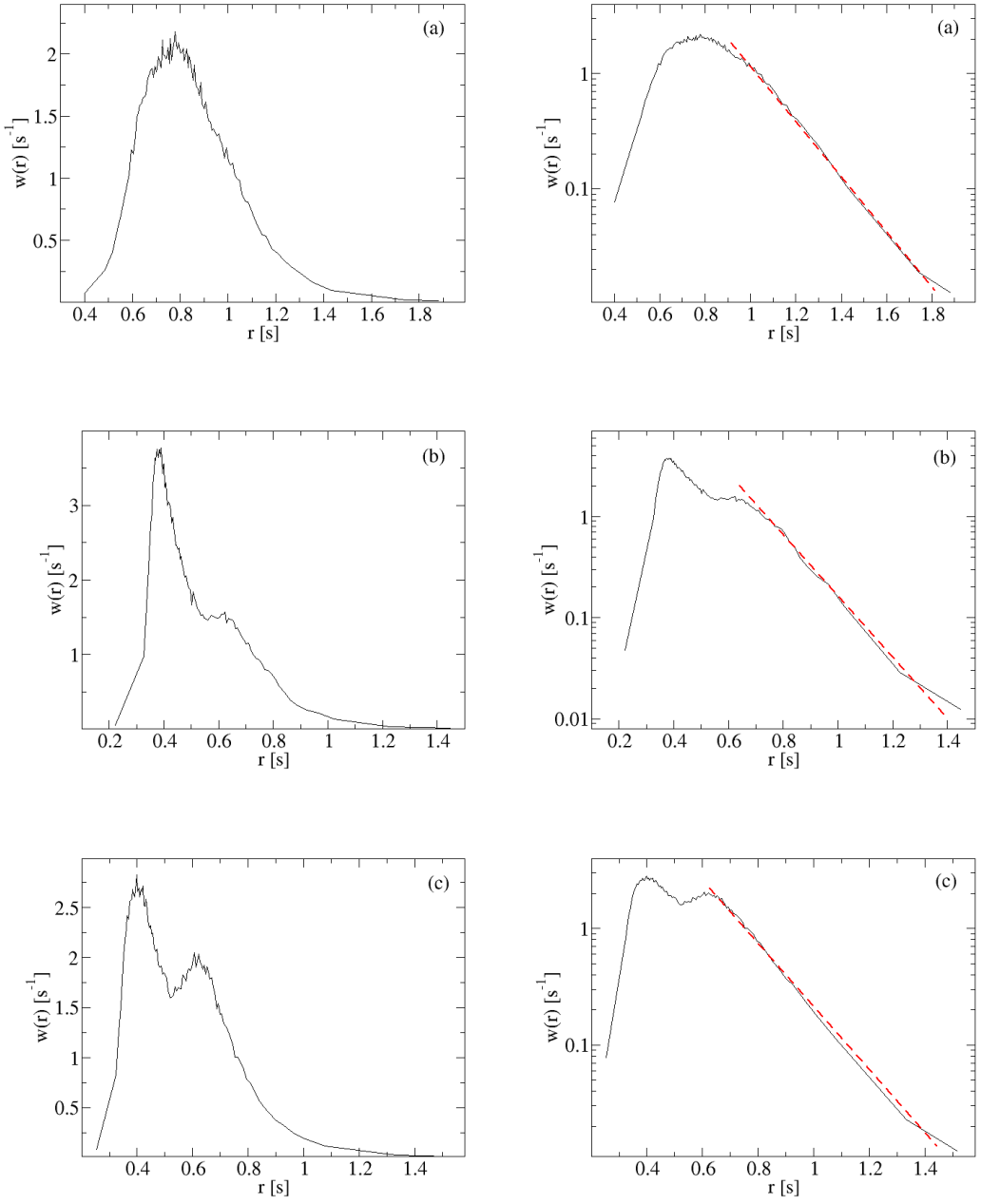

Figure 6.5: Probability densities $w(r)$ of intervals r during AF for three representative patients on linear (left panels) and semi-logarithmic scale (right panels). Uni-modal (a) and multimodal (c) patterns are observed as well as the occurrence of *shoulders* (b). All distributions $w(r)$ exhibit a characteristic exponential decay for large intervals r which can be well fitted to eq. (6.6).

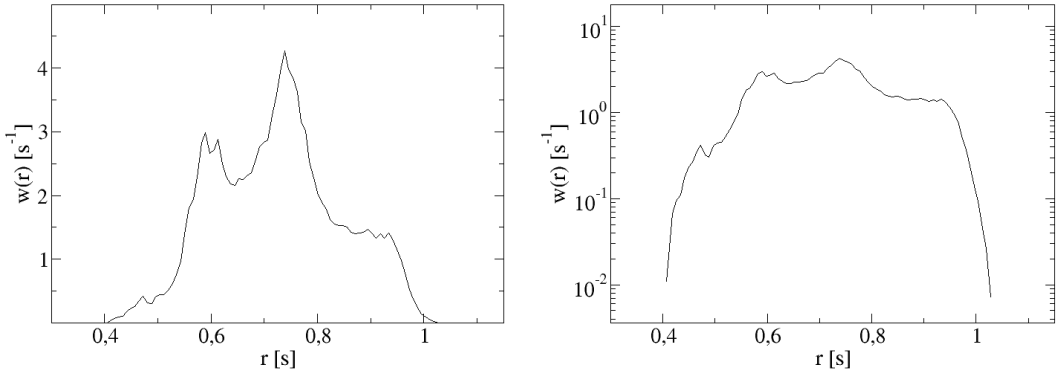

Figure 6.6: Probability density $w(r)$ of intervals r observed during sinus rhythm for a representative person on linear (left panel) and semi-logarithmic scale (right panel).

tribution $w(r)$. For other patterns the quality of the suggested definition depends on the individual patient. Only 78 of all 130 AF patients pass a Kolmogorov-Smirnov test with a standard significance level of 10%. To improve the analysis we replace the global definition of the tail region based on relation (6.6) by more sophisticated and more shape-sensitive definitions, which identify the tail region in $w(r)$ individually for each patient. To ensure a sufficient statistical meaning of the result we require the estimated region to encompass at least 0.3s and at least 2% of all observed intervals. Based on this definition 106 of all 130 AF patients pass the test, which strongly supports the significance of the exponential tail.

In order to evaluate if the observed tail is not only a significant but also a characteristic statistical feature of AF, we perform a counter check and study the distributions $w(r)$ for the healthy persons in data pool 3. Figure 6.6 shows the distribution $w(r)$ for a representative of this group. Contrary to the $w(r)$ for the AF patients the distribution is not right skewed and signatures of an exponential tail can not be identified. Only 6 of the 72 healthy persons are accepted by the Kolmogorov-Smirnov test specified above. Then we analyse the distributions $w(r)$ for the CHF patients and for the PAF patients in data-pool 3. Distributions $w(r)$ for representatives of these groups are shown in fig. 6.7 (left panel: CHF patient, right panel: PAF patient). All CHF patients fail the Kolmogorov-Smirnov test while three of the 22 PAF patients pass the specified test. However, the result for the PAF patients changes when we take into account only those intervals r that occurred during periods of atrial fibrillation. To ensure a sufficient statistical meaning of the obtained Kolmogorov-Smirnov probabilities p_{Kol} we require that these episodes should encompass at least 5000 intervals. According to this constraint we have to remove seven patients from the analysis and find that seven of the remaining 15 ones pass the test specified above. Thus, we conclude that the occurrence of an exponential decay in the distribution $w(r)$ is a significant and also a characteristic feature of atrial fibrillation.

In the following we study the parameters p_∞ and γ_{dist} of the exponential decay. In order to estimate these parameters we perform a linear regression of the tail region in the semi-logarithmic representation of $w(r)$. To ensure an accurate determination of p_∞ and γ_{dist}, we use the following methods to estimate the tail region in $w(r)$ for each patient separately.

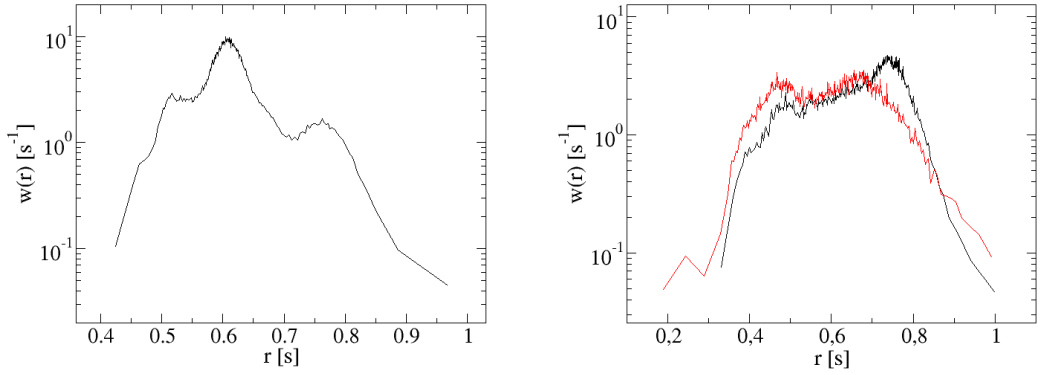

Figure 6.7: Semi-logarithmic representation of distributions $w(r)$ of intervals r for a CHF patient (left panel) and a PAF patient (right panel). The black curve in the right panel displays the distribution $w(r)$ off all observed intervals r. The red curve displays the distribution $w(r)$ of all intervals r which are observed during episodes of atrial fibrillation.

- **method 1:** Interval of best linear regression

  The tail region is defined as that interval $[r_1, r_2]$, that yields the largest absolute regression coefficient for a linear regression of $\ln(w(r))$.

- **method 2:** Interval of largest Kolmogorov-Smirnov probability p_{Kol}

  The tail region is defined as that interval $[r_1, r_2]$, in which the Kolmogorov-Smirnov deviation is smallest - which corresponds to a maximal Kolmogorov-Smirnov probability. We require that the tail region should yield a Kolmogorov-Smirnov probability larger than 5%.

For both methods the borders of the interval $[r_1, r_2]$ are varied under the constraints $r_2 - r_1 \geq 0.3\ s$ and $r_1 > 0.7\ s$. With the first constraint we guarantee that the width of the fitting region covers at least one decay time $1/\gamma_{\mathrm{dist}}$ for small γ_{dist} values. The combination of the first and the second constraint ensures that the fitting region lies right to the maximum of $w(r)$.

Figure 6.8 display the tail regions according to eq. (6.6) and those obtained by applying method 1 and 2 for two representative AF patients. The regions estimated by method 1 are much broader than the ones got by the Kolmogorov-Smirnov test and do not provide a valid fitting region. Better results are obtained when defining the tail region based on the Kolmogorov-Smirnov test. Accordingly for the further analysis we will use the tail regions estimated by method 2. On average these regions encompass about 0.42s and take 8.6% of all intervals r. Before we estimate the parameters p_∞ and γ_{dist}, we take the Kolmogorov-Smirnov probabilities found during the estimation of the tail region and repeat the check of significance. Now, 125 of the 130 AF patients pass the test with a standard significance level of 10%. In the further analysis only these 125 patients are taken into account.

The histogram of the estimated γ_{dist} values is displayed in the left panel of fig. 6.9. Most values lie in the range 2-12 Hz. This is a remarkable finding since the range of γ_{dist} values correspond to the range of fibrillation rates published in the literature. Motivated by this finding we investigate the relation between γ_{dist} and the fibrillation rate. For uni-modal

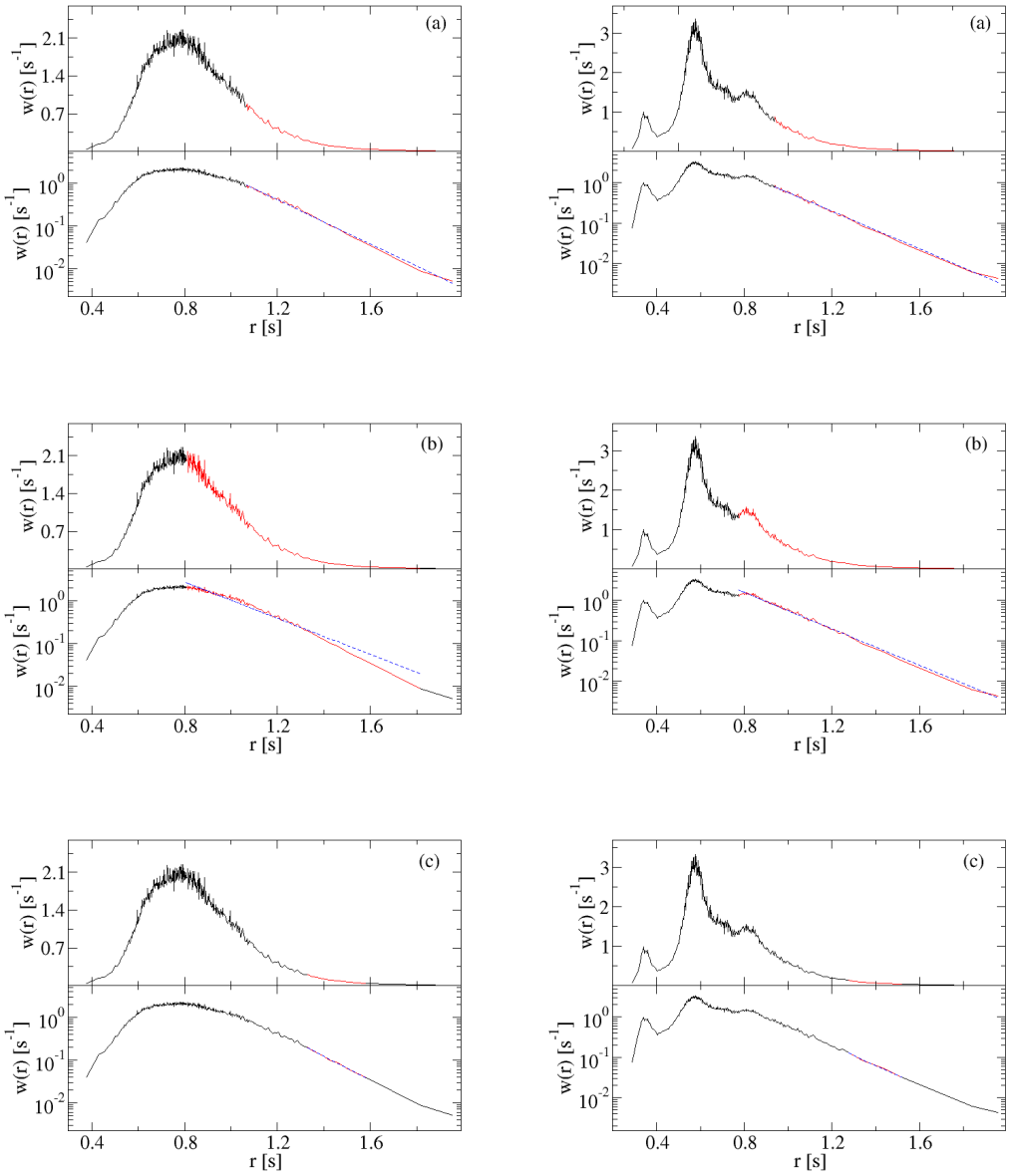

Figure 6.8: Probability density $w(r)$ (black curve) of intervals r during AF and estimated tail regions (red curves) on linear (upper panels) and semi-logarithmic (lower panels) scale for two representative patients. The tail regions are estimated (a) according to relation (6.6), (b) to the interval of best linear regression and (c) to the interval of largest Kolmogorov-Smirnov probability. The dashed blue lines represent the linear regressions of $\ln(w(r))$ in the estimated tail regions.

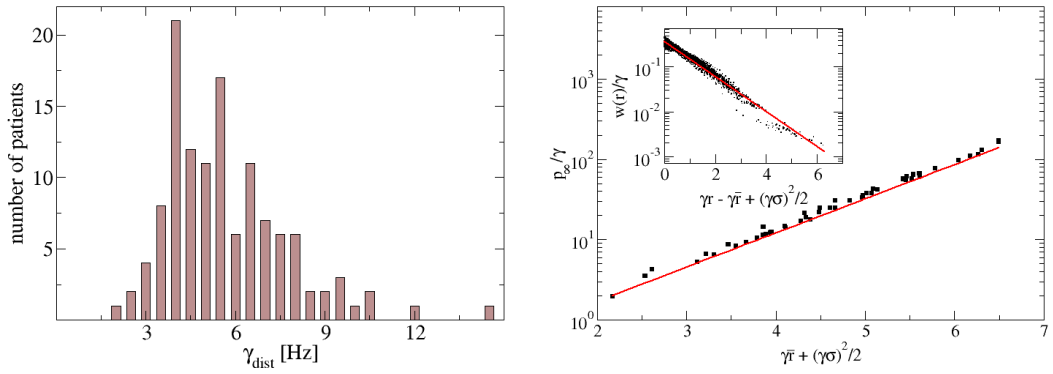

Figure 6.9: Left panel: Histogram of γ_{dist} values for all 125 patients in data pool 1 that pass the Kolmogorov-Smirnov test of significance with a standard significance level of 10%. The values are estimated by a linear regression in the tail regions in the semi-logarithmic representation of the distributions. The γ_{dist} values have a mean 5.4 Hz and a standard deviation 2.1 Hz. Right panel: Semi-logarithmic representation of $p_\infty/\gamma_{\text{dist}}$ as a function of $\gamma_{\text{dist}}\bar{r} + \gamma_{\text{dist}}^2\sigma^2/2$ for the subgroup of 48 patients in data pool 1 with uni-modal distributions $w(r)$. The straight line marks the theoretical behaviour according to eq. (6.8). The inset shows the rescaled probability density for this subgroup of patients.

distributions $w(r)$ a full mathematical description can be given, when assuming that the intervals r result from a superposition of two statistically independent times, $r = r' + \eta$. Here r' is drawn from a Gaussian distribution $\psi_G(r')$ with mean $\bar{r}_G$ and variance σ_G^2, and η is drawn from an Exponential distribution $\phi_E(\eta) = \gamma_{\text{dist}} \exp(-\gamma_{\text{dist}}\eta)$. We note, that formally $\psi_G(r')$ should be introduced as a truncated Gaussian due to the positive character of the times r'. We neglect this truncation because we consider $\psi_G(r')$ to be sufficiently sharply peaked at $\bar{r}_G$. Then the theoretical distribution $\hat{w}(r)$ is given by

$$\begin{aligned}\hat{w}(r) &= \int_{-\infty}^{r} \psi_G(r')\,\phi_E(r-r')\,dr' \\ &= \frac{1}{2}\gamma_{\text{dist}} \exp(\gamma_{\text{dist}}\bar{r}_G + \gamma_{\text{dist}}^2\sigma_G^2/2)\,\text{erfc}\left(\frac{\bar{r}_G + \gamma_{\text{dist}}\sigma_G^2 - r}{\sqrt{2}\sigma_G}\right)\exp(-\gamma_{\text{dist}}r) \qquad (6.7)\end{aligned}$$

with mean $\bar{r} = \bar{r}_G + \gamma_{\text{dist}}^{-1}$ and variance $\sigma^2 = \sigma_G^2 + \gamma_{\text{dist}}^{-2}$, respectively. In fig. 6.10 both the real distribution $w(r)$ (black curve) and the theoretical distribution $\hat{w}(r)$ (red curve) are shown for two representative AF patients. For all 48 patients with unimodal-distributions $w(r)$, the parameters $\bar{r}_G$ and σ_G are in the ranges 0.3s−0.85s and 0.04s−0.17s, respectively.

In the limit of large intervals r the theoretical distribution $\hat{w}(r)$ exhibits an exponential decay with amplitude factor

$$p_\infty = \gamma_{\text{dist}} \exp\left(\gamma_{\text{dist}}\bar{r}_G + \frac{\gamma_{\text{dist}}^2\sigma_{\text{G}}^2}{2}\right) = \gamma_{\text{dist}} \exp\left(\gamma_{\text{dist}}\bar{r} + \frac{\gamma_{\text{dist}}^2\sigma^2}{2} - \frac{3}{2}\right). \qquad (6.8)$$

The values of p_∞ determined by the linear regression closely follow this theoretical value,

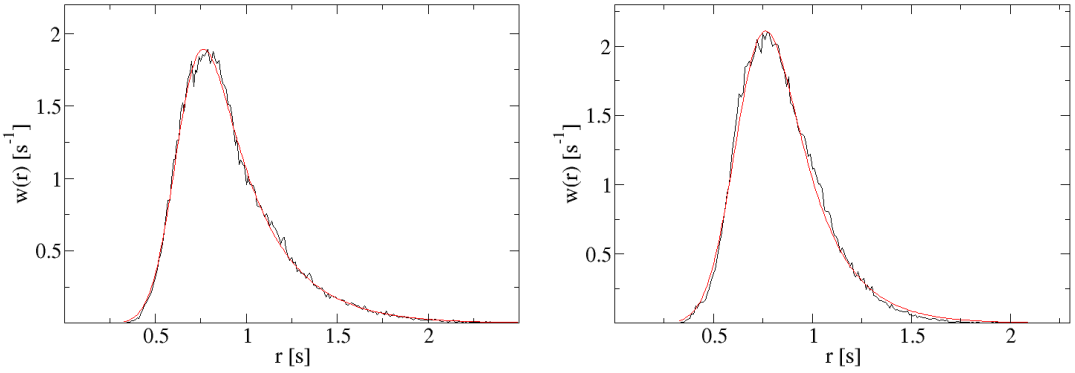

Figure 6.10: Probability densities $w(r)$ (black curve) and fits according to eq. (6.7) (red curve) of ventricular intervals r for two representative patients undergoing AF.

as it is shown in the right panel of fig. 6.9. Furthermore, eq. (6.8) allows us to scale the exponential tails for all 48 patients onto a common master curve. This is displayed in the inset of the right panel of fig. 6.9. The good agreement between the theoretical prediction and the measured data justifies our assumption for $\hat{w}(r)$.

The fact that the range of γ_{dist} corresponds to the one of the fibrillation rate suggest that γ_{dist} exhibits a medical meaning. Thus it may be subjected to diurnal variations as it is reported for the fibrillation rate, [Meurling01]. To test this, we study the correlation between γ_{dist} and $\bar{r}$, which can be expected to be larger during night time than during day time. We split the time series of intervals r into N overlapping segments of 2^{14} elements which correspond to typically 4.5 hours. To achieve a good temporal resolution the segments are shifted by 2^{12} heart beats, approximately 1 hour. In each segment i we determine the decay rate $\gamma_{\text{dist,i}}$ from the distribution $w_i(r)$ and calculate the mean $\bar{r}_i$.

The left panel in figure 6.11 shows $\gamma_{\text{dist,i}}$ and $\bar{r}_i$ as a function of time for a representative AF patient. Both parameters are assigned to the beginning of the segments. The graphs in the figure display remarkable diurnal fluctuations of the decay rate and indicate strong anticorrelation between $\gamma_{\text{dist,i}}$ and $\bar{r}_i$. Periods with larger means $\bar{r}_i$ correspond to periods of smaller γ_i and vice versa. One might argue, that the observed anticorrelation is a simple effect, since lower $\gamma_{\text{dist,i}}$ values correspond to larger intervals r and therefore influence the observed mean value $\bar{r}_i$. To exclude such an effect, we also calculate the mean value $\bar{r}_{\text{G,i}} = \bar{r}_i - \gamma^{-1}_{\text{dist,i}}$ of the Gaussian distribution $\psi_G(r')$ and find that the pronounced anti-correlation is still present.

To quantify the strength of the observed anticorrelation we calculate the cross-correlation coefficient

$$C_{\text{cross,dist}} = \frac{1}{N}\sum_{i=1}^{N}\frac{(\bar{r}_i - \tilde{r})(\gamma_{\text{dist,i}} - \tilde{\gamma})}{\sigma_{\gamma,i}\,\sigma_{r,i}} \tag{6.9}$$

where $\tilde{r}$ and $\tilde{\gamma}$ are the means and $\sigma_{r,i}$ and $\sigma_{\gamma,i}$ are the standard deviations of $\bar{r}_i$ and $\bar{\gamma}_{\text{dist,i}}$ respectively. The histogram of the $C_{\text{cross,dist}}$ values is displayed in fig. 6.12. For the major

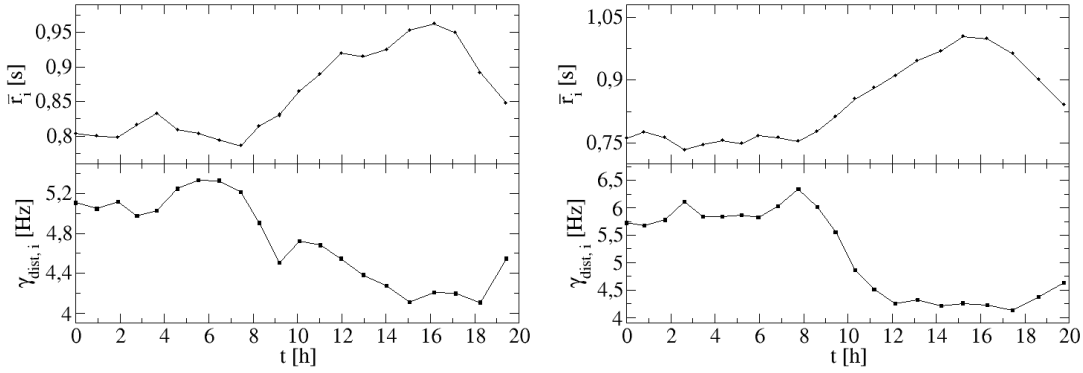

Figure 6.11: Time dependence of $\bar{r}_i$ and decay rate $\gamma_{\text{dist,i}}$ during AF for two representative patients from data pool 1. The values are estimated in segments of 2^{14} successive intervals r. The segments are shifted by 2^{12} intervals. The local values $\bar{r}_i$ and $\gamma_{\text{dist,i}}$ are assigned to the starting point of each segment i.

part of patients we obtain coefficients $C_{\text{cross,dist}} < -0.8$, which clearly confirm the presence of strong anticorrelation between $\gamma_{\text{dist,i}}$ and $\bar{r}_i$.

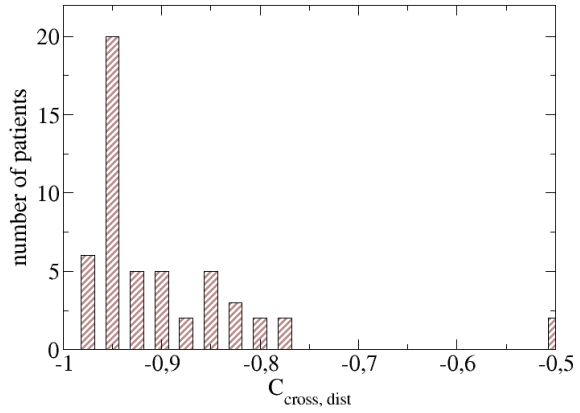

Figure 6.12: Histogram of cross-correlation coefficients $C_{\text{cross,dist}}$ for mean intervals $\bar{r}_i$ and decay rate $\gamma_{\text{dist,i}}$. The mean cross correlation coefficient is $\bar{C}_{\text{cross,dist}} = -0.86$ and reflects strong anticorrelation between $\gamma_{\text{dist,i}}$ and $\bar{r}_i$.

6.3 Interrelation of characteristic features

Beside the exponential decay in $w(r)$ the ventricular response during AF is characterised by a constant signal to noise ratio and a breakpoint in the PSD at which the $1/f$ behaviour of $S(f)$ changes into a white noise behaviour. The fact that the disease is reflected in different statistical properties gives rise to the question if there exist interrelations between these features. In particular we ask if the long, exponentially distributed intervals r are associated with the white noise part in the power spectrum.

It was shown before that during AF unimodal distributed intervals r can be decomposed

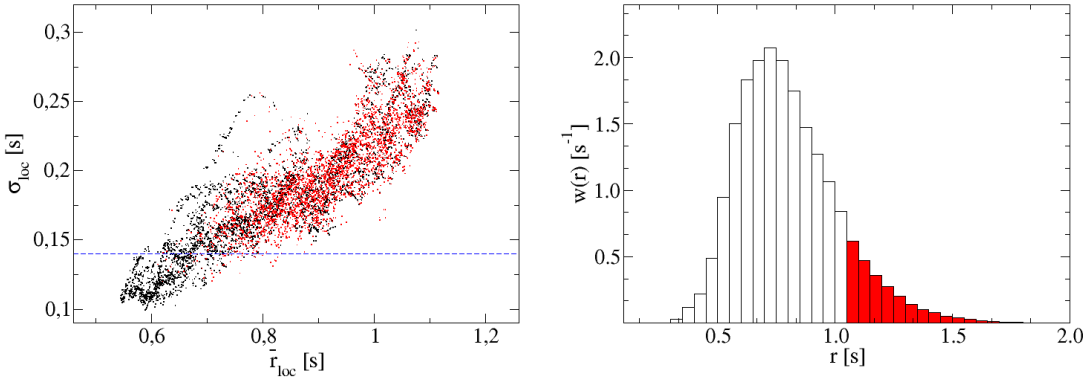

Figure 6.13: Left panel: Local standard deviation σ_{loc} vs. local mean $\bar{r}_{\mathrm{loc}}$ for a representative patient undergoing atrial fibrillation. The local values are calculated for segments of 100 consecutive intervals r and are rounded to 10^{-4}sec to achieve a better representation. The red points mark those pairs $(\bar{r}_{\mathrm{loc}}, \sigma^{*}_{\mathrm{loc}})$ that are obtained in segments centred around intervals r fulfilling eq. (6.6). The dashed blue line marks the threshold $\sigma^{(\mathrm{c})}_{\mathrm{loc}}$. Right panel: Distribution $w(r)$ of interbeat intervals r for the same subject. The red bars mark the exponential tail according to eq. (6.6).

into two statistically independent times r' and η drawn from a Gaussian and an Exponential distribution, respectively. Now we assume the times r' to be correlated and to reflect the regulation by the autonomous nervous system. The times η on the other hand are considered to be uncorrelated or to exhibit correlation only on very short times scales. As a consequence, we expect the white noise part in the PSD to result from the times η.

To test this we decompose the original time series of intervals r into two sub-sequences $\mathcal{S}_{r'}$ and $\mathcal{S}_{\eta}$. $\mathcal{S}_{r'}$ contains only those intervals for which η gives only a small contribution, $\eta \ll r'$, whereas $\mathcal{S}_{\eta}$ contains intervals for which η cannot be neglected. Given such a decomposition we expect the white noise part in the power spectrum of $\mathcal{S}_{r'}$ to be less significant than the one in the PSD of the original time series. On the other hand we expect the white noise part in the PSD of $\mathcal{S}_{\eta}$ to be more pronounced than the one in the PSD of the original time series.

Note that $\mathcal{S}_{\eta}$ can not simply be identified as the sequence of intervals r belonging to the exponential tail in $w(r)$, since also short intervals contribute to the white noise part in the power spectrum. A more successful procedure for decomposing the original time series is based on the analysis of the constant signal to noise ratio $\sigma_{\mathrm{loc}}/\bar{r}_{\mathrm{loc}}$ [Hennig06a]. We find that segments of intervals r, centred around those that contribute to the tail region in $w(r)$, exhibit standard deviations $\sigma^{*}_{\mathrm{loc}}$ which exceed a certain threshold $\sigma^{(\mathrm{c})}_{\mathrm{loc}}$. This is demonstrated in fig. 6.13 where both the scatter plot (left) and the distribution $w(r)$ (right) are shown for a representative AF patient. The dashed blue marks the threshold $\sigma^{(\mathrm{c})}_{\mathrm{loc}}$ and the red points mark the pairs $(\bar{r}_{\mathrm{loc}}, \sigma^{*}_{\mathrm{loc}})$. For comparison, the red bars in the right panel mark the exponential tail according to eq. (6.6). The demonstrated behaviour is mostly independent from the chosen length of the segments. We note, that there also exist segments, not centred around intervals fulfilling eq. (6.6), for which the local standard deviation also exceed the threshold $\sigma^{(\mathrm{c})}_{\mathrm{loc}}$.

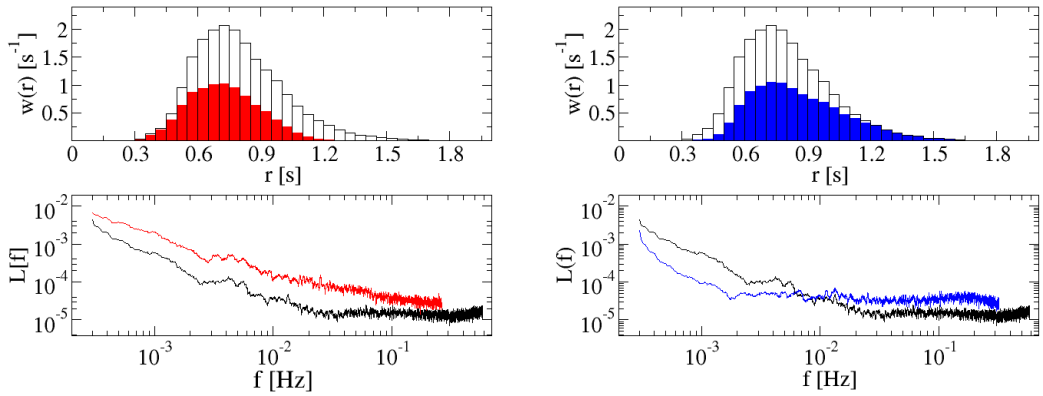

Figure 6.14: Distributions of interbeat intervals (upper panel) and Lomb periodograms $L(f)$ (lower panel) for the full sequence of intervals (black) and the sub-sequences $\mathcal{S}_{r'}$ (blue, left panel) and $\mathcal{S}_\eta$ (blue, right panel). The Lomb-periodograms are smoothed with a moving average filter.

Motivated by our finding, we define $\mathcal{S}_\eta$ as the sequence of those intervals r, for which segments centred around these intervals satisfy $\sigma_{\mathrm{loc}} > \sigma_{\mathrm{loc}}^{(\mathrm{c})}$. Accordingly $\mathcal{S}_{r'}$ is the sequence of the remaining intervals. Best results are achieved when the time series of intervals r is splitted in very short segments of 10 consecutive intervals only and for a lower threshold $\sigma_{\mathrm{loc}}^{(\mathrm{c})}$ given by:

$$\sigma_{\mathrm{loc}}^{(\mathrm{c})} = \bar{\sigma}^* - \sigma_{\sigma^*}$$

where $\bar{\sigma}^*$ is the mean and σ_{σ^*} is the standard deviation of all σ_{loc}^*.

A straightforward calculation of the power spectra of $\mathcal{S}_{r'}$ and $\mathcal{S}_\eta$ is not possible since the estimated sub-sequences are unevenly sampled. This problem can be solved by approximating the power spectra with Lomb periodograms. The lower panels in fig. 6.14 display the Lomb-periodograms for the two sub-sequences $\mathcal{S}_{r'}$ (red) and $\mathcal{S}_\eta$ (blue) and for the full sequence of intervals (black) for a representative AF patient. The corresponding distributions of the different sequences are displayed in the upper panels. We note, that $\mathcal{S}_{r'}$ and $\mathcal{S}_\eta$ contain of about 40% to 60% of all intervals r in the data sets. Furthermore, for both sub-sequences the fluctuations of the sampling intervals do not significantly differ.

As can be seen from the left panel of fig. 6.14 the Lomb-periodogram of $\mathcal{S}_{r'}$ shows the $1/f$-type behaviour over almost the whole frequency range. In comparison with the periodogram of the original sequence the white noise region is shifted to the high frequency region. The distribution $w(r)$ of intervals r belonging to $\mathcal{S}_{r'}$ barely contributes to the exponential tail seen in the distribution of all intervals. In contrast, the white noise part in the periodogram of $\mathcal{S}_\eta$ extends to much lower frequencies compared to the one of the full sequence of intervals (right panel). The corresponding distribution accounts for nearly the whole exponential tail of $w(r)$ but also contains smaller intervals r.

These results show that the long and exponentially distributed intervals r contribute to the white noise part in the PSD of the ventricular response during AF. Furthermore they support that during AF ventricular intervals r result from the superposition of two independent

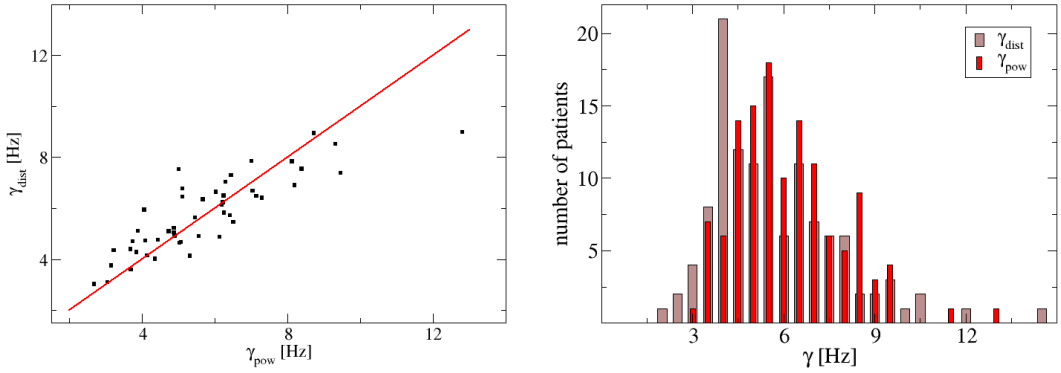

Figure 6.15: Left panel: γ_{dist} vs. γ_{pow} for the group of 48 patients undergoing AF with uni-modal $w(r)$. The red line marks the theoretical relation $\gamma_{\text{dist}} = \gamma_{\text{pow}}$. Right panel: Histograms of γ values (brown bars: γ_{dist} calculated from $w(r)$; red bars: γ_{pow} calculated from the PSD of the ventricular response).

processes as described above. The exponentially distributed times η are uncorrelated and hence are associated with the white noise part in the PSD. The times r' on the other hand reflect a strongly correlated process and thus are associated with the $1/f$ part in the power spectrum.

In accordance to this the PSD of the original time series is given by:

$$S(f) = S_{r'}(f) + S_{\eta}(f) \tag{6.10}$$

where $S_{r'}(f) \sim S_0 f^{-\xi}$ and $S_{\eta}(f) \simeq S_{\infty}$ are the power spectra of the two contributions. The strength of the white noise in $S(f)$ corresponds to the variance σ_{η}^2 of the times η. Hence, we obtain

$$S_{\infty} = \sigma_{\eta}^2 = 1/\gamma_{\text{dist}}^2 \tag{6.11}$$

since the times η are exponentially distributed.

Eq. (6.11) allows us to determine the rate of the exponential decay in $w(r)$ from the PSD of the ventricular response directly. In contrast to the rate estimated from the distribution, we denote the one estimated according to eq. (6.11) as γ_{pow}. The left panel of fig. 6.15 shows γ_{pow} in comparison with γ_{dist} for all 48 patients in data pool 1 for which the ventricular intervals r are uni-modal distributed. The straight line in the plot marks the theoretical relation $\gamma_{\text{dist}} = \gamma_{\text{pow}}$. Clearly to see, the points $(\gamma_{\text{pow}}, \gamma_{\text{dist}})$ are arranged closely around the theoretical line indicating a good agreement between the estimated rates. Except of one patient the values γ_{dist} and γ_{pow} differ only of about ± 1.5Hz. The right panel in fig. 6.15 shows both the histogram of γ_{dist} (brown bars) and γ_{pow} (red bars).

As next we ask if γ_{pow} is also subjected to diurnal fluctuations, as it was found for γ_{dist}. To tackle this question we perform the same time-dependent analysis for the parameter γ_{pow} as it was performed for γ_{dist} in sec. 6.2. As a result the lower left panel in fig. 6.16 displays both γ_{pow} (red) and γ_{dist} (black) as a function of time for one representative patient. Again the

upper panel shows the diurnal fluctuation of the mean interval $\bar{r}$. Obviously, γ_{pow} exhibits pronounced diurnal fluctuations. The values of γ_{pow} closely follow the diurnal variations of γ_{dist} and thus are also strongly anticorrelated to the diurnal fluctuations of $\bar{r}$. To quantify the anticorrelation between γ_{pow} and $\bar{r}$ we calculate the cross-correlation coefficients $C_{\text{cross,pow}}$ between the γ_{pow} and $\bar{r}$ according to eq. (6.9). For both γ_{dist} and γ_{pow} the histograms of the cross-correlation coefficients are shown in the right panel in fig. 6.16 (full bars: γ_{dist}, hatched bars: γ_{pow}).

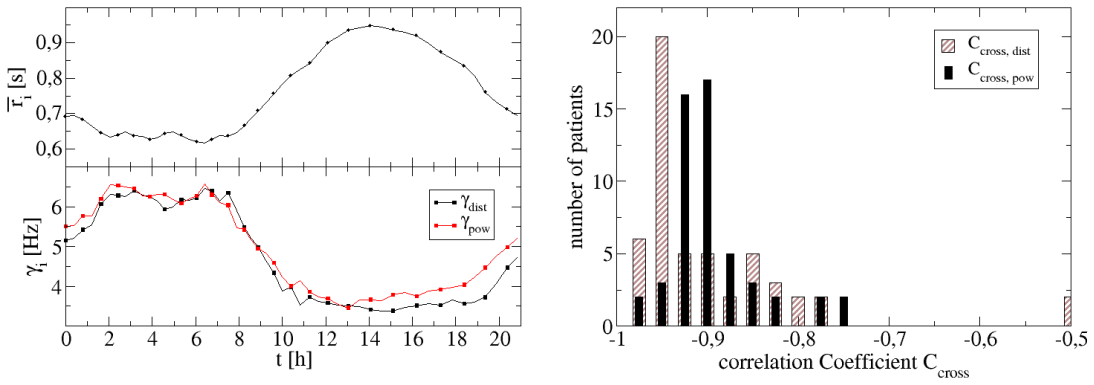

Figure 6.16: Left panel: Time dependency of $\bar{r}$ and of γ_{dist} (black curve) and of γ_{pow} (red curve). Right panel: Histogram of cross-correlation coefficients for the local mean interval $\bar{r}$ and γ_{dist} (hatched bars) and γ_{pow} (full bars).

We note, that the gamma values obtained by the time-resolved analysis are not as close as displayed in fig. 6.16 for every patient. This is due to the fact, that a precise determination of γ_{dist} from the interval distribution becomes rather difficult for a comparatively small number of intervals. The white noise part in the power spectrum on the other hand, can be clearly identified already for segments comprising 2^{10} beats only. Hence with view to practical applications, we propose to estimate the characteristic decay rate γ from the PSD.

7 Numerical and analytical modelling of the conduction process through the AV node during atrial fibrillation

The present chapter concentrates on modelling of the ventricular response during AF. In particular it questions (i) in which way the conduction of electrical impulses through the AV node can be described in a mathematical manner and (ii) in which way mathematical models are useful for determining the AFR from surface tachograms.

After a short introduction to the basic concepts of conduction models we discuss in detail the one proposed by Jørgensen *et al.* [Jørgensen02]. This model is most suitable for predicting the statistical properties of tachograms during AF. Systematical investigations will determine the influence of the different parameters in the model on the statistical properties of the predicted response and will yield a first approach for determining the fibrillation rate.

It will be shown, that the conduction model of Jørgensen *et al.* can be described analytically. The formal solution of the model as well as particular ones, obtained for different modifications of the model, will be presented.

7.1 Mathematical models of the AV node

7.1.1 Mathematical models of the AV node: General overview

Two major concepts can be distinguished in models suggested for the biological processes in the heart during atrial fibrillation.

The first one focuses on the electrophysiological properties of the atrium and assumes that the behaviour of the atrium differs between sinus rhythm and AF [Cohen83]. According to this approach the differences between sinus rhythm and AF are expressed only in changes of atrial parameters, such as the correlation properties of atrial interbeat intervals or the duration of the mean atrial interval.

The second one assumes, that during AF the intrinsic behaviour of the AV node junctions differs from the one during sinus rhythm ([Moe64], [Zeng96]). Most commonly accepted is the *concealed conduction approach* [Langendorf48]. According to this, atrial impulses arriving at the AV node either (i) are successfully conducted to the ventricles, (ii) are totally blocked by the AV node, or (iii) penetrate the AV node only partly. In the following we concentrate only on models following this concept, since we find that it is most suitable for predicting the ventricular response during AF.

The time that it takes to conduct an atrial excitation through the AV node is named *conduction time* t_{con}. This time can be associated with the time between the occurrence of an excitation in the atrial ECG and the observation of the corresponding ventricular excitation in the surface ECG. After the conduction the AV node is *absolutely refractory* for a given time t_{ref}, the so-called *refractory period*. Impulses arriving at the node during this period are blocked and thus are not conducted. The time interval between the end of the refractory period and the arrival of the next atrial impulse is the so-called *recovery time* t_{rec}. Since the early 1920s it is known, that the conduction time t_{con} decreases when t_{rec} increases [Lewis25b]. The functional relation $t_{\mathrm{con}}(t_{\mathrm{rec}})$ is described by the *recovery curve* [Shrier87].

Several medical studies focused on the determination of the exact analytical form of the recovery curve (e.g. [Shrier87], [Glass91]). These studies are usually done by invasive measurements and ECG-recordings under controlled pacing of the atrium. A major problem in the determination of the recovery curve is, that the exact position and the exact size of the node are not well defined. In addition to sums of several exponentials ([Chorro88], [Teague76], [Ferrier74]) , non-steady functions or hyperbolic functions ([Chorro88], [Simson79]), the recovery curve is often assumed to exhibit a single exponential decay:

$$t_{\mathrm{con}} = t_{\mathrm{con}}(t_{\mathrm{rec}}) = \alpha + \beta\, e^{-t_{\mathrm{rec}}/\tau_{\mathrm{AV}}} \tag{7.1}$$

where α denotes the minimal conduction time and $\alpha + \beta$ the maximal one. The parameter τ_{AV} denotes the characteristic timescale of the recovering process.

Besides the analytical form of the recovery curve, established conduction models differ (i) in the exact definition of the refractory state of the AV node and (ii) in the way in which the blocking of impulses affects its electrophysiological state. Apart from this, the models contain the following major mechanisms:

1. **Blocking mechanism**
   The AV node is absolutely refractory after an atrial excitation is conducted to the ventricle. Excitations reaching the node in this state are blocked.
2. **Conduction process**
   Impulses reaching the AV node are not conducted immediately. The conduction time t_{con} depends on the time that it takes to recover the electrophysiological neutral state of the AV node.

7.1.2 Conduction model of Jørgensen *et al.*

The conduction model proposed by Jørgensen *et al.* [Jørgensen02] basically follows the one of Zeng and Glass [Zeng96] and considers the AV node to be capable of existing in two different states: neutral and absolutely refractory.

Impulses are conducted only during the neutral state of the node. The conduction time t_{con} is determined by the foregoing recovery time t_{rec}, which in contrast to [Zeng96] is defined as the time interval between the end of the refractory period and the onset of the first atrial impulse successfully conducted. The recovery curve is considered to be a single exponential according to eq. (7.1). Impulses occurring at the node during the conduction process, are

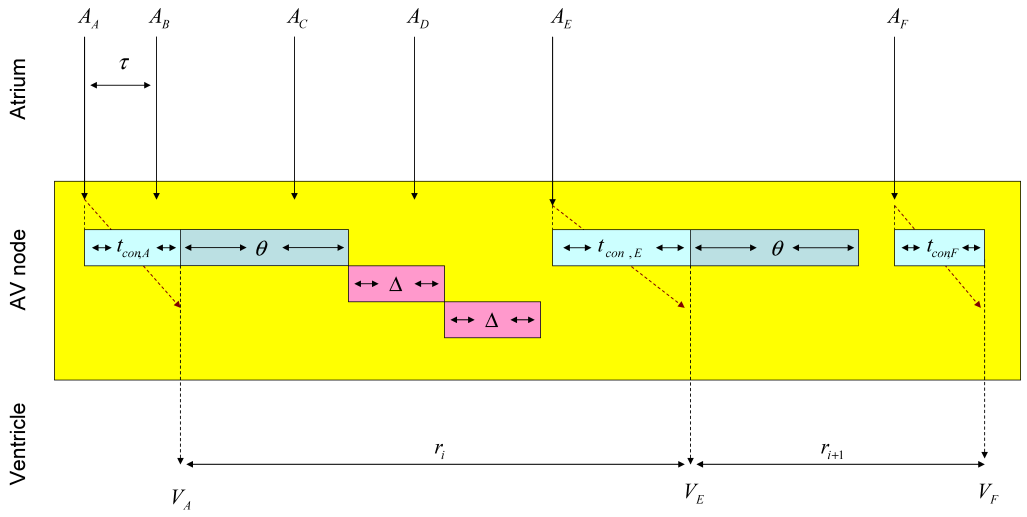

Figure 7.1: Schematic representation of the AV node conduction model for AF proposed by Jørgensen *et al.*. Atrial impulses arriving at the AV node are conducted to the ventricle and initiate a ventricular excitation (atrial impulses A_A, A_E and A_F). The conduction time t_{con} depends on the foregoing recovery time t_{rec}, which is defined as the time between the end of the refractory period and the onset of the next successfully conducted atrial impulse. Impulses arriving at the AV node during the conduction process are blocked but do not influence the electrophysiological state of the node (atrial impulse A_B). After the conduction of an impulse the node is absolutely refractory for the time $t_{\mathrm{ref}} = \Theta$. Impulses occurring at the node during this time are not conducted (atrial impulses A_C and A_D) and extend t_{ref} by the time increment Δ.

blocked but do not affect its electrophysiological state. After the conduction, the AV node is absolutely refractory for the time $t_{\mathrm{ref}} = \Theta$. Impulses arriving during t_{ref} are blocked and extend this period by the *time increment* Δ. As such the *absolute refractory period* $t_{\mathrm{ref,abs}}$ is given by

$$t_{\mathrm{ref,abs}} = \Theta_k = \Theta + k\Delta \tag{7.2}$$

where k denotes the number of blocked excitations. A schematic representation of the model is shown in fig. 7.1.

Jørgensen *et al.* showed, that the proposed model predicts the ventricular response during AF and during atrial flutter. Based on atrial tachograms obtained by invasive measurements, they predicted ventricular responses and afterwards compared them with the real ones. Their remarkable results ($p_{\mathrm{Kol}} \sim 70\%$) showed that the suggested model is suitable for describing the medical state of the heart during AF.

Figure 7.2 shows normalised histograms $h(r)$ of intervals r simulated according to the model. The detailed parameters are given in the figure caption.[1] The insets of the panels display the histograms in a semi-logarithmic plot. The histograms are superposed by several striking and nearly equidistant spikes. The positions of the spikes mark the end

[1] If not otherwise noted, atrial interbeat intervals τ are considered to be random numbers drawn from a truncated Gaussian distribution with mean $\bar{\tau}$ and standard deviation σ_τ.

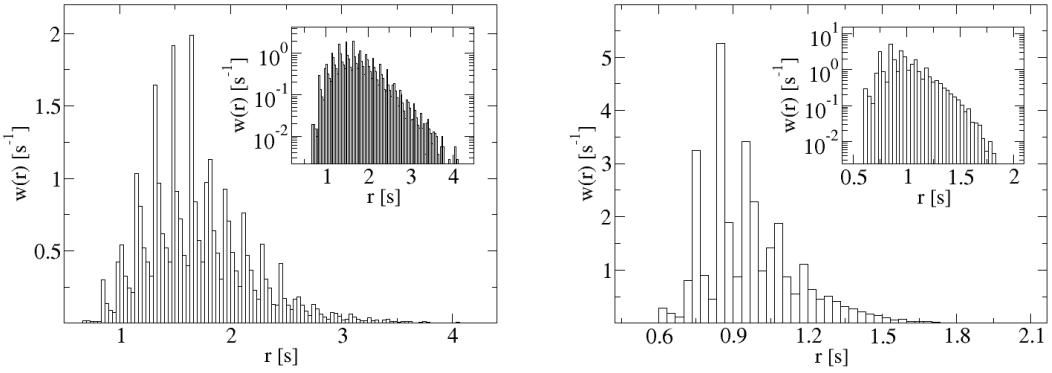

Figure 7.2: Normalised histograms $h(r)$ of ventricular interbeat intervals r simulated according to the conduction model of Jørgensen *et al.*. The insets of the panels display the histograms on a semi-logarithmic scale. The following parameters are used in the simulations: $\bar{\tau} = 0.2s$, $\sigma_\tau = 0.04s$, $\Theta = 0.33s$, $\Delta = 0.16s$, $\alpha = 0.1s$, $\beta = 0.5s$ and $\tau_{AV} = 0.02s$ (left panel) and $\bar{\tau} = 0.17s$, $\sigma_\tau = 0.03s$, $\Theta = 0.26s$,$\Delta = 0.11s$, $\alpha = 0.2s$, $\beta = 0.7s$ and $\tau_{AV} = 0.01s$ (right panel).

of the different absolute refractory periods. Between the peaks the histograms exhibit exponential decays reflecting the exponential form of the recovery curve. The $h(r)$ show an exponential tail for large intervals r, which is caused by the multiple blocking of impulses during t_{ref}.

The statistical properties of the responses are mainly determined by the relation between the increment Δ and the mean atrial interval $\bar{\tau}$. It is obvious that $\Delta \leq \bar{\tau}$. Otherwise the multiple incrementation yields infinitive refractory periods and hence no atrial impulse will be conducted anymore. The closer is Δ to $\bar{\tau}$, the more atrial impulses are blocked.

The Jørgensen *et al.* model has been studied by several other groups. Cammarota *et al.* [Cammarota05] discussed the model with respect to their finding that during AF ventricular intervals exhibit a constant signal to noise ratio. They argued that the model does not predict this statistical feature and suggested to introduce a non-stationary modification (replacing the fixed values of $\bar{\tau}$, Θ and Δ by random ones). A similar approach and also comparable results have been presented by Mangin *et al.* [Mangin05] who studied the influence of a randomly chosen increment Δ on the predicted response.

7.2 Discussion of the Jørgensen *et al.* conduction model

We study the influence of certain parameters in the Jørgensen *et al.* model on the statistical properties of the predicted response. According to the model the ventricular intervals r are given by:

$$r = t_{\text{con}} + t_{\text{ref,abs}} + t_{\text{rec}}.$$

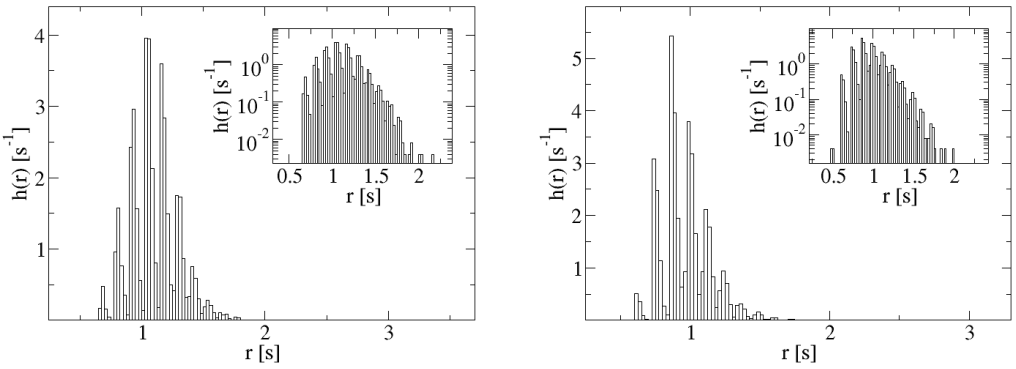

Figure 7.3: Normalised histograms $h(r)$ of intervals r generated according to modified Jørgensen *et al.* models. The insets of the panels display the histograms on semi-logarithmic scales. The left panel refers to a simulation with constant conduction time $t_{\mathrm{con}} = 0.3$s and the right one to a simulation with $t_{\mathrm{con}} = 0$s. The generated ventricular response have a mean $\bar{r} = 1.1$s and a standard deviation $\sigma_r = 0.19$s (left panel) and $\bar{r} = 0.97$s and $\sigma_r = 0.176$s (right panel). In both simulations the following parameters are used: $\bar{\tau} = 0.17$s, $\sigma_{AA} = 0.03$s, $\Theta = 0.25$s, $\Delta = 0.12$s.

The time t_{rec} is mainly determined by the statistical properties of the intervals τ. On average t_{rec} is the shorter the shorter $\bar{\tau}$ is. According to eq. (7.1) the times t_{con} vary between α and $\alpha+\beta$. The times $t_{\mathrm{ref,abs}}$ on the other hand are not limited. A multiple blocking of impulses causes multiple prolongations of t_{ref} and allows the generation of refractory periods of arbitrary length. Hence in comparison to times $t_{\mathrm{ref,abs}}$ the influence of the times t_{con} on the statistical properties of the intervals r can be neglected.

To test this, we modify the original conduction model and replace the variable conduction time t_{con} by a constant averaged value: (i) $t_{\mathrm{con}} > 0$, (ii) $t_{\mathrm{con}} = 0$. Normalised histograms $h(r)$ of intervals r, generated according to these modified models, are shown in fig. 7.3. The insets of the panels display the histograms on a semi-logarithmic scale. The statistical properties of the responses noted in the figure caption do not strongly vary between both realisations. Furthermore, the histograms do not differ qualitatively from the ones displayed in fig. 7.2. They are right-skewed, exhibit the typical multimodal patterns and exponential decays for large intervals r.

Replacing the variable time t_{con} by a constant value decreases the variability of the ventricular response and yields pronounced multimodal patterns in the histogram. The onsets of the peaks mark the end of the different absolute refractory periods Θ_k. In the presence of a fluctuating conduction time these times differ and yield a broadening of the peaks. This becomes particular clear when comparing the histograms displayed in fig. 7.3 with the ones shown in fig. 7.2. The histograms obtained for the original model exhibit a more realistic shape than the ones obtained for the modified versions.

As next we ask, if a conduction model in which $t_{\mathrm{con}}$is set to $t_{\mathrm{con}} = 0$s, exhibits a medical meaning. To tackle this question, we (i) generate a ventricular response according to the model originally proposed, (ii) fit the parameters of the modified model to this response,

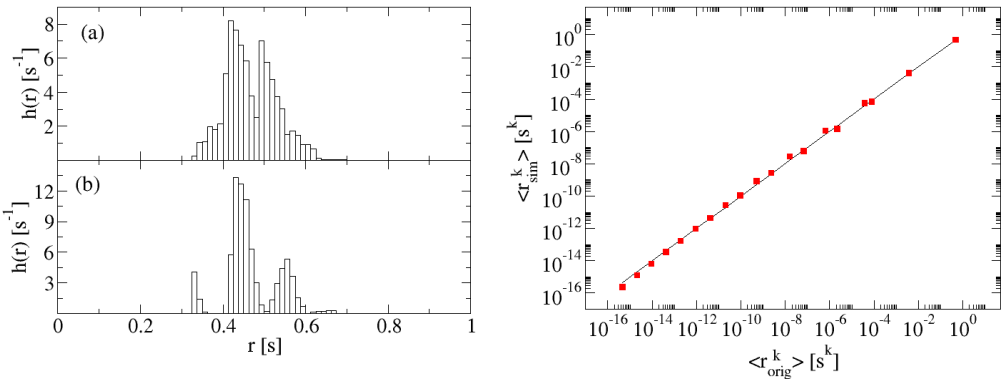

Figure 7.4: Left panel: Normalised histograms $h(r)$ of intervals r generated according to the original conduction model of Jørgensen *et al.* (panel a) and according to a modified conduction model in which t_{con} is set to $t_{\text{con}} = 0$s (panel b). The parameters for the simulations are taken from [Jørgensen02]. Right panel: Comparison of the central moments of the generated ventricular responses. The black line marks the theoretical curve for complete identity. The parameters of the modified conduction model are estimated by fitting Θ and Δ with respect to the lowest AAREM value to the original response.

(iii) generate the response of the modified model, and (iv) perform a Kolmogorov-Smirnov test to compare the different responses. To ensure that the response generated according to the original model exhibits a sufficient medical meaning we use the set of parameters presented in the original work of Jørgensen *et al.* ($\bar{\tau} = 0.146$s, $\sigma_{AA} = 0.016$s, $\Theta = 0.114$s, $\Delta = 0.081$s, $\alpha = 0.065$s, $\beta = 0.290$s and $\tau_{AV} = 0.055$s). The normalised histograms $h(r)$ of the generated responses are displayed in the left panel of fig. 7.4 (upper panel: original model, lower panel: modified model). At first view, the histograms are not in a good agreement ($p_{Kol} \sim 1.3\%$). This points out that the modified conduction model is not capable of predicting the exact statistical properties of the original response.

Before rejecting the modified model, we ask if the model is capable of predicting at least some statistical properties of the original response (e.g. the first moments of the distribution $w(r)$). As such we perform a counter check and fit the parameters Θ and Δ to the original response, with respect to the first moments of the intervals r only. To quantify the agreement between the first k moments of the responses we introduce the *absolute averaged relative error of moments* (AAREM)

$$AAREM_k = \left| \frac{1}{k} \sum_{i=1}^{k} \left(1 - \frac{\left\langle r_{\text{sim}}^i \right\rangle}{\left\langle r_{\text{orig}}^i \right\rangle} \right) \right| + \left| \frac{1}{k} \sum_{i=1}^{k} \left(1 - \frac{\left\langle (r_{\text{sim}} - \bar{r}_{\text{sim}})^i \right\rangle}{\left\langle (r_{\text{orig}} - \bar{r}_{\text{orig}})^i \right\rangle} \right) \right| \tag{7.3}$$

where $|x|$ denotes the absolute value of x and where $\langle x \rangle$ denotes the average of x over all elements in the time series. The index "orig" indicates intervals r generated according to the original model and the index "sim" the intervals generated according to the modified model.

We repeat our test and fit the parameters Θ and Δ with respect to the lowest AAREM value.

The right panel of fig. 7.4 shows the first 20 central moments of the different responses plotted against each other on a double-logarithmic scale. The black line marks the theoretical behaviour in case $\left\langle r^k_{\mathrm{orig}} \right\rangle = \left\langle r^k_{\mathrm{sim}} \right\rangle$. The points in the representation closely follow the theoretical line, which shows that the modified model predicts the main statistical properties of the original response. It has to be mentioned that this result can not be obtained for every response. The agreement between the moments is the better the smaller t_{con} is in comparison with the times Θ_k. We conclude that at least in certain cases modified models also predict the main statistical features of ventricular responses predicted by the original model during AF.

The medical meaning of the exponential tail

The multiple extension of the refractory period is the main mechanism for the origin of the characteristic tail in $w(r)$. Conduction models that do not consider this mechanism (e.g. the model proposed by Moe and Abildskov [Moe64]), do not predict exponential decays in $w(r)$. Furthermore, the smaller t_{con} is in comparison with the times Θ_k, the more pronounced the tail is. This shows that the exponential decay carries information about both the electrophysiological properties of the AV node and the statistical properties of the atrial interbeat intervals. Here we ask if this information is helpful for determining the fibrillation rate from the ventricular response.

We consider a conduction model with (i) $t_{\mathrm{con}} = 0$, and in which (ii) each blocked excitation initiates a complete new refractory cycle $t_{\mathrm{ref}} = \Theta$. Due to the second modification the time between the arrival of the last blocked impulse and the end of the new refractory period is constant. Hence, only those impulses are conducted that occur at the node after the time Θ is passed by.

The probability P_{b} for an arriving impulse to be blocked at the node is:

$$P_{\mathrm{b}} = \int_0^{\Theta} \rho_{AA}(\tau)\, d\tau \tag{7.4}$$

where $\rho_{AA}(\tau)$ is the distribution of the atrial interbeat intervals τ.

Accordingly, the probability $P_{\mathrm{c,k}}$ for an atrial impulse to be conducted after k successive atrial impulses have been blocked, is

$$P_{\mathrm{c,k}} = P_{\mathrm{b}}^k \, (1 - P_{\mathrm{b}}) \; . \tag{7.5}$$

Numerical simulations show that distributions $w(r)$ predicted by the suggested model, exhibit an exponential decay, which can be well fitted by:

$$w(r) \sim p_\infty \exp(-\gamma r) \, , \tag{7.6}$$

with decay rate γ and amplitude factor p_∞.

Let be $w(r_1)dr$ the probability for a ventricular interval r to lie in the interval $[r_1; r_1 + dr]$ and let be $w(r_2 = r_1 + \Theta)dr$ the probability to observe a ventricular interval r in the interval

$[r_1 + \Theta; r_1 + \Theta + dr]$. Then $w(r_2)dr$ can be approximated by

$$w(r_2)dr \approx P_\mathrm{b}\, w(r_1)dr. \tag{7.7}$$

Here we have considered that the generations of the intervals r_2 and r_1 differ only by one additional blocked impulse.[2] In combination with eq. (7.6), relation (7.7) yields:

$$\frac{w(r_2)dr}{w(r_1)dr} = e^{-\gamma\Theta} \approx P_\mathrm{b} \tag{7.8}$$

which allows to approximate the rate γ of the exponential decay in $w(r)$ by

$$\gamma \approx -\frac{1}{\Theta}\,\ln(P_\mathrm{b})\,. \tag{7.9}$$

Figure 7.5 shows distributions $w(r)$ of ventricular responses generated according to the modified model (black curves) and the exponential decays according to relation (7.9) (red dashed curves). The amplitude factors p_∞ of the theoretical decays are adjusted by fitting the theoretical decay to the real distributions. The insets of the panels display the distributions on a semi-logarithmic scale. As it can be clearly seen, the theoretical and the real exponential decays are in a good agreement. The rates of the real decays seem to be slightly higher than the ones of the theoretical tails. This is due to the fact, that the generations of ventricular interbeat intervals r_1 and $r_1 + \Theta$ can differ in more than one additional blocked impulse. The higher the number of blockings is the lower is the probability for the realisation of such generation processes. Hence in practise, the probability to observe a ventricular interval r_1 of a given length is lower than the one approximated in eq. (7.7).

Next we consider the refractory period Θ to be prolonged by the time increment Δ every time an atrial impulse is blocked at the node. We follow a mean field approach and study the averaged time intervals (i) between the last blocked impulses and the end of the refractory period and (ii) between the occurrences of successively blocked impulses.

Let be x_k the time interval between the arrival of the impulse k and the end of the corresponding refractory period $t_\mathrm{ref} = \Theta_k = \Theta + k\Delta$. Then $x_0 = \Theta$ denotes the time interval between a successful conduction and the end of the refractory period $t_\mathrm{ref} = \Theta$. On average the first atrial impulse blocked at the node occurs after the time $\bar{\tau}_{\mathrm{b},1}$.

$$\bar{\tau}_{\mathrm{b},1} = \int_0^\Theta \tau\, \rho_{AA}(\tau)\, d\tau \tag{7.10}$$

If the impulse is blocked, the refractory period is extended by the time increment Δ and thus becomes $t_\mathrm{ref} = \Theta_1 = \Theta + \Delta$. On average the time interval x_1 between the occurrence of the last blocked impulse and the end of the new refractory period is $x_1 = \Theta + \Delta - \bar{\tau}_{\mathrm{b},1}$.

On average the next atrial impulse blocked at the node, occurs after the time interval $\bar{\tau}_{\mathrm{b},2}$

[2] We note, that the number of blocked impulses participating in the generation of a ventricular interval of a given length, cannot be predicted a priori. On the other hand is is obvious to consider that at least one additional atrial impulse has been blocked during the generation of an interval $r_1 + \Theta$, than during the generation of an interval r_1 since atrial interbeat intervals τ, are narrow distributed during AF.

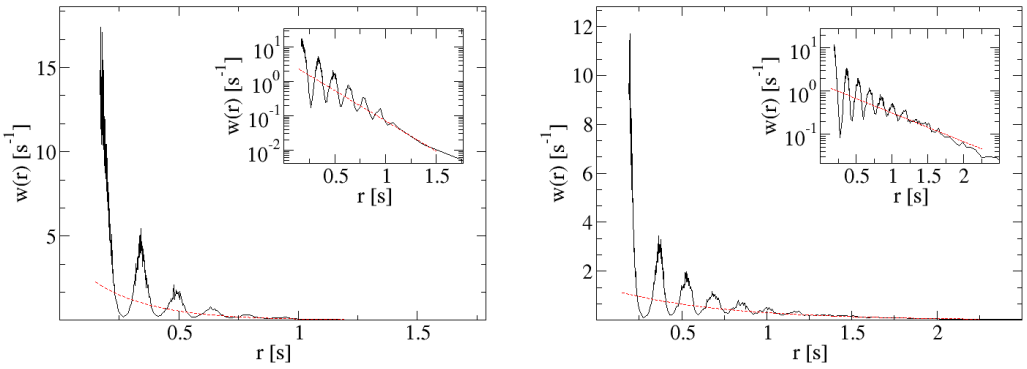

Figure 7.5: Distributions $w(r)$ of ventricular intervals r generated according to a modified Jørgensen model, in which (i) every atrial impulse blocked at the AV node initiates a complete new refractory cycle and with (ii) $t_{\mathrm{con}} = 0$. The insets of the panels display the distributions on semi-logarithmic scales. In both simulations the atrial intervals τ are considered to be random variables drawn from a Gaussian distribution with mean $\bar{\tau} = 0.15s$ and standard deviation $\sigma_\tau = 0.03$. The refractory period is: $\Theta = 0.17s$ (left panel) and $\Theta = 0.19s$ (right panel) respectively. The red dashed lines mark the theoretical exponential decays of $w(r)$ according to eq. 7.9.

has passed.

$$\bar{\tau}_{\mathrm{b},2} = \int_0^{\Theta+\Delta-\bar{\tau}_{\mathrm{b},1}} \tau\, \rho_{AA}(\tau)\, d\tau \tag{7.11}$$

In accordance to the previous calculation, we use $\bar{\tau}_{\mathrm{b},2}$ to determine the time interval $x_2 = \Theta + 2\Delta - \bar{\tau}_{\mathrm{b},1} - \bar{\tau}_{\mathrm{b},2}$, which afterwards is used to estimate the time $\bar{\tau}_{\mathrm{b},3}$, and so on.

In table 7.1 the times x_k and $\bar{\tau}_{\mathrm{b,k}}$ are listed for a given set of parameters ($\bar{\tau} = 0.15$s, $\sigma_{AA} = 0.03$s, $\Theta = 0.3$s and $\Delta = 0.09$s). Both x_k and $\bar{\tau}_{\mathrm{b,k}}$ decrease when k increases. For large numbers k, the time interval $\bar{\tau}_{\mathrm{b,k}}$ converges to a limit value, which corresponds to Δ and the time delay x_k becomes constant. Hence the probability for the next atrial impulse to be blocked at the node becomes constant. Therefore, for a large number of blockings we find the same situation as discussed for the previous conduction model. In the limit $k \to \infty$, the following approximations can be made:

1. The influence of Θ on the refractory period Θ_k can be neglected.

$$t_{\mathrm{ref,abs}} = \Theta_k = \Theta + k\Delta \approx k\Delta \quad , \quad k \to \infty \tag{7.12}$$

2. The influence of t_{rec} on the statistical properties of the intervals r can be neglected. Hence, $r \approx t_{\mathrm{ref,abs}}$, which in combination with eq. (7.12) yields:

$$k \approx r/\Delta\,. \tag{7.13}$$

numbers of blocked impulses k	0.	1.	2.	3.	4.
$\bar{\tau}_{\mathrm{b,k}}$ [s]	0.15	0.1498	0.1414	0.111	0.0941
x_k [s]	0.3	0.24	0.180	0.1288	0.1077
numbers of blocked impulses k	5.	6.	7.	8.	
$\bar{\tau}_{\mathrm{b,k}}$ [s]	0.0906	0.0901	0.0900	0.0900	
x_k [s]	0.1036	0.1030	0.1029	0.1029	

Table 7.1: Mean intervals $\bar{\tau}_{\mathrm{b,k}}$ between the successively blocked impulses k and $k+1$ and time delays x_k between the blocked impulse k and the end of the corresponding refractory period Θ_k. The values are calculated based on the parameter set: $\bar{\tau} = 0.15$s, $\sigma_{AA} = 0.03$s, $\Theta = 0.3$s and $\Delta = 0.09$s.

3. The probability P_{b} becomes constant

$$P_{\mathrm{b}} = \text{constant} = \int_0^{\mathrm{x}^*} \rho_{\mathrm{AA}}(\tau)\,\mathrm{d}\tau \quad , \quad \mathrm{k} \to \infty \tag{7.14}$$

with

$$\int_0^{x^*} \tau\rho_{AA}(\tau)\,d\tau = \Delta \tag{7.15}$$

since $\bar{\tau}_{\mathrm{b,k}} \to \Delta$ for $k \to \infty$.

We combine eqs. (7.13), (7.14), (7.15) and obtain:

$$P_{\mathrm{c,k}} = (1 - P_{\mathrm{b}})\,P_{\mathrm{b}}^k \approx P_{\mathrm{b}}^k = P_{\mathrm{b}}^{\frac{r}{\Delta}} = \left(P_{\mathrm{b}}^{\frac{1}{\Delta}}\right)^r = e^{-\gamma r} \tag{7.16}$$

with

$$P_{\mathrm{b}}^{\frac{1}{\Delta}} = \left[\int_0^{x^*} \rho_{AA}(\tau)\,d\tau\right]^{1/\kappa} = e^{-\gamma} \tag{7.17}$$

and

$$\kappa = \int_0^{x^*} \tau\rho_{AA}(\tau)\,d\tau\,. \tag{7.18}$$

According to eq. 7.17 the rate γ of the exponential decay in $w(r)$ is directly related to the statistical properties of the atrial interbeat intervals τ. We will show in the next section, that relation 7.17, although approximate, provides a first approach for the estimation of the fibrillation rate from $w(r)$.

Estimation of the fibrillation rate : First approach

The decay rate γ is related to the statistical properties of the intervals τ and to the electrophysiological properties of the AV node. This relation can be used for determining the

AFR from the statistical properties of the ventricular response during AF. The method presented in the following has been applied as invention and has been protected by a patent [Hennig06b].

We consider the following conduction model:

- intervals τ are uncorrelated random numbers drawn from a truncated Gaussian distribution with mean $\bar{\tau}$ and standard deviation σ_τ
- the blocking of atrial impulses extend the refractory period Θ by the time increment Δ
- $t_{\text{con}} = 0$.

To determine the fibrillation rate f_{fib} from a sequence r_i , $i = 1, 2, \ldots, N$ of N ventricular interbeat intervals observed during AF, we perform the following steps:

1. Estimating the decay rate γ of the distribution $w(r)$ by (i) a linear regression of $\ln(w(r))$ in the tail region or (ii) based on the PSD of the sequence
2. Approximating the refractory period Θ by the smallest interval $r_{\min}$
3. Determining the increment Δ_0 from the combination of eqs. (7.14) and (7.15) for the estimated decay rate γ and a randomly chosen set of parameters $(\bar{\tau}_0, \sigma_{\tau,0})$.
4. Calculating the expected percentage/amount N_{theo} of ventricular intervals r_i originated without a blocking of atrial impulses.
5. Comparing the expected number N_{theo} with the number N_{real} of real intervals r_i fulfilling: $\Theta \leq r \leq \Theta + \Delta_0$.
6. In case that N_{theo} significantly differs from N_{real}, the set of parameters $(\bar{\tau}_0, \sigma_{\tau,0})$ is rejected and the steps (3) to (5) are repeated. Otherwise the set of parameters is accepted and f_{fib} is determined by the inverse of $\bar{\tau}$.

To demonstrate the potential of the presented approach, we apply the method to the data sets in data pool 2. The left panel in fig. 7.6 shows the distribution $w(r)$ for one representative of this group. For this patient the sequence of ventricular intervals consists of $N = 1331$ elements, with mean $\bar{r} = 0.448$s and standard deviation of $\sigma_r = 0.0049$s. The right panel in fig. 7.6 shows both the distribution of intervals τ obtained from the atrial ECG-recording (black curve) and the expected one estimated with the proposed method (red curve).

The real and the estimated fibrillation rate are in a good agreement (real value: $f_{\text{fib}} = 6.33$Hz, estimated value: $f_{\text{fib}} = 5.81$Hz) and differ only of about 0.52Hz (8%). This is a remarkable result. It has to be taken into account, that the result is obtained for a very short data set and without any further information about the atrial signal.

The expected distribution is broader than the original one. This is due to the absence of a fluctuating conduction time, which causes a loss of variability in the predicted ventricular response. To balance this loss the suggested method automatically pursues broader atrial distributions. Hence, the method does not only allow to determine the fibrillation rate, but also provides an upper limit for the standard deviation σ_τ of the distribution $\rho_{AA}(\tau)$.

The number N of ventricular intervals observed in the ECG-recording determines the quality of the attained result. The longer the time of the ECG-recording is the better the agreement between the real and the estimated AFR will be. The approximation $\Theta = r_{\min}$ is

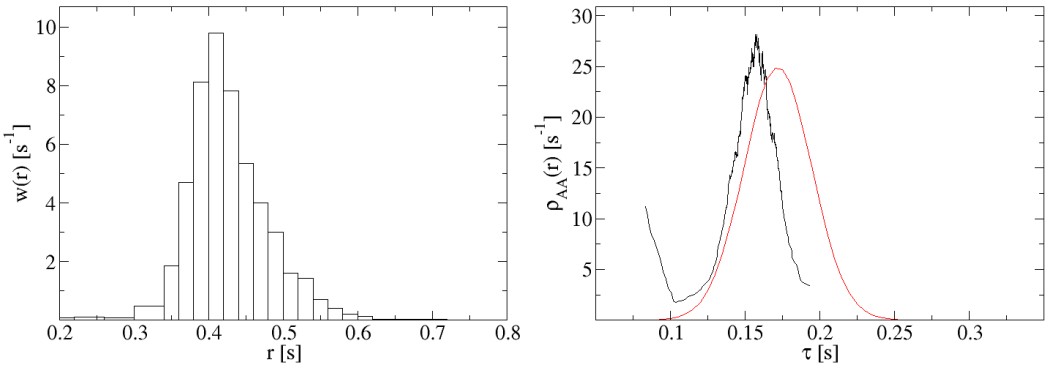

Figure 7.6: Left panel: Distribution of ventricular interbeat intervals during atrial fibrillation for a representative patient. The sequence of ventricular intervals consists of $N = 1331$ elements with mean $\bar{r} = 0.448$s and standard deviation of $\sigma_r = 0.049$s respectively. Right panel: Distribution $\rho_{AA}(\tau)$ of the corresponding atrial interbeat intervals estimated from a atrial ECG-recording (black curve) and theoretical distribution estimated from the statistical properties of the ventricular response. The fibrillation rates (real value: $f_{\text{fib}} = 6.33$Hz, theoretical value: $f_{\text{fib}} = 5.81$Hz) are in a good agreement and differ only of about 0.52Hz (8%).

sufficient only for large sequences r_i. The estimation of γ also requires sequences of appropriate length. Obviously such difficulties can be easily avoided when increasing the recording time of the surface ECG, which in contrast to atrial recordings does not yield any inconvenient effects for the patient.

Best results are obtained when applying the suggested algorithm to ventricular intervals which are uni-modal distributed. This is due to the fact, that in these distributions the estimation of the decay rate γ is less complicated. In case of bimodal or uni-modal distributed intervals r on the other hand, the range of the parameter space can be reduced from the beginning. In multimodal distributions the distance between the observed peaks mostly corresponds to the time increment Δ, while the onset of the peaks mark the end of the different refractory periods (see above). In contrast to this, the presence of pronounced bimodal structures often indicates a restricted variability in the conduction ratio and the distance between the observed peaks indicates the time increment Δ or the mean atrial interval $\bar{\tau}$ in maximum.

7.3 Analytical solutions

7.3.1 Formal solution of the conduction model

We model the sequence of atrial impulses $\mathcal{A}_n$ by a waiting time process and consider the atrial impulses to occur after uncorrelated random time intervals τ drawn from a given probability density $\rho(\tau)$. In contrast to $\mathcal{A}_n$, the sequence A_n denotes the times of conducted

impulses and the times V_n the times of the following ventricular excitations. Note, that in presence of sinus rhythm the times A_n correspond to the times $\mathcal{A}_n$. Furthermore during sinus rhythm the times A_n correspond to the P peaks in the surface ECG and the times V_n are associated with the sequence of R peaks in the surface ECG.

We follow the notations of the previous sections and consider the times t_{con} for the conduction of an atrial impulse through the AV node to depend on the foregoing recovery time t_{rec}. In order to provide a general solution of the conduction model we do not specify the AV nodal recovery curve at this point of the work. In accordance to Jørgensen *et al.* we define the recovery time t_{rec} as the time interval between the end of the refractory period Θ_k and the onset of the first conducted atrial impulse.

$$t_{\mathrm{rec}} = A - V' - \Theta_k \tag{7.19}$$

The stochastic process (A_n, V_n), $n = 1, 2, \ldots$ is completely described by the specification of all n-point joint probability densities $p_n(A_1, V_1; \ldots; A_n, V_n)$, which is the probability that n conducted atrial impulses occur at times $A_1 < \ldots < A_n$ and that each of them is followed by a ventricular excitation V_j, $A_j < V_j < A_{j+1}$, $j = 1, \ldots, n-1$, $A_n < V_n$. [3] Note, that the stochastic process (A_n, V_n), $n = 1, 2, \ldots$ is Markovian in (A, V) space. According to the general electrophysiological properties of the AV node (recovery curve, refractory periods, etc.) random sequences (A_j, V_j), $j = 1, 2, \ldots$ can be generated for every given starting pair (A_0, V_0). Therefore the process is fully determined by the transition probability density $\psi(A, V|A', V') = p_{1|1}(A, V|A', V')$ which is the probability that an event (A, V) follows the event (A', V'). In particular, the one-point probability density $p_1(A, V)$ must satisfy the integral equation

$$p_1(A, V) = \int dA' \int dV'\, p_1(A', V')\, \psi(A, V|A', V')\,. \tag{7.20}$$

The solution of this integral equation becomes unique if we require normalisation. Without loss of generality we set $A' = 0$, which is due to the time translational invariance of the process. While $\psi(A, V|A', V')$ is different from zero only for $A' < V' < A < V$, eq. (7.20) can be rewritten as

$$p(v) \quad = \quad p_1(0, V-A) \;=\; \int_0^\infty dv'\, p(v')\, h(v, v') \tag{7.21}$$

$$h(v, v') \quad = \quad \int_0^\infty du\, \psi(v' + u, v' + v + u|0, v')\,, \tag{7.22}$$

when introducing $v = V - A$, $v' = V' - A'$ and $u = A - V'$ respectively. Note that $p(V-A)$ corresponds to the probability density for the PR intervals in a surface ECG. Hence we obtain the n-point joint probability densities $p_n(A_1, V_1; \ldots; A_n, V_n)$ by multiplying the one-point probability $p_1(A_1, V_1)$ for the first event (A_1, V_1) with the Markov chain that propagates

[3] We here deliberately suppress differential measures to specify the probability densities in terms of probabilities to avoid lengthy wording. As such we simply say that $p_1(A, V)$ is the probability for the event (A, V), while correctly $p_1(A, V)dAdV$ is the probability for a conducted atrial excitation A' and a corresponding ventricular excitation V' to occur in the infinitesimal time intervals $A < A' < A + dA$ and $V < V' < V + dV$.

the first event to the nth event.

$$p_n(A_1, V_1; \ldots; A_n, V_n) = p_1(A_1, V_1) \prod_{i=1}^{n-1} \psi(A_{i+1}, V_{i+1}|A_i, V_i) \tag{7.23}$$

In order to calculate the transition probability density $\psi(A, V|A', V')$ we define $\phi_{k'k}(A|A', V')$ as

$$\phi_{k'k}(A|A', V') = \text{Prob}\left\{\begin{array}{l}\text{following an event } (A', V'), \text{ the first con-}\\ \text{ducted atrial impulse occurs at a time } A\\ \text{after exactly } k' \text{ blocked atrial impulses}\\ \text{during the AV conduction period } V'-A'\\ \text{and after exactly } k \text{ blocked atrial impulses}\\ \text{during the refractory period } \Theta_k\end{array}\right\}. \tag{7.24}$$

With

$$\phi_k(A|A', V') = \sum_{k'=0}^{\infty} \phi_{k'k}(A|A', V') \tag{7.25}$$

and with eq. (7.19) the transition probability density $\psi(A, V|A', V')$ writes:

$$\psi(A, V|A', V') = \sum_{k=0}^{\infty} \phi_k(A|A', V')\, \delta\big(V - A - t_{\text{con}}(A - V' - \Theta_k)\big)\,. \tag{7.26}$$

Introducing the accumulated time intervals

$$U_j = \sum_{i=1}^{j} u_i\,, \quad j = 0, \ldots, k' \qquad , \qquad T_j = \sum_{i=1}^{j} \tau_i\,, \quad j = 1, \ldots, k+1 \tag{7.27}$$

for atrial excitations during the conduction process and during the refractory period respectively, allows us to specify the conditions for the realisation of the particular process underlying $\phi_{k'k}(A|A', V')$.

$$\begin{aligned} A' + U_{k'} &\le V' \\ A' + U_{k'} + \tau_1 &> V' \\ A' + U_{k'} + T_j &\le V' + \Theta_{j-1}\,, \quad j = 1, \ldots, k \\ A = A' + U_{k'} + T_{k+1} &> V' + \Theta_k\,. \end{aligned} \tag{7.28}$$

Accordingly we obtain:

$$\begin{aligned} \phi_{k'k}(A|A', V') = &\int du_1\, \rho(u_1) \ldots \int du_{k'}\, \rho(u_{k'}) \int d\tau_1\, \rho(\tau_1) \ldots \int d\tau_{k+1}\, \rho(\tau_{k+1}) \\ &\times H(A - V' - \Theta_k)\, H(V' - A' - U_{k'})\, H(A' - V' + U_{k'} + \tau_1) \\ &\times \Big[\prod_{j=1}^{k} H(V' - A' - U_{k'} + \Theta_{j-1} - T_j)\Big]\, \delta(A - A' - U_{k'} - T_{k+1}) \end{aligned} \tag{7.29}$$

where $H(.)$ denotes the Heaviside jump function ($H(x)$=1 for $x > 0$ and zero else).

Eq. (7.29) can be rewritten as:

$$\phi_{k'k}(A|A',V') = \int du_1\,\rho(u_1)\ldots\int du_{k'}\,\rho(u_{k'})\,F_k(V'-A'-U_{k'},A-V') \tag{7.30}$$

when introducing

$$\begin{aligned} F_k(\hat{x},a) = {} & H(\hat{x})\,H(a-\Theta_k)\int d\tau_1\,\rho(\tau_1)\ldots\int d\tau_{k+1}\,\rho(\tau_{k+1}) \\ & \times H(\tau_1-\hat{x})\Big[\prod_{j=1}^{k} H(\hat{x}+\Theta_{j-1}-T_j)\Big]\,\delta(\hat{x}+a-T_{k+1})\,. \end{aligned} \tag{7.31}$$

Note, that the time $\hat{x}$ denotes the interval between the ventricular excitation V' and the onset of the last atrial impulse $\mathcal{A}_{k'}$ blocked during the conduction time t_{con}. Accordingly the next atrial impulse occurs after a time interval $\tau_1 > \hat{x}$, as it is displayed by the Heaviside jump function $H(\tau_1-\hat{x})$. Eq. (7.30) can be simplified to:

$$\begin{aligned} \phi_{k'k}(A|A',V') &= \int dz\,F_k(v'-z,a)\int du_1\,\rho(u_1)\ldots\int du_{k'}\,\rho(u_{k'})\,\delta(z-U_{k'}) \\ &= \int dz\,F_k(v'-z,a)\int du_1\,\rho(u_1)\ldots\int du_{k'}\,\rho(u_{k'}) \\ &\quad\times\int\frac{dq}{2\pi}\,\exp\Big(\mathrm{i}qz-\mathrm{i}q\sum_{j=1}^{k'}u_j\Big) \\ &= \int\frac{dq}{2\pi}\,\hat{\rho}(q)^{k'}\int dz\,F_k(v'-z,a)\,e^{\mathrm{i}qz} = \int\frac{dq}{2\pi}\,\hat{\rho}(q)^{k'}\,\hat{F}_k(q,a)\,e^{\mathrm{i}qv'} \end{aligned} \tag{7.32}$$

where

$$\hat{\rho}(q) = \int d\tau\,\rho(u)\,e^{-\mathrm{i}qu}\,,\quad \hat{F}_k(q,a) = \int dx\,F_k(\hat{x},a)\,e^{-\mathrm{i}q\hat{x}} \tag{7.33}$$

denote the Fourier Transform of $\rho(u)$ and $F_k(x,a)$ respectively. Inserting (7.33) and (7.32) into eq. (7.25) yields

$$\phi_k(A|A',V') = \int\frac{dq}{2\pi}\,\frac{\hat{F}_k(q,A-V')}{1-\hat{\rho}(q)}\,e^{\mathrm{i}q(V'-A')}\,. \tag{7.34}$$

Hence performing the integrals in eqs. (7.31) and (7.33) allows us to calculate $\phi_k(A|A',V')$ directly from eq. (7.34). Given $\phi_k(A|A',V')$ from eq. (7.26) we obtain $\psi(A,V|A',V')$ and finally $p_n(A_1,V_1;\ldots;A_n,V_n)$ from eq. (7.23).

7.3.2 General solution: First passage time problem

In this section we present another approach for calculating the transition probability $\phi_{k',k}(A|A',V')$ and express the stochastic process (A_n,V_n), $n=1,2,\ldots$ in terms of a *first passage time problem of an one-dimensional discrete random walk with moving boundary conditions*.

We consider a random walker, starting his walk at position $V' - \hat{x}$. The lengths of the steps of the walker correspond to the intervals τ between successive atrial excitations. With the first step the walker pass the point V', since $\tau_1 > \hat{x}$. The end of the refractory period $V' + \Theta$ marks an absorbing border which is shifted by the increment Δ with every step of the walker until the border is passed. Hence, the probability $F_k(\hat{x}, a)$ in eq. 7.31 equals the probability that the walker generates a first passage time interval of length a by $k + 1$ steps given a starting point $V' - \hat{x}$.

Let $T_k = \sum_{j=1}^{k} \tau_j$ be the position of the walker after k steps and let $\tilde{\varphi}_k(T_k)$ be the corresponding distribution function. Then

$$\begin{aligned}\tilde{\varphi}_{k+1}(T_{k+1}) &= \int_{\hat{x}}^{\Theta_{k-1}+\hat{x}} dT_k \int_0^{\Theta_k+\hat{x}-T_k} d\tau \;\; \tilde{\varphi}_k(T_k)\rho(\tau)\,\delta(T_{k+1} - T_k - \tau) \\ &= H(\Theta_k + \hat{x} - T_{k+1}) \int_{\hat{x}}^{\Theta_{k-1}+\hat{x}} dT_k\, \tilde{\varphi}_k(T_k)\,\rho(T_{k+1} - T_k) \end{aligned} \tag{7.35}$$

is the probability to find the walker after $k + 1$ steps at position T_{k+1} in front of the border and:

$$\begin{aligned}\phi_k(A) &= \int_{\hat{x}}^{\Theta_{k-1}+\hat{x}} dT_k \int_{\Theta_k+\hat{x}-T_k}^{\infty} d\tau \;\; \tilde{\varphi}_k(T_k)\,\rho(\tau)\,\delta(A - T_k - \tau) \\ &= H(A - \Theta_k - \hat{x}) \int_{\hat{x}}^{\Theta_{k-1}+\hat{x}} dT_k\, \tilde{\varphi}_k(T_k)\,\rho(A - T_k) \end{aligned} \tag{7.36}$$

is the probability of realising a first passage time interval of duration A by performing $k + 1$ steps respectively.

Equation (7.35) provides a recursive relation for the calculation of the distribution functions $\tilde{\varphi}_k(T_k)$, which simplifies when introducing the displacement x_k between the walker and the absorbing boundary after k steps.

$$x_k = \Theta_{k-1} + \hat{x} - T_k = \Theta + (k-1)\Delta + \hat{x} - T_k \tag{7.37}$$

Note, that x_k denotes the displacement after the step k is performed but before the border is shifted. Hence, after the first step the displacement between the walker and the absorbing border is $x_0 = \Theta + \hat{x} - \tau_1$. Expressing τ in terms of the successive displacements x_k and x_{k+1}

$$\tau = x_k - x_{k+1} + \Delta \tag{7.38}$$

yields

$$\varphi_{k+1}(x) = \int_0^{\infty} \varphi_k(x')\,\rho(x' - x + \Delta)dx' \tag{7.39}$$

where $x = x_{k+1}$, $x' = x_k$ and $\varphi_k(x) = \tilde{\varphi}_k(x)H(x)H(\Theta_k - x)$.

As next we introduce the generating function $G(x, s)$ of the distribution functions $\varphi_k(x)$

$$G(x, s) = \sum_{k=1}^{\infty} \varphi_k(x)\; s^k \tag{7.40}$$

and write

$$\sum_{k=1}^{\infty} \varphi_{k+1}(x)\; s^k = \sum_{k=2}^{\infty} \varphi_k(x)\; s^{k-1} = \sum_{k=1}^{\infty} \varphi_k(x)\; s^{k-1} - \varphi_1(x) = \frac{1}{s} G(x,s) - \varphi_1(x)\,. \tag{7.41}$$

This allows us to rewrite eq. (7.39) into

$$G(x,s) - \int_0^{\infty} G(x',s)\; s\, \rho(x' - x + \Delta)\, dx' = s\varphi_1(x)\,. \tag{7.42}$$

Equation (7.42) displays an *inhomogeneous Wiener-Hopf integral equation* which completely determines the generating function $G(x,s)$ for any given distribution $\rho(x')$, since $\varphi_1(x)$ is determined by:

$$\varphi_1(x_1) = \rho(\Theta + \hat{x} - x_1)\, H(x_1)\, H(\Theta - x_1)\,. \tag{7.43}$$

Note, that eq. (7.42) provides a general solution of the discussed first passage time problem for any considered distribution $\rho(\tau)$.[4]

Wiener Hopf problem : Principle solution

Before discussing several particular solutions of eq. (7.42) we give a brief overview to the general method for solving Wiener-Hopf equations. A so-called *inhomogeneous Wiener-Hopf integral* is a equation of kind:

$$y(x) - \int_0^{\infty} K(x-t)\, y(t)\, dt = g(x) \quad , \quad 0 \le x < +\infty \tag{7.44}$$

which in the special case $g(x) = 0$ turns into a so-called *homogeneous Wiener-Hopf integral*. Given the functions $K(x)$ and $g(x)$, eq. (7.44) fully determines the function $y(x)$. The estimation of $y(x)$ is the so-called *Wiener-Hopf problem*.

First we focus on the analytical properties of the Fourier Transformation and introduce the Fourier Transform $\tilde{y}(u)$ of the function $y(x)$ as

$$\tilde{y}(u) = \frac{1}{\sqrt{2\pi}} \int_{-\infty}^{\infty} y(x)\, e^{\mathrm{i}ux}\, dx\,. \tag{7.45}$$

In accordance to

$$y(x) = y_-(x)\, H(-x) + y_+(x)\, H(x) \tag{7.46}$$

[4]Note, that the deduction of the Wiener-Hopf equation is independent from the considered distribution $\rho(\tau)$. Eq. (7.42) provides a general solution of the first passage time problem. On the other hand it has to be mentioned, that a basic method for the solution of the Wiener-Hopf problem is given only for a special class of functions $\rho(\tau)$. However, this fact does not affect the general character of relation (7.42).

the Fourier Transform $\tilde{y}(u)$ can be written as

$$\begin{aligned}\tilde{y}(u) &= \tilde{y}_-(u) + \tilde{y}_+(u)\\ \tilde{y}_+(u) &= \frac{1}{\sqrt{2\pi}} \int_0^\infty y_+(x)\, e^{\mathrm{i}ux}\, dx\\ \tilde{y}_-(u) &= \frac{1}{\sqrt{2\pi}} \int_{-\infty}^0 y_-(x)\, e^{\mathrm{i}ux}\, dx\end{aligned} \tag{7.47}$$

where $\tilde{y}_+(u)$ and $\tilde{y}_-(u)$ denote the Fourier Transform of $y_+(x)$ and $y_-(x)$ respectively. The function $\tilde{y}_+(u)$ is analytical in the subspace $Im(u) > k_-$, in the case

$$|y_+(x)| < M\, e^{k_- x} \quad , \quad x \to \infty\,. \tag{7.48}$$

In accordance to eqs. (7.47) the homogeneous Wiener-Hopf equation can be rewritten into

$$y_+(x) + y_-(x) = \int_0^\infty K(x-t)\, y_+(t)\, dt \tag{7.49}$$

with

$$\begin{aligned}y_+(x) &= \int_0^\infty K(x-t)\, y_+(t)\, dt \quad , \quad x > 0\\ y_-(x) &= \int_0^\infty K(x-t)\, y_+(t)\, dt \quad , \quad x < 0\,.\end{aligned} \tag{7.50}$$

The Fourier Transform $\tilde{K}(u)$ of $K(x)$ is analytical for $k_- < Im(u) < k_+$, in case that $K(x)$ satisfies:

$$\begin{aligned}|K(x)| &< M\, e^{k_- x} \quad , \quad x \to +\infty\\ |K(x)| &< M\, e^{k_+ x} \quad , \quad x \to -\infty\,.\end{aligned} \tag{7.51}$$

Furthermore, given that

$$|y_+(x)| < M_1\, e^{\mu x} \quad , \quad x \to +\infty \tag{7.52}$$

for $\mu < k_+$, the integrals in eqs. (7.50) converge and $y_-(x)$ fulfils

$$|y_-(x)| < M_2\, e^{k_+ x} \quad , \quad x \to -\infty\,. \tag{7.53}$$

In order to solve eq. (7.49) we perform the Fourier Transformation and obtain

$$\tilde{y}_+(u)[1 - \tilde{K}(u)] + \tilde{y}_-(u) = 0\,. \tag{7.54}$$

As next the term $[1 - \tilde{K}(u)]$ is factorised in that way

$$[1 - \tilde{K}(u)] = \frac{\omega_+(u)}{\omega_-(u)} \tag{7.55}$$

that the functions $\omega_+(u)$ and $\omega_-(u)$ are (i) analytical for $Im(u) > \mu$ and $Im(u) < k_+$ re-

spectively and (ii) do not increase faster than a polynomial u^n of order n for $|u| \to \infty$. Accordingly eq. (7.54) is rewritten into

$$\omega_+(u)\,\tilde{y}_+(u) = -\omega_-(u)\,\tilde{y}_-(u)\,. \tag{7.56}$$

Note, that the left hand side of eq. (7.56) is analytical in the upper half space of the complex plane for $Im(u) > \mu$, while the right hand side is analytical in the lower half for $Im(u) < k_+$. Hence both sides of the equation are analytical for $\mu < k_+$. As such there exists a complex function, analytical in the entire complex plane which is equal to the left hand side of eq. (7.56) in the upper half plane and which is equal to the right hand side in the lower half respectively. In accordance to the sentence of Liouville, this function is a polynomial $P_{n-1}(u)$ of order $n-1$, if not one of the functions in eq. (7.56) increase faster than u^n for $|u| \to \infty$. Given that, we write

$$\omega_+(u)\,\tilde{y}_+(u) = -\omega_-(u)\,\tilde{y}_-(u) = P_{n-1}(u) \tag{7.57}$$

and obtain

$$\tilde{y}_+(u) = \frac{P_{n-1}(u)}{\omega_+(u)} \qquad , \qquad \tilde{y}_-(u) = -\frac{P_{n-1}(u)}{\omega_-(u)}\,. \tag{7.58}$$

The Fourier Transformation of eq. (7.58) yields the desired functions $y_+(u)$ and $y_-(u)$, except of the constant factors in the polynomial $P_{n-1}(u)$. These factors can be determined by further conditions which are due to the observed physical problem.

In case of an inhomogeneous Wiener-Hopf equation, eq. (7.54) writes

$$\tilde{y}_+(u)\,[1 - \tilde{K}(u)] + \tilde{y}_-(u) = \tilde{g}(u) \tag{7.59}$$

where $\tilde{g}(u)$ is the Fourier Transform of $g(x)$. Factorising $[1 - \tilde{K}(u)]$ according to eq. (7.55) yields

$$\omega_+(u)\,\tilde{y}_+(u) = -\omega_-(u)\,\tilde{y}_-(u) + \omega_-(u)\,\tilde{g}(u) = -\omega_-(u)\,\tilde{y}_-(u) + d(u)\,. \tag{7.60}$$

One now express $d(u)$ as $d(u) = d_-(u) + d_+(u)$, where $d_-(u)$ and $d_+(u)$ are analytical for $Im(u) < h_+$ and for $Im(u) > h_-$ respectively. In case (i) that the regions, in which the functions in eq. (7.60) are analytical, overlap and share a region $k''_- < Im(u) < k''_+$ and (ii) that the functions $d_-(u)$ and $d_+(u)$ do not increase faster than a polynomial u^n of order n for $|u| \to \infty$, eq. (7.60) can be rewritten into

$$\tilde{\omega}_+(u)\,\tilde{y}_+(u) - d_+(u) = d_-(u) - \omega_-(u)\,\tilde{y}_-(u) = P_{n-1}(u) \tag{7.61}$$

where again $P_{n-1}(u)$ denotes a polynomial in u of order $n-1$. Note, that the left hand side in eq. (7.61) is analytical for $k''_- < Im(u)$ while the right hand side is analytical for $Im(u) < k''_+$. Thus one finally obtain

$$\tilde{y}_+(u) = \frac{P_{n-1}(u) + d_+(u)}{\omega_+(u)} \qquad , \qquad \tilde{y}_-(u) = -\frac{P_{n-1}(u) - d_-(u)}{\omega_-(u)} \tag{7.62}$$

and the functions $y_+(x)$ and $y_-(x)$ after Fourier Transformation.

7.3.3 Specific models

We study the statistical properties of ventricular intervals r predicted by the proposed conduction model for different waiting time densities (WTD) $\rho(\tau)$. In particular we concentrate on an exponential WTD

$$\rho(\tau) = f \exp(-f\tau)\, H(\tau) \tag{7.63}$$

and on an Erlang WTD[5]

$$\rho(\tau) = f^p \, \frac{\tau^{p-1}}{(p-1)!} \, e^{-f\tau} \, H(\tau) \,. \tag{7.64}$$

Often the atrial interbeat intervals are suggested to be Gaussian distributed since the transduction of impulses through the atrium is influenced by the electrophysiological states of all cells and hence is affected by different times and timescales. In contrast to this, we consider the intervals τ to be Erlang distributed. This is due to the fact that (i) distributions of real intervals τ can be well approximated by this class of distributions and that (ii) the general solution of the Wiener-Hopf problem can be successfully applied for this kind of distribution.

Furthermore we consider an exponential AV nodal recovery curve

$$t_{\mathrm{con}}(t_{\mathrm{rec}}) = \alpha + \beta \exp(-t_{\mathrm{rec}}/\tau_{\mathrm{AV}}) \,. \tag{7.65}$$

Without loss of generality we define τ_{AV} as our time unit and set $\tau_{\mathrm{AV}} = 1$. Hence achieved results are transformed into standard time units when dividing times (e.g. α, β, Θ_k, etc.) and probability densities of time intervals by τ_{AV}.

We also consider two specific forms of refractory periods Θ_k:

- a constant one $\Theta_k = \Theta$, not affected by a blocking of atrial impulses during t_{ref}
- a variable one $\Theta_j = \Theta + j\Delta \,, \quad j = 0, 1, \ldots$, extended by the time increment Δ whenever an atrial impulse is blocked during t_{ref}.

Exponential WTD and constant refractory period

At first we discuss a conduction model with constant refractory period $\Theta_k = \Theta$ and consider the atrial intervals τ to be generated by a Poisson process. Due to the absence of memory in the Poisson process, the transition probability density $\phi(A|A', V')$, that the first conducted atrial impulse occurs at the AV node at time A after an event (A', V'), is independent of A'.

$$\phi(A|A', V') = \sum_{k=0}^{\infty} \phi_k(A|A', V') \tag{7.66}$$

Consequently we write $\phi(A|A', V') = \phi_{\mathrm{P}}(A - V')$, where the subscript P marks the presence of the Poisson process. The probability that an atrial impulse does not occur at the node

[5] The Erlang distribution is a special case of the Gamma distribution in which the order p is an integer.

during the interval $A-V'-\Theta$, is $\exp[-f(A-V'-\Theta)]$. Hence we write:

$$\phi_{\mathrm{P}}(A-V') = \phi(A|A', V') = f\exp[-f(A-V'-\Theta)]H(A-V'-\Theta) \tag{7.67}$$

which in combination with eqs. (7.26) and (7.65) yields:

$$\begin{aligned}\psi_{\mathrm{P}}(A-V', V-V') &= \psi(A, V|A', V') \\ &= \delta(V - A - \alpha - \beta e^{-(A-V'-\Theta)}) f e^{-f(A-V'-\Theta)}\, H(A-V'-\Theta)\,. \end{aligned} \tag{7.68}$$

We introduce the times $a = A-V'$ and $r = V-V'$ and rewrite eq. (7.68) into:

$$\psi_{\mathrm{P}}(a, r) = \delta(r-a-\alpha-\beta\, e^{-(a-\Theta)})\, f e^{-f(a-\Theta)}\, H(a-\Theta)\,. \tag{7.69}$$

If we take into account the normalisation of $p(v)$, eq. (7.69) yields

$$\begin{aligned} p(v) &= \int_0^\infty da\, \psi_{\mathrm{P}}(a, v+a) && (7.70)\\ &= \int_0^\infty da\, \delta(v - \alpha - \beta\, e^{-(a-\Theta)/\tau_{\mathrm{AV}}})\, f e^{-f(a-\Theta)} H(a-\Theta) \\ &= \frac{f}{\beta}\left(\frac{\beta}{v-\alpha}\right)^{1-f}, \quad \alpha < v \le \alpha+\beta\,. && (7.71)\end{aligned}$$

We find $p(V-A) = 0$ for all $V-A < \alpha$ and $V-A > \alpha+\beta$, which is due to the fact that the interval $V-A$ cannot not be smaller than the minimal conduction time but also not be larger than the maximal conduction time. We note, that eq. (7.70) can be derived directly without referring to the formal solution: Without loss of generality we can set $V' = 0$ and project out from all possible time instants A only those that satisfy $v = V-A = t_{\mathrm{con}}(A-\Theta)$. Note, that $p(v)$ in eq. (7.68) corresponds to the probability density distribution of PR intervals in the surface ECG.

While in the presence of AF the P waves cannot be identified we here concentrate on the distribution $w(r)$ of ventricular interbeat intervals. Therefore we introduce $r = a + t_{\mathrm{con}}(a-\Theta)$ and project out from the possible time instants $a = A - V'$ only those which satisfy $r = a + t_{\mathrm{con}}(a-\Theta)$.

$$\begin{aligned} w(r) &= \int_\Theta^\infty da\, f e^{-f(a-\Theta)}\, \delta(r - a - \alpha - \beta\, e^{-(a-\Theta)}) \\ &= \int_0^\infty du\, f e^{-fu}\, \delta(r - u - \Theta - \alpha - \beta\, e^{-u}) \end{aligned} \tag{7.72}$$

The same result is obtained when following the formal solution and calculating the n-point joint probabilities $w_n(V_1, \ldots, V_n)$ for the sequence $V_1, \ldots, V_n$ of ventricular excitation

times

$$\begin{aligned} w_n(V_1,\ldots,V_n) &= \int dA_1 \ldots \int dA_n\, p_n(A_1,V_1;\ldots;A_n,V_n) \\ &= \int dA_1 \ldots \int dA_n\, p_1(A_1,V_1) \prod_{i=1}^{n-1} \psi(A_{i+1},V_{i+1}|A_i,V_i) \\ &= \int dA_1\, p(V_1-A_1) \prod_{i=1}^{n-1} \int dA_{i+1}\, \psi_{\mathrm{P}}(A_{i+1}-V_i, V_{i+1}-V_i) \\ &= \prod_{i=1}^{n-1} w(V_{i+1}-V_i) \end{aligned} \tag{7.73}$$

where

$$w(r) = \int du\, \psi_{\mathrm{P}}(u,r)\,. \tag{7.74}$$

Note, that eq. (7.73) implies that the intervals r_i are uncorrelated and that eq. (7.74) agrees with eq. (7.72).

To solve the integral in eq. (7.72), we have to find the zeros of the argument of the δ-function with respect to $u = a-\Theta > 0$. As such we introduce $\tilde{r} = (r–\alpha–\Theta)$ and obtain the determining equation:

$$g(u) = u + \beta\, e^{-u} = \tilde{r}\,. \tag{7.75}$$

For the further work two different cases have to be distinguished, *(i)* $\beta > 1$ and *(ii)* $\beta \le 1$. For the first case *(i)* the function $g(u)$ exhibits a minimum at $u_{\min} = \ln[\beta] > 0$. Depending on the value of $\tilde{r}$ we can distinguish different scenarios. We find two distinct positive solutions $u_{1,2} = u_{1,2}(\tilde{r})$ (with $u_1 < u_{\min} < u_2$) for $g(u_{\min}) = 1 + \ln[\beta] < \tilde{r} < g(0) = \beta$. These solutions merge when $\tilde{r} = g(u_{\min}) = 1 + \ln[\beta]$. Hence, $u_{\min} = u_{1,2} = \ln[\beta]$ becomes a double root of eq. (7.75) which yields a square root singularity of $w(r)$ for $\tilde{r} \to 1+\ln[\beta]$ (see eqs. (7.80) and (7.81) below). For $\tilde{r} > g(0) = \beta$, only the root u_2 remains positive. For large intervals a and hence large $\tilde{r}$ values this root can be approximated by the asymptotic solution $u_2^{\mathrm{as}} = \tilde{r}$. In case *(ii)* on the other hand, there exists only the solution $u_2(\beta,\tilde{r})$ for $\tilde{r} > g(0) = \beta$.

Thus we finally obtain:

$$\beta \le 1: \qquad w(r) = w_2(r)\,, \qquad r_2 \equiv \Theta + \alpha + \beta < r \tag{7.76}$$

$$\beta > 1: \qquad w(r) = \begin{cases} w_1(r) + w_2(r)\,, & r_1 \equiv \Theta + \alpha + 1 + \ln\beta < r < r_2 \\ w_2(r)\,, & r_2 \le r \end{cases} \tag{7.77}$$

$$w_1(r) = \frac{f e^{-f u_1}}{\beta\, e^{-u_1} - 1}\,, \qquad w_2(r) = \frac{f e^{-f u_2}}{1 - \beta\, e^{-u_2}}\,. \tag{7.78}$$

The times r_1 and r_2 mark the smallest ventricular interval that can be observed for the special cases $\beta > 1$ and $\beta \le 1$ respectively. Note, that the smallest interval r_2 observed for $\beta \le 1$ is longer than the smallest interval r_1 in case $\beta > 1$. This feature can be easily understood from the AV nodal recovery curve (eq. (7.65)).

Again we note, that in case of a constant refractory period the ventricular response is mostly

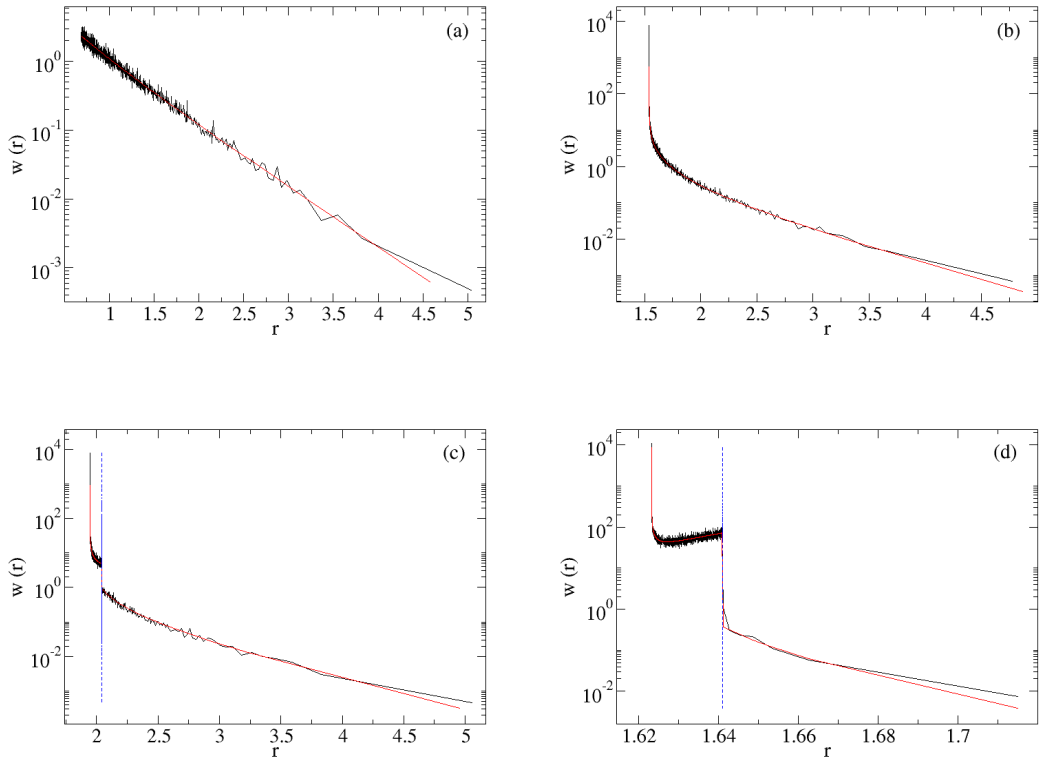

Figure 7.7: Possible shapes of the probability density $w(r)$ of intervals r for exponentially distributed intervals τ and a constant refractory period. The AV conduction process is characterised by an exponential AV nodal recovery curve $\alpha + \beta \exp(-t_{\mathrm{rec}}/\tau_{\mathrm{AV}})$: *(a)* $\beta < 1$, *(b)* $\beta = 1$, *(c)* $\beta > 1$ and $f < f_c$, *(d)* $\beta > 1$ and $f > f_c$. The time τ_{AV} is chosen as time unit.

determined by the recovery time t_{rec} and the conduction time t_{con}. Ventricular intervals of a given length result either from long recovery times and hence small conduction times or vice versa. This fact is reflected in the two distinct roots u_1 and u_2 found for $\beta > 1$. In this particular case the conduction time t_{con} is limited to $t_{\mathrm{rec}} < \ln\beta$. Hence we observe the smallest ventricular interval $r_1 = \Theta + \alpha + 1 + \ln\beta$, when the conducted impulse occurs at the node at time $A = V' + \Theta + \ln\beta$. This becomes different for $\beta \leq 1$. In this case the conduction time does not increase strong enough to balance the sum $t_{\mathrm{rec}} + t_{\mathrm{con}}$ of both times, when the recovery time decreases. This fact becomes particular clear when we focus on the derivate $d(t_{\mathrm{rec}} + t_{\mathrm{con}})/dt_{\mathrm{rec}} = 1 - \beta \exp(-t_{\mathrm{rec}})$ which is always greater than zero for $\beta \leq 1$. Accordingly the smallest ventricular interval $r_2 = \Theta + \alpha + \beta$ is observed when the conducted atrial impulse occur at the node right after the end of the refractory period. The functions $w_1(r)$ and $w_2(r)$ follow

$$\beta < 1: \qquad w(r) = \frac{f}{1-\beta} - \frac{f[f(1-\beta)+\beta]}{(1-\beta)^3}(r-r_2) + O\left((r-r_2)^2\right) \tag{7.79}$$

$$\beta = 1: \qquad w(r) = \frac{f\beta^{-f}}{\sqrt{2(r-r_2)}} - f^2\beta^{-f} + O\left((r-r_2)^{1/2}\right) \tag{7.80}$$

$$\beta > 1: \qquad w(r) = \frac{2f\beta^{-f}}{\sqrt{2(r-r_1)}} + O\left((r-r_1)^{1/2}\right) \tag{7.81}$$

for small time intervals $r - r_{1,2}$, and follow

$$w(r) \sim f e^{f(\Theta+\alpha)} e^{-fr}, \qquad r \to \infty \tag{7.82}$$

in the limit of large ventricular intervals. The exponential decay in (7.82) equals the decay of the exponential WTD of the atrial impulses (see eq. (7.63)) and hence directly reflects this distribution. Due to the constant refractory period and due to the limited conduction time t_{con},in the considered model large intervals r are originated from large atrial intervals. Hence the statistics of those intervals is not affected by the special shape of the recovery curve.

The discussion of the monotonic behaviour of $w_{1,2}(r)$ points out, that the considered model predicts several shapes of the distributions (see Appendix A). As an example, fig. 7.7 displays the distribution $w(r)$ for different sets of parameters. For $\beta \leq 1$, $w(r)$ is a smooth and monotonously decaying function as it can be seen in the panels (a) and (b). In case $\beta < 1$ the distribution $w(r)$ approaches $f/(1-\beta)$ for $r \to r_2$ and exhibits a square root singularity for $r \to r_2$ (see eq. (7.80)). For $\beta > 1$ on the other hand, we observe a discontinuity $\Delta w = f/(\beta - 1)$ in $w(r)$ at $r = r_2$, which is clear to see in panels the (c) and (d) in fig. 7.7. For intervals $r \geq r_2$, $w(r)$ monotonously decreases but exhibits a square root singularity in the limit $r \to r_1$. For ventricular intervals $r_1 < r < r_2$ the behaviour of $w(r)$ strongly depends on the rate f of the atrial impulses: $w(r)$ is a monotonic decaying function for atrial rates f smaller than a critical frequency $f_c > \beta/(\beta - 1) > 1$. For frequencies $f > f_c$ the function exhibits a minimum at $r = r_{\min}$ with $r_1 < r_{\min} < r_2$ as displayed in panel (d) of fig. 7.7.

Exponential WTD and fluctuating refractory period

We consider the atrial excitations to generate a Poisson process with rate f and a refractory period Θ_k which is extended by Δ, whenever an atrial impulse is blocked by the node during its refractory state. We note, that the transition probability $\psi(A, V|A', V')$ is still independent of A'. Due to the stationarity of the process we again introduce $a = A - V'$ and $v = V - V'$ and express $\psi(A, V|A', V')$ by the function $\psi_{\mathrm{P}}(a, v)$. The results (7.70), (7.73) and (7.74) remain valid, since they are independent of the specific form of $\psi_{\mathrm{P}}(a, v)$. The absence of memory in the Poisson process enables us to calculate $\phi_k(A|A', V') = \varphi_k(A - V')$ directly without referring to eq. (7.34), since the probability distribution for the times of the first atrial excitation after a ventricular one does not depend on the time of the foregoing atrial excitation. With the notations in section 7.3.1 [see eq. (7.27)] we write

$$\begin{aligned}
\varphi_k(a) &= H(a-\Theta_k) \int d\tau_1\, \rho(\tau_1) \ldots \int d\tau_{k+1}\, \rho(\tau_{k+1}) \Big[\prod_{j=1}^{k} H(\Theta_{j-1} - T_j)\Big] \delta(a - T_{k+1}) \\
&= H(a-\Theta_k) \int d\tau_1\, \rho(\tau_1) \ldots \int d\tau_k\, \rho(\tau_k) \Big[\prod_{j=1}^{k} H(\Theta_{j-1} - T_j)\Big] f e^{-f(a-T_k)}
\end{aligned}$$

$$
\begin{aligned}
&= H(a-\Theta_k)\, f^{k+1} e^{-fa} \int_0^\infty d\tau_1 \ldots \int_0^\infty d\tau_k \prod_{j=1}^{k} H(\Theta_{j-1}-T_j) \\
&= H(a-\Theta_k)\, f^{k+1} e^{-fa} I_k
\end{aligned} \tag{7.83}
$$

where I_k is given by:

$$
\begin{aligned}
I_k &= \int_0^{\Theta_0} d\tau_1 \int_0^{\Theta_1-\tau_1} d\tau_2 \int_0^{\Theta_2-\tau_1-\tau_2} d\tau_3 \ \ldots \int_0^{\Theta_{k-1}-\tau_1-\ldots-\tau_{k-1}} d\tau_k \\
&= \int_0^{\Theta_0} d\tau_1 \int_{\tau_1}^{\Theta_1} d\tau_2 \int_{\tau_2}^{\Theta_2} d\tau_3 \ldots \int_{\tau_{k-1}}^{\Theta_{k-1}} d\tau_k \\
&= \frac{\Theta_0 \Theta_k^{k-1}}{k!} \,.
\end{aligned} \tag{7.84}
$$

Note, that I_k satisfies the recursive relation $I_{k+1}(\Theta_0, \Delta) = \int_0^{\Theta_0} d\tau_1 I_k(\Theta_1 - \tau_1, \Delta)$ which follows from the first line of eq. (7.84) when substituting $\tau_j \rightarrow \tau'_j = \tau_j - \tau_1$ for $j = 2, 3, \ldots, k+1$. The solution in eq. (7.84) can be proven by complete induction.

$$
\begin{aligned}
&\int_0^{\Theta_0} I_k(\theta_1 - \tau_1, \Delta)\, d\tau_1 = \int_0^{\Theta_0} \frac{(\Theta_1 - \tau_1)(\Theta_1 - \tau_1 + k\Delta)^k}{k!}\, d\tau_1 = \\
&= -\frac{1}{k!} \int_0^{-\Theta_0} (\Theta_1 + \tau_1)(\Theta_1 + \tau_1 + k\Delta)^{k-1} = -\frac{1}{k!} \int_{\Theta_1}^{\Theta_1 - \Theta_0} \tau_1 (\tau_1 + k\Delta)^{k-1}\, d\tau_1 = \\
&= -\frac{1}{k!} \int_{\Theta_1 + k\Delta}^{\Theta_{k+1} - \Theta_0} \left[\tau_1^k - k\Delta\tau_1^{k-1}\right] d\tau_1 = -\frac{1}{k!} \left[\frac{\tau_1^{k+1}}{k+1} - \Delta\tau_1^k\right]_{\Theta_{k+1}}^{\Theta_{k+1}-\Theta_0} = \\
&= -\frac{1}{(k+1)!} \left[(k+1)\Delta\tau_1^k - \tau_1^{k+1}\right]_{\Theta_{k+1}-\Theta_0}^{\Theta_{k+1}} = \left(\frac{\tau_1^k}{(k+1)!} \left[(\Theta_{k+1} - \Theta_0) - \tau_1\right]_{\Theta_{k+1}-\Theta_0}^{\Theta_{k+1}}\right) \\
&= \frac{\Theta_{k+1}^k}{(k+1)!}\Theta_0
\end{aligned}
$$

In accordance to eq. (7.84) we obtain

$$
\phi_k(A|A', V') = \varphi_k(A - V') = H(A - V' - \Theta_k)\, \frac{f\Theta_0 (f\Theta_k)^{k-1}}{k!}\, f\, e^{-f(A-V')} \,. \tag{7.85}
$$

For $\Delta = 0$, we get the same results as in eq. (7.67) after summation over k, since $(f^{k-1} I_k)$ equals the Taylor series of $exp(-f\Theta)$. According to the eqs. (7.26) and (7.65) the transition probability $\psi_{\mathrm{P}}(A - V', V - V')$ writes:

$$
\psi_{\mathrm{P}}(A - V', V - V') = \sum_{k=0}^{\infty} \frac{f\Theta_0 (f\Theta_k)^{k-1}}{k!}\, f\, e^{-f(A-V')}\, H(A - V' - \Theta_k)\, \delta(V - A - \alpha - \beta e^{-(A-V'-\Theta)})
$$

and one obtains

$$
\psi_{\mathrm{P}}(a, r) = \sum_{k=0}^{\infty} \frac{f\Theta_0 (f\Theta_k)^{k-1}}{k!}\, f\, e^{-f(a)}\, H(a - \Theta_k)\, \delta(r - a - \alpha - \beta e^{-(a-\Theta_k)}) \tag{7.86}
$$

after inserting $a = A - V'$ and $r = V - V'$.

To achieve $w(r)$ we project out only those times $a = A - V'$ which satisfy $r = t_{\mathrm{con}}(a - \Theta_k)$ and thus finally obtain

$$\begin{aligned} w(r) &= \sum_{k=0}^{\infty} \frac{f\Theta_0(f\Theta_k)^{k-1}}{k!} \int_{\Theta_k}^{\infty} da\, f\, e^{-f(a)}\, \delta(r - a - \alpha - \beta e^{-(a-\Theta_k)}) \\ &= \sum_{k=0}^{\infty} \frac{f\Theta_0(f\Theta_k)^{k-1}}{k!}\, e^{f\,\Theta_k} \int_0^{\infty} du\, f\, e^{-f\,u_k} \\ &= \sum_{k=0}^{\infty} \frac{f\Theta_0(f\Theta_k)^{k-1}}{k!}\, e^{f\,\Theta_k} \tilde{w}(r) \end{aligned} \tag{7.87}$$

where $\tilde{w}(r)$ denotes the solutions expressed in eq. (7.78).

Possible shapes of distributions $w(r)$ are displayed in fig. 7.8 (black curves: distributions of simulated intervals r, red curves: distributions according to eq. (7.87). The parameters are chosen in that way, that the influence of the conduction time t_{con} on the ventricular response continuously increase. Thus, the representation in panel (a) refer to a realisation of the model in which the conduction time is completely neglected and the one in panel (d) refer to a realisation for which the ventricular response is mainly determined by t_{con}. The model predicts both distributions with a pronounced maximum and those that are monotonously decaying. The weaker the influence of the conduction time t_{con} the more pronounced the maximum in $w(r)$ is. The striking equidistant spikes that are observed in panel (c) and panel (d) mark the end of the different refractory periods Θ_k. Between the spikes the distributions exhibit exponential decays, caused by the multiple prolongation of the refractory period, and several discontinuities, caused by the considered AV nodal recovery curve. For $t_{\mathrm{con}} = 0$, the ventricular intervals r equal the time intervals a and hence $w(r)$ writes

$$w(r) = \; e^{-fr} \sum_{k=0}^{\infty} \frac{f\Theta_0(f\Theta_k)^{k-1}}{k!}\, H(r - \Theta_k)\,. \tag{7.88}$$

In this case the monotonic behaviour of $w(r)$ is determined only by the convergence behaviour of the sum in eq. (7.88), since e^{-fr} always decays. The sum only converges for $f\Delta \leq e^{-1}$. Otherwise the sum decreases until

$$ef\Delta > \left(1 + \frac{1}{k}\right)^{3/2} \tag{7.89}$$

and diverges for larger values in k.

Erlang WTD and constant conduction time $t_{\mathrm{con}} = 0$

We consider a conduction model with Erlang distributed intervals τ and constant conduction time $t_{\mathrm{con}} = 0$. Every atrial impulse blocked during the refractory period Θ_k extend this period by the time increment Δ. Hence, the parameter $\hat{x}$ in eq. (7.31) becomes zero, the Heaviside jump function $H(\hat{x})$ in eq. (7.31) vanishes, the times between successfully conducted atrial impulses equal the time interval between the corresponding ventricular

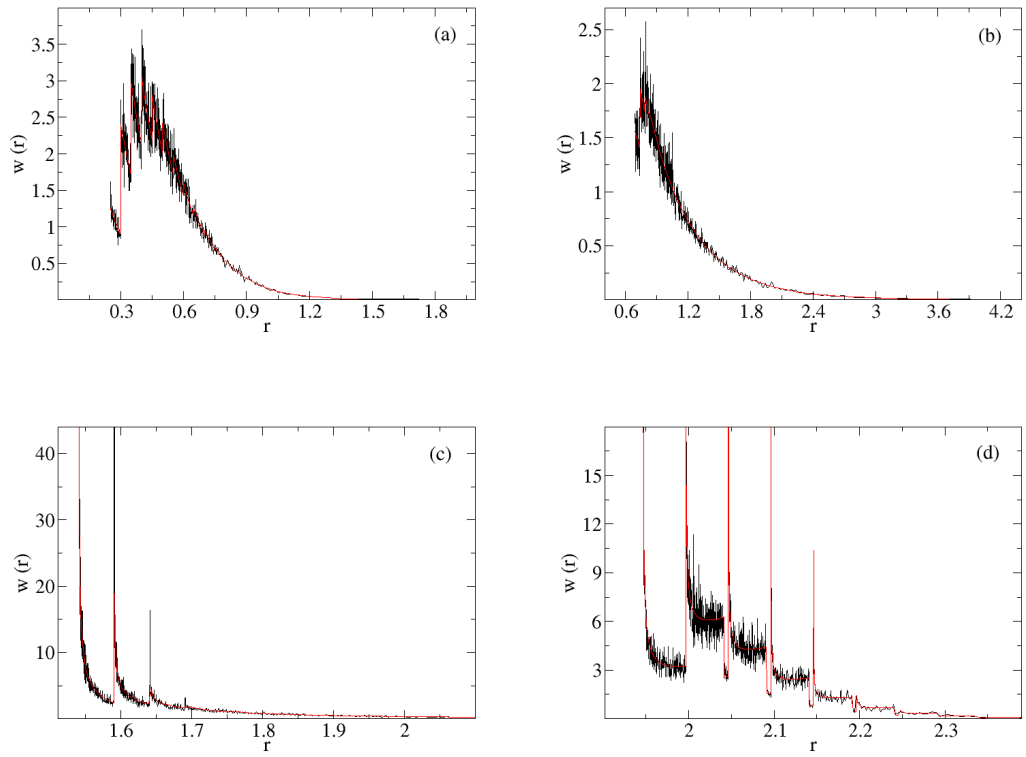

Figure 7.8: Possible shapes of the probability density $w(r)$ of intervals r for exponentially distributed intervals τ. The AV conduction process is characterised by a variable refractory period Θ_k and an exponential AV nodal recovery curve $\alpha + \beta \exp(-t_{\text{rec}}/\tau_{\text{AV}})$ (eq. (7.65)): (panel a) $t_{\text{con}} = 0$, (panel b) $\beta < 1$, (panel c) $\beta = 1$, (panel d) $\beta > 1$ and $f > f_c$. $\tau_{\text{AV}} = 1$ is chosen as time unit. The panels show both distributions of simulated intervals r (black curves) and distributions calculated according to eq. (7.88) (red curves).

excitations and the stochastic process (A_n, V_n) becomes (A_n). Furthermore the probability $\phi(A|A')$ for the first successfully conducted atrial impulse to arrive at the AV node at time A after an event (A'), becomes independent of A'. Accordingly we write $\phi_k(A) = \phi_k(A|A', V')$, which now denotes the probability for an interval $r = A$ to be originated by the blocking k atrial impulses during the refractory period Θ_k.

For the considered model the functions $K(x)$ and $g(x)$ are given as:

$$K(x) = s\,\rho(\Delta - x) \;= sf^p\,\frac{(\Delta - x)^{p-1}}{(p-1)!}\,e^{-f(\Delta - x)}\,H(\Delta - x) \tag{7.90}$$

and

$$g(x) = s\,\varphi_1(x) = sf^p\,\frac{(\Theta - x)^{p-1}}{(p-1)!}\,e^{-f(\Theta - x)}\,H(\Theta - x)\,H(x) \tag{7.91}$$

respectively (see eqs. (7.42), (7.44) and (7.64). The Fourier Transform $\tilde{K}(u)$ and $\tilde{g}(u)$ of

$K(x)$ and of $g(x)$

$$\begin{aligned}\tilde{K}(u) &= \int_{-\infty}^{+\infty} K(x)\, e^{\mathbb{i}ux}\, dx = \frac{s\, f^p\, e^{\mathbb{i}u\Delta}}{(f+\mathbb{i}u)^p} \\ \tilde{g}(u) &= \int_{-\infty}^{+\infty} g(x)\, e^{\mathbb{i}ux}\, dx = \frac{s\, f^p\, e^{\mathbb{i}u\Theta}}{(f+\mathbb{i}u)^p} - \sum_{g=0}^{p-1} \frac{\Theta^{p-1-g}\, s\, f^p\, e^{-f\Theta}}{(p-1-g)!\,(f+\mathbb{i}u)^{(g+1)}}\end{aligned} \tag{7.92}$$

are analytical for $k_- = -\infty < Im(u) < k_+ = f$, since

$$K(x), g(x) = \begin{cases} 0 & , x \to +\infty \quad , \quad k_- = -\infty \\ Me^{fx} & , x \to -\infty \quad , \quad k_+ = f \end{cases} . \tag{7.93}$$

(7.94)

In accordance to eq. (7.55) we factorise the term $\left[1 - \tilde{K}(u)\right]$ as

$$\left[1 - \tilde{K}(u)\right] = 1 - \frac{sf^p e^{\mathbb{i}u\Delta}}{(f+\mathbb{i}u)^p} = \frac{(f+\mathbb{i}u)^p - sf^p e^{\mathbb{i}u\Delta}}{(f+\mathbb{i}u)^p} = \frac{\tilde{\omega}_+(u)}{\tilde{\omega}_-(u)} \tag{7.95}$$

with

$$\tilde{\omega}_+(u) = (f+\mathbb{i}u)^p - sf^p e^{\mathbb{i}u\Delta} \qquad , \qquad \tilde{\omega}_-(u) = (f+\mathbb{i}u)^p . \tag{7.96}$$

Both $\tilde{\omega}_+(u)$ and $\tilde{\omega}_-(u)$ are analytical in the entire complex plane, since

$$\begin{aligned}\tilde{\omega}_+(u) &\sim (f+\mathbb{i}u)^p \quad , \quad u \to +\infty \quad , \quad Im(u) > \mu \\ \tilde{\omega}_-(u) &\sim (f+\mathbb{i}u)^p \quad , \quad |u| \to \infty .\end{aligned} \tag{7.97}$$

Inserting $\tilde{\omega}_-(u)$ into eq. (7.60) yields

$$\begin{aligned} d(u) &= (f+\mathbb{i}u)^p \left[\frac{s\, f^p\, e^{\mathbb{i}u\Theta}}{(f+\mathbb{i}u)^p} - \sum_{g=0}^{p-1} \frac{\Theta^{p-1-g}\, s\, f^p\, e^{-f\Theta}}{(p-1-g)!\,(f+\mathbb{i}u)^{(g+1)}} \right] \\ &= s\, f^p e^{\mathbb{i}u\Theta} - \sum_{g=0}^{p-1} \frac{\Theta^{p-1-g}\, s\, f^p\, e^{-f\Theta}}{(p-1-g)!}\, (f+\mathbb{i}u)^{(p-1-g)} \\ &= d_+(u) + d_-(u) \end{aligned} \tag{7.98}$$

with

$$\begin{aligned} d_+(u) &= s\, f^p e^{\mathbb{i}u\Theta} \\ d_-(u) &= -\sum_{g=0}^{p-1} \frac{\Theta^{p-1-g}\, s\, f^p\, e^{-f\Theta}}{(p-1-g)!}\, (f+\mathbb{i}u)^{(p-1-g)} . \end{aligned} \tag{7.99}$$

Note, that the so-defined functions are analytical in the entire complex plane, since $p-1 \geq p-1-g \geq 0$.

Due to the particular factorisation of $\left[1 - \tilde{K}(u)\right]$ and due to the particular splitting of $d(u)$, eq. (7.61) writes:

$$\tilde{G}_+(u)\,\omega_+(u) - d_+(u) = d_-(u) - \omega_-(u)\tilde{G}_-(u) = C(u) \tag{7.100}$$

where $\tilde{G}_+(u)$ and $\tilde{G}_-(u)$ are the half sided Fourier Transform of the generating function $G(x, s)$ and where

$$C(u) = P_{p-1}(u) = \sum_{j=0}^{p-1} a_j\, u^j \tag{7.101}$$

is a polynomial in u of order $p-1$, since both $\omega_+(u)$ and $\omega_-(u)$ are polynomials in u of order p. Inserting $d_+(u)$ and $\omega_+(u)$ into eq. (7.100) yields

$$\tilde{G}_+(u) = \frac{C(u) + d_+(u)}{\omega_+(u)} = \frac{s\, f^p e^{\mathrm{i}u\Theta} + \sum_{j=0}^{p-1} a_j\, u^j}{(f + \mathrm{i}u)^p - s f^p e^{\mathrm{i}u\Delta}}\,. \tag{7.102}$$

In order to calculate $G(x, s)$ we perform the inverse Fourier Transformation of $\tilde{G}_+(u)$ and obtain

$$\begin{aligned} G(x,s) = &\sum_{k=0}^{\infty} \frac{s^{k+1} f^{pk+p}}{(pk+p-1)!}\,(\Theta_k - x)^{pk+p-1}\, e^{-f(\Theta_k - x)}\, H(\Theta_k - x) + \\ &+ \sum_{k=0}^{\infty} H(\Delta_k - x)\,\frac{s^k\, e^{-f\,(\Delta_k - x)}}{(pk+p-1)!} \times \\ &\times \left(\sum_{l=0}^{z} \sum_{j=z-l}^{p-1} \binom{z}{l} (\Delta_k - x)^l\, f^{pk+j-z+l} a_j\, \frac{\mathrm{i}^{j-z+2l-pk-p+1}\, j!}{(j-z+l)!} \right) \end{aligned} \tag{7.103}$$

where $z = pk + p - 1$. Expanding the coefficients a_j with respect to s^k and rearranging the sums in eq. (7.103) yields:

$$\begin{aligned} \varphi_k(x) = &\frac{f^{pk}}{(pk-1)!}\,(\Theta_{k-1} - x)^{pk-1}\, e^{-f(\Theta_{k-1} - x)}\, H(\Theta_{k-1} - x) \\ &+\; f^{pk}\, e^{-f\,(\Theta_{k-1} - x)} \sum_{m=1}^{k-1} \sum_{l=0}^{p-1} H(\Delta_{k-m} - x)\, z_{l,m}\, \frac{(\Delta_{k-m} - x)^{l+p(k-m)}}{(l + p(k-m))!} \end{aligned} \tag{7.104}$$

where the coefficients $z_{l,m}$ satisfy the recursive relation:

$$z_{l,k} \;=\; -\frac{\Theta_{k-1}^{pk-1-l}}{(pk-1-l)!} \;-\; \sum_{m=1}^{k-1} \sum_{g=0}^{p-1} z_{g,m}\, \frac{\Delta_{k-m}^{g+p(k-m)-l}}{(g + p(k-m) - l)!}\,. \tag{7.105}$$

In order to calculate the probability $\phi_k(A)$ we substitute the displacement x by $x = \Theta_{k-1} - T_k$,

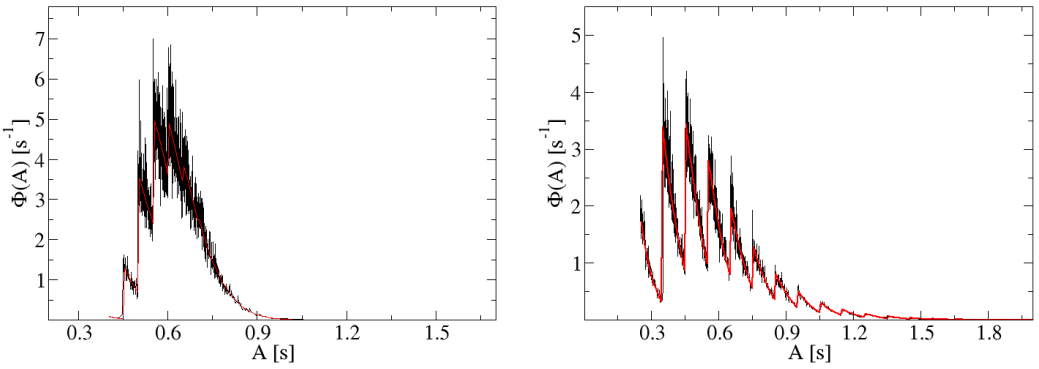

Figure 7.9: Distributions of intervals r for a conduction model with Erlang distributed atrial intervals τ and $t_{\text{con}} = 0$. The black curves display distributions of simulated intervals r while the red ones display theoretical distributions according to eq. (7.106). The parameters used in the simulations are: $\bar{\tau} = 0.157$s, $p = 5$, $\Theta = 0.4$s, $\Delta = 0.05$s (left panel) and $\bar{\tau} = 0.157$s, $p = 5$, $\Theta = 0.25$s, $\Delta = 0.1$s (right panel).

insert eq. (7.104) into eq. (7.36) and thus finally obtain

$$\phi_k(A) = f^{pk+p}\, e^{-fA}\, H(A-\Theta_k) \sum_{g=0}^{p-1} \frac{(A-\Theta_{k-1})^{p-1-g}}{(p-1-g)!} \times \left[\frac{(\Theta_{k-1})^{pk+g}}{(pk+g)!} + \sum_{m=1}^{k-1} \sum_{l=0}^{p-1} \frac{z_{l,m}\,(\Delta_{k-m})^{l+p(k-m)+g+1}}{(l+p(k-m)+1+g)!} \right] \tag{7.106}$$

and the distribution function $\phi(A)$ of the first passage times A after the summation over k.

Note, that for $p = 1$, eq. (7.106) equals eq. (7.85), since in this special case the Erlang distribution becomes an Exponential one. Accordingly eq. (7.67) equals eq. (7.106) for $p = 1$ and $\Delta = 0$.

Fig. (7.9) shows both distributions of simulated intervals r (black curve) and $\phi(A)$ according to eq. (7.106) (red curves). The sets of parameters are chosen as follows: $\bar{\tau} = 0.157$s, $p = 5$, $\Theta = 0.4$s, $\Delta = 0.05$s (left panel) and $\bar{\tau} = 0.157$s, $p = 5$, $\Theta = 0.25$s, $\Delta = 0.1$s (right panel). In the first simulation (left panel in fig. 7.9) the statistical properties of the ventricular response are mainly determined by the blocking of atrial impulses during the original refractory period Θ. In this realisation the incrementation of the refractory period plays only a minor role, since $\Delta = 0.05s \ll \bar{\tau} \ll \Theta$. $w(r)$ exhibits a pronounced maximum and fastly decays for large intervals r. In contrast to this, the distribution in the right panel of fig. 7.9 exhibits a pronounced exponential tail superposed by several striking peaks. These peaks mark the end of the different refractory periods Θ_k.

Erlang WTD and fluctuating conduction time

We expand the model discussed in the previous section by including a variable conduction time $t_{\mathrm{con}} \neq 0$. Accordingly we consider (i) the random walker to start at position $A_{k'} = V' - \hat{x}$ and (ii) the absorbing border to be at position $\Theta^* = \Theta + \hat{x}$ in the beginning of the walk. The length of the first step τ_1 satisfies

$$\tau_1 > \hat{x} \tag{7.107}$$

since $\hat{x}$ is the time when the last atrial impulse occurs at the node during t_{con}. We introduce the displacement $x_k = \Theta_{k-1} + \hat{x} - T_k$ and obtain

$$\varphi_1^*(x) = \varphi_1^*(x_1) = A \, \frac{f^p}{(p-1)!} \, (\Theta + \hat{x} - x_1)^{p-1} \, e^{-f(\Theta+\hat{x}-x_1)} \, H(\Theta - x_1) \, H(x_1) \tag{7.108}$$

as the probability to find the walker after the first step in a distance x_1 in front of the border. Here

$$A = \left[\sum_{h=0}^{p-1} \frac{f^{p-1-h}}{(p-1-h)!} \, e^{-f\hat{x}} \, (\hat{x})^{p-1-h} \right]^{-1} \tag{7.109}$$

denotes the factor of normalisation. Note, that the displacement x_1 is still restricted to be within $0 \leq x_1 \leq \Theta$ and therefore is not affected by $\hat{x}$. This fact is reflected by the two Heaviside jump functions in eq. (7.108).

For the considered model the Wiener-Hopf equation writes

$$G(x,s) - \int_0^\infty G(x',s) \; s \, \rho(x' - x + \Delta) \, dx' = s\varphi_1^*(x) \tag{7.110}$$

with $x = x_{k+1}$ and $x' = x_k$, which except of the particular form of the right hand side of eq. (7.110) equals the Wiener-Hopf equation discussed in the previous section. Hence all parts of previous calculation that are independent from $\varphi_1^*(x)$ stay remain. For the present calculation we take both eq. (7.90) and the particular splitting of $\left[1 - \tilde{K}(u)\right]$ and thus write

$$\omega_+(u) \, \tilde{G}_+(u) + \omega_-(u) \, \tilde{G}_-(u) = \omega_-(u) \, \tilde{g}^*(u) = d^*(u) \tag{7.111}$$

where $\tilde{g}^*(u)$

$$\begin{aligned}
\tilde{g}^*(u) &= \int_{-\infty}^{+\infty} s\varphi_1^*(x) \, e^{\mathrm{i}ux} \, dx \\
&= A \; s \, \frac{f^p}{(p-1)!} \, e^{-f(\Theta^*)} \int_0^\Theta (\Theta^* - x)^{p-1} \, e^{x(f+\mathrm{i}u)} \, dx \\
&= \sum_{g=0}^{p-1} \frac{s \, f^p \, A \, e^{-f\hat{x}} e^{\mathrm{i}u\Theta} \, (\hat{x})^{p-1-g}}{(p-1-g)! \, (f+\mathrm{i}u)^{g+1}} - \sum_{g=0}^{p-1} \frac{s \, f^p \, A \, e^{-f(\Theta^*)} \, (\Theta^*)^{p-1-g}}{(p-1-g)! \, (f+\mathrm{i}u)^{g+1}}
\end{aligned} \tag{7.112}$$

is the Fourier Transform of $s\varphi_1^*(x)$. To calculate $\tilde{G}_+(u)$ we insert $\omega_-(u)$ into eq. (7.111),

split the right hand side of eq. (7.111) into $d^*(u) = d^*_+(u) + d^*_-(u)$ and obtain

$$\begin{aligned}\tilde{G}_+(u) &= \frac{C(u) + d_+(u)}{\omega_+(u)} \\ &= -\sum_{g=0}^{p-1} \frac{s\, f^p\, A\, e^{-f\hat{x}} e^{\mathbb{i}u\Theta}\, (\hat{x})^{p-1-g}\, (p-1-g)!^{-1}\, (f+\mathbb{i}u)^{p-g-1} + C(u)}{(f+\mathbb{i}u)^p - s f^p e^{\mathbb{i}u\Delta}}\end{aligned} \tag{7.113}$$

where the function $C(u) = \sum_{j=0}^{p-1} a_j\, u^j$ is a polynomial in u of order $p-1$. After Fourier Transformation and after expanding the coefficients a_j with respect to s^k we finally obtain

$$\begin{aligned}F_k(\hat{x}, a) = H(a - \Theta_k + \hat{x})\, f^{pk+p}\, e^{-fa} \sum_{r=0}^{p-1} \frac{(a-\Theta_{k-1})^{p-1-r}}{(p-1-r)!} \times \\ \left[\sum_{g=0}^{p-1} \frac{A\, (\hat{x})^{p-1-g} (\Theta_{k-1})^{pk-p+g+1+r}}{(p-1-g)!\, (pk-p+g+1+r)!} - e^{f\hat{x}} \sum_{m=1}^{k-1} \sum_{l=0}^{p-1} z_{l,m} \frac{(\Delta_{k-m})^{l+p(k-m)+1+r}}{(l+p(k-m)+1+r)!}\right].\end{aligned} \tag{7.114}$$

The coefficients $z_{l,k}$ in eq. (7.114) are determined by the recursive relation

$$\begin{aligned}z_{l,k} \;=\; &-\sum_{g=0}^{p-1} \frac{e^{-f\hat{x}}\, A\, (\hat{x})^{p-1-g}}{(p-1-g)!}\, \frac{(\Theta_{k-1})^{pk-p+g-l}}{(pk-p+g-l)!} \\ &-\sum_{m=1}^{k-1} \sum_{g=0}^{p-1} z_{g,m}\, \frac{\Delta_{k-m}^{g+p(k-m)-l}}{(g+p(k-m)-l)!} \quad .\end{aligned} \tag{7.115}$$

In accordance to eq. (7.34), we have to perform the Fourier Transformation of $F_k(\hat{x}, a)$ with respect to $\hat{x}$ in order to calculate the transition probability $\phi_k(A|A', V')$. Note, that both $F_k(\hat{x}, a)$ and the coefficients $z_{l,k}$ are functions of $\hat{x}$ and that the coefficients $z_{l,k} = z_{l,k}(\hat{x})$ are determined only by a recursive relation. Due to this we can neither perform the Fourier Transformation of $F_k(\hat{x}, a)$ with respect to $\hat{x}$ nor calculate $\phi_k(A|A', V')$. On the other hand, for any given time $\hat{x}$ we can calculate the distribution $\hat{\phi}(a)$ of the first passage times a when performing the summation over k in eq. (7.114).

8 Estimation of the fibrillation rate

The present chapter is devoted to the main question of the work.

> *Can the fibrillation rate be estimated from the statistical properties of the ventricular response during atrial fibrillation?*

The analytical results previously presented pointed out a direct relation between the statistical properties of the ventricular intervals and the fibrillation rate. Hence it is an obvious approach to estimate the fibrillation rate by fitting the analytical solutions to ventricular responses of real patients.

8.1 Estimating the fibrillation rate

We concentrate on those models which consider the atrial interbeat intervals to be Erlang distributed. This is due to the fact (i) that the assumption of Exponential distributed intervals τ does not exhibit a medical meaning and (ii) that distributions of intervals τ observed during AF can be well fitted to Erlang distributions (see fig. 8.1). We find, that on average a good agreement between the real and the considered distributions is obtained for Erlang distributions of orders $p \gg 20$ and with decay rates $f \gg 100$. For the two representative patients in fig. 8.1 the fitted parameters are p=75, f=500Hz (left panel) and p=70, f=420Hz (right panel).

Determining the AFR based on the statistical properties of ventricular intervals r is a difficult task. The original conduction model contains the seven parameters: $\bar{\tau}$, σ_τ, Θ, Δ, α, β and τ_{AV}. Several of them affect the ventricular response in similar ways. For example, $\bar{r}$ increases when at least one of the times Θ, Δ, α and β increases or when at least one of the times $\bar{\tau}$ and τ_{AV} decreases. Furthermore we did not obtain a full analytical solution for the complete model, including Erlang distributed intervals τ and variable conduction times.

To tackle these problems we determine the AFR in the following way:

1. For conduction models considering t_{con} to be $t_{\mathrm{con}} = 0$ we determine the AFR by fitting the analytical solution to distributions of real ventricular responses. To quantify the agreement between the real and the fitted distribution we perform a Kolmogorov-Smirnov test and define that set of parameters as the true one that yields the highest Kolmogorov-Smirnov probability p_{Kol}.
2. For conduction models which consider t_{con} to be $t_{\mathrm{con}} \neq 0$ we determine the AFR based on numerical simulations. As such we simulate ventricular responses, compare their statistical properties with the ones of real intervals r and quantify the agreement between the real and the predicted response (i) by performing Kolmogorov-Smirnov tests and (ii) by calculating the $AAREM_k$ values. For every set of parameters we

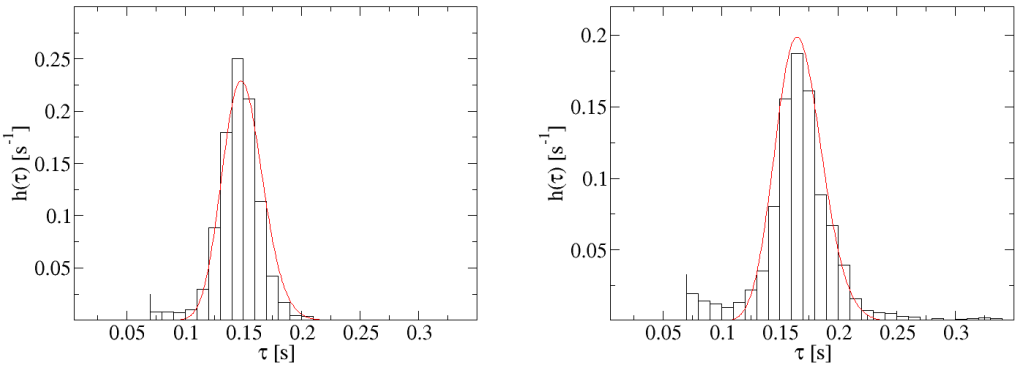

Figure 8.1: Normalised histograms $h(\tau)$ of atrial interbeat intervals τ and fitted Erlang distributions $\rho(\tau)$ for two patients from data pool 2. The parameters of the Erlang distributions are: p=75, f=500Hz (left panel) ; p=70, f=420Hz (right panel).

generate 30000 ventricular intervals. We define that set of parameters as the true one that either (i) yields the highest Kolmogorov-Smirnov probability p_{Kol} or (ii) yields the lowest $AAREM_7$ value.

In accordance to our previous work, the following conduction models are taken into account in the study.

- **Conduction model - Type I**

  Type I conduction models consider t_{con} to be $t_{\mathrm{con}} = 0$. Atrial impulses arriving at the node after the end of the refractory period are conducted immediately to the ventricle and cause the beginning of a new refractory cycle. The class of of Type I conduction models contains (i) the conduction model I.1, which considers a constant refractory period Θ and (ii) the conduction model I.2, which considers a fluctuating refractory period Θ_k, that is extended by Δ whenever an atrial impulse is blocked.

- **Conduction model - Type II**

  A Type II model contains a fluctuating refractory period Θ_k and a constant conduction time $t_{\mathrm{con}} > 0$. Impulses arriving at the node during t_{con} or during the refractory period are blocked. Impulses blocked during t_{con} do not influence the electrophysiological state of the node. In contrast to this, impulses blocked during the refractory period extend Θ by the time increment Δ. The model includes the five parameters: $\bar{\tau}$, σ_τ, Θ, Δ and t_{con}.

- **Conduction model - Type III**

  The Type III model corresponds to the one proposed by Jørgensen *et al.* [Jørgensen02]. It includes the seven parameters: $\bar{\tau}$, σ_τ, Θ, Δ, α, β and τ_{AV}.

According to chosen approach, for the group of Type I conduction models we determine the AFR by fitting the analytical solution to real ventricular responses. In case of Type II and Type III conduction models we determine the AFR based on numerical simulations. In this case we apply three different methods for scanning the parameter space:

- **method 1: Equidistant scanning**
  The parameter space is scanned in equidistant steps of a given size.
- **method 2: Pure random steps**
  The parameter space is scanned in non-equidistant steps. Each set of parameters that is taken into account is chosen randomly and independently from the previous one.
- **method 3: Random Walk approach**
  The parameter space is scanned while performing random walks. The steps are excepted if the new set of parameters yields a better agreement between the real and the predicted response than the former one. Performing various walks with randomly chosen starting points allows to estimate that set of parameters that yields the best level of agreement in the entire parameter space.

To support the fitting, we restrict the parameter spaces to medical sufficient ranges which are chosen in accordance to our own investigations and to the ranges published in the literature ([Jørgensen02], [Mangin05]).[1]

As such we vary the refractory period Θ between 0.0s and an upper threshold $\Theta_{\max}$, defined as the mean of the 50 smallest intervals r in the ECG of a patient and by 0.45s at maximum. This definition ensures that the range in which Θ varies is (i) in a sufficient medical range and (ii) is not influenced by mistakes in the detection of the peaks in the surface ECG.

The mean atrial interval $\bar{\tau}$ is varied between $\bar{\tau}_{\min} = 0.1$s and a maximum value $\bar{\tau}_{max}$, which is set to $\bar{\tau}_{max} = \Theta_{max}/1.5$ and to 0.33s at maximum. The upper limit $\Theta_{max}/1.5$ is chosen to restrict the fraction of blocked atrial impulses to a medical sufficient range. In case of an equidistant scanning both Θ and $\bar{\tau}$ are varied in steps of 0.02s.

The standard deviation σ_τ is varied between $\bar{\tau}/20$ and $\bar{\tau}/5$. In contrast to the other parameters σ_τ is not varied in steps of a fixed time duration but in 25 equidistant steps between the lower and upper threshold. This is due to the fact, that both the upper threshold and the lower one are not fixed values but depend on $\bar{\tau}$.

The time increment Δ is varied in steps of 0.02s between 0.0s and $\bar{\tau}$. Both t_{con} and α are varied in steps of 0.02s between 0.0s and 0.33s.

To estimate the parameters of the Type III model we follow the approach suggested by Mangin *et al.* [Mangin05] and fix the parameters β and τ_{AV} to the constant values: $\beta = 0.2$s and $\tau_{\text{AV}} = 0.1$s. Approximately these values are the midpoints of the physiological parameters ([Shrier87], [Nattel87], [Nayebpour91].

8.2 Discussion of results

We study the ECG-signals for all patients in data pool 2, since both surface ECG and atrial ECG-recordings are provided. The results obtained by the different studies are listed in in the tables 8.1... 8.8.[2] In order to relieve the interpretation of the results, the last columns in

[1] The step sizes mentioned in the text are used for the equidistant scanning of the plane, when determining the AFR based on numerical simulations.

[2] To support the reading we do not display all but only a subset of the results. We note that the displayed results are representative and are in agreement with the ones that are not listed.

patient	p_{Kol}	$\bar{\tau}_{\mathrm{real}}$ [s]	$\bar{\tau}_{\mathrm{fit}}$ [s]	σ_{fit} [s]	Θ [s]	Δ_{AFR} [Hz]	δ_{AFR}
2006_01_03	0.454	0.158	0.216	0.030	0.369	1.70	1.37
2006_01_16	1.371e-69	0.155	0.210	0.041	0.313	1.69	1.35
2006_04_05	1.275e-110	0.180	0.283	0.056	0.425	2.02	1.57
2006_11_20	1.122e-300	0.233	0.333	0.066	0.445	1.29	1.43
2007_01_31	2.157e-302	0.185	0.314	0.062	0.448	2.22	1.70
2007_02_01	1.883e-252	0.140	0.197	0.055	0.298	2.07	1.41

Table 8.1: Estimated parameters and Kolmogorov-Smirnov probabilities for conduction model I.1. The results are obtained by fitting the analytical solution to the real ventricular responses.

patient	p_{Kol}	$\bar{\tau}_{\mathrm{real}}$ [s]	$\bar{\tau}_{\mathrm{fit}}$ [s]	σ_{fit} [s]	Θ [s]	Δ [s]	Δ_{AFR} [Hz]	δ_{AFR}
2006_01_03	0.449	0.158	0.217	0.029	0.335	0.037	1.72	1.37
2006_01_16	1.860e-08	0.155	0.122	0.023	0.214	0.077	-1.75	0.78
2006_04_05	1.682e-07	0.180	0.240	0.046	0.313	0.165	1.39	1.33
2006_11_20	0.017	0.233	0.306	0.052	0.443	0.211	1.02	1.31
2007_01_31	6.893e-05	0.185	0.232	0.046	0.378	0.144	1.10	1.25
2007_02_01	2.944e-24	0.140	0.105	0.019	0.209	0.076	-2.38	0.75

Table 8.2: Estimated parameters and Kolmogorov-Smirnov probabilities for conduction model I.2. The results are obtained by fitting the analytical solution to the real ventricular responses.

the tables display the absolute differences Δ_{AFR} and the relative differences δ_{AFR} between the estimated and the real fibrillation rates.

$$\Delta_{\mathrm{AFR}} = f_{\mathrm{real,fib}} - f_{\mathrm{est,fib}}$$
$$\delta_{\mathrm{AFR}} = f_{\mathrm{real,fib}} / f_{\mathrm{est,fib}}$$

At first we concentrate on Type I conduction models and estimate the parameters by fitting the analytical solutions to the real ventricular responses. The obtained results are listed in table 8.1 (Type I.1 model) and in table 8.2 (Type I.2 model).

The probabilities p_{Kol} indicate a strong disagreement between the real and the predicted ventricular responses, which is in accordance to our previous findings (see sec. 7.2). However, the probabilities obtained for the Type I.2 conduction model are significantly larger than the ones for the Type I.1 model. This underlines that the blocking mechanism of the AV node strongly influence the statistical properties of the ventricular response during AF.

Furthermore we find pronounced differences in the p_{Kol} values obtained for the different patients. At least in some cases the modified models are capable of predicting the statistical properties of the ventricular response. On the other hand, even in case of high p_{Kol} values the real and the estimated fibrillation rates differ about more than 1Hz. Thus we conclude that fitting the analytical solutions of Type I conduction models to real ventricular responses is not suitable for determining the AFR.

As next we study the Type II conduction model and determine the parameters based on numerical simulations. The obtained results are listed in the tables 8.3, . . ., 8.5.

The Kolmogorov-Smirnov probabilities are significantly higher than the ones for the previous models. This indicates that for the given group of patients the statistical properties of the intervals r are strongly influenced by the conduction of impulses through the AV node. Notwithstanding the strong improvement of the results, the Kolmogorov-Smirnov probabilities are significantly lower than the ones presented by Jørgensen *et al.* [Jørgensen02] and by Mangin *et al.* [Mangin05]. We note, that these differences are not only due to the introduced modifications. In contrast to their work our study does not include any information about the statistical properties of the atrial intervals τ.

The probabilities p_{Kol} slightly increase when replacing the equidistant scanning by the random one. This indicates that the function $p_{\mathrm{Kol}}(\bar{\tau}, \sigma_{tau}, \Theta \ldots)$ exhibits several local maxima and that some of them are may not detected when scanning the parameter space with equidistant steps. Furthermore it underlines the fact that certain parameters influence the statistical properties of the response in a similar way.

For some patients the true parameters estimated with the first method are close to the ones obtained by second method. For other patients the sets of parameters significantly differ. Note, that in some cases the differences between the estimated parameters are larger then the step size chosen for the equidistant scanning. Hence, we conclude that parameters obtained by the first method only provide an indication of the true ones.

The best agreement between the fibrillation rates is obtained when estimating the parameters with view to the lowest $AAREM_7$ value. On average the rates differ only of about ± 0.63Hz and only of about $\pm 11.5\%$. In comparison, the rates estimated with respect to the highest p_{Kol} differ of about ± 1.33Hz and of about $\pm 29\%$. Furthermore, in contrast to the Kolmogorov-Smirnov probabilities the $AAREM_7$ values for the different subjects do only slightly differ.

As last step we study the complete conduction model, originally proposed by Jørgensen *et al.* [Jørgensen02]. The obtained results are listed in the tables 8.6,. . ., 8.8.

At first view it is clear to see, that the transition from the Type II conduction models to the original one, does not yield improved Kolmogorov-Smirnov probabilities. In contrast, the listed p_{Kol} values are significantly lower than the ones displayed in table 8.3. The AAREM values on the other hand, are only slightly larger then the ones for the Type II model. Again we find pronounced differences between the parameter sets estimated with an equidistant and a random scanning.

For all methods the estimated and the real fibrillation rates differ in a broad range. This reflects that several parameters affect the ventricular response in a similar way. Therefore the true set of parameters is no longer unambiguously determinable. As such we conclude, that the combination of the applied methods and the considered conduction model is not suitable for determining the fibrillation rate.

patient	p_{Kol}	$\bar{\tau}_{\mathrm{real}}$ [s]	$\bar{\tau}_{\mathrm{fit}}$ [s]	σ_{fit} [s]	Θ [s]	Δ [s]	t_{con} [s]	Δ_{AFR} [Hz]	δ_{AFR}
2006_01_03	0.212	0.158	0.14	0.025	0.18	0.04	0.16	-0.81	0.89
2006_01_16	4.556e-05	0.155	0.20	0.040	0.12	0.10	0.20	1.45	1.29
2006_04_05	3.142e-08	0.180	0.24	0.048	0.18	0.14	0.26	1.39	1.33
2006_11_20	0.001	0.233	0.22	0.043	0.28	0.14	0.20	-0.25	0.94
2007_01_31	0.022	0.185	0.22	0.041	0.24	0.12	0.20	0.86	1.12
2007_02_01	1.187e-05	0.140	0.18	0.030	0.16	0.10	0.16	1.59	1.29

Table 8.3: Estimated parameters and Kolmogorov-Smirnov probabilities for the numerical simulation of conduction model II. The results are obtained for a equidistant scanning of the parameter plane (see text).

patient	p_{Kol}	$\bar{\tau}_{\mathrm{real}}$ [s]	$\bar{\tau}_{\mathrm{fit}}$ [s]	σ_{fit} [s]	Θ [s]	Δ [s]	t_{con} [s]	Δ_{AFR} [Hz]	δ_{AFR}
2006_01_03	0.433	0.158	0.216	0.031	0.262	0.030	0.080	1.70	1.37
2006_01_16	0.0003	0.155	0.195	0.037	0.135	0.082	0.203	1.32	1.26
2006_04_05	2.548e-05	0.180	0.257	0.047	0.161	0.146	0.242	1.66	1.43
2006_11_20	0.00012	0.233	0.219	0.043	0.257	0.144	0.191	-0.27	0.94
2007_01_31	0.024	0.185	0.231	0.041	0.246	0.121	0.222	1.08	1.25
2007_02_01	1.5146e-06	0.140	0.192	0.029	0.162	0.099	0.175	1.93	1.37

Table 8.4: Estimated parameters and Kolmogorov-Smirnov probabilities for the numerical simulation of conduction model II. The results are obtained for a random scanning of the parameter plane (see text).

patient	*AAREM*	$\bar{\tau}_{\text{real}}$ [s]	$\bar{\tau}_{\text{fit}}$ [s]	σ_{fit} [s]	Θ [s]	Δ [s]	t_{con} [s]	Δ_{AFR} [Hz]	δ_{AFR}
2006_01_03	0.732	0.158	0.153	0.014	0.303	0.001	0.013	-0.21	0.97
2006_01_16	0.920	0.155	0.168	0.011	0.278	0.005	0.088	0.50	1.08
2006_04_05	0.751	0.180	0.160	0.020	0.256	0.088	0.154	-0.70	0.89
2006_11_20	0.321	0.233	0.304	0.059	0.471	0.186	0.038	1.00	1.30
2007_01_31	0.701	0.185	0.191	0.024	0.314	0.131	0.043	0.17	1.03
2007_02_01	0.923	0.140	0.120	0.007	0.279	0.070	0.029	-1.20	0.86

Table 8.5: Estimated parameters and Kolmogorov-Smirnov probabilities for the numerical simulation of conduction model II. The results are obtained for a random scanning of the parameter plane (see text).

patient	p_{Kol}	$\bar{\tau}_{\text{real}}$ [s]	$\bar{\tau}_{\text{fit}}$ [s]	σ_{fit} [s]	Θ [s]	Δ [s]	α [s]	Δ_{AFR} [Hz]	δ_{AFR}
2006_01_03	4.042e-07	0.158	0.24	0.018	0.02	0.10	0.20	2.17	1.52
2006_01_16	1.151e-29	0.155	0.12	0.024	0.10	0.08	0.04	-1.88	0.77
2006_04_05	1.899e-13	0.180	0.10	0.010	0.12	0.08	0.04	-4.44	0.56
2006_11_20	1.474e-06	0.233	0.18	0.020	0.16	0.14	0.16	-1.26	0.77
2007_01_31	6.651e-10	0.185	0.12	0.023	0.20	0.08	0.04	-2.93	0.65
2007_02_01	5.442e-33	0.140	0.14	0.011	0.10	0.10	0.08	0.00	1.00

Table 8.6: Estimated parameters and Kolmogorov-Smirnov probabilities for the numerical simulation of conduction model III. The results are obtained for a equidistant scanning of the parameter plane (see text). The parameters α and τ_{AV} are set to be $\alpha = 0.2$s and $\tau_{AV} = 0.1$s

patient	p_{Kol}	$\bar{\tau}_{\text{real}}$ [s]	$\bar{\tau}_{\text{fit}}$ [s]	σ_{fit} [s]	Θ [s]	Δ [s]	α [s]	Δ_{AFR} [Hz]	δ_{AFR}
2006_01_03	1.883e-09	0.158	0.235	0.026	0.018	0.095	0.205	2.07	1.49
2006_01_16	4.298e-19	0.155	0.103	0.017	0.094	0.069	0.055	-3.26	0.66
2006_04_05	6.713e-14	0.180	0.106	0.013	0.098	0.08	0.149	-3.88	0.59
2006_11_20	7.865e-07	0.233	0.152	0.019	0.185	0.116	0.090	-2.29	0.65
2007_01_31	4.915e-10	0.185	0.110	0.022	0.186	0.075	0.063	-3.69	0.59
2007_02_01	7.114e-32	0.140	0.110	0.012	0.110	0.083	0.006	-1.95	0.79

Table 8.7: Estimated parameters and Kolmogorov-Smirnov probabilities for the numerical simulation of conduction model III. The results are obtained for a random scanning of the parameter plane (see text). The parameters α and τ_{AV} are set to be $\alpha = 0.2$s and $\tau_{AV} = 0.1$s

patient	*AAREM*	$\bar{\tau}_{\text{real}}$ [s]	$\bar{\tau}_{\text{fit}}$ [s]	σ_{fit} [s]	Θ [s]	Δ [s]	α [s]	Δ_{AFR} [Hz]	δ_{AFR}
2006_01_03	1.473	0.158	0.114	0.014	0.236	0.013	0.196	-2.44	0.72
2006_01_16	0.995	0.155	0.114	0.014	0.236	0.013	0.196	-2.32	0.74
2006_04_05	0.878	0.180	0.137	0.012	0.265	0.079	0.157	-1.74	0.76
2006_11_20	0.874	0.233	0.276	0.021	0.466	0.116	0.252	0.67	1.18
2007_01_31	0.841	0.185	0.124	0.011	0.202	0.086	0.207	-2.66	0.67
2007_02_01	1.010	0.140	0.104	0.011	0.187	0.008	0.352	-2.47	0.74

Table 8.8: Estimated parameters and AAREM values for the numerical simulation of conduction model III. The results are obtained for a random scanning of the parameter plane (see text). The parameters α and τ_{AV} are set to be $\alpha = 0.2$s and $\tau_{AV} = 0.1$s

8.3 Conclusion

We questioned if the AFR can be determined from the statistical properties of the ventricular response during AF. To answer this question we studied several conduction models and determined the fibrillation rate by fitting analytical solutions and by numerical simulations.

We find, that for the given data pool of patients the most suitable approach is fitting the parameters of the Type II conduction model with respect to the lowest AAREM value and by performing random walks in the parameter space. On average the fibrillation rates differ only of about ±0.63Hz and only of about ±11.5%. This result is remarkable. One has to take into account (i) that except of the statistical properties of the ventricular response, no further information has been taken into account and that (ii) data pool 2 contains only short ECG-recordings.

Furthermore, we find that it is not suitable to introduce further modifications or to analyse the original conduction model directly. In addition, fitting the parameters with respect to the lowest AAREM value is favoured over a fitting with respect to the highest Kolmogorov-Smirnov probability. As such we finally conclude:

The fibrillation rate can be determined from the statistical properties of the ventricular response by fitting the response to the Type II conduction model.

9 Conclusion

The present work is devoted to the question:

> *Can the fibrillation rate be determined from the statistical properties of the ventricular response during atrial fibrillation?*

To tackle this question we first studied the statistical properties of ECG recordings and related signals and asked (i) in which way those signals differ during different states of health and (ii) if these signals exhibit statistical properties which are characteristic for atrial fibrillation.

To investigate all information contained in an ECG recording we introduced new time series, so-called normalised morphograms. In contrast to tachograms these time series do not contain any information about the lenghts of the heart beats but only about the shape of the ECG. Thus they carry information which are complementary to the ones carried by tachograms.

We found that during all states of health, the fluctuations in the normalised morphograms exhibit pronounced long-range anticorrelation. The same result is found for time series containing information only about the deviation of the ECG signal shape, so-called delta morphograms. In the normalised morphograms the long-range anticorrelation are most pronounced for patients undergoing paroxysmal AF (averaged Hurst exponent: 0.034 ± 0.034) while in case of delta morphograms the anticorrelation are most pronounced for healthy subjects (averaged Hurst exponent: 0.0075 ± 0.0008). With view to an automatic detection of different states of health we found, that for both types of morphograms a comparison of the fluctuations on certain timescales is suitable for determining the presence or absence of sinus rhythm. Healthy subjects show lower fluctuations in the normalised morphograms and higher fluctuations in the delta morphograms than diseased persons. ROC values close or even higher than 90% on nearly all timescales, confirm the potential of this approach.

The other states of health can be distinguished when analysing so-called non-normalised morphograms in which the information about the signal shape and about the duration of a single heart beat is concatenated. The different states can be diagnosed either by comparing the averaged strengths of fluctuations of the increments or by comparing the Hurst exponents of the corresponding fluctuation functions $F(s)$. For all states of health the increments in the non-normalised morphograms show long-range anticorrelation. These anticorrelation are most pronounced for healthy subjects and for patients undergoing paroxysmal AF (averaged Hurst exponent: 0.0358 ± 0.0247 (healthy subjects); 0.0336 ± 0.0334 (PAF patients)). For PAF and CHF patients the ROC values, obtained while comparing the averaged strengths of fluctuations on different timescales, are significantly higher then the ones obtained for the normalised morphograms.

Hence with view to an automatic detection of different states of health we suggest to study the statistical properties of different kinds of morphograms together. While the study of normalised morphograms and delta morphograms allows to distinguish between healthy and non-healthy subjects, the study of non-normalised morphograms allows to distinguish between different diseased states.

As next we followed a more classical approach and investigated the statistical properties of ventricular responses during different states of health. We found a new specific and characteristic feature in the statistical properties of ventricular intervals occurring during atrial fibrillation, that has not been investigated so far. Besides the earlier reported features - a striking breakpoint in the power spectrum and a constant signal to noise ratio - ventricular intervals during AF are characterised by an exponentially decaying distribution. This decay can be well fitted to an single exponential. We showed, that the exponential tail can be also observed during paroxysmal AF when rejecting all intervals occurring during episodes without fibrillation. The decay rate of the tail exhibits pronounced diurnal fluctuations which are strongly anticorrelated to the ones observed for the mean ventricular interval. This suggests that the decay rate exhibits a medical meaning and thus carries important information about the disease.

The occurrence of three different statistical properties which are specific and characteristic for the ventricular response during AF raised the question whether or not these features are interrelated. To answer this question we first concentrated on the relation between the breakpoint in the power spectrum and the occurrence of the exponential decay in the distribution. We analysed the correlation properties of different subsamples in tachograms during AF. We found the long and exponentially distributed intervals during AF to be mostly uncorrelated while shorter intervals are mostly correlated.

In detail, we showed that during AF the time series of ventricular intervals can be decomposed into two sub-sequences in such way, that (i) the first of them mainly contains intervals which are mostly correlated and which barely contribute to the exponential tail in the distribution and that (ii) the other one contains mostly uncorrelated intervals that encompass accounts for nearly the whole exponential tail in the distribution. We found that the decomposition is most pronounced when taken into account the information stored in the constant signal to noise ratio of the intervals. Hence, our analysis concatenated all characteristic features in the statistical properties of ventricular responses during AF.

Furthermore it was shown that the decay rate of the exponential decay can be estimated directly from the white noise part of the power spectrum. The strength of the white noise underlies diurnal fluctuations which are strongly anticorrelated to the ones of the mean ventricular interval. This finding clearly proofed the relation between the exponential tail in the distribution, the breakpoint in the power spectrum and the constant signal to noise ratio in the ventricular response during AF.

As next we concentrated on mathematical models for the process of conducting electrical impulses from the atrium to the ventricles through the AV node. In particular we focused on the model suggested by Jørgensen *et al* [Jørgensen02] since it is most suitable for predicting the statistical properties of the ventricular response during AF. We showed, that the occurrence of the exponential decay in the distribution of the ventricular intervals is directly predicted by this model.

Based on numerical simulations and analytical calculations we developed a first approach for estimating the fibrillation rate from the ventricular response. We found that this method yields a good agreement between the real and the estimated fibrillation rates in case of ECG recordings with sufficient statistical meaning and for distributions with pronounced exponential decays. Even in case of short recordings in which only 1331 heart beats are observed, the estimated and the real fibrillation rate differ only of about $0.52Hz$ (8%). The suggested method has been panded as invention and as patent [Hennig06b] and is a first provement for the possibility of detecting the fibrillation rate based only on the statistical properties of heart beat intervals.

In the further work we showed that the model proposed by Jørgensen *et al* [Jørgensen02] can be formally described in a mathematical manner. For the original and several particular models we presented complete analytical solutions. These solutions pointed out that the exponential decay in the distribution of the ventricular intervals carries information not only about the fibrillation rate but also about other biological parameters which are important for the conduction process. For certain modified conduction models these parameters can be estimated directly by fitting the analytical solution to real responses. For other conduction models numerical simulations can be used.

We found that the most suitable approach is to fit the parameters of a Type II conduction model to a real ventricular response with respect to the lowest AAREM value (absolute averaged relative error of moments). For the analysed data pool the estimated rates differ only of about ±0.63Hz (±11.5%), which is comparable to the result obtained with the first suggested method. We expect this agreement to be improved when analysing ECG recordings that contain much more heart beat intervals, than the ones analysed in the present study. However, the fair agreement between the real and the estimated rates clearly points out, that the proposed approach is suitable for estimating the fibrillation rate.

The present work makes a contribution to the development of statistical time series analysis of medical datasets. We presented novel methods for analysing the information stored in an ECG recording without complicated pattern recognition, found a new characteristic feature in the statistical properties of ventricular responses during AF and proved that different characteristic features are interrelated. Moreover we showed that these different features carry important information about the disease, which has not been shown so far. Finally we performed comprehensive analytical and numerical investigations to present a complete solution of a well established conduction model and showed that in principle the fibrillation rate can be detected from the statistical properties of the ventricular response.

Appendices

A Discussion of the monotonic behaviour of the distributions w(r)

In this appendix we discuss the monotonic behaviour of the functions $w_1(r)$ and $w_2(r)$ in the solution (7.78) with respect to the time intervals $r_1 < r < r_2$ and $r_2 \leq r < \infty$.

We first focus on the case $\beta < 1$ where only the solution $u_2 = u_2(\tilde{r})$ is positive. The lower border $\tilde{r}_2$ is given by the value $g(0) = \beta$. To estimate the behaviour of $w_2(r)$ for small values $r \to r_2$ we set $\tilde{r} = \tilde{r}_2 + \epsilon$ in eq. (7.75) and expand $g(u_2)$ up to linear order in u_2. We thus obtain

$$u_2 = \frac{\epsilon}{1-\beta} + O(\epsilon^2)\,. \tag{A.1}$$

Inserting this relation into eq. (7.76) yields eq. (7.79). The derivative $dw_2(r)/dr$ of $w_2(r) = fe^{-fu_2}/g'(u_2)$ is

$$w_2'(r) = \frac{d\,w_2(r)}{d\,r} = -u_2'\,\frac{fe^{-fu_2}}{g'(u_2)^2}\,[fg'(u_2) + g''(u_2)] \tag{A.2}$$

with

$$g'(u_2) = 1 - \beta e^{-u_2} \quad , \quad g''(u_2) = \beta e^{-u_2} \quad , \quad u_2' = 1/g'(u_2) \quad . \tag{A.3}$$

Hence we conclude that $w(r) = w_2(r)$ decays monotonously since $g'(u_2) > 0$ and $u_2' > 0$.

In the second case $\beta > 1$ the minimum of $g(u)$ at $u = u_{\min} = \ln(\beta)$ determines the lower bound $\tilde{r}_1 = 1 + \ln(\beta)$. In accordance we set $\tilde{r} = \tilde{r}_1 + \epsilon$ in eq. (7.75) but now expand $g(u)$ up to the second order in u around $u_{\min}$, since $g'(u_{\min}) = 0$). We thus obtain

$$u_{1,2} = \ln\beta \mp \sqrt{2\epsilon} + O(\epsilon)\,. \tag{A.4}$$

Again we insert this into the corresponding eq. (7.77) and yield eq. (7.81). In accordance with eq. (A.2) the derivative $dw_1(r)/dr$ of $w_1(r) = fe^{-fu_1}/g'(u_1)$ is

$$w_1'(r) = u_1'\,\frac{fe^{-fu_1}}{g'(u_1)^2}\,[fg'(u_1) + g''(u_1)] \tag{A.5}$$

with

$$g'(u_1) = 1 - \beta e^{-u_1} \quad , \quad g''(u_1) = \beta e^{-u_1} \quad , \quad u_1' = 1/g'(u_1) \quad . \tag{A.6}$$

Depending of the rate f of the atrial impulses we here have to distinguish two different cases for the monotonic behaviour of $w_1(r)$. Since $u_1' = 1/g'(u_1) < 0$ for $u_1 < u_{\min}$, the derivative $w_1'(r)$ is negative in the interval $r_1 < r < r_2$, when the sum $fg'(u_1) + g''(u_1)$ is positive in the corresponding interval $0 < u_1 < \ln(\beta)$. This is the case if f is smaller than the critical value given by $f_c^{(1)} = \beta/(\beta - 1) > 1$. For $f > f_c^{(1)}$ on the other hand $fg'(u_1) + g''(u_1)$

is zero at $u_1 = \ln[\beta(f-1)/f)]$. Hence $u_1 = \ln[\beta(f-1)/f)]$ goes through a minimum at $r_{\min}^{(1)} = \Theta + \alpha + f/(f-1) + \ln[\beta(f-1)/f)]$ with value $w_1(r_{\min}^{(1)}) = [f/(\beta(f-1))]^f f(f-1)$. In contrast the monotonic behaviour of the second part of the solution $w_2(r)$ is independent of f. The function always decreases in the interval $r_1 < r < r_2$ (see above). Consequently the full solution $w(r) = w_1(r) + w_2(r)$ does not exhibit a minimum in $r_1 < r < r_2$ for $f = f_c^{(1)}$. For sufficiently large $f > f_c$ on the other hand, $w(r) = w_1(r) + w_2(r)$ exhibit a minimum in $r_1 < r < r_2$. This is due to the fact that u_2 is always $u_2 > u_1$ and that hence the part $w_2(r) \propto fe^{-fu_2}$ does less influence $w(r)$ for large fibrillation rates f then the solution $w_1(r) \propto fe^{-fu_1}$.

On the other hand in case $\beta > 1$, $w(r)$ always exhibit a discontinuity at $r = r_2$ with a jump value

$$\Delta w = \lim_{\epsilon \to +0} [w(r_2 - \epsilon) - w(r_2 + \epsilon)] = \lim_{\epsilon \to +0} w_1(r_2 - \epsilon) = \frac{f}{\beta - 1} \tag{A.7}$$

Note that the special case $\beta = 1$, eq. (A.4) still remains valid. Inserting $u_2 = \ln\beta + \sqrt{2\epsilon} + O(\epsilon)$ into eq. (7.76) yields eq. (7.80).

B Solution of the Wiener-Hopf problem for Erlang WTD for $t_{\mathrm{con}} = 0$

In this appendix we discuss in detail the solution of the Wiener-Hopf problem (sec. 7.3.2)

$$G(x,s) - \int_0^\infty G(x',s)\, s\, \rho(x'-x+\Delta)\, dx' = s\varphi_1(x) \tag{B.1}$$

which is derived from the analytical description of a conduction model (i) with atrial inter-beat intervals τ drawn from an Erlang distribution

$$\rho(\tau) = f^p \frac{\tau^{p-1}}{(p-1)!}\, e^{-f\tau}\, H(\tau) \tag{B.2}$$

and (ii) with constant conduction time $t_{\mathrm{con}} = 0$. We note, that we follow the notation of sec. 7.3.2.

B.A Solution of the Wiener-Hopf problem

The inhomogeneous Wiener-Hopf integral equation is a equation of kind

$$y(x) - \int_0^\infty K(x-t)\, y(t)\, dt = g(x) \quad , \quad 0 \le x < +\infty\,. \tag{B.3}$$

For the considered conduction model the functions $K(x)$ and $g(x)$ in eq. (B.3) are given as:

$$K(x) = s\,\rho(\Delta - x) = s\, f^p \frac{(\Delta-x)^{p-1}}{(p-1)!}\, e^{-f(\Delta-x)}\, H(\Delta - x) \tag{B.4}$$

$$g(x) = s\,\varphi_1(x) = s\, f^p \frac{(\Theta-x)^{p-1}}{(p-1)!}\, e^{-f(\Theta-x)}\, H(\Theta - x)\, H(x)\,. \tag{B.5}$$

After Fourier Transformation of eq. (B.3) we obtain

$$\tilde{g}(u) = \tilde{G}_+(u) + \tilde{G}_-(u) - \tilde{K}(u)\,\tilde{G}_+(u) = \left[1 - \tilde{K}(u)\right]\,\tilde{G}_+(u) + \tilde{G}_-(u) \tag{B.6}$$

where $\tilde{G}_+(u)$ and $\tilde{G}_-(u)$ are the positive and the negative half sided Fourier Transforms of the generating function $G(x, s)$ and where

$$\tilde{K}(u) = \frac{s\, f^p\, e^{\mathrm{i}u\Delta}}{(f + \mathrm{i}u)^p}, \qquad \tilde{g}(u) = \frac{s\, f^p\, e^{\mathrm{i}u\Theta}}{(f + \mathrm{i}u)^p} - \sum_{g=0}^{p-1} \frac{\Theta^{p-1-g}\, s\, f^p\, e^{-f\Theta}}{(p-1-g)!\,(f + \mathrm{i}u)^{(g+1)}} \tag{B.7}$$

are the Fourier Transforms of $K(x)$ and $g(x)$ respectively. We insert (B.7) into (B.6) and factorise the term $\left[1 - \tilde{K}(u)\right]$ as:

$$\left[1 - \tilde{K}(u)\right] = 1 - \frac{sf^p e^{\mathrm{i}u\Delta}}{(f + \mathrm{i}u)^p} = \frac{(f + \mathrm{i}u)^p - sf^p e^{\mathrm{i}u\Delta}}{(f + \mathrm{i}u)^p} = \frac{\omega_+(u)}{\omega_-(u)} \tag{B.8}$$

with $\tilde{\omega}_+(u) = (f+\mathrm{i}u)^p - sf^p e^{\mathrm{i}u\Delta}$ and $\tilde{\omega}_-(u) = (f+\mathrm{i}u)^p$. Due to this particular factorisation, eq. (B.6) writes

$$\omega_+(u)\, \tilde{G}_+(u) + \omega_-(u)\, \tilde{G}_-(u) = \omega_-(u)\, \tilde{g}(u) = d(u) \tag{B.9}$$

with

$$d(u) = s\, f^p e^{\mathrm{i}u\Theta} - s\, f^p\, e^{-f\Theta} \sum_{g=0}^{p-1} \frac{\Theta^{p-1-g}}{(p-1-g)!}\, (f + \mathrm{i}u)^{(p-1-g)}\,. \tag{B.10}$$

Next we express $d(u)$ as the sum $d(u) = d_+(u) + d_-(u)$, with

$$d_+(u) = s\, f^p e^{\mathrm{i}u\Theta}, \qquad d_-(u) \;= -s\, f^p\, e^{-f\Theta} \sum_{g=0}^{p-1} \frac{\Theta^{p-1-g}}{(p-1-g)!}\, (f + \mathrm{i}u)^{(p-1-g)}\,. \tag{B.11}$$

Both $d_+(u)$ and $d_-(u)$ are (i) analytical in the entire complex plane, since g is always in the range $0 \le g \le p-1$ and (ii) do not increase faster than a polynomial u^{p-1} for $|u| \to \infty$. Hence we obtain

$$\tilde{G}_+(u) = \frac{C(u) + d_+(u)}{\omega_+(u)} \tag{B.12}$$

where $C(u)$ is a polynomial in u of degree $p-1$.

In order to calculate $G(x, s)$ we perform the Inverse Fourier Transformation of $\tilde{G}_+(u)$. To support the reading we split $G_+(u)$ into:

$$\begin{aligned}
\tilde{G}_+(u) &= \tilde{G}_{+,1}(u) + \tilde{G}_{+,2}(u) \\
\tilde{G}_{+,1}(u) &= -\frac{d_+(u)}{\omega_+(u)} = \frac{s\, f^p e^{\mathrm{i}u\Theta}}{(f + \mathrm{i}u)^p - sf^p e^{\mathrm{i}u\Delta}} \\
\tilde{G}_{+,2}(u) &= \frac{C(u)}{\omega_+(u)} = \frac{C(u)}{(f + \mathrm{i}u)^p - sf^p e^{\mathrm{i}u\Delta}}\,.
\end{aligned} \tag{B.13}$$

First we rewrite $\tilde{G}_{+,1}(u)$ as

$$\tilde{G}_{+,1}(u) = \frac{s\, f^p e^{\mathbb{i}u\Theta}}{(f+\mathbb{i}u)^p}\, \frac{1}{1-\frac{sf^p e^{\mathbb{i}u\Delta}}{(f+\mathbb{i}u)^p}} = \sum_{k=0}^{\infty} \frac{s^{k+1} f^{pk+p} e^{\mathbb{i}u(k\Delta+\Theta)}}{(f+\mathbb{i}u)^{pk+p}} = \sum_{k=0}^{\infty} \frac{s^{k+1} f^{pk+p} e^{\mathbb{i}u(k\Delta+\Theta)}}{\mathbb{i}^{pk+p}(u-\mathbb{i}f)^{pk+p}} \quad \text{(B.14)}$$

since $|(sf^p e^{\mathbb{i}u\Delta})/((f+\mathbb{i}u)^p)| < |s| < 1$. Note, that $\tilde{G}_{+,1}(u)$ exhibits a singularity of order $pk+p$ on the imaginary axis of the complex plane at position $u^* = \mathbb{i}f$.

Then we perform the Inverse Fourier Transformation and obtain:

$$\begin{aligned} G_{+,1}(x,s) &= \frac{1}{2\pi} \int_{-\infty}^{+\infty} \sum_{k=0}^{\infty} \frac{s^{k+1} f^{pk+p} e^{\mathbb{i}u(k\Delta+\Theta)}}{\mathbb{i}^{pk+p}(u-\mathbb{i}f)^{pk+p}} e^{-\mathbb{i}ux}\, du \\ &= \sum_{k=0}^{\infty} \frac{1}{2\pi\mathbb{i}}\, \frac{s^{k+1} f^{pk+p}}{\mathbb{i}^{pk+p-1}} \int_{-\infty}^{+\infty} \frac{e^{\mathbb{i}u(\Theta_k - x)}}{(u-\mathbb{i}f)^{pk+p}}\, du \end{aligned} \quad \text{(B.15)}$$

The integral in eq. (B.15) vanishes for $u \to \infty$, when $(\Theta_k - x) > 0$. Hence we expand the integral over the whole upper half complex plane and obtain:

$$\begin{aligned} G_{+,1}(x,s) &= \sum_{k=0}^{\infty} \frac{s^{k+1} f^{pk+p}}{\mathbb{i}^{pk+p-1}(pk+p-1)!}\, H(\Theta_k - x)\, \frac{\partial^{pk+p-1}}{\partial u^{pk+p-1}} \Big|_{u^*=\mathbb{i}f}\; e^{\mathbb{i}u(\Theta_k - x)} \\ &= \sum_{k=0}^{\infty} \frac{s^{k+1} f^{pk+p}}{\mathbb{i}^{pk+p-1}(pk+p-1)!}\, H(\Theta_k - x)\, \mathbb{i}^{pk+p-1}\, (\Theta_k - x)^{pk+p-1}\, e^{-f(\Theta_k - x)} \\ &= \sum_{k=0}^{\infty} \frac{s^{k+1} f^{pk+p}}{(pk+p-1)!}\, (\Theta_k - x)^{pk+p-1}\, e^{-f(\Theta_k - x)}\, H(\Theta_k - x) \end{aligned} \quad \text{(B.16)}$$

where we used the Cauchy integral formula

$$h^{(n)}(z) = n! \oint \frac{dz'}{2\pi\mathbb{i}} \frac{h(z')}{(z'-z)^{n+1}}\,. \quad \text{(B.17)}$$

In accordance with the previous calculation we rewrite $\tilde{G}_{+,2}(u)$ as

$$\tilde{G}_{+,2}(u) = \frac{C(u)}{(f+\mathbb{i}u)^p - sf^p e^{\mathbb{i}u\Delta}} = \sum_{k=0}^{\infty} \frac{C(u)\, s^k f^{pk} e^{\mathbb{i}u(k\Delta)}}{(f+\mathbb{i}u)^{pk+p}}\,. \quad \text{(B.18)}$$

Note that, $\tilde{G}_{+,2}(u)$ also exhibits a singularity of order $pk+p$ at position $u^* = \mathbb{i}f$ on the imaginary axis of the complex plane. Again we perform the Inverse Fourier Transformation, expand the integral over the whole upper complex plane and obtain

$$G_{+,2}(x,s) = \sum_{k=0}^{\infty} \frac{s^k f^{pk}}{\mathbb{i}^{pk+p-1}}\, \frac{H(\Delta_k - x)}{(pk+p-1)!}\, \frac{\partial^{pk+p-1}}{\partial u^{pk+p-1}} \Big|_{u^*=\mathbb{i}f}\; C(u)\, e^{\mathbb{i}u(\Delta_k - x)}\,. \quad \text{(B.19)}$$

To calculate the deviations of $C(u)\, e^{\mathbb{i}u(\Delta_n - x)}$ we use the formula of Leibniz

$$\frac{\partial^r}{\partial u^r}\,[h(u)b(u)] = \sum_{k=0}^{r} \binom{r}{k} h(u)^{(k)}\, b(u)^{(r-k)} \quad \text{(B.20)}$$

and write

$$\frac{\partial^z}{\partial u^z}[C\, e^{\mathbb{i}u(\Delta_k - x)}] = \sum_{l=0}^{z} \binom{z}{l} \left[e^{\mathbb{i}u(\Delta_k - x)}\right]^{(l)} \left[\sum_{j=0}^{p-1} a_j\, u^j\right]^{(z-l)}$$
$$= \sum_{l=0}^{z} \binom{z}{l} \left[\mathbb{i}^l\, (\Delta_k - x)^l\, e^{\mathbb{i}u\,(\Delta_k - x)}\right] \left[\sum_{j=z-l}^{p-1} \frac{a_j\, u^{j-z+l}\, j!}{(j-z+l)!}\right] \tag{B.21}$$

with $z = pk + p - 1$. We evaluate eq. (B.21) at $u = u^*$

$$\frac{\partial^z}{\partial u^z}\,|_{u=\mathbb{i}f} \left[C\, e^{\mathbb{i}u(\Delta_k - x)}\right] = \sum_{l=0}^{z} \sum_{j=z-l}^{p-1} \binom{z}{l} (\Delta_k - x)^l\, a_j\, f^{j-z+l}\, \frac{\mathbb{i}^{j-z+2l}\, j!}{(j-z+l)!}\, e^{-f\,(\Delta_k - x)}\,, \tag{B.22}$$

apply the Cauchy integral formula and thus finally obtain

$$G_{+,2}(x,s) = \sum_{k=0}^{\infty} \sum_{l=0}^{z} \sum_{j=z-l}^{p-1} H(\Delta_k - x)\, \frac{s^k f^{pk+j-z+l}}{(pk+p-1)!}\, e^{-f\,(\Delta_k - x)} \binom{z}{l} (\Delta_k - x)^l\, a_j\, \frac{\mathbb{i}^{j-z+2l-pk-p+1}\, j!}{(j-z+l)!}\,. \tag{B.23}$$

B.B Calculating the probabilities $\varphi_k(x)$

In accordance to the splitting of $G_+(x,s)$ into $G_{+,1}(x,s)$ and $G_{+,2}(x,s)$ the probabilities $\varphi_k(x)$ also write $\varphi_k(x) = \varphi_{1,k}(x) + \varphi_{2,k}(x)$. In order to calculate these different terms we simplify and rearrange the analytical expressions in eq. (B.16) and eq. (B.23) with respect to s^k.

First we rewrite $G_{+,1}(x,s)$ as

$$G_{+,1}(x,s) = \sum_{k=1}^{\infty} \frac{s^k f^{pk}}{(pk-1)!}\, (\Theta_{k-1} - x)^{pk-1}\, e^{-f(\Theta_{k-1} - x)}\, H(\Theta_{k-1} - x) \tag{B.24}$$

and therefore obtain

$$\varphi_{1,k}(x) = \frac{(\Theta_{k-1} - x)^{pk-1}}{(pk-1)!}\, f^{pk}\, e^{-f(\Theta_{k-1} - x)}\, H(\Theta_{k-1} - x)\,. \tag{B.25}$$

Next we expand the coefficients a_j in eq. (B.23) with respect to s^k,

$$a_j \to \sum_{m=1}^{\infty} a_{j,m}\, s^m \tag{B.26}$$

insert $z = pk + p - 1$ and obtain

$$G_{+,2}(x,s) = \sum_{k=1}^{\infty} \sum_{m=1}^{k} H(\Delta_{k-m} - x)\, \frac{s^k}{(p(k-m)+p-1)!}\, e^{-f\,(\Delta_{k-m} - x)} \times$$

$$\times \sum_{l=0}^{p(k-m)+p-1} \sum_{j=p(k-m)+p-1-l}^{p-1} \binom{p(k-m)+p-1}{l} f^{j+l-p+1} \frac{(\Delta_{k-m}-x)^l \, a_{j,m} \, \mathbb{i}^{j+2l-2p(k-m)-2p+2} \, j!}{(j+l-p(k-m)-p+1)!} \tag{B.27}$$

when performing the following transformations: $k+m \to k'$, $k'-m \to k$, $k' \to k$.

To simplify eq. (B.27) we introduce $\tilde{z} = p(k-m)+p-1$ and rewrite the last two sums into

$$\sum_{l=0}^{\tilde{z}} \sum_{j=0}^{l-p(k-m)} \binom{\tilde{z}}{l} f^{j+\tilde{z}-p+1} \, (\Delta_{k-m}-x)^l \, a_{j+\tilde{z}-l,m} \frac{\mathbb{i}^{j+l-\tilde{z}} \, (j+\tilde{z}-l)!}{j!} \tag{B.28}$$

As next we change the lower border in the sum over l into $p(k-m)$, since the sum over j contributes to $G_{+,2}(x,s)$ only for $l \geq p(k-m)$ and write

$$\sum_{l=0}^{\tilde{z}-p(k-m)} \sum_{j=0}^{l} \binom{\tilde{z}}{l+p(k-m)} f^{j+\tilde{z}-p+1} \, (\Delta_{k-m}-x)^{l+p(k-m)} \, a_{j+\tilde{z}-l+p(k-m),m} \times \\ \times \frac{\mathbb{i}^{j+l+p(k-m)-\tilde{z}} \, (j+\tilde{z}-l-p(k-m))!}{j!} \, . \tag{B.29}$$

Replace $\tilde{z}$ by $p(k-m)+p-1$ and introducing $\tilde{A}_{-l+p-1,m}$ as

$$\tilde{A}_{-l+p-1,m} = \sum_{j=0}^{l} a_{j-l+p-1,m} f^j \, \frac{\mathbb{i}^{j+l-p+1} \, (j-l+p-1)!}{j!} \tag{B.30}$$

yields

$$G_{+,2}(x,s) = \sum_{k=1}^{\infty} \sum_{m=1}^{k} H(\Delta_{k-m}-x) \, \frac{s^k \, e^{-f \, (\Delta_{k-m}-x)}}{(p(k-m)+p-1)!} \times \\ \times \sum_{l=0}^{p-1} \binom{p(k-m)+p-1}{l+p(k-m)} f^{p(k-m)} \, (\Delta_{k-m}-x)^{l+p(k-m)} \tilde{A}_{-l+p-1,m} \tag{B.31}$$

and

$$\varphi_{2,k}(x) = \sum_{m=1}^{k} \sum_{l=0}^{p-1} H(\Delta_{k-m}-x) \, \tilde{A}_{-l+p-1,m} \, e^{-f \, (\Delta_{k-m}-x)} \, \frac{f^{p(k-m)} \, (\Delta_{k-m}-x)^{l+p(k-m)}}{(l+p(k-m))! \; (p-1-l)!} \tag{B.32}$$

after expanding the binomial coefficient in eq. (B.31). For further simplifications we chose the following ansatz:

$$\frac{1}{(p-1-l)!} \sum_{j=0}^{l} \tilde{a}_{j-l+p-1,m} = \frac{\tilde{A}_{-l+p-1,m}}{(p-1-l)!} = z_{l,m} \, f^{pm} \, e^{-f\Theta_{m-1}} \tag{B.33}$$

and accordingly write

$$\varphi_{2,k}(x) = f^{pk}\, e^{-f\ (\Theta_{k-1}-x)} \sum_{m=1}^{k} \sum_{l=0}^{p-1} H(\Delta_{k-m} - x)\, z_{l,m}\, \frac{(\Delta_{k-m} - x)^{l+p(k-m)}}{(l + p(k-m))!}\,. \tag{B.34}$$

We combine the solutions $\varphi_{1,k}(x)$ and $\varphi_{2,k}(x)$ and thus finally obtain

$$\begin{aligned}\varphi_k(x) &= \varphi_{1,k}(x) + \varphi_{2,k}(x) \\ &= \frac{(\Theta_{k-1} - x)^{pk-1}}{(pk-1)!}\, f^{pk}\, e^{-f(\Theta_{k-1}-x)}\, H(\Theta_{k-1} - x) + \\ &+ f^{pk}\, e^{-f\ (\Theta_{k-1}-x)} \sum_{m=1}^{k} \sum_{l=0}^{p-1} H(\Delta_{k-m} - x)\, z_{l,m}\, \frac{(\Delta_{k-m} - x)^{l+p(k-m)}}{(l + p(k-m))!}\,.\end{aligned} \tag{B.35}$$

B.C Estimation of the coefficients $z_{l,m}$

The present section discuss in detail the estimation of the coefficients $z_{l,m}$ in eq. (B.35). The probabilities $\varphi_k(x)$ satisfies equation (B.1) since they are solutions of this Wiener-Hopf problem. To determine the coefficients $z_{l,m}$ we compare the theoretical probability density $\varphi_{k+1,\mathrm{theo}}(x)$, which is achieved when setting k to $k+1$ in eq. (B.35), with the real density $\varphi_{k+1,\mathrm{real}}(x)$ obtain when inserting eq. (B.35) into

$$\varphi_{k+1}(x) = \int_0^\infty \varphi_k(x')\, \rho(x' - x + \Delta) dx' \tag{B.36}$$

and when solving the integral.

We note, that the coefficients $z_{1,m}$ can not be estimated in the proposed way, since $\varphi_1(x)$ is not a solution of the Wiener-Hopf problem. However we can determine the first coefficients $z_{l,m}$ directly since $\varphi_k(x)$ equals $\varphi_1(x)$ for $k = 1$.

$$\varphi_1(x) = f^p\, e^{-f(\Theta-x)} \frac{(\Theta - x)^{p-1}}{(p-1)!}\, H(\Theta - x)\, H(x) \tag{B.37}$$

We set $k = 1$ in eq. (B.35) and obtain

$$\varphi_{1,\mathrm{theo}}(x) = f^p\, e^{-f(\Theta-x)} \left(\frac{(\Theta - x)^{p-1}}{(p-1)!}\, H(\Theta - x) + \sum_{l=0}^{p-1} H(-x)\, z_{l,1}\, \frac{(-x)^l}{(l)!} \right). \tag{B.38}$$

Clearly $\varphi_{1,\mathrm{theo}}(x)$ equals $\varphi_1(x)$ and for $x > 0$. In case $x < 0$ we obtain

$$0 \;= f^p\, e^{-f(\Theta-x)}\, H(-x) \left(\frac{(\Theta - x)^{p-1}}{(p-1)!} + \sum_{l=0}^{p-1} z_{l,1}\, \frac{(-x)^l}{(l)!} \right) \tag{B.39}$$

and thus

$$-\frac{(\Theta - x)^{p-1}}{(p-1)!} \;=\; \sum_{l=0}^{p-1} z_{l,1}\, \frac{(-x)^l}{(l)!}\,. \tag{B.40}$$

Both sides in eq. (B.41) display polynomials in x. Hence we can determine $z_{l,1}$ when comparing those coefficients of the polynomials that belongs to the same order of x. We rewrite eq. (B.40) as

$$-\sum_{g=0}^{p-1} \binom{p-1}{g} \Theta^{p-1-g}\, (-x)^g \;=\; \sum_{l=0}^{p-1} \binom{p-1}{l} (p-1-l)!\; z_{l,1}\, (-x)^l \tag{B.41}$$

and obtain

$$z_{l,1} \;=\; -\frac{\Theta^{p-1-l}}{(p-1-l)!}\,. \tag{B.42}$$

Before calculating the coefficients $z_{k,m}$ we rewrite $\varphi_k(x)$ by splitting the sum over m in eq. (B.35) as follows

$$\begin{aligned}\varphi_k(x) = {} & f^{pk}\frac{(\Theta_{k-1} - x)^{pk-1}}{(pk-1)!}\; e^{-f(\Theta_{k-1}-x)}\; H(\Theta_{k-1} - x) + \\ & +\; f^{pk}\, e^{-f\,(\Theta_{k-1}-x)} \left(\sum_{m=1}^{k-1} \sum_{l=0}^{p-1} H(\Delta_{k-m} - x)\; z_{l,m}\; \frac{(\Delta_{k-m} - x)^{l+p(k-m)}}{(l + p(k-m))!} + \sum_{l=0}^{p-1} H(-x)\; z_{l,k}\; \frac{(-x)^l}{(l)!} \right).\end{aligned} \tag{B.43}$$

Note, that the summand for $m = k$ is different from zero only for negative values in x and therefore does not affect the solution of eq. (B.1). Therefore without loss of generality we reject this summand from the further calculations and write

$$\begin{aligned}\varphi_k(x) = {} & \frac{f^{pk}}{(pk-1)!}\; (\Theta_{k-1} - x)^{pk-1}\; e^{-f(\Theta_{k-1}-x)}\; H(\Theta_{k-1} - x) \\ & +\; f^{pk}\, e^{-f\,(\Theta_{k-1}-x)} \sum_{m=1}^{k-1} \sum_{l=0}^{p-1} H(\Delta_{k-m} - x)\; z_{l,m}\; \frac{(\Delta_{k-m} - x)^{l+p(k-m)}}{(l + p(k-m))!}\,.\end{aligned} \tag{B.44}$$

For a better handling of the equations we again split $\varphi_k(x)$ into the parts $\varphi_{k,1}(x)$ and $\varphi_{k,2}(x)$.

$$\varphi_{k,1}(x) = \; \frac{f^{pk}}{(pk-1)!}\; (\Theta_{k-1} - x)^{pk-1}\; e^{-f(\Theta_{k-1}-x)}\; H(\Theta_{k-1} - x) \tag{B.45}$$

$$\varphi_{k,2}(x) \;=\; f^{pk}\, e^{-f\,(\Theta_{k-1}-x)} \sum_{m=1}^{k-1} \sum_{l=0}^{p-1} H(\Delta_{k-m} - x)\; z_{l,m}\; \frac{(\Delta_{k-m} - x)^{l+p(k-m)}}{(l + p(k-m))!} \tag{B.46}$$

For both parts we (i) calculate the theoretical distribution functions $\varphi_{k+1,1,\text{theo}}(x)$ and $\varphi_{k+1,2,\text{theo}}(x)$

by setting k to $k + 1$ and (ii) the real distribution functions $\varphi_{k+1,1,\text{real}}(x)$ and $\varphi_{k+1,2,\text{real}}(x)$ by inserting the parts into eq. (B.1) and by solving the integral. Afterwards we combine the results, compare the real and the theoretical distributions and thus determine the coefficients $z_{k,m}$.

To calculate the theoretical distribution $\varphi_{k+1,1,\text{theo}}(x)$ we set k to $k + 1$ in eq. (B.45) and obtain

$$\varphi_{k+1,1,\text{theo}}(x) = \frac{f^{pk+p}}{(pk+p-1)!}\,(\Theta_k - x)^{pk+p-1}\,e^{-f(\Theta_k-x)}\,H(\Theta_k - x)\,. \tag{B.47}$$

Next we calculate $\varphi_{k+1,1,\text{real}}(x)$ by inserting eq. (B.45) into (B.1).

$$\varphi_{k+1,1,\text{real}}(x) = \frac{f^{pk+p}\,e^{-f(\Theta_k-x)}}{(pk-1)!\,(p-1)!}\int_0^{\Theta_{k-1}}(\Theta_{k-1}-x')^{pk-1}(x'-x+\Delta)^{p-1}\,H(x'-x+\Delta)\,dx'$$

According to the borders of the integral and according to the Heaviside jump function $H(x'-x+\Delta)$ we have to distinguish two cases. The integral writes

$$\int_0^{\Theta_{k-1}}(\Theta_{k-1}-x')^{pk-1}\,(x'-x+\Delta)^{p-1}\,H(\Delta-x)dx'$$

for $\Delta > x$ and

$$\int_{x-\Delta}^{\Theta_{k-1}}(\Theta_{k-1}-x')^{pk-1}\,(x'-x+\Delta)^{p-1}\,H(x-\Delta)\,H(\Theta_k-x)dx'$$

for $\Delta \le x \le \Theta_k$ respectively. We solve the integrals with the technique of fractional integration and obtain

$$\begin{aligned}\varphi_{k+1,1,\text{real}}(x) &= H(\Theta_k-x)\,f^{pk+p}\,e^{-f(\Theta_k-x)}\,\frac{(\Theta_k-x)^{pk+p-1}}{(pk+p-1)!}\,+\\ &+\;H(\Delta-x)\,f^{pk+p}\,e^{-f(\Theta_k-x)}\left[\left(\sum_{g=0}^{p-1}\frac{(\Theta_{k-1})^{pk+g}\,(\Delta-x)^{p-1-g}}{(pk+g)!\,(p-1-g)!}\right)-\frac{(\Theta_k-x)^{pk+p-1}}{(pk+p-1)!}\right].\end{aligned} \tag{B.48}$$

As next we calculate the distributions $\varphi_{k+1,2,theo}(x)$ and $\varphi_{k+1,2,real}(x)$ and obtain

$$\begin{aligned}\varphi_{k+1,2,theo}(x) &= f^{pk+p}\,e^{-f\,(\Theta_k-x)}\sum_{m=1}^{k-1}\sum_{l=0}^{p-1}H(\Delta_{k+1-m}-x)\,z_{l,m}\frac{(\Delta_{k+1-m}-x)^{l+p(k+1-m)}}{(l+p(k+1-m))!}\,+\\ &+\;f^{pk+p}\,e^{-f\,(\Theta_k-x)}\sum_{l=0}^{p-1}H(\Delta-x)\,z_{l,k}\,\frac{(\Delta-x)^{l+p}}{(l+p)!}\end{aligned} \tag{B.49}$$

and

$$\varphi_{k+1,2,\text{real}}(x) = f^{pk+p}\,e^{-f\,(\Theta_k-x)}\,H(\Delta-x)\left(\sum_{m=1}^{k-1}\sum_{l=0}^{p-1}\sum_{g=0}^{p-1}\frac{z_{l,m}\,(\Delta_{k-m})^{l+p(k-m)+g+1}\,(\Delta-x)^{p-1-g}}{(l+p(k-m)+g+1)!\,(p-1-g)!}\right)+$$

$$+\ f^{pk+p}\ e^{-f\ (\Theta_k - x)} \sum_{m=1}^{k-1} \sum_{l=0}^{p-1} \frac{z_{l,m}\ (\Delta_{k+1-m} - x)^{l+p(k-m)+p}}{(l+p(k-m)+p)!}\ H(\Delta_{k-m+1} - x) -$$

$$-\ f^{pk+p}\ e^{-f\ (\Theta_l - x)}\ H(\Delta - x)\ H(\Delta_{k-m+1} - x) \left(\sum_{m=1}^{k-1} \sum_{l=0}^{p-1} \frac{z_{l,m}\ (\Delta_{k+1-m} - x)^{l+p(k-m)+p}}{(l+p(k-m)+p)!} \right). \tag{B.50}$$

respectively.

We combine eqs. (B.47) and (B.49) and eqs. (B.48) and (B.50) and compare the theoretical distribution $\varphi_{k+1,\text{theo}}(x)$ with the real one $\varphi_{k+1,\text{real}}(x)$.

$$\begin{aligned}
& f^{pk+p}\ e^{-f\ (\Theta_k - x)}\ H(\Delta - x) \sum_{l=0}^{p-1} z_{l,k}\ \frac{(\Delta - x)^{k+p}}{(k+p)!} = \\
&= f^{pk+p}\ e^{-f(\Theta_k - x)}\ H(\Delta - x) \left[\left(\sum_{g=0}^{p-1} \frac{(\Theta_{k-1})^{pk+g}\ (\Delta - x)^{p-1-g}}{(pk+g)!\ (p-1-g)!} \right) - \frac{(\Theta_k - x)^{pk+p-1}}{(pk+p-1)!} \right] + \\
&+\ f^{pk+p}\ e^{-f\ (\Theta_k - x)}\ H(\Delta - x) \left[\sum_{m=1}^{k-1} \sum_{l=0}^{p-1} \sum_{g=0}^{p-1} \frac{z_{l,m}\ (\Delta_{k-m})^{l+p(k-m)+g+1}\ (\Delta - x)^{p-1-g}}{(l+p(k-m)+g+1)!\ (p-1-g)!} \right] - \\
&-\ f^{pk+p}\ e^{-f\ (\Theta_k - x)}\ H(\Delta - x)\ H(\Delta_{k-m+1} - x) \left[\sum_{m=1}^{k-1} \sum_{l=0}^{p-1} \frac{z_{l,m}\ (\Delta_{k+1-m} - x)^{l+p(k-m)+p}}{(l+p(k-m)+p)!} \right].
\end{aligned} \tag{B.51}$$

Eq. (B.51) simplifies to

$$\begin{aligned}
\sum_{l=0}^{p-1} z_{l,k}\ \frac{(\Delta - x)^{l+p}}{(l+p)!} = & \left[\left(\sum_{g=0}^{p-1} \frac{(\Theta_{k-1})^{pk+g}\ (\Delta - x)^{p-1-g}}{(pk+g)!\ (p-1-g)!} \right) - \frac{(\Theta_k - x)^{pk+p-1}}{(pk+p-1)!} \right] + \\
& + \left[\sum_{m=1}^{k-1} \sum_{l=0}^{p-1} \sum_{g=0}^{p-1} \frac{z_{l,m}\ (\Delta_{k-m})^{l+p(k-m)+g+1}\ (\Delta - x)^{p-1-g}}{(l+p(k-m)+g+1)!\ (p-1-g)!} \right] - \\
& - \left[\sum_{m=1}^{k-1} \sum_{l=0}^{p-1} \frac{z_{l,m}\ (\Delta_{k+1-m} - x)^{l+p(k-m)+p}}{(l+p(k-m)+p)!} \right].
\end{aligned} \tag{B.52}$$

when taking into account that $H(\Delta - x)\ H(\Delta_{k-m+1} - x) = H(\Delta - x)$, since the second Heaviside jump function $H(\Delta_{k-m+1} - x)$ writes $H(\Delta_2 - x)$ for the maximal value $m = k - 1$.

For further simplifications we rearrange and expand the different sums and terms in eq. (B.52) and write

$$\begin{aligned}
\sum_{l=0}^{p-1} z_{l,k}\ \frac{(\Delta - x)^{l+p}}{(l+p)!} = & - \sum_{g=0}^{pk-1} \frac{\Theta_{k-1}^{pk-1-g}}{(pk-1-g)!} \frac{(\Delta - x)^{g+p}}{(g+p)!} - \\
& - \sum_{m=1}^{k-1} \sum_{l=0}^{p-1} \sum_{g=0}^{l+p(k-m)} z_{l,m}\ \frac{\Delta_{k-m}^{l+p(k-m)-g}}{(l+p(k-m)-g)!} \frac{(\Delta - x)^{g+p}}{(g+p)!}.
\end{aligned} \tag{B.53}$$

Both sides in eq. (B.53) display polynomials in $(\Delta - x)$. Hence we can determine the coefficients $z_{l,k}$ by comparing those coefficients of the polynomials that belongs to the same order of $(\Delta - x)$. The left hand side of eq. (B.53) is a polynomial of order $p-1$ and the right hand side is one of order $pk + p - 1$. As such we conclude that all parts of the right hand side polynomial, belonging to an order higher than $p - 1$ vanish. Therefore we replace the upper borders in the sum over g by $p - 1$, substitute g by l in the second term on the right hand side and thus finally obtain

$$z_{l,k} \;=\; -\frac{\Theta_{k-1}^{pk-1-l}}{(pk-1-l)!} \;-\sum_{m=1}^{k-1}\sum_{g=0}^{p-1} z_{g,m}\,\frac{\Delta_{k-m}^{g+p(k-m)-l}}{(g+p(k-m)-l)!}\,. \tag{B.54}$$

This recursive relation allows us to calculate all coefficients $z_{l,k}$. Note, that eq. (B.54) also predict the first coefficients $z_{l,1}$. We obtain eq. (B.42) when setting $k = 1$.

B.D Estimation of first passage time probability $\phi_k(a)$

In order to calculate the first passage time probability $\phi_k(a)$ we replace x by $\Theta_{k-1} - T_k$ in eq. (B.44).

$$\tilde{\varphi}_k(x) = f^{pk}\, e^{-fT_k}\left(\frac{T_k^{pk-1}}{(pk-1)!}\,H(T_k) + \sum_{m=1}^{k-1}\sum_{l=0}^{p-1} H(T_k-\Theta_{m-1})\, z_{l,m}\,\frac{(T_k-\Theta_{m-1})^{l+p(k-m)}}{(l+p(k-m))!}\right). \tag{B.55}$$

We insert eq. (B.55) into eq. (7.36) obtain

$$\begin{aligned}\phi_k(A) = \frac{f^{pk+p}}{(p-1)!}\,e^{-fA}\,H(A-\Theta_k)\sum_{g=0}^{p-1}\frac{(A-\Theta_{k-1})^{p-1-g}}{(p-1-g)!}\times \\ \times\left[\frac{(\Theta_{k-1})^{pk+g}}{(pk+g)!} + \sum_{m=1}^{k-1}\sum_{l=0}^{p-1}\frac{z_{l,m}\,(\Delta_{k-m})^{l+p(k-m)+g+1}}{(l+p(k-m)+1+g)!}\right].\end{aligned} \tag{B.56}$$

Note, that in the special case $p = 1$ the Erlang distribution equals the Exponential distribution. Hence $\phi_k(A)$ in eq. (B.56) equals eq. (7.85). In accordance, for $p = 1$ and $\Delta = 0$ we obtain the same result as in sec. 7.3.3.

C Solution of the Wiener-Hopf problem for Erlang WTD for $t_{\mathrm{con}} \neq 0$

C.1 Solution of the Wiener-Hopf problem

The present appendix discuss the solution of the Wiener-Hopf problem (see sec. 7.3.2) which is derived from the analytical description of a conduction model with (i) Erlang distributed atrial interbeat intervals τ and (ii) a conduction time $t_{\mathrm{con}} \neq 0$. As such the random walker starts at a position $V' - \hat{x}$, where $\hat{x}$ denotes the time interval between the onset of the ventricular excitation V' and the occurrence of the last atrial impulse $A_{k'}$, blocked during t_{con}. Accordingly we substitute Θ by $\Theta^* = \Theta + \hat{x}$ and consider the first step of the walker to be of appropriate length $\tau_1 > \hat{x}$, in order to pass V' with the first step.

Hence the distribution $\rho_1(\tau_1)$ of the lengths of the first step τ_1 writes:

$$\rho_1(\tau_1) = A\, f^p \frac{\tau_1^{p-1}}{(p-1)!}\, e^{-f\tau_1}\, H(\tau_1 - \hat{x}) \tag{C.1}$$

where

$$A = \left[\sum_{h=0}^{p-1} \frac{f^{p-1-h}}{(p-1-h)!}\, e^{-f\hat{x}}\, (\hat{x})^{p-1-h}\right]^{-1} \tag{C.2}$$

is the factor of normalisation. We introduce $\varphi_1^*(T_1)$ as the probability to find the walker after one step at position $T_1 = \tau_1$, in front of the border Θ^* and write

$$\varphi_1^*(T_1) = A\, f^p \frac{T_1^{p-1}}{(p-1)!}\, e^{-fT_1}\, H(T_1 - \hat{x})\, H(\Theta^* - T_1)\,. \tag{C.3}$$

In accordance with the substitution of Θ, we introduce the displacement x between the walker and the border as:

$$x_k = \Theta_{k-1}^* - T_k = [\Theta + (k-1)\Delta] + \hat{x} - T_k \tag{C.4}$$

and obtain

$$\varphi_1^*(x) = Af^p\, \frac{(\Theta^* - x)^{p-1}}{(p-1)!}\, e^{-f(\Theta^* - x)}\, H(\Theta - x)\, H(x) \tag{C.5}$$

as the probability to find the walker after the first step in distance x in front of the border Θ^*. We note, that the relation $\tau = x' - x + \Delta$ (eq. (7.38)) stays remain and that the further

displacements x_k, $(k > 1)$ are not affected by the constraint of the first step. Accordingly for the considered conduction model the final Wiener-Hopf equation writes

$$G(x,s) - \int_0^\infty G(x',s)\; s\,\rho(x'-x+\Delta)\,dx' = s\varphi_1^*(x)\,. \tag{C.6}$$

Furthermore, the eqs. (B.4) and (B.7) from the calculation in the previous appendix are also valid, since they are not affected by the particular form of the distribution $\varphi_1^*(x)$. Accordingly we can split the term $\left[1-\tilde{K}(u)\right]$ in the same way as in the previous calculation and thus can directly refer to eq. (B.9) which now writes

$$\omega_+(u)\,\tilde{G}_+(u) + \omega_-(u)\,\tilde{G}_-(u) = \omega_-(u)\,\tilde{g}^*(u) = d^*(u) \tag{C.7}$$

where $\tilde{g}^*(u)$

$$\tilde{g}^*(u) = \sum_{g=0}^{p-1} \frac{s\,f^p\,A\,e^{-f\hat{x}}e^{\mathrm{i}u\Theta}\,(\hat{x})^{p-1-g}}{(p-1-g)!\,(f+\mathrm{i}u)^{g+1}} - \sum_{g=0}^{p-1} \frac{s\,f^p\,A\,e^{-f(\Theta^*)}\,(\Theta^*)^{p-1-g}}{(p-1-g)!\,(f+\mathrm{i}u)^{g+1}} \tag{C.8}$$

is the Fourier Transform of $s\varphi_1^*(x)$.

According to the particular factorisation of $\left[1-\tilde{K}(u)\right]$ we split $s\varphi_1^*(x)$ into

$$\begin{aligned}
d^*(u) &= d_+^*(u) + d_-^*(u)\\
d_+^*(u) &= \sum_{g=0}^{p-1} \frac{s\,f^p\,A\,e^{-f\hat{x}}e^{\mathrm{i}u\Theta}\,(\hat{x})^{p-1-g}}{(p-1-g)!}\,(f+\mathrm{i}u)^{p-g-1}\\
d_-^*(u) &= -\sum_{g=0}^{p-1} \frac{s\,f^p\,A\,e^{-f(\Theta^*)}\,(\Theta^*)^{p-1-g}}{(p-1-g)!}\,(f+\mathrm{i}u)^{p-g-1}\,.
\end{aligned} \tag{C.9}$$

Both functions $d_+^*(u)$ and $d_-^*(u)$ are analytical in the entire complex plane since $g \leq p-1$. In order to to calculate $\tilde{G}_+(u)$, we insert $d_+^*(u)$ and $\omega_+(u)$ into eq. (7.62) and obtain

$$\tilde{G}_+(u) = -\sum_{g=0}^{p-1} \frac{s\,f^p\,A\,e^{-f\hat{x}}e^{\mathrm{i}u\Theta}\,(\hat{x})^{p-1-g}\,(p-1-g)!^{-1}\,(f+\mathrm{i}u)^{p-g-1} + C(u)}{(f+\mathrm{i}u)^p - sf^pe^{\mathrm{i}u\Delta}} \tag{C.10}$$

where $C(u) = \sum_{j=0}^{p-1} a_j\,u^j$ is a polynomial in u of degree $p-1$.

As next we perform the Inverse Fourier Transformation of $\tilde{G}_+(u)$ to calculate the generating function $G(x,s)$. To support the reading we split $G_+(u)$ as follows:

$$\begin{aligned}
\tilde{G}_+(u) &= \tilde{G}_{+,1}(u) + \tilde{G}_{+,2}(u)\\
\tilde{G}_{+,1}(u) &= \frac{d_+(u)}{\omega_+(u)} = -\sum_{g=0}^{p-1} \frac{s\,f^p\,A\,e^{-f\hat{x}}e^{\mathrm{i}u\Theta}\,(\hat{x})^{p-1-g}\,(p-1-g)!^{-1}\,(f+\mathrm{i}u)^{p-g-1}}{(f+\mathrm{i}u)^p - sf^pe^{\mathrm{i}u\Delta}}\\
\tilde{G}_{+,2}(u) &= \frac{C(u)}{\omega_+(u)} = \frac{C(u)}{(f+\mathrm{i}u)^p - sf^pe^{\mathrm{i}u\Delta}}
\end{aligned} \tag{C.11}$$

We rewrite $\tilde{G}_{+,1}(u)$ into

$$\tilde{G}_{+,1}(u) = -\sum_{k=0}^{\infty}\sum_{g=0}^{p-1} \frac{s^{k+1} f^{pk+p} e^{-f\hat{x}} e^{\mathbb{i}u(\Theta+k\Delta)}\, A\,(\hat{x})^{p-1-g}}{(f+\mathbb{i}u)^{pk+g+1}\,(p-1-g)!} \tag{C.12}$$

and obtain

$$G_{+,1}(x,s) = \sum_{k=0}^{\infty}\sum_{g=0}^{p-1} H(\Theta_k - x)\frac{s^{k+1} f^{pk+p} A\,(\hat{x})^{p-1-g}(\Theta_k - x)^{pk+g}\; e^{-f(\Theta_k^*-x)}}{(p-1-g)!\,(pk+g)!}\,. \tag{C.13}$$

when performing the Inverse Fourier Transformation of $\tilde{G}_{+,1}(u)$.

The second part $G_{+,2}(x,s)$ of $G(x,s)$ corresponds to eq. (B.23) in the previous Appendix, since $\tilde{G}_{+,2}(u)$ equals eq. (B.18).

C.2 Calculating the probabilities $\varphi_k(x)$

In accordance to the splitting of $G(x,s)$ into $G_{+,1}(x,s)$ and $G_{+,2}(x,s)$ the distribution $\varphi_k(x)$ writes $\varphi_k(x) = \varphi_{k,1}(x) + \varphi_{k,2}(x)$. In order to calculate $\varphi_{k,1}(x)$ we rearrange the sum over k in $G_{+,1}(x,s)$ which yields:

$$\varphi_{k,1}(x) = \sum_{g=0}^{p-1} H(\Theta_{k-1} - x)\frac{f^{pk} A\,(\hat{x})^{p-1-g}(\Theta_{k-1} - x)^{pk-p+g}\; e^{-f(\Theta_{k-1}^*-x)}}{(p-1-g)!\,(pk-p+g)!}\,. \tag{C.14}$$

The second part $\varphi_{k,2}(x)$ on the other hand equals eq. (B.34) in the previous Appendix, since $G_{+,2}(u)$ equals eq. (B.23). We thus finally obtain

$$\begin{aligned}\varphi_k(x) = &\sum_{g=0}^{p-1} H(\Theta_{k-1} - x)\frac{f^{pk} A\,(\hat{x})^{p-1-g}(\Theta_{k-1} - x)^{pk-p+g}\; e^{-f(\Theta_{k-1}^*-x)}}{(p-1-g)!\,(pk-p+g)!} + \\ &+ f^{pk}\; e^{-f\;(\Theta_{k-1}-x)} \sum_{m=1}^{k}\sum_{l=0}^{p-1} H(\Delta_{k-m} - x)\; z_{l,m}\; \frac{(\Delta_{k-m} - x)^{l+p(k-m)}}{(l+p(k-m))!}\end{aligned} \tag{C.15}$$

C.3 Estimation of the coefficients $z_{l,m}$

We follow the same approach as in the previous section and estimate the coefficients $z_{l,m}$ in that way, that the functions $\varphi_k(x)$ satisfy eq. (C.6). As such we compare the theoretical distribution $\varphi_{k+1,1,\text{theo}}(x)$, which is achieved when setting k to $k+1$ in eq. (C.15), with the real distribution $\varphi_{k+1,1,\text{real}}(x)$ obtained by inserting eq. (C.15) into

$$\varphi_{k+1}(x) = \int_0^{\infty} \varphi_k(x')\,\rho(x' - x + \Delta)dx'\,. \tag{C.16}$$

and by solving the integral.

Again we note, that $\varphi_1(x)$ is not a direct solution of eq. (C.16). We determine the coefficients $z_{1,m}$ by comparing $\varphi_{1,\mathrm{theo}}(x)$

$$\varphi_{1,\mathrm{theo}}(x) = H(\Theta - x) f^p A \, \frac{(\Theta^* - x)^{p-1}}{(p-1)!} \, e^{-f(\Theta^* - x)} \; + \; f^p \, e^{-f(\Theta - x)} \, \sum_{l=0}^{p-1} H(-x) \, z_{l,1} \, \frac{(-x)^l}{(l)!} \, . \tag{C.17}$$

which is obtain by setting k to $k+1$ in eq. (C.15) with $\varphi_1^*(x)$

$$\varphi_1^*(x) = A \, \frac{f^p}{(p-1)!} \, (\Theta^* - x)^{p-1} \, e^{-f(\Theta^* - x)} \, H(\Theta - x) \, H(x) \, . \tag{C.18}$$

Obviously, both functions are equal for $x > 0$. For $x < 0$ on the other hand, we obtain

$$0 = \sum_{l=0}^{p-1} z_{l,1} \, \frac{(-x)^l}{(l)!} + A \, \frac{(\Theta^* - x)^{p-1}}{(p-1)!} \, e^{-f\hat{x}} \tag{C.19}$$

which can be rewritten into

$$-A \, e^{-f\hat{x}} \sum_{g=0}^{p-1} \binom{p-1}{g} (\Theta^*)^{p-1-g} \, (-x)^g \; = \; \sum_{l=0}^{p-1} \binom{p-1}{l} (p-1-l)! \, z_{l,1} \, (-x)^l \, . \tag{C.20}$$

Both sides in eq. (C.20) display polynomials in x of order $p-1$. This allows us to determine the coefficients $z_{l,1}$ by comparing those coefficients of the polynomials that belongs to same order in x. Thus we we obtain

$$z_{l,1} = -A \, e^{-f\hat{x}} \frac{(\Theta^*)^{p-1-l}}{(p-1-l)!} \, . \tag{C.21}$$

which for $\hat{x} = 0$ equals the solution in the previous Appendix (eq. (B.42)).

We insert $z_{l,1}$ into eq. (C.15) and rewrite the expression for $\varphi_k(x)$ into:

$$\begin{aligned} \varphi_k(x) = & \sum_{g=0}^{p-1} H(\Theta_{k-1} - x) \frac{f^{pk} A \, (\hat{x})^{p-1-g} (\Theta_{k-1} - x)^{pk-p+g} \, e^{-f(\Theta^*_{k-1} - x)}}{(p-1-g)! \, (pk-p+g)!} \; + \\ & + \; f^{pk} \, e^{-f \, (\Theta_{k-1} - x)} \sum_{m=1}^{k-1} \sum_{l=0}^{p-1} H(\Delta_{k-m} - x) \, z_{l,m} \, \frac{(\Delta_{k-m} - x)^{l+p(k-m)}}{(l + p(k-m))!} \\ & + \; f^{pk} \, e^{-f \, (\Theta_{k-1} - x)} \sum_{l=0}^{p-1} H(-x) \, z_{l,k} \, \frac{(-x)^l}{(l)!} \end{aligned} \tag{C.22}$$

Obviously the last summand in this expression is different from zero only for negative values in x and therefore does not affect the solution of eq. (C.16). Therefore and without loss of generality, we neglect this summand for the further calculations and write

$$\varphi_k(x) = \varphi_{k,1}(x) + \varphi_{k,2}(x)$$

$$\varphi_{k,1}(x) = \sum_{g=0}^{p-1} H(\Theta_{k-1} - x) \frac{f^{pk} A\ (\hat{x})^{p-1-g} (\Theta_{k-1} - x)^{pk-p+g}\ e^{-f(\Theta^*_{k-1}-x)}}{(p-1-g)!\ (pk-p+g)!}$$

$$\varphi_{k,2}(x) = \ f^{pk}\ e^{-f\ (\Theta_{k-1}-x)} \sum_{m=1}^{k-1} \sum_{l=0}^{p-1} H(\Delta_{k-m} - x)\ z_{l,m}\ \frac{(\Delta_{k-m} - x)^{l+p(k-m)}}{(l + p(k-m))!}\ . \tag{C.23}$$

To determine the coefficients $z_{l,m}$ we compare the theoretical distribution $\varphi_{k+1,1,\text{theo}}(x)$ with the real one $\varphi_{k+1,1,\text{real}}(x)$. The functions $\varphi_{k,2,\text{theo}}(x)$ and $\varphi_{k,2,\text{real}}(x)$ correspond to eq. (B.49) and to eq. (B.50) respectively, since $\varphi_{k,2}(x)$ equals eq. (B.46) in the previous Appendix.

For $\varphi_{k,1}(x)$ the theoretical distribution $\varphi_{k+1,1,\text{theo}}(x)$ writes:

$$\varphi_{k+1,1,\text{theo}}(x)\ = \sum_{g=0}^{p-1} H(\Theta_k - x) \frac{f^{pk+p} A\ (\hat{x})^{p-1-g} (\Theta_k - x)^{pk+g}\ e^{-f(\Theta^*_k - x)}}{(p-1-g)!\ (pk+g)!}\ . \tag{C.24}$$

To calculate $\varphi_{k+1,1,\text{real}}(x)$ we insert $\varphi_{k,1}(x)$ into eq. (C.16) and obtain

$$\begin{aligned}\varphi_{k+1,1,\text{real}}(x) = H(\Theta_k - x) \sum_{g=0}^{p-1} \frac{f^{pk+p}\ e^{-f(\Theta_k + \hat{x} - x)}\ A\ (\hat{x})^{p-1-g}}{(p-1-g)!}\ \frac{(\Theta_k - x)^{pk+g}}{(pk+g)!}\ + \\ + H(\Delta - x) \sum_{g=0}^{p-1} \frac{f^{pk+p}\ e^{-f(\Theta_k+\hat{x}-x)}\ A\ (\hat{x})^{p-1-g}}{(p-1-g)!}\ \times \\ \times \left[\sum_{h=0}^{p-1} \frac{(\Theta_{k-1})^{pk-p+g+1+h}\ (\Delta - x)^{p-1-h}}{(pk-p+g+1+h)!\ (p-1-h)!} - \frac{(\Theta_k - x)^{pk+g}}{(pk+g)!} \right]\end{aligned} \tag{C.25}$$

Comparing $\varphi_{k+1,\text{theo}}(x)$ with $\varphi_{k+1,\text{real}}(x)$ yields

$$\begin{aligned}&H(\Delta - x) \sum_{l=0}^{p-1} z_{l,k}\ \frac{(\Delta - x)^{k+p}}{(k+p)!}\ = \\ &H(\Delta - x) \sum_{g=0}^{p-1} \frac{e^{-f\hat{x}}\ A\ (\hat{x})^{p-1-g}}{(p-1-g)!} \left[\sum_{h=0}^{p-1} \frac{(\Theta_{k-1})^{pk-p+g+1+h}\ (\Delta - x)^{p-1-h}}{(pk-p+g+1+h)!\ (p-1-h)!} - \frac{(\Theta_k - x)^{pk+g}}{(pk+g)!} \right] + \\ &+\ H(\Delta - x) \left[\sum_{m=1}^{k-1} \sum_{l=0}^{p-1} \sum_{g=0}^{p-1} \frac{z_{l,m}\ (\Delta_{k-m})^{l+p(k-m)+g+1}\ (\Delta - x)^{p-1-g}}{(l + p(k-m) + g + 1)!\ (p-1-g)!} \right] - \\ &-\ H(\Delta - x)\ H(\Delta_{k-m+1} - x) \left[\sum_{m=1}^{k-1} \sum_{l=0}^{p-1} \frac{z_{l,m}\ (\Delta_{k+1-m} - x)^{l+p(k-m)+p}}{(l + p(k-m) + p)!} \right]\ .\end{aligned} \tag{C.26}$$

We simplify this expression by rearranging and expanding the different terms and sums and obtain

$$\sum_{l=0}^{p-1} z_{l,k}\ \frac{(\Delta - x)^{l+p}}{(l+p)!}\ = \ -\sum_{g=0}^{p-1} \sum_{l=0}^{pk-p+g} \frac{e^{-f\hat{x}}\ A\ (\hat{x})^{p-1-g}}{(p-1-g)!}\ \frac{(\Theta_{k-1})^{pk-p+g-l}\ (\Delta - x)^{l+p}}{(pk-p+g-l)!\ (l+p)!}\ -$$

$$- \sum_{m=1}^{k-1} \sum_{g=0}^{p-1} \sum_{l=0}^{g+p(k-m)} z_{g,m} \frac{\Delta_{k-m}^{g+p(k-m)-l}}{(g+p(k-m)-l)!} \frac{(\Delta - x)^{l+p}}{(l+p)!} . \tag{C.27}$$

The right hand side of eq. (C.27) is a polynomial of $(\Delta - x)$ of order $pk + p - 1$ and the left hand side is a polynomial of $(\Delta - x)$ of order $p - 1$. Hence we conclude that, all parts of the right hand polynomial, which belong to an order in $(\Delta - x)$ higher than $p - 1$, vanish.

To determine the parameters $z_{l,k}$ we first rewrite the sum $\sum_{l=0}^{g+p(k-m)}$ in the second term of the right handed polynomial into $\sum_{l=0}^{p-1}$, since $g + p(k - m) \geq p$ for all combinations of m, k and g. Next we rewrite the sum $\sum_{l=0}^{pk-p+g}$ in the first term of the right handed polynomial. Note, that we have to distinguish two different cases. The upper border $pk - p + g$ in the second sum is greater than p only for $k > 1$. Hence we replace the upper border $pk - p + g$ (i) by $p - 1$ for $k > 1$ and (ii) by g for $k = 1$. In the latter case we substitute g by l and thus finally obtain:

$$z_{l,k} = - \sum_{g=0}^{p-1} \frac{e^{-f\hat{x}} A (\hat{x})^{p-1-g}}{(p-1-g)!} \frac{(\Theta_{k-1})^{pk-p+g-l}}{(pk-p+g-l)!} \tag{C.28}$$

in case $k = 1$ and

$$z_{l,k} = - \sum_{g=0}^{p-1} \frac{e^{-f\hat{x}} A (\hat{x})^{p-1-g}}{(p-1-g)!} \frac{(\Theta_{k-1})^{pk-p+g-l}}{(pk-p+g-l)!} - \sum_{m=1}^{k-1} \sum_{g=0}^{p-1} z_{g,m} \frac{\Delta_{k-m}^{g+p(k-m)-l}}{(g+p(k-m)-l)!} \tag{C.29}$$

for $k > 1$ respectively.

Note, that in the special case $\hat{x} = 0$ the eqs. (C.28) and (C.29) equal the result of the previous Appendix (eq. (B.54)).

C.4 Estimation of first passage time probability $\phi_k(a)$

To calculate the first passage time probability $\phi_k(a)$ we first replace x by $x = \Theta_{k-1}^* - T_k$ in eq. (C.15) and afterwards insert $\tilde{\varphi}_k(T_k)$ into eq. (7.36). Thus we obtain

$$\phi_k(a) = H(a - \theta_k^*) \int_0^{\theta_{k-1}^*} \tilde{\varphi}_k(T_k) \rho(a - T_k) \, dT_k = I_1 + I_2 \tag{C.30}$$

with

$$\begin{aligned} I_1 &= H(a-\theta_k^*) \sum_{g=0}^{p-1} \frac{f^{pk+p} A e^{-fa} (\hat{x})^{p-1-g}}{(p-1)!\,(p-1-g)!\,(pk-p+g)!} \int_{\hat{x}}^{\Theta_{k-1}^*} (T_k - \hat{x})^{pk-p+g} (a - T_k)^{p-1} dT_k \\ &= H(a-\theta_k^*) f^{pk+p} A e^{-fa} \sum_{g=0}^{p-1} \sum_{r=0}^{p-1} \frac{(\hat{x})^{p-1-g} (\Theta_{k-1})^{pk-p+g+1+r} (a - \Theta_{k-1}^*)^{p-1-r}}{(p-1-g)!\,(pk-p+g+1+r)!\,(p-1-r)!} \end{aligned} \tag{C.31}$$

and

$$I_2 = H(a-\theta_k^*)\sum_{m=1}^{k-1}\sum_{l=0}^{p-1}\frac{f^{pk+p}\ e^{-f(a-\hat{x})}}{(p-1)!\ (l+p(k-m))!}\int_{\Theta_{m-1}^*}^{\Theta_{k-1}^*}(T_k-\Theta_{m-1}^*)^{l+p(k-m)}(a-T_k)^{p-1}dT_k$$
$$= H(a-\theta_k^*)\ f^{pk+p}\ e^{-f(a-\hat{x})}\sum_{m=1}^{k-1}\sum_{l=0}^{p-1}\sum_{r=0}^{p-1} z_{l,m}\frac{(\Delta_{k-m})^{l+p(k-m)+1+r}\ (a-\Theta_{k-1}^*)^{p-1-r}}{(l+p(k-m)+1+r)!\ (p-1-r)!} \tag{C.32}$$

respectively. Solving the integrals finally yields

$$\phi_k(a) = H(a-\theta_k^*)\ f^{pk+p}\ e^{-fa}\ \sum_{r=0}^{p-1}\frac{(a-\Theta_{k-1})^{p-1-r}}{(p-1-r)!}\times$$
$$\left[\sum_{g=0}^{p-1}\frac{A\ (\hat{x})^{p-1-g}(\Theta_{k-1})^{pk-p+g+1+r}}{(p-1-g)!\ (pk-p+g+1+r)!} - e^{f\hat{x}}\sum_{m=1}^{k-1}\sum_{l=0}^{p-1} z_{l,m}\frac{(\Delta_{k-m})^{l+p(k-m)+1+r}}{(l+p(k-m)+1+r)!}\right] \tag{C.33}$$

Statement

Ich versichere, daß ich die vorliegende Arbeit ohne unzulässige Hilfe Dritter und ohne Benutzung anderer als der angegebenen Hilfsmittel angefertigt habe. Die aus anderen Quellen direkt oder indirekt übernommenen Daten und Konzepte sind unter Angabe der Quelle gekennzeichnet.

Weitere Personen waren an der inhaltlichen und materiellen Erstellung der vorliegenden Arbeit nicht beteiligt. Insbesondere habe ich hierfür nicht die entgeltliche Hilfe von Vermittlungs- oder Beratungsdiensten (Promotionsberatern oder anderer Personen) in Anspruch genommen. Niemand hat von mir unmittelbar oder mittelbar geldwerte Leistungen für Arbeiten erhalten, die im Zusammenhang mit dem Inhalt der vorgelegten Dissertation stehen.

Die Arbeit wurde bisher weder im In- noch im Ausland in gleicher oder ähnlicher Form einer Prüfungsbehörde vorgelegt.

Ich bin darauf hingewiesen worden, daß die Unrichtigkeit der vorstehenden Erklärung als Täuschungsversuch angesehen wird und den erfolglosen Abbruch des Promotionsverfahrens zur Folge hat.

(Ilmenau, Datum) (Thomas Hennig)

Acknowledgment

Maßgebend für den Erfolg meiner Arbeit war eine vielseitige fachliche und menschliche Unterstützung. Dafür habe ich zu danken.

Als erstes gilt mein Dank Herrn Prof. Dr. Philipp Maaß , der mir während der vergangenen Jahre Unterstützung und fachliche Kritik gewährte und durch seine Hinweise maßgeblich zur Struktur der vorliegenden Arbeit beitrug.

Desweiteren möchte ich mich bei den Mitarbeitern der Arbeitsgruppen „ Theoretische Physik II / Computational Physics“und „Theoretische Physik I“ der Technischen Universität Ilmenau für die konstruktive und kollegiale Zusammenarbeit und den fachlichen Austausch bedanken.

Zum Zustandekommen und Gelingen meiner Arbeit haben viele Menschen beigetragen und mich bei der Arbeit an diesem Thema fachlich und menschlich unterstützt. Besonders herausheben möchte ich dabei die folgenden Personen: Dr. Hartmut Grille, Prof.Erich Runge, Dr. Wichard J. D. Beenken. Desweiteren gilt mein Dank Frau Yvonne Raab.

Nicht nur für die Durchsicht und Korrektur dieses Manuskriptes, sondern auch für ihre Geduld, ihr Interesse und ihre vielen kleinen Hilfeleistungen danke ich meiner Frau, meinen Freunden und Schopenhauer.

Abbildungsverzeichnis

Tabellenverzeichnis

Literaturverzeichnis

[Allessie76] M.A. Allessie, F.I. Bonke, and F.J. Schopman. Circus movement in rabbit atrial muscle as a mechanism of tachycardia. II. the role of nonuniform recovery of excitability in the occurrence of unidirectional block, as studied with multiple microelectrodes. Circulation, 39:168–177, 1976.

[Allessie85] M.A. Allessie, W.J.P.E. Lammers, F.I.M. Bonke, and J. Hollen. Experimental evaluation af Moe's multiple wavelet hypothesis of AF. New York: Grune & Stratton, 1985.

[Allessie96] M.A. Allessie, K. Konings, C.J. Kirchhof, and M. Wijffels. Electrophysiologic mechanisms of perpetuation of atrial fibrillation. Am. J. Cardiol., 77:10A–23A, 1996.

[Andresen98] D. Andresen and T. Brüggemann. Heart rate variability preceding onset of atrial fibrillation. J. Cardiovasc. Electrophysiol. Supp., 9:26–29, 1998.

[Arnar96] D.O. Arnar and R. Danielsen. Factors predicting maintenance of sinus rhythm after direct current cardioversion of atrial fibrillation and flutter: a reanalysis with recently acquired data. Cardiology, 87:181–188, 1996.

[Asano92] Y. Asano, J. Saito, K. Matsumoto, K. Kaneko, T. Yamamoto, and M. Uchida. On the mechanism of termination and perpetuation of atrial fibrillation. Am. J. Cardiol., 69(12):1033–1038, April 1992.

[Aysha88] M.H. Aysha and A.S. Hassan. Diagnostic importance of fibrillatory wave amplitude: a clue to echocardiographic left atrial size and etiology of atrial fibrillation. J. Electrocardiol., 21:247–251, 1988.

[Aytemir99] K. Aytemir, S. Aksoyek, A. Yildirir, N. Ozer, and A. Oto. Prediction of atrial fibrillation recurrence after cardioversion by p wave signal-averaged electrocardiography. Int. J. Cardiol., 70:15–21, 1999.

[Barning63] F.J.M. Barning. The numerical analysis of the light-curve of 12 lacertae. Bulletin of the Astronomical Institutes of the Netherlands, 17:22—28, 1963.

[Bartall78] H. Bartall, K.B. Desser, A. Benchimol, and B.J. Massey. Assessment of echocardiographic left atrial enlargement in patients with atrial fibrillation. an electrovectorcardiographic study. J. Electrocardiol., 11:269–272, 1978.

[Bartsch05] R. Bartsch, Th. Hennig, A. Heinen, St. Heinrichs, and P. Maass. Sta-

tistical analysis of fluctuations in the ecg morphology. Physica A, 354:415, 2005.

[Bauernfeind81] R.A. Bauernfeind, C.R. Wyndham, S.P. Swiryn, E.V. Palileo, B. Strasberg, W. Lam, D. Westveer, and K.M. Rosen. Paroxysmal atrial fibrillation in the Wolff-Parkinson-White syndrome. Am. J. Cardiol., 47(3):562–569, March 1981.

[Bellet71] S. Bellet. Clinical disorders of the heart beat. Philadelphia: Lea and Febiger, 3rd edition, 1971.

[Ben-Avraham00] D. Ben-Avraham and S. Havlin. Diffusion and reactions in fractals and disordered system. Cambridge University Press, 2000.

[Bigger95] J.T. Bigger, L.F. Fleiss, R.C. Steinman, L.M. Rolnitzky, W.J. Schneider, and P.K. Stein. Rr variability in healthy, middle-age persons compared with patients with chronic coronary heart disease or recent acute myocardial infarction. Circulation, 91:1936–1943, 1995.

[Blackshear96] J.L. Blackshear, R.E. Safford, and L.A. Pearce. F-amplitude, left atrial appendage velocity, and thromboembolic risk in nonrheumatic atrial fibrillation. stroke prevention in atrial fibrillation investigators. Clin. Cardiol., 19:309–313, 1996.

[Boahene90] K.A. Boahene, G.J. Klein, R. Yee, A.D. Sharma, and O. Fujimura. Termination of acute atrial fibrillation in the Wolff-Parkinson-White syndrome by procainamide and propafenone: importance of atrial fibrillatory cycle length. J. Am. Coll. Cardiol., 16(6):1408–1414, November 1990.

[Bollmann98] A. Bollmann, N.K. Kanuru, K.K. McTeague, P.F. Walter, D.B. DeLurgio, and J.J. Langberg. Frequency analysis of human atrial fibrillation using the surface electrocardiogram and its response to ibutilide. Am. J. Cardiol., 81:1439–1445, 1998.

[Bollmann99] A. Bollmann, K. Sonne, H.D. Esperer, I. Toepffer, J.J. Langberg, and H.U. Klein. Non-invasive assessment of fibrillatory activity in patients with paroxysmal and persistent atrial fibrillation using the holter ecg. Cardiovasc. Res., 44:60–66, 1999.

[Bollmann00] A. Bollmann, K. Sonne, and H.D. Esperer et al. Circadian variations in atrial fibrillatory frequency in persistent human atrial fibrillation. Pacing Clin. Electrophysiol, 23:1867–1871, 2000.

[Bootsma70] B. Bootsma, A. Hollen, and J. Strackee. Analysis of RR intervals in patients with atrial fibrillation at rest and during exercise. Circulation, 41:783–794, 1970.

[Botteron95] G.W. Botteron and J.M. Smith. A technique for measurements of the extent of spatial organization of atrial activation during atrial fibrillation in the intact human heart. IEEE Trans. Biom. Eng., 42:579–586, 1995.

[Britton85] M. Britton and C.l Gustafsson et a. Non-rheumatic atrial fibrillation

as a risk factor for stroke. Stroke, 14:182–188, 1985.

[Bunde00] A. Bunde, S. Havlin, J.W. Kantelhardt, T. Penzel, J.H. Peter, and K. Voigt. Correlated and uncorrelated regions in heart-rate fluctuations during sleep. Phys. Rev. Lett., 85:3736–3739, 2000.

[Cammarota02] C. Cammarota, G. Guarini, E. Rogora, and M. Ambrosini. Non stationary model of the heart beat time series in atrial fibrillation. In Mathematical Modelling and Computing in Biology and Medicine. Milan, 2002.

[Cammarota05] C. Cammarota and E. Rogora. Validation of a nonstationary modification of a model due to Zeng and Glass. In Applied and Industrial Mathematics in Italy, pages 179–188. World Scientific, New Jersey, Venezia, September 2005.

[Capucci95] A. Capucci, M. Biffi, and G. Boriani et al. Dynamic electrophysiological behavior of human atria during paroxysmal atrial fibrillation. Circulation, 92:1193–1202, 1995.

[Castiglioni96] P. Castiglioni and M.D. Rienzo. On the evaluation of heart rate spectra : the lomb periodogram. Computers in Cardiology, pages 505–508, 1996.

[Censi00] F. Censi, V. Barbaro, P. Bartolini, G. Calcagnini, A. Michelucci, G.F. Gensini, and S. Cerutti. Recurrent patterns of atrial depolarization during atrial fibrillation assessed by recurrence plot quantification. Ann. Biomed. Eng., 28:61–70, 2000.

[Chialvo90] D.R. Chialvo, R.F. Gilmour, and J. Jalife. Low dimensional chaos in cardiac tissue. Nature, 343:653–657, 1990.

[Chorro88] F.J. Chorro, R. Ruiz-Granell, E. Casadan, R. Garcia-Civera, L. Such, and V. Lopez-Merino. Mathematical description of av nodal function curves in dogs. Pace, 11:679–686, 1988.

[Cinca86] J. Cinca, A. Moya, and J. Figueras et al. Circadian variations in the electrical properties of the human heart assessed by sequential bedside electrophysiologic testing. Am. Heart J., 112:315–321, 1986.

[Clifford02] G.D. Clifford. Signal Processing Methods for Heart Rate Variability. Ph.D. thesis, University of Oxford, Department of Engineering Science, 2002.

[Cohen83] R.J. Cohen, R.D. Berger, and T.E. Dushane. A quantitative model for the ventricular response during atrial fibrillation. IEEE Trans. Biomed. Eng., 30(12):769–781, 1983.

[Eichner03] J.F. Eichner, E. Koscielny-Bunde, A. Bunde, S. Havlin, and H.J. Schellnhuber. Power-law persistence and trends in the atmosphere: a detailed study of long temperature records. Phys. Rev. E, 68, 2003.

[Engelse79] W.A.H. Engelse and C. Zeelenberg. A single scan algorithm for qrs-

detection and feature extraction. Computers in Cardiology, 6:37–42, 1979.

[Feld94] G. Feld, P. Fleck, and O. Fujimura. Control of rapid ventricular response by radiofrequency catheter modification of the atrioventricular node in patients with medically refractory atrial fibrillation. Circulation, 90:2299–2307, 1994.

[Ferrier74] G.R. Ferrier and P.E. Dresel. Relationship of the functional refractory period to conduction in the atrioventricular node. Circ. Res., 35:204–214, 1974.

[Flegel87] K.M. Flegel, M.J. Shipley, and G. Rose. Risk of stroke in non-rheumatic atrial fibrillation. Lancet, 1:526–529, 1987.

[Fujiki01] A. Fujiki, H. Nagasawa, and M. Sakabe et al. Spectral characteristics of human atrial fibrillation waves of the right atrial free wall with respect to the duration of atrial fibrillation and effect of class i antiarrhythmic drugs. Jpn. Circ. J., 65:1047–1051, 2001.

[Furberg94] C.D. Furberg, B.M. Psaty, T.A. Manolio, J.M. Gardin, V.E. Smith, and P.M. Rautaharju. Prevalence of atrial fibrillation in elderly subjects (the Cardiovascular Health Study). Am. J. Cardiol., 74(3):236–241, 1994.

[Fuster01] V. Fuster and L.E. Ryden. Acc/aha/esc guidelines for the management of patients with atrial fibrillation - a report of the american college of cardiology/american heart association task force on practice guidelines and the european society of cardiology committee for practice guidelines and policy conferences (committee to develop guidelines for the management of patients with atrial fibrillation). Journal of the American College of Cardiology, 38(4):1265–1335, 2001.

[Gaita98] F. Gaita, R. Riccardi, L. Calo, M. Scaglione, L. Garberoglio, R. Antolini, M. Kirchner, F. Lamberti, and E. Richiardi. Atrial mapping and radiofrequency catheter ablation in patients with idiopathic atrial fibrillation. electrophysiological findings and ablation results. Circulation, 97:2136–2145, 1998.

[Garfinkel97] A. Garfinkel, P.S. Chen, D.O. Walter, H.S. Karagueuzian, B. Kogan, B.J. Evans, M. Karpoukhin, C. Hwang, T. Uchida, M. Gotoh, O. Nwasakwa, P. Sager, and J.N. Weiss. Quasiperiodicity and chaos in cardiac fibrillation. J. Clin. Invest., 99:305–314, 1997.

[Gelzer00] A.R. Gelzer, N.S. Moise, D. Vaidya, K.A. Wagner, and J. Jalife. Temporal organization of atrial activity and irregular ventricular rhythm during spontaneous atrial fibrillation: an in vivo study in the horse. J. Cardiovasc. Electrophysiol., 11(7):773–784, 2000.

[Glass91] L. Glass, P.J. Hunter, and A. McCulloch, editors. Biomechanics, Biophysics, and Nonlinear Dynamics of Cardiac Function, pages 313–358. Springer-Verlag, 1991.

[Glass05] L. Glass and K. Tateno. Detection of cardiac arrhythmia using mathematical representation of standard δrr probability density histograms. US Patent 10382385 Issued on December 5, 2006, 2005.

[Goldberger00] A.L. Goldberger, L.A.N. Amaral, L. Glass, J.M. Hausdorff, P.Ch. Ivanov, R.G. Mark, J.E. Mietus, G.B. Moody, C.-K. Peng, and H.E. Stanley. Physiobank, physiotoolkit, and physionet : Components of a new research resource for complex physiologic signals. Circulation, 101:215–220, 2000.

[Goldsmith92] R.L. Goldsmith, J.T. Bigger, and R.C. Steinman. Comparison of 24-hour parasympathetic activity in endurance-trained and untrained young men. J. Am. Coll. Cardiol., 20:552–558, 1992.

[Goldstein67] R.E. Goldstein and G.O. Barnett. A statistical study of the ventricular irregularity of atrial fibrillation. Comput. Biomed. Res., 1:146, 1967.

[Haissaguerre98] M. Haissaguerre, P. Jais, and D.C. Shah. Spontaneous initiation of atrial fibrillation by ectopic beats originating in the pulmonary veins. N. Engl. J. Med., 339:1998, 1998.

[Hayano97] J. Hayano, F. Yamasaki, S. Sakata, A. Okada, S. Mukai, and T. Fujinami. Spectral characteristics of ventricular response to atrial fibrillation. Am. J. Physiol., 273:2811–2816, 1997.

[Heinrichs04] S. Heinrichs, Z.R. Struzik, J. Hayano, and Y. Yamamoto. Probing temporal correlation in ventricular interbeat intervals during atrial fibrillation with local continuous dfa, *proceedings of spie second international symposium on fluctuations and noise*. Proceedings of SPIE Second International Symposium on Fluctuations and Noise, 5467:404–410, 2004.

[Hennig06a] Th. Hennig and P. Maass. Long exponentially distributed interbeat intervals in the ecg of af patients show white noise behaviour in power spectrum. Berichte der ESGCO 2006, S. 31-35, 2006.

[Hennig06b] Th. Hennig and P. Maass. Verfahren zur nicht-invasiven bestimmung der vorhofflimmerrate. Patentanmeldung 12.07.06, 2006.

[Hennig06c] Th. Hennig, P. Maass, J. Hayano, and S. Heinrichs. Exponential distribution of long heart beat intervals during atrial fibrillation and their relevance for white noise behaviour in power spectrum. J. Biol. Phys., 32:383, 2006.

[Henry76] W.L. Henry, J. Morganroth, A.S. Pearlman, C.E. Clark, D.R. Redwood, S.B. Itscoitz, and S.E. Epstein. Relation between echocardiographically determined left atrial size and atrial fibrillation. Circulation, 53:273–279, 1976.

[Hobbs00] W.J. Hobbs, S. Fynn, D.M. Todd, P. Wolfson, M. Galloway, and C.J. Garratt. Reversal of atrial electrical remodeling after cardioversion of persistent atrial fibrillation in humans. Circulation, 101:1145–

1151, 2000.

[Hoekstra95] B.P. Hoekstra, C.G. Diks, M.A. Allessie, and J. DeGoede. Nonlinear analysis of epicardial atrial electrograms of electrically induced atrial fibrillation in man. J. Cardiovasc. Electrophysiol., 6:419–440, 1995.

[Hoffmann02] E. Hoffmann, S. Janko, C. Reithmann, and G. Steinbeck. Auslösemechanismen von Vorhofflimmern. Kardiol, 91:24–32, 2002.

[Hoglund85] C. Hoglund and G. Rosenhamer. Echocardiographic left atrial dimension as a predictor of maintaining sinus rhythm after conversion of atrial fibrillation. Acta Med. Scand., 217:411–415, 1985.

[Honerkamp94] J. Honerkamp. Stochastic Dynamical Systems: Concepts, Numerical Methods, Data Analysis. VCH Publishers, Cambridge, 1994.

[Huikuri95] H.V. Huikuri, S. Yli-Mayry, and M.K. Linnaluoto et al. Diurnal fluctuations in human ventricular and atrial refractoriness. Pacing Clin. Electrophysiol, 18:1362–1368, 1995.

[Hurst51] H.E. Hurst. Long-term storage capacity of reservoirs. Transactions of the American Society of Civil Engineering, 116:770, 1951.

[Ivanov99] P.Ch. Ivanov, A. Bunde, L.A.N. Amaral, S. Havlin, J. Fritsch-Yelle, R.M. Baevsky, H.E. Stanley, and A.L. Goldberger. Sleep-wake differences in scaling behavior of the human heartbeat: analysis of terrestrial and long-term space flight data. Europhysics Letters, 48(5):594–600, 1999.

[Jais96] P. Jais, M. Haissaguerre, D.C. Shah, S. Chouairi, and J. Clementy. Regional disparities of endocardial atrial activation in paroxysmal atrial fibrillation. PACE, 19:1998–2003, 1996.

[Jais97] P. Jais, M. Haissaguerre, and D.C. Shah. A focal source of atrial fibrillation treated by discrete radiofrequency ablation. Circulation, 95:572–576, 1997.

[Jalife98] J. Jalife, O. Berenfeld, A. Skanes, and R. Mandapati. Mechanisms of atrial fibrillation: mother rotors or multiple daughter wavelets, or both? J. Cardiovasc. Electrophysiol., 9:2–12, 1998.

[Jørgensen02] P. Jørgensen, C. Schaefer, P. Guerra, M. Talajic, S. Nattel, and L. Glass. A mathematical model of human atrioventricular nodal function incorporating concealed conduction. Bull. Math. Bio., 64:1083, 2002.

[Kannel82] W.B. Kannel, R.D. Abbott, D.D. Savage, and P.M. McNamara. Epidemiologic features of chronic atrial fibrillation: the Framingham study. N. Engl. J. Med., 306:1018–1022, 1982.

[Kannel83] W.B. Kannel, R.D. Abbott, D.D. Savage, and P.M. McNamara. Coronary heart disease and atrial fibrillation: the Framingham study.

Am. Heart. J., 106:389–396, 1983.

[Kantelhardt01] J.W. Kantelhardt, E. Koscielny-Bunde, H.H.A. Rego, S. Havlin, and A. Bunde. Detecting long-range correlations with detrended fluctuation analysis. Physica A, 295:441–454, 2001.

[Kantelhardt02] J.W. Kantelhardt, Y. Ashkenazy, P.Ch. Ivanov, A. Bunde, S. Havlin, T. Penzel, H.-J. Peter, and H.E. Stanley. Characterization of sleep stages by correlations of magnitude and sign of heartbeat increments. Phys. Rev. E, 65, 2002.

[Kim96] K.B. Kim, M.D. Rodefeld, and R.B. Schuessler et al. Relationship between local atrial fibrillation interval and refractory period in the isolated canine atrium. Circulation, 94:2961–2967, 1996.

[Kirsh88] J.A. Kirsh, A.V. Sahakian, J.M. Baerman, and S. Swiryn. Ventricular response to atrial fibrillation: role of atrioventricular conduction pathways. J. Am. Coll. Cardiol., 12(5):1265–1272, November 1988.

[Kneller02] J. Kneller, R. Zou, E.J. Vigmond, Zh. Wang, Joshua Leon. L., and S. Nattel. Cholinergic atrial fibrillation in a computer model of a two-dimensional sheet of canine atrial cells with realistic ionic properties. Circ. Res., 90:73–87, 2002.

[Konings94] K.T. Konings, C.J. Kirchhof, J.R. Smeets, H.J. Wellens, O.C. Penn, and M.A. Allessie. High-density mapping of electrically induced atrial fibrillation in humans. Circulation, 89:1665–1680, April 1994.

[Koscielny-Bunde96] E. Koscielny-Bunde, A. Bunde, S. Havlin, and Y. Goldreich. Analysis of daily temperature fluctuations. Physica A, 231(393):393–396, 1996.

[Koscielny-Bunde98] E. Koscielny-Bunde, A. Bunde, S. Havlin, H.E. Roman, Y. Goldreich, and H.-J. Schellnhuber. Indication of a universal persistence law governing atmospheric variability. Phys. Rev. Lett., 81:729–732, 1998.

[Krahn95] A.D. Krahn, J. Manfreda, R.B. Tate, F.A. Mathewson, and T.E. Cuddy. The natural history of atrial fibrillation: incidence, risk factors, and prognosis in the manitoba follow-up study. Am. J. Med., 98:476–484, 1995.

[Laguna98] P. Laguna, G.B. Moody, and R.G. Mark. Power spectral density of unevenly sampled data by least-square analysis: Performance and application to heart rate signals. IEEE Transcations in Biomedical Engineering, 45(6):1998, June 1998.

[Langberg98] J.J. Langberg and A. Bollmann. Method, system and apparatus for determining prognosis in atrial fibrillation. US Patent 5772604, Issued on June 30, 1998, 1998.

[Langendorf48] R. Langendorf. Concealed a-v conduction: the effect of blocked impulses on the formation and conduction of subsequent impulses. Am. Heart J., 35:542–552, 1948.

[Leier80] C.V. Leier and S.F. Schaal. Biatrial electrograms during coarse atrial fibrillation and flutter-fibrillation. Am. Heart J., 99:331–341, 1980.

[Levy98] S. Levy. Epidemiology and classification of atrial fibrillation. J. Cardiovasc. Electrophysiol, 9:78–82, 1998.

[Levy99] S. Levy, M. Maarek, and P. Coumel. Characterization of different subsets of atrial fibrillation in general practice in France: the ALFA study. Circulation, 99:3028–3035, 1999.

[Lewis25a] T. Lewis. The mechanism and graphic registration of the heart beat. Shaw and Sons London, 1925.

[Lewis25b] T. Lewis and A.M. Master. Observations upon conduction in the mammalian heart. a-v conduction. Heart, 12:209–269, 1925.

[Li95] Y.H. Li, J.J. Hwang, Y.Z. Tseng, P. Kuan, and W.P. Lien. Clinical significance of fibrillatory wave amplitude - a clue to left atrial appendage function in nonrheumatic atrial fibrillation. Chest, 108:359–363, 1995.

[Li96] H. Li, J. Hare, K. Mughal, D. Krum, M. Biehl, S. Deshpande, A. Dhala, Z. Blanck, J. Sra, M. Jazayeri, and M. Akhtar. Distribution of atrial electrogram types during atrial fibrillation: effect of rapid atrial pacing and intercaval junction ablation. J. Am. Coll. Cardiol., 27:1713–1721, 1996.

[Lomb76] N.R. Lomb. Least-squares frequency analysis of unequally spaced data. Astrophysics and Space Science, 39:447–462, 1976.

[Manabe97] K. Manabe, T. Oki, T. Tabata, H. Yamada, K. Fukuda, M. Abe, A. Iuchi, N. Fukuda, and S. Ito. Transesophageal echocardiographic prediction of initially successful electrical cardioversion of isolated atrial fibrillation. effects of left atrial appendage function. Jpn. Heart J., 38:487–495, 1997.

[Mandelbrot68] B.B. Mandelbrot and J.W. van Ness. Fractional brownian motions, fractional noises and applications. SIAM Review, 10(4):422–437, 1968.

[Mangin05] L. Mangin, A. Vinetb, P. Pagéb, and L. Glass. Effects of antiarrhythmic drug therapy on atrioventricular nodal function during atrial fibrillation in humans. Europace, 7:71–82, 2005.

[Meurling01] C.J. Meurling, J.E.P. Waktare, I. Holmqvist, A. Hedman, A.J. Camm, S.B. Olsson, and M. Malik. Diurnal variations of the dominant cycle length of chronic atrial fibrillation. Am. J. Physiol. Heart Circ. Physiol., 280:401–406, 2001.

[Mietus02] J.E. Mietus, C.-K. Peng, I. Henry, R.L. Goldsmith, and A.L. Goldberger. The pnnx files: re-examining a widely used heart rate variability measure. Heart, 88:378–380, 2002.

[Misier92] A.R. Misier, T. Opthof, and N.M. van Hemel et al. Increased disper-

sion of refractoriness in patients with idiopathic paroxysmal atrial fibrillation. J. Am. Coll. Cardiol., 19:1531–1535, 1992.

[Moe59] G.K. Moe and J.A. Abildskov. Atrial fibrillation as a self sustaining arrhythmia independent of focal discharge. Am. Heart. J., 58:59–70, 1959.

[Moe62] G. Moe. On the multiple wavelet hypothesis of atrial fibrillation. Arch. Int. Pharmacodyn. Ther., 140:183–188, 1962.

[Moe64] G.K. Moe and J.A. Abildskov. Observations on the ventricular dysrhythmia associated with atrial fibrillation in the dog heart. Circulation Res., 14:447–460, 1964.

[Morady97] F. Morady, C. Hasse, and S. Strickberger. Long-term followup after radiofrequency modification of the atrioventricular node in patients with atrial fibrillation. J. Am. Coll. Cardiol., 27:113–121, 1997.

[Morganroth79] J. Morganroth, L.N. Horowitz, M.E. Josephson, and J.A. Kastor. Relationship of atrial fibrillatory wave amplitude to left atrial size and etiology of heart disease. an old generalization re-examined. Am. Heart J., 97:184–186, 1979.

[Murgatroyd95] F. Murgatroyd, B. Xie, X. Copie, I. Blankoff, A. Camm, and M. Malik. Identification of atrial fibrillation episodes in ambulatory electrocardiographic recordings: validation of a method for obtaining labeled R-R interval files. Pacing Clin. Electrophysiol., 18:1315—1320, 1995.

[Nagayoshi97] H. Nagayoshi, T. Janota, and K. Hnatkova. Autonomic modulation of ventricular rate in atrial fibrillation. Am. J. Physiol., 272(4):1643–1649, 1997.

[Nattel87] S. Nattel, M. Talajic, and M. Quantz. Frequency-dependent effects of amiodarone on atrioventricular nodal function and slow-channel action potentials: evidence for calcium channel-blocking activity. Circulation, 76:442–449, 1987.

[Nattel02] S. Nattel. New ideas about atrial fibrillation 50 years on. Nature, 415(6868):219–226, 2002.

[Nayebpour91] M. Nayebpour, M. Talajic, and S. Nattel. Quantitation of dynamic av nodal properties and application to predict rate-dependent av conduction. Am. J. Physiol., 261:292–300, 1991.

[NCC06] The National Collaborating Centre for Chronic Conditions NCC. Atrial fibrillation national clinical guideline for management in primary and secondary care. http://www.rcplondon.ac.uk/pubs/books/AF/ AtrialFibGuide.pdf, 2006.

[NHS06] National Institute for Health NHS and Clinical Excellence. Atrial fibrillation - the management of atrial fibrillation. http://guidance.nice.org.uk/CG36/niceguidance/pdf/

English/download.dspx, 2006.

[Olsson86] S. Olsson, N. Cai, and M. Dohnal. Non-invasive support for and characterization of multiple intranodal pathways in patients with mitral valve disease and atrial fibrillation. Eur. Heart J., 7:320 –333, 1986.

[Omran98] H. Omran, W. Jung, R. Schimpf, D. MacCarter, R. Rabahieh, C. Wolpert, S. Illien, and B. Luderitz. Echocardiographic parameters for predicting maintenance of sinus rhythm after internal atrial defibrillation. Am. J. Cardiol., 81:1446–1449, 1998.

[Ossadnik94] S.M. Ossadnik, S.B. Buldyrev, A.L. Goldberger, S. Havlin, R.N. Mantegna, C.-K. Peng, M. Simons, and H.E. Stanley. Correlation approach to identify coding regions in dna sequences. Biophys. J., 67:64–70, 1994.

[Pamboucas02] C. Pamboucas, S. Chatzidou, S. Voyatzis, S. Stambola, I. Antonelli, and S. Rokas. The predictive accuracy of the RR interval distribution pattern in the detection of dual AV node physiology in patients with chronic atrial fibrillation. Hellenic J. Cardiol, 43:204–208, 2002.

[Pan85] J. Pan and J. Tompkins, W. A real-time qrs detection algorithm. IEEE Transactions on Biomedical Engineering,, 32:230–236, 1985.

[Pappone04] C. Pappone and S. Rosanio. Cardiac Electrophysiology - From Cell to Bedside. Saunders, jalife j edition, 2004.

[Peng91] C.-K. Peng, S. Havlin, M. Schwartz, and H.E. Stanley. Directed-polymer and ballistic deposition growth with correlated noise. Phys. Rev. A, 44:2239–2243, 1991.

[Peng94] C.K. Peng, S.V. Buldyrev, S. Havlin, M. Simons, H.E. Stanley, and A.L. Goldberger. Mosaic organization of DNA nucleotides. Phys. Rev. E, 49:1685–1689, 1994.

[Peter66] R.H. Peter, J.J. Morris, and H.D. McIntosh. Relationship of fibrillatory waves and p waves in the electrocardiogram. Circulation, 33:599–606, 1966.

[Petrucci05] E. Petrucci, V. Balian, G. Filippini, and L.T. Mainardi. Atrial fibrillation detection algorithms for very long term ECG monitoring. Computers in Cardiology, 32:623–626, 2005.

[Pherson98] St. Pherson, M. Holm, , C. Meurling, M. Ingemansson, B. Smideberg, L. Sornmo, and S.B. Olsson. Non-invasive assessment of magnitude and dispersion of atrial cycle length during chronic atrial fibrillation in man. European Heart Journal, 19:1836–1844, 1998.

[Piechulla00] W. Piechulla. Herzratenindikatoren, arbeit zum pflichtwahlpraktikum: Workload konzepte und messmethoden fuer belastung und beanspruchung. http://www.psychologie.uni-wuerzburg.de/methoden/mitarbeiter/ehemalige/piechulla.php.de, 2000.

[Pinciroli86] F. Pinciroli and A. Castelli. Pre-clinical experimentation of a quan-

titative synthesis of the local variability in the original R-R interval sequence in the presence of arrhythmia. Automedica, 6:295—317, 1986.

[Pitschner98] H.F. Pitschner, A. Berkovic, S. Grumbrecht, and J. Neuzner. Multielectrode basket catheter mapping for human atrial fibrillation. J. Cardiovasc. Electrophysiol., 9:48–56, 1998.

[Poon97] C.-S. Poon and C.K. Merrill. Decrease of cardiac chaos in congestive heart failure. Nature, 389(6650):492–495, October 1997.

[Prystowsky97] E.N. Prystowsky. Atrioventricular node reentry: physiology and radiofrequency ablation. Pacing. Clin. Electrophysiol., 20:552–571, 1997.

[Raitt00] M.H. Raitt, K.D. Ingram, and S.M. Thurman. Signal-averaged p wave duration predicts early recurrence of atrial fibrillation after cardioversion. Pacing Clin. Electrophysiol., 23:259–265, 2000.

[Rensma88] P.L. Rensma, M.A. Allessie, W.J. Lammers, F.I. Bonke, and M.J. Schalij. Length of excitation wave and susceptibility to reentrant atrial arrhythmias in normal conscious dogs. Circ. Res., 62:395–410, 1988.

[Rokas01] S. Rokas, S. Gaitanidou, S. Chatzidou, C. Pamboucas, D. Achtipis, and S. Stamatelopoulos. Atrioventricular node modification in patients with chronic atrial fibrillation. role of morphology of RR interval variation. Circulation, 103:2942–2948, 2001.

[Ropella89] K.M. Ropella, A.V. Sahakian, J.M. Baerman, and S. Swiryn. The coherence spectrum. a quantitative discriminator of fibrillatory and nonfibrillatory cardiac rhythms. Circulation, 80:112–119, 1989.

[Rosenbaum90] D.S. Rosenbaum and R.J. Cohen. Frequency based measures of atrial fibrillation in man. IEEE-EMBS, 12:582–583, 1990.

[Sahakian92] A. Sahakian, K. Ropella, and S. Swiryn. Atrial electrograms and the characterization of atrial fibrillation. J. Electrocardiol., 24:131–133, 1992.

[Saul87] J.P. Saul, P. Albrecht, and R.J. Berger. Analysis of long term heart rate variability: methods, 1/f scaling and implications. Comp. Cardiol., 14:419–422, 1987.

[Saur03] Ch. Saur. Simultanes multipolares Mapping von anhaltendem und nichtanhaltendem Vorhofflimmern beim Menschen. Ph.D. thesis, Technische Universität München, February 2003.

[Scargle82] J.D. Scargle. Studies in astronomical time series analysis. ii - statistical aspects of spectral analysis of unevenly spaced data. Astrophysical Journal, 263:835–853, 1982.

[Scherf48] D. Scherf, F.J. Romano, and R. Terranova. Experimental setudies on auricular flutter and auricular fibrillation. Am. Heart J., 36:241–251,

1948.

[Scherf53] D. Scherf, A.I. Schaffer, and S. Blumenfeld. Mechanism of flutter and fibrillation. Arch. Intern Med., 91:333–352, 1953.

[Schuessler92] R.B. Schuessler, T.M. Grayson, B.I. Bromberg, J.L. Cox, and J.P. Boineau. Cholinergically mediated tachyarrhythmias induced by a single extrastimulus in the isolated canine right atrium. Circ. Res., 71:1254–1267, 1992.

[Shlesinger87] M.F. Shlesinger, B.J. West, and J. Klafter. Lévy dynamics of enhanced diffusion: Application to turbulence. Phys. Rev. Lett., 58:1100, 1987.

[Shrier87] A. Shrier, H. Dubarsky, M. Rosengarten, M.R. Guevara, S. Nattel, and L. Glass. Prediction of complex atrioventricular conduction rhythms in humans with use of the atrioventricular nodal recovery curve. Circulation, 76:1196–1205, 1987.

[Shrout79] P.E. Shrout and J.L. Fleiss. Intraclass correlations: uses in assessing rater reliability. Psychol. Bull., 86:420–428, 1979.

[Sih99] H.J. Sih, D.P. Zipes, E.J Berbari, and J.E. Olgin. A high temporal resolution algorithm for quantifying organization during atrial fibrillation. IEEE Trans BME, 46:440–450, 1999.

[Simson79] M.B. Simson, J. Spear, and E.N. Moore. The relationship between atrioventricular nodal refractoriness and the functional refractory period in the dog. Circ. Res., 44:121–126, 1979.

[Skanes97] A.C. Skanes, R.A. Gray, C.L. Zuur, and J. Jalife. Spatio-temporal patterns of atrial fibrillation: role of the subendocardial structure. Semin. Interv. Cardiol., 2:185–193, 1997.

[Skanes98] A.C. Skanes, R. Mandapati, O. Berenfeld, J.M. Davidenko, and J. Jalife. Spatiotemporal periodicity during atrial fibrillation in the isolated sheep heart. Circulation, 98:1236–1248, 1998.

[Slocum92] J. Slocum, A. Sahakian, and S. Swiryn. Diagnosis of atrial fibrillation from surface electrocardiograms based on computer-detected atrial activity. J. Electrocardiol., 25:1–8, 1992.

[Slocum94] J.E. Slocum and K.M. Ropella. Correspondence between the frequency domain characteristics of simultaneous surface and intra-atrial recordings of atrial fibrillation. IEEE Computers in Cardiology, 21:781–784, 1994.

[Stackee71] J. Stackee, A.J. Hoelen, N.E. Zimmerman, and F.L. Meijler. Artificial atrial fibrillation in the dog. An artifact? Circ. Res., 28:441–445, 1971.

[Stambler97] B.S. Stambler, M.A. Wood, and K.A. Ellenbogen. Antiarrhythmic actions of intravenous ibutilide compared with procainamide during human atrial flutter and fibrillation : Electrophysiological determi-

nants of enhanced conversion efficacy. Circulation, 96:4298–4306, December 1997.

[Stein99] K.M. Stein, J. Walden, N. Lippman, and B.B. Lerman. Ventricular response in atrial fibrillation: random or deterministic? Am. J. Physiol., 277:452–458, 1999.

[Taqqu95] M.S. Taqqu, V. Teverovsky, and W. Willinger. Estimators for long-range dependence: an empirical study. Fractals, 3:785, 1995.

[Tateno01] K. Tateno and L. Glass. Automatic detection of atrial fibrillation using the coefficient of variation and density histograms of RR and ΔRR intervals. Med. Biol. Eng. Comput., 39:664–671, 2001.

[Teague76] S. Teague, S. Collins, D. Wu, P. Denes, K. Rosen, and R. Arzbaecher. A quantitative description of normal av nodal conduction curve in man. J. Appl. Physiol., 40:74–78, 1976.

[Toivonen90] L. Toivonen, A. Kadish, W. Kou, and F. Morday. Determinants of the ventricular rate during atrial fibrillation. Am. J. Physiol., 16(5):1194–1200, 1990.

[Van den Berg94] M. P. Van den Berg, H.J.G.M. Crijns, J. Haaksma, J. Brouwer, and K.I. Lie. Analysis of vagal effects on ventricular rhythm in patients with atrial fibrillation. Clin. Sci. (Lond.), 86:531–535, 1994.

[Vanicek71] P. Vanicek. Further development and properties of the spectral analysis by least-squares. Astrophysics and Space Science, 12:10—33, 1971.

[Verhorst97] P.M. Verhorst, O. Kamp, R.C. Welling, M.J. Van Eenige, and C.A. Visser. Transesophageal echocardiographic predictors for maintenance of sinus rhythm after electrical cardioversion of atrial fibrillation. Am. J. Cardiol., 79:1355–1359, 1997.

[Vjushin04] D. Vjushin, I. Zhidkov, S. Havlin, A. Bunde, and S. Brenner. Volcanic forcing improves atmosphere-ocean coupled general circulation model scaling performance. Geophys. Res. Lett., 31:10206, 2004.

[Wasmund03] S.L. Wasmund, J.M. Li, R.L. Page, J.A. Joglar, and R.C. Kowal. Effect of atrial fibrillation and an irregular ventricular response on sympathetic nerve activity in human subjects. Circulation, 107(15):2001–2015, 2003.

[Wells78] J.L.Jr. Wells, R.B. Karp, N.T. Kouchoukos, W.A. MacLean, T.N. James, and A.L. Waldo. Characterization of atrial fibrillation in man: studies following open heart surgery. Pacing Clin. Electrophysiol, 1:426–438, 1978.

[Williamson94] B. Williamson, K. Man, and E. Daoud. Radiofrequency catheter modification of atrioventricular conduction to control the ventricular rate during atrial fibrillation. N. Engl. J. Med., 331:910–917, 1994.

[Wittkampf88] F.H. Wittkampf, M.J.L. de Jongste, H.I. Lie, and F.L. Meijler. Ef-

fect of right ventricular pacing on ventricular rhythm during atrial fibrillation. J. Am. Coll. Cardiol., 11:539–545, 1988.

[Wolf87] P.A. Wolf, R.D. Abbott, and W.B. Kannel. Atrial fibrillation a major contributor to stroke in the elderly. the framingham study. Arch. Intern. Med., 147:1561–1544, 1987.

[Wolf91] P.A. Wolf, R.D. Abbott, and W.B. Kannel. Atrial fibrillation as an independent risk factor for stroke: the framingham study. Stroke, 22:983–988, 1991.

[Yamada99] T. Yamada, M. Fukunami, T. Shimonagata, K. Kumagai, S. Sanada, H. Ogita, Y. Asano, M. Hori, and N. Hoki. Dispersion of signal-averaged p wave duration on precordial body surface in patients with paroxysmal atrial fibrillation. Eur. Heart J., 20:211–220, 1999.

[Yamamoto94] Y. Yamamoto and R.L. Hughson. On the fractal nature of heart rate variability in humans: effects of data length and b-adrenergic blockade. Am. J. Physiol., 266:40–49, 1994.

[Zeng96] W. Zeng and L. Glass. Statistical properties of heartbeat intervals during atrial fibrillation. Phys. Rev. E., 54:1779–1784, 1996.

[Zweig93] H. Zweig, M. and G. Cambell. Receiver-operating characteristic (roc) plots: a fundamental evaluation tool in clinical medicine. Clin. Chem., 39(8):561, August 1993.

Abbreviations

AF	atrial fibrillation	7
AFDB	Atrial Fibrillation Database	39
AFR	rate of atrial fibrillation	61
AREEM	absolute averaged relative error of moments	66
AV node	atrioventricular node	11
atrial tachogram	time series of consecutive atrial interbeat intervals	13
CHF	Congestive Heart Failure Database	39
DFA	detrended fluctuation analysis	28
ECG	electrocardiogram	11
NSRDB	Normal Sinus Rhythm RR Interval Database	38
NSR2DB	Normal Sinus Rhythm Database	38
SNR	signal to noise ratio	23
tachogram	time series of consecutive ventricular interbeat intervals r	13
PSD	power spectral density	25
ventricular response	time series of consecutive ventricular interbeat intervals r	13
WTD	waiting time density	80

Notations

r	ventricular interbeat interval 13
$w(r)$	distribution of ventricular interbeat intervals r 22
$\bar{r}$	mean of ventricular intervals r 23
σ_r	standard deviation of ventricular intervals r 23
$\bar{r}_{\text{loc}}$	local mean of ventricular intervals r calculated in time windows of certain length 23
$\sigma_{r,\text{loc}}$	local standard deviation of ventricular interbeat intervals r calculated in time windows of certain length 23
$S(f)$	power spectral density 25
$F(s)$	fluctuation function 28
$L(\omega)$	Lomb-periodogram of the unevenly sampled time series x_i 32
$\vec{F}_n$	form vector of the time and voltage normalized ECG segment of a single heartbeat n 42
M_n	normalized-morphogram 43
dM_n	delta morphograms 43
N_n	non-normalized morphogram 47
γ	rate of the exponential decay of $w(r)$ for large intervals r 48
p_∞	amplitude factor of the exponential decay of $w(r)$ for large intervals r 48
t_{con}	time for the conduction of an atrial impulse through the AV node 62
t_{ref}	refractory period of the AV node 62
t_{rec}	recovery time of the AV node 62
α	minimal conduction time of the AV node 62
Δ	time increment of the refractory period in the conduction model of Jørgensen *et al* 63

Index

T

V

W